This is to certify that the

dissertation entitled

ANALYTICAL AND EXPERIMENTAL TECHNIQUES FOR THE ELECTROMAGNETIC CHARACTERIZATION OF MATERIALS

presented by

Michael John Havrilla

has been accepted towards fulfillment
of the requirements for

Ph.D. degree in Electrical and Computer Engineering

D. R. Wyglinski
Major professor

Date 19 April 2001

DATE DUE	DATE DUE	DATE DUE
MAY 1 7 2005 0 9 1 6 0 3		
AUG 3 1 2016		

ANALYTICAL AND EXPERIMENTAL TECHNIQUES FOR THE ELECTROMAGNETIC CHARACTERIZATION OF MATERIALS

By

Michael John Havrilla

A DISSERTATION

Submitted to
Michigan State University
in partial fulfillment of the requirements
for the degree of

DOCTOR OF PHILOSOPHY

Department of Electrical and Computer Engineering

2001

ABSTRACT

ANALYTICAL AND EXPERIMENTAL TECHNIQUES FOR THE ELECTROMAGNETIC CHARACTERIZATION OF MATERIALS

By

Michael John Havrilla

Electromagnetic material characterization is the process of determining the permittivity and permeability of matter. This process is predominantly employed in stealth and integrated-circuit technologies with the aid of the analytical Nicolson-Ross-Weir (NRW) formulation. The increasing demands of industry have rendered the NRW technique invalid under certain conditions due to theoretical violations, leading to erroneous results. In rectangular waveguide measurements, for example, it is assumed that sample material is comprised of a single layer only, that walls are perfectly conducting and that no gaps exist between the sample and conducting boundaries. However, in the industry environment, samples are often multi-layered due to material integrity and high-temperature measurements lead to sample-to-wall gaps and involve waveguide metals that are typically poorly conducting. In addition, high-temperature strip and microstrip field applicators also involve imperfectly-conducting boundaries, leading to gross errors in the material characterization process. This dissertation provides several techniques to accommodate these errors.

Chapter 2 provides two methods, the direct and deembed techniques, for characterizing materials that are embedded in multi-layered samples. Although both formulations utilize wave-transmission matrices, it is shown that the direct method must

be used if sample homogeneity is to be accurately monitored. Errors due to sample-to-wall gaps are accommodated in Chapter 3 by regarding the waveguide as inhomogeneously filled in the cross-sectional plane with *LSM* and *LSE* propagation modes supported in the sample/gap regions. This analysis leads to corrections in the scattering parameters and ideal TE_{10} propagation constant of a uniformly-filled guide. Chapter 4 investigates the effects of waveguide wall loss by using a coupled-mode perturbation theory which is based upon an impedance boundary condition at the imperfectly-conducting walls. The result is a complex correction to the ideal TE_{10} propagation constant.

Strip and microstrip field applicators having imperfectly-conducting boundaries are investigated in Chapters 5-7 using a spectral-domain integral-operator formulation with the aid of electric-field dyadic Green's functions. The resulting electric field integral equations, which follow from enforcement of impedance boundary conditions on the imperfect strip conductors, are solved using a non-Galerkin's Method of Moments technique employing Chebyshev basis functions of the first and second kind. The analysis in Chapters 5-6 and 7 leads to a correction in the ideal principal-mode propagation constant for the strip and microstrip transmission lines, respectively.

In loving memory of my father

Albert L. Havrilla

ACKNOWLEDGEMENTS

I would like to express sincerest thanks to my committee members. My advisor and mentor, Dr. Dennis Nyquist, has given generously of his time throughout the years. His expertise, physical insight, enthusiasm and guidance made this dissertation possible. It's difficult to express in words just how grateful I am to have studied under such a gifted and talented scholar. Dr. Edward Rothwell's academic abilities, patience and kindness will always be an example to me. Like many others, I am indebted to Dr. Kun-Mu Chen for establishing a tradition of excellence in the electromagnetics research group at Michigan State University. Dr. Byron Drachman also gave freely of his time and provided valuable mathematical insight. I would also like to express my appreciation to Dr. Lydell Frasch for his insightful comments. A majority of this dissertation was supported by GE Aircraft Engines and I would like to thank Matt Kress and John Nelson for their guidance and expertise in material measurements. Jeff Meese and Dennis Kelly provided valuable computer consultation. The secretaries were very kind and made me feel right at home.

The support of my parents, family and friends was equally important. Special thanks go to my parents, Margaret and Albert, and to my colleagues and friends Chris Coleman, Dave Infante, Mark Perrin and Dave Story. My friends from the marketing group, especially Rose, were endlessly entertaining. Ken Noren, my friend and winter mountaineering partner, and his wife, Deb, have been exceedingly gracious and hospitable over the years. My loving girlfriend, Som, is a constant encouragement and support to me. Finally, and most importantly, I am forever grateful to Christ Jesus.

TABLE OF CONTENTS

LIST OF FIGURES

Chapter 1

INTRODUCTION AND OVERVIEW

This dissertation deals with aspects of theoretical and experimental techniques in electromagnetic material characterization, which is the process of determining the permittivity and/or permeability of a material. Permittivity and permeability are specific values that describe the effect that an externally applied electric and magnetic field has on matter. Several disciplines rely heavily on the material characterization process; including stealth, integrated circuit and agricultural technologies. For example, in stealth technology, the permittivity and permeability describe how effectively a particular material can absorb incoming radar signals. Due to the increasing demands on industry, accurate characterization is vital if stringent design specifications are to be realized.

Typically, materials are first measured in the small-scale laboratory environment prior to large-scale application. In stealth technology, it's common for a radar absorbing coating to encounter months or years of testing and design changes in the laboratory before it can be applied to the structure of a vehicle. Several laboratory devices (operating in their fundamental mode) can be exploited in the material characterization process, including rectangular and circular waveguides, coaxial transmission lines, free-field measurement systems, strip transmission lines, microstrip field applicators and cavity resonators. In each case, the material must be machined to fit the particular geometry of the given apparatus and a corresponding theory must be developed that ultimately relates the permittivity and permeability of the sample to the experimental

measurement. Rectangular waveguides, strip transmission lines and, to a lesser extent, microstrip field applicators are most often used in the industry environment due to the ease of machining rectangular samples and the relative broadband nature of such devices.

As an overview, the material characterization process generally involves the following steps. First, as mentioned above, a material sample is appropriately machined to fit into the testing device. Next, the device is connected to a network analyzer, which launches an incident wave towards the sample and subsequently measures the amount of signal that is reflected from and transmitted through the material. These experimental measurements are then correlated with suitable theoretical expressions and the permittivity and permeability are computed using numerical algorithms. The predominant algorithm used in industry is the Nicolson, Ross and Weir (NRW) technique [1], [2].

The fundamental underlying assumptions in the NRW technique are as follows. First, the material sample is assumed to be simple (i.e., linear, homogeneous and isotropic) and have front and back interfaces that are coplanar. In addition, the sample is assumed to be comprised of a single layer only. Furthermore, if a rectangular waveguide is used, it is assumed that the waveguide walls are perfectly conducting and no gaps exist between the sample and conducting boundaries. In the stripline or microstrip environments, it is also assumed that the boundaries are perfectly conducting. However, in the industry environment, these assumptions are often violated. Samples that are thin and susceptible to warping must be attached to known substrates to facilitate measurement, thus violating the single-layer assumption. Materials are frequently inhomogeneous due to sample preparation methods. Samples that are measured at high

temperatures must involve field applicators made of special alloys that typically have poor conductivities. Gaps can also occur in high-temperature applications due to differing rates of thermal expansion for the sample material and metallic walls. These NRW violations can lead to significant errors in the material characterization process and render standard methods useless. The main objective of this thesis is to develop various techniques to accommodate for and subsequently reduce these errors.

Chapter 2 presents two material characterization techniques for analyzing multi-layered samples, the direct and deembed methods. Both methods utilize wave matrices [3] for extracting the unknown layer parameters from the known substrate layer(s). It will be shown that the direct method has a distinct advantage over the deembed method when monitoring for sample inhomogeneity. Chapter 3 addresses the issue of sample-to-wall gaps in rectangular waveguide-based measurements [4]-[6]. These gaps are analyzed by regarding the waveguide as inhomogeneously filled in the cross-sectional plane with longitudinal section magnetic (LSM) and longitudinal section electric (LSE) propagating modes supported in the sample/gap region [3]. It will be shown that this leads to a correction to the ideal TE_{10} mode propagation constant and interfacial reflection and transmission coefficients, thus allowing for accurate determination of the constitutive parameters for the sample material. Chapter 4 accommodates rectangular waveguide wall loss [7]-[13] by invoking an impedance boundary condition at the imperfect conducting boundaries, which leads to a coupled mode perturbation theory that is subsequently specialized to single mode operation [3]. The result is a complex correction to the ideal TE_{10} propagation constant. It will be demonstrated that this complex correction is critical in the material characterization process via comparison

with the standard power-loss method [3], [14]-[19]. Therefore, Chapters 2-4 present techniques for accommodation of NRW violations when using rectangular waveguides in electromagnetic material characterization measurements.

The focus and intent of Chapters 5-7 are to account for imperfect conductors in stripline and microstrip field applicators using a full-wave analysis in the Fourier transform domain [20]-[24]. First, in Chapter 5, the Green's function for the fields excited by a general 3D current source immersed in a stripline background environment is developed using two different methods. The primary method involves the use of Hertzian potential boundary conditions [25]-[27] for a symmetric slab waveguide in which the outer cover regions are allowed to become highly conducting. The secondary method utilizes Hertzian potential impedance boundary conditions, which are developed in Appendix D. Although both methods produce identical results, it will be shown that considerably less effort is required when utilizing Hertzian potential impedance boundary conditions.

The lossy stripline field applicator is analyzed in Chapter 6 by specializing the general 3D current source of chapter 5 to an infinitely-long strip surface current symmetrically located between imperfectly-conducting plates. An EFIE (electric field integral equation) is subsequently developed [28] by satisfying an impedance boundary condition on the strip conductor. The EFIE is solved numerically using a MoM (method of moments) technique [29] and the principal-mode propagation constant and corresponding surface current distribution are identified and examined. Chapter 7 is exclusively devoted to the lossy microstrip field applicator. Similar to Chapters 5 and 6, the electric-field dyadic Green's function is developed for a general 3D current source

immersed within a microstrip background environment. An EFIE is formulated and solved by confining the 3D current to a strip conductor, implementing impedance boundary conditions on the surface of the imperfect strip and invoking the MoM technique. A complex propagation constant, vital to the material characterization process, is identified and investigated, along with the strip surface current density. Chapter 8 provides conclusions and future recommendations of study.

Chapter 2

DIRECT AND DEEMBED METHODS FOR MATERIAL CHARACTERIZATION

2.1 Introduction

The well-known Nicolson-Ross-Weir (NRW) [1], [2] algorithm is predominantly used in industry for computing the permittivity and permeability (ε, μ) of an unknown single-layered material from forward measured scattering parameters S_{11}, S_{21}. Constitutive parameters can also be computed using the reverse S-parameters S_{22}, S_{12}. It is common practice to use both sets of S-parameters since a comparison between them can provide a measure of sample isotropy and homogeneity, which are important criteria in the NRW technique. Unknown materials which are subject to warping or bending are frequently attached (through deposition, spraying, etc.) on a known substrate layer to facilitate measurement. In this case, the standard NRW method cannot be employed since it can only handle single-layered environments. Although ignoring the substrate layer would allow application of the NRW technique, experience shows that this leads to gross errors.

Wave transmission matrices (i.e., A-parameters) [3] can be utilized to account for the multi-layered environment so that the constitutive parameters of the unknown layer can be properly determined. Two schemes for extracting the material parameters of the unknown layer will be discussed, the direct and deembed methods. It will be shown through comparison that only the direct method is reliable for monitoring the important property of sample homogeneity.

2.2 Material Characterization for a Single-Layered Environment

2.2.1 Overview

The overall scheme of the material measurement process is to experimentally obtain the sample S-parameters ($S_{11}^{exp}, S_{21}^{exp}$) and compare them with their theoretical expressions ($S_{11}^{thy}, S_{21}^{thy}$). Mathematically, the above condition leads to the following set of coupled equations

$$\begin{aligned} S_{11}^{thy}(\omega,\varepsilon,\mu) - S_{11}^{exp}(\omega) = 0 \\ S_{21}^{thy}(\omega,\varepsilon,\mu) - S_{21}^{exp}(\omega) = 0 \end{aligned} \tag{2.1}$$

The constitutive parameters (ε, μ) in (2.1) can be determined analytically using the NRW technique or numerically using a two-dimensional Newton's root search. If the sample is non-magnetic, then the permittivity can be computed using S_{11} or S_{21}, that is

$$S_{11}^{thy}(\omega,\varepsilon) - S_{11}^{exp}(\omega) = 0 \quad or \quad S_{21}^{thy}(\omega,\varepsilon) - S_{21}^{exp}(\omega) = 0 \tag{2.2}$$

A one-dimensional root-search must be used in (2.2) since no closed-form solution exists. A similar scheme applies if $S_{22}^{exp}, S_{12}^{exp}$ are measured. That is, if the material has both dielectric and magnetic properties, then the following coupled equations must be solved (either analytically or numerically) for the reverse direction

$$\begin{aligned} S_{22}^{thy}(\omega,\varepsilon,\mu) - S_{22}^{exp}(\omega) = 0 \\ S_{12}^{thy}(\omega,\varepsilon,\mu) - S_{12}^{exp}(\omega) = 0 \end{aligned} \tag{2.3}$$

If the material is non-magnetic, then the permittivity must be computed numerically using either of the following relations

$$S_{22}^{thy}(\omega,\varepsilon) - S_{22}^{exp}(\omega) = 0 \quad or \quad S_{12}^{thy}(\omega,\varepsilon) - S_{12}^{exp}(\omega) = 0 \tag{2.4}$$

A review of the analytical NRW technique is given next for the benefit of the reader.

2.2.2 General NRW Formulation

It can be shown (see section 2.4, for example) that the theoretical (forward) S-parameters of a single-layered planar material are

$$S_{11}^{thy} = \frac{R(1-P^2)}{1-R^2P^2} \tag{2.5}$$

$$S_{21}^{thy} = \frac{P(1-R^2)}{1-R^2P^2} \tag{2.6}$$

where $R = R(\omega, \varepsilon, \mu)$ is the interfacial reflection coefficient and $P = P(\omega, \varepsilon, \mu)$ is the one-way phase delay and attenuation through the material. Equation (2.1) suggests that (2.5) and (2.6) can be written

$$S_{11}^{exp} = \frac{R(1-P^2)}{1-R^2P^2} \tag{2.7}$$

$$S_{21}^{exp} = \frac{P(1-R^2)}{1-R^2P^2} \tag{2.8}$$

A closed-form inverse solution exists for the above nonlinear equations. That is, R and P can be solved in terms of S_{11}^{exp} and S_{21}^{exp}. Once these values have been determined, the constitutive parameters (ε, μ) can be computed. The inverse solution can be obtained by first solving (2.7) for P^2 and (2.8) for P, leading to

$$P^2 = \frac{R - S_{11}^{exp}}{R(1 - RS_{11}^{exp})} \tag{2.9}$$

$$P = \frac{S_{21}^{exp}(1-R^2P^2)}{1-R^2} \tag{2.10}$$

Substituting equation (2.9) into the P^2 term of (2.10) results in

$$P = \frac{S_{21}^{exp}}{1 - RS_{11}^{exp}} \quad \Rightarrow \quad P^2 = \left(\frac{S_{21}^{exp}}{1 - RS_{11}^{exp}} \right)^2 \tag{2.11}$$

Equating (2.9) and (2.11) gives

$$\frac{R - S_{11}^{exp}}{R(1 - RS_{11}^{exp})} = \left(\frac{S_{21}^{exp}}{1 - RS_{11}^{exp}} \right)^2 \quad \Rightarrow \quad \frac{R - S_{11}^{exp}}{R} = \frac{(S_{21}^{exp})^2}{1 - RS_{11}^{exp}} \tag{2.12}$$

Cross-multiplying and grouping terms leads to the following quadratic equation

$$R^2 - 2QR + 1 = 0 \quad , \quad Q = \frac{(S_{11}^{exp})^2 - (S_{21}^{exp})^2 + 1}{2S_{11}^{exp}} \tag{2.13}$$

whose solution is

$$R = Q \pm \sqrt{Q^2 - 1} \tag{2.14}$$

The proper root choice is based on the requirement that the magnitude of the interfacial reflection coefficient must be less than unity for a passive material, that is, $|R| < 1$. Equation (2.14) produces two roots. One will have a magnitude greater than unity and the other root must have a magnitude less than unity. To see this, let $R_1 = Q + \sqrt{Q^2 - 1}$ and $R_2 = Q - \sqrt{Q^2 - 1}$. Note the following relationship between the two roots

$$\frac{1}{R_1} = \frac{1}{Q + \sqrt{Q^2 - 1}} = \frac{1}{Q + \sqrt{Q^2 - 1}} \frac{Q - \sqrt{Q^2 - 1}}{Q - \sqrt{Q^2 - 1}} = Q - \sqrt{Q^2 - 1} = R_2 \tag{2.15}$$

therefore

$$\left| \frac{1}{R_1} \right| = \frac{1}{|R_1|} = |R_2| \tag{2.16}$$

Now that R and P have been related to S_{11}^{exp} and S_{21}^{exp} in equations (2.14) and (2.11), the permittivity and permeability can be determined. The details of this calculation are provided in the following two sections. Note, a similar analysis holds for the reverse S-parameters S_{22}^{exp} and S_{12}^{exp}.

2.2.3 Computation of Constitutive Parameters for a TEM System

If the sample (having length ℓ) is measured using a transverse electromagnetic (TEM) field applicator (i.e., coaxial, stripline, free-field, etc.) operating in its fundamental mode, then the interfacial reflection coefficient R and one-way propagation term P are related to the relative permittivity and permeability (ε_r, μ_r) in the following manner

$$R = \frac{Z - Z_0}{Z + Z_0} = \frac{z-1}{z+1} \quad , \quad z = \frac{Z}{Z_0} = \sqrt{\frac{\mu_r}{\varepsilon_r}} \tag{2.17}$$

$$P = e^{-\gamma \ell} \quad , \quad \gamma = -\frac{\ln P}{\ell} = j\beta = j(\omega / c)\sqrt{\varepsilon_r \mu_r} = j\omega y / c \tag{2.18}$$

Solving the above equations for y and z produces

$$z = \sqrt{\frac{\mu_r}{\varepsilon_r}} = \frac{1+R}{1-R} \tag{2.19}$$

$$y = \sqrt{\varepsilon_r \mu_r} = \frac{\gamma c}{j\omega} = \frac{jc \ln P}{\omega \ell} \tag{2.20}$$

Therefore, ε_r and μ_r are computed using the relations

$$\varepsilon_r = \frac{y}{z} = j\frac{c \ln P}{\omega \ell}\left(\frac{1-R}{1+R}\right) \quad , \quad \mu_r = yz = j\frac{c \ln P}{\omega \ell}\left(\frac{1+R}{1-R}\right) \tag{2.21}$$

2.2.4 Computation of Constitutive Parameters for a Waveguide System

If the sample is measured using a rectangular waveguide operating in the principal TE_{10} mode, then R and P are related to ε_r and μ_r in the following manner (assuming no gaps exist between the sample and perfectly-conducting waveguide walls)

$$R = \frac{z-1}{z+1} \quad , \quad z = \frac{Z}{Z_0} = \frac{j\omega\mu_0\mu_r/\gamma}{j\omega\mu_0/\gamma_0} = \mu_r\frac{\gamma_0}{\gamma} \tag{2.22}$$

$$\gamma^2 = k_c^2 - k^2 \quad , \quad \gamma_0^2 = k_c^2 - k_0^2 \quad , \quad k_0^2 = \omega^2\varepsilon_0\mu_0 \quad , \quad k^2 = k_0^2\varepsilon_r\mu_r \quad , \quad k_c^2 = \frac{\pi^2}{a^2} \tag{2.23}$$

$$P = e^{-\gamma\ell} \quad , \quad \gamma = -\frac{\ln P}{\ell} = \sqrt{k_c^2 - k_0^2\varepsilon_r\mu_r} \tag{2.24}$$

Solving (2.22) for μ_r and (2.24) for ε_r gives

$$\mu_r = z\frac{\gamma}{\gamma_0} = -\frac{\ln P}{\gamma_0\ell}\left(\frac{1+R}{1-R}\right) \tag{2.25}$$

$$\varepsilon_r = \frac{k_c^2 - \gamma^2}{\mu_r k_0^2} = -\frac{k_c^2 - (\ln P/\ell)^2}{k_0^2\dfrac{\ln P}{\gamma_0\ell}\left(\dfrac{1+R}{1-R}\right)} \tag{2.26}$$

2.3 Geometry of Multi-Layered Environment

Figure 2.1 shows the multi-layered environment under consideration. The system, which is assumed to be immersed in free space, is comprised of N layers and $N+1$ interfaces. The thickness, effective complex permittivity and permeability of the i^{th} layer are ε_i, μ_i and ℓ_i. The terms c_i, b_i are the complex wave amplitudes of the incident and reflected waves immediately to the left of the i^{th} interface. The interfacial reflection and transmission coefficients at the i^{th} interface are R_i and T_i.

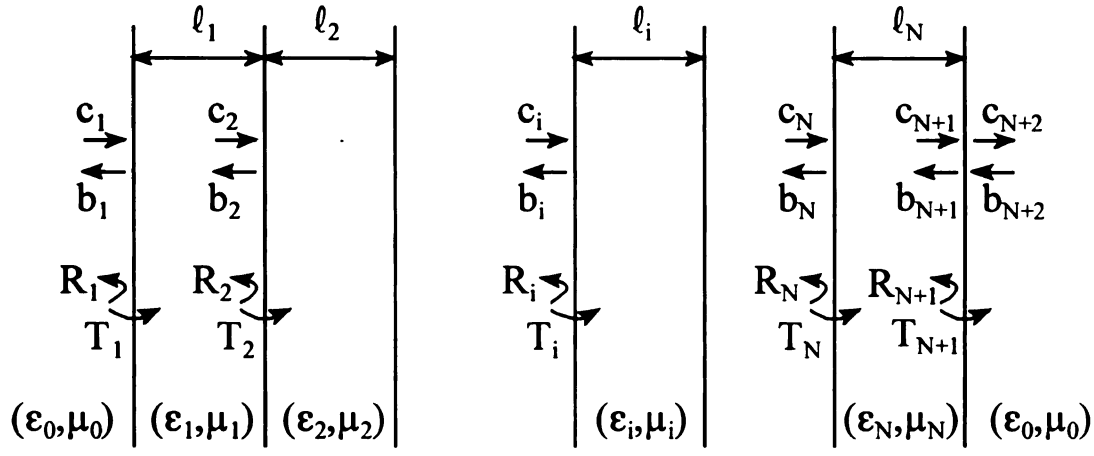

Figure 2.1 Multi-layered environment.

2.4 A-Parameter Description of a Multi-Layered System

Wave transmission matrices or A parameters describe the relationship between incident and reflected wave amplitudes at a prescribed input terminal plane to those at a prescribed output terminal plane. The general A-parameter formulation is developed as follows [3]. Consider a wave c_1 incident on an interface from the left and a second wave b_2' incident on the interface from the right, as shown in Figure 2.2.

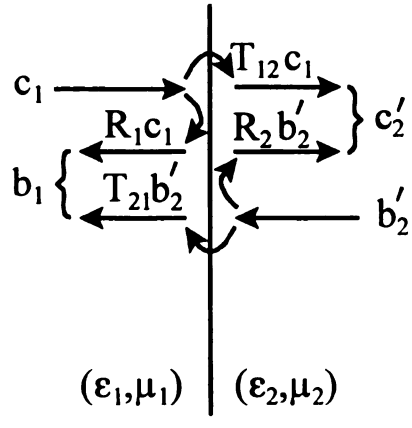

Figure 2.2 Reflected and transmitted waves at a planar interface.

If R_1, T_{12} and R_2, T_{21} are the respective interfacial reflection and transmission coefficients experienced by waves c_1 and b_2', then the following relations prevail

$$\begin{aligned} c_2' &= T_{12}c_1 + R_2 b_2' \\ b_1 &= R_1 c_1 + T_{21} b_2' \end{aligned} \quad \Rightarrow \quad \begin{aligned} c_1 &= \frac{1}{T_{12}} c_2' - \frac{R_2}{T_{12}} b_2' \\ b_1 &= \frac{R_1}{T_{12}} c_2' + \frac{T_{12}T_{21} - R_1 R_2}{T_{12}} b_2' \end{aligned} \tag{2.27}$$

where (using continuity of the tangential electric and magnetic fields)

$$R_1 = -R_2 = \frac{Z_2 - Z_1}{Z_2 + Z_1} \ , \ T_{12} = 1 + R_1 \ , \ T_{21} = 1 + R_2 = 1 - R_1 \tag{2.28}$$

Substitution of (2.28) into (2.27) leads to the matrix expression

$$\begin{bmatrix} c_1 \\ b_1 \end{bmatrix} = \frac{1}{T_{12}} \begin{bmatrix} 1 & R_1 \\ R_1 & 1 \end{bmatrix} \begin{bmatrix} c_2' \\ b_2' \end{bmatrix} \tag{2.29}$$

Thus, (2.29) describes the relationship between the forward and reverse traveling waves (c_1, b_1) immediately to the left of the interface to the forward and reverse traveling waves (c_2', b_2') immediately to the right of the interface.

Before considering the cascade connection of N sections, it must be shown how the waves (c_2', b_2') are related to waves (c_2, b_2) that are located a distance ℓ from the interface as depicted in Figure 2.3. Since the region is assumed to be linear, homogeneous and isotropic, a simple relationship exists between the waves, namely $c_2 = c_2' e^{-\gamma_2 \ell}$ and $b_2' = b_2 e^{-\gamma_2 \ell}$. Therefore, the relationship between (c_2', b_2') and (c_2, b_2) can be written

$$\begin{aligned} c_2' &= c_2 e^{\gamma_2 \ell} \\ b_2' &= b_2 e^{-\gamma_2 \ell} \end{aligned} \quad \Rightarrow \quad \begin{bmatrix} c_2' \\ b_2' \end{bmatrix} = \begin{bmatrix} e^{\gamma_2 \ell} & 0 \\ 0 & e^{-\gamma_2 \ell} \end{bmatrix} \begin{bmatrix} c_2 \\ b_2 \end{bmatrix} \tag{2.30}$$

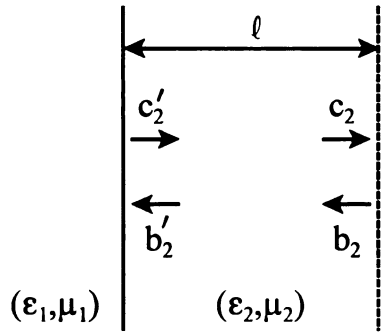

Figure 2.3 Wave description for shift of distance ℓ.

The A-parameter relationship between waves (c_1, b_1) and (c_2, b_2) is obtained by substituting (2.30) into (2.29), leading to

$$\begin{bmatrix} c_1 \\ b_1 \end{bmatrix} = \frac{1}{T_{12}} \begin{bmatrix} e^{\gamma_2 \ell} & R_1 e^{-\gamma_2 \ell} \\ R_1 e^{\gamma_2 \ell} & e^{-\gamma_2 \ell} \end{bmatrix} \begin{bmatrix} c_2 \\ b_2 \end{bmatrix} = \begin{bmatrix} A_{11} & A_{12} \\ A_{21} & A_{22} \end{bmatrix} \begin{bmatrix} c_2 \\ b_2 \end{bmatrix} \tag{2.31}$$

The overall A-parameter description of the multi-layered system of Figure 2.1 can now be obtained by generalizing (2.31), leading to the desired result

$$\begin{bmatrix} c_1 \\ b_1 \end{bmatrix} = \prod_{i=1}^{N+1} \frac{1}{T_i} \begin{bmatrix} e^{\gamma_i \ell_i} & R_i e^{-\gamma_i \ell_i} \\ R_i e^{\gamma_i \ell_i} & e^{-\gamma_i \ell_i} \end{bmatrix} \begin{bmatrix} c_{N+2} \\ b_{N+2} \end{bmatrix} = \begin{bmatrix} A_{11}^{sys} & A_{12}^{sys} \\ A_{21}^{sys} & A_{22}^{sys} \end{bmatrix} \begin{bmatrix} c_{N+2} \\ b_{N+2} \end{bmatrix} \tag{2.32}$$

$$\begin{bmatrix} A_{11}^{sys} & A_{12}^{sys} \\ A_{21}^{sys} & A_{22}^{sys} \end{bmatrix} = \prod_{i=1}^{N+1} \frac{1}{T_i} \begin{bmatrix} e^{\gamma_i \ell_i} & R_i e^{-\gamma_i \ell_i} \\ R_i e^{\gamma_i \ell_i} & e^{-\gamma_i \ell_i} \end{bmatrix} = \prod_{i=1}^{N+1} \begin{bmatrix} A_{11}^{i} & A_{12}^{i} \\ A_{21}^{i} & A_{22}^{i} \end{bmatrix} \tag{2.33}$$

where

$$R_i = \frac{Z_i - Z_{i-1}}{Z_i + Z_{i-1}} \quad , \quad T_i = 1 + R_i \tag{2.34}$$

Note that the upper limit on the product is $N+1$ since there are $N+1$ interfaces and because the relationship between (c_1, b_1) and (c_{N+2}, b_{N+2}) is desired.

As an example, consider a single-layered sample of length ℓ immersed in free space. Since there will be two interfaces, equation (2.32) specializes to

$$\begin{bmatrix} c_1 \\ b_1 \end{bmatrix} = \prod_{i=1}^{2} \frac{1}{T_i} \begin{bmatrix} e^{\gamma_i \ell_i} & R_i e^{-\gamma_i \ell_i} \\ R_i e^{\gamma_i \ell_i} & e^{-\gamma_i \ell_i} \end{bmatrix} \begin{bmatrix} c_3 \\ b_3 \end{bmatrix} = \begin{bmatrix} A_{11} & A_{12} \\ A_{21} & A_{22} \end{bmatrix} \begin{bmatrix} c_3 \\ b_3 \end{bmatrix} \tag{2.35}$$

where $R_1 = -R_2 = R$, $T_1 = 1+R$, $T_2 = 1-R$, $\gamma_1 = \gamma$, $\gamma_2 = \gamma_0$, $\ell_1 = \ell$ and $\ell_2 = 0$. The wave matrix for the system is therefore

$$\begin{bmatrix} A_{11} & A_{12} \\ A_{21} & A_{22} \end{bmatrix} = \frac{1}{1+R} \begin{bmatrix} e^{\gamma \ell} & R e^{-\gamma \ell} \\ R e^{\gamma \ell} & e^{-\gamma \ell} \end{bmatrix} \frac{1}{1-R} \begin{bmatrix} 1 & -R \\ -R & 1 \end{bmatrix} \tag{2.36}$$

Carrying out the matrix multiplication and letting $P = e^{-\gamma \ell}$ leads to the following A-parameters for a single-layered sample

$$\begin{bmatrix} A_{11} & A_{12} \\ A_{21} & A_{22} \end{bmatrix} = \frac{1}{P(1-R^2)} \begin{bmatrix} 1-R^2P^2 & -R(1-P^2) \\ R(1-P^2) & P^2-R^2 \end{bmatrix} \tag{2.37}$$

The S-parameters of the above single-layered sample can be obtained by using the well-known relations [3]

$$\begin{bmatrix} S_{11} & S_{12} \\ S_{21} & S_{22} \end{bmatrix} = \frac{1}{A_{11}} \begin{bmatrix} A_{21} & A_{11}A_{22} - A_{21}A_{12} \\ 1 & -A_{12} \end{bmatrix} \tag{2.38}$$

$$\begin{bmatrix} A_{11} & A_{12} \\ A_{21} & A_{22} \end{bmatrix} = \frac{1}{S_{21}} \begin{bmatrix} 1 & -S_{22} \\ S_{11} & S_{21}S_{12} - S_{11}S_{22} \end{bmatrix} \tag{2.39}$$

Although (2.39) is not required here, it has been given for the sake of completeness. Substituting (2.37) into (2.38) produces the familiar result

$$S_{11} = S_{22} = \frac{R(1-P^2)}{1-R^2P^2} \quad , \quad S_{21} = S_{12} = \frac{P(1-R^2)}{1-R^2P^2} \tag{2.40}$$

The direct and deembed methods will now be discussed.

2.5 Direct Method of Constitutive Parameter Extraction

The direct method is one scheme for determining the constitutive parameters of an unknown layer immersed in a multi-layered system. The overall procedure for the direct method is as follows. First, a guess for the permittivity and permeability of the unknown layer is provided. Next, the theoretical A-parameters of the known/unknown layers are calculated and the overall system wave matrix is determined using (2.33), that is

$$\varepsilon_i, \mu_i, \ell_i \rightarrow \left[A^i\right] \quad , \quad \left[A_{sys}^{thy}\right] = \prod_{i=1}^{N+1} \left[A^i\right] \tag{2.41}$$

Note that the permittivity and permeability of layers 0 and $N+1$ are (ε_0, μ_0) and the length of the $N+1$ layer is $\ell_{N+1} = 0$. The theoretical A-parameters of the system are then converted into the theoretical S-parameters of the system using (2.38), namely

$$\left[A_{sys}^{thy}\right] \rightarrow \left[S_{sys}^{thy}\right] \tag{2.42}$$

The theoretical S-parameters of the system are then compared to the experimentally measured system S-parameters using the relations

$$\left.\begin{aligned} S_{11,sys}^{thy}(\omega, \varepsilon, \mu) - S_{11,sys}^{exp}(\omega) = 0 \\ S_{21,sys}^{thy}(\omega, \varepsilon, \mu) - S_{21,sys}^{exp}(\omega) = 0 \end{aligned}\right\} \Rightarrow \varepsilon_f, \mu_f \tag{2.43}$$

for the forward direction and, independently,

$$\left.\begin{aligned} S_{22,sys}^{thy}(\omega,\varepsilon,\mu) - S_{22,sys}^{exp}(\omega) = 0 \\ S_{12,sys}^{thy}(\omega,\varepsilon,\mu) - S_{12,sys}^{exp}(\omega) = 0 \end{aligned}\right\} \Rightarrow \quad \varepsilon_r, \mu_r \tag{2.44}$$

for the reverse direction. The permittivity and permeability values for the forward direction and reverse direction are numerically iterated until conditions (2.43) and (2.44) are satisfied. If the unknown layer is non-magnetic, then the following forward and reverse relations are used

$$\left. S_{11,sys}^{thy}(\omega,\varepsilon) - S_{11,sys}^{exp}(\omega) = 0 \;\; or \;\; S_{21,sys}^{thy}(\omega,\varepsilon) - S_{21,sys}^{exp}(\omega) = 0 \right\} \Rightarrow \quad \varepsilon_f \tag{2.45}$$

$$\left. S_{22,sys}^{thy}(\omega,\varepsilon) - S_{22,sys}^{exp}(\omega) = 0 \;\; or \;\; S_{12,sys}^{thy}(\omega,\varepsilon) - S_{12,sys}^{exp}(\omega) = 0 \right\} \Rightarrow \quad \varepsilon_r \tag{2.46}$$

Comments regarding the advantage/disadvantage of the direct method will be delayed until the deembed method has been discussed.

2.6 Deembed Method of Constitutive Parameter Extraction

2.6.1 Modification of A-Parameters for Deembedding

In the deembed method, the constitutive parameters of the unknown layer are extracted by first mathematically removing the known layers until only the unknown single layer is remaining. The NRW procedure is then invoked and (ε,μ) are analytically computed. Since the NRW technique assumes that free space exists on either side of the single-layered sample, the multi-layered system must be mathematically viewed as having infinitesimal artificial air layers on either side of the unknown layer. These zero-length air layers will be introduced between all layers, however, since this is computationally easier to implement. Note that because the A and S-parameters are based on tangential fields, the validity of the above procedure is provided by continuity

of the tangential electric and magnetic field components. The artificial air layers are shown in Figure 2.4.

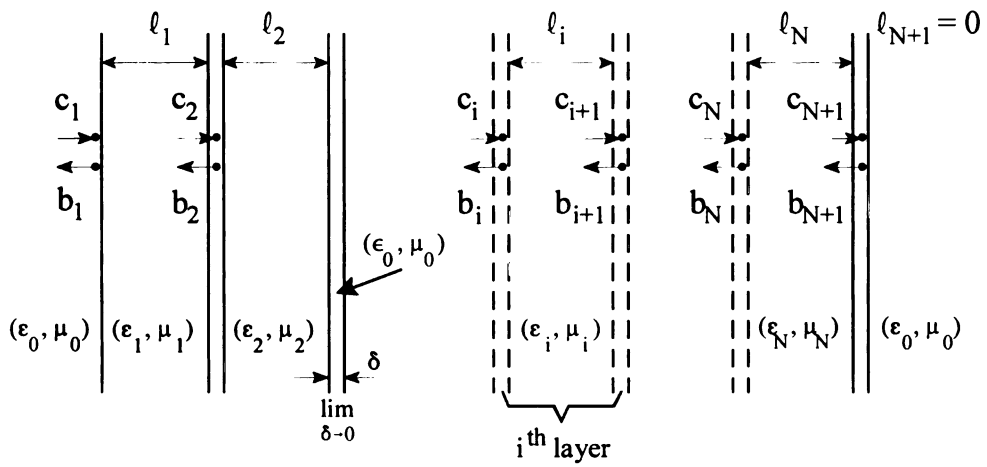

Figure 2.4 Introduction of zero-length air layers for deembedding.

Previously, the A-parameters of the i^{th} layer described the relationship between the waves (c_i, b_i) immediately to the left of the i^{th} interface to the waves (c_{i+1}, b_{i+1}) immediately to the left of the $i+1$ interface. In the deembed technique, the waves (c_i, b_i) immediately to the left of the i^{th} interface must be related to the waves (c_{i+1}, b_{i+1}) immediately to the right of the $i+1$ interface. This A-parameter modification is easily accomplished using the result of equation (2.33), leading to

$$\left[\tilde{A}^i\right] = \lim_{\delta \to 0} \frac{1}{1+R_i} \begin{bmatrix} e^{\gamma_i \ell_i} & R_i e^{-\gamma_i \ell_i} \\ R_i e^{\gamma_i \ell_i} & e^{-\gamma_i \ell_i} \end{bmatrix} \frac{1}{1-R_i} \begin{bmatrix} e^{\gamma_0 \delta} & -R_i e^{-\gamma_0 \delta} \\ -R_i e^{\gamma_0 \delta} & e^{-\gamma_0 \delta} \end{bmatrix} \tag{2.47}$$

where the interfacial reflection coefficient between layer i and the infinitesimally thin air

layer is

$$R_i = \frac{Z_i - Z_0}{Z_i + Z_0} \tag{2.48}$$

Taking the limit in (2.47) produces the following appropriate A-parameter modification for the deembed scheme

$$\left[\tilde{A}^i\right] = \frac{1}{P_i(1-R_i^2)} \begin{bmatrix} 1-R_i^2P_i^2 & -R_i(1-P_i^2) \\ R_i(1-P_i^2) & P_i^2-R_i^2 \end{bmatrix} \tag{2.49}$$

where

$$P_i = e^{-\gamma_i \ell_i} \tag{2.50}$$

is the one-way propagation delay and attenuation within the i^{th} layer. This result should have been anticipated from (2.37).

2.6.2 Deembed Procedure for Constitutive Parameter Extraction

The deembed method for material characterization is accomplished through the following procedure. First, the A-parameters of each known layer are computed using (2.49), that is

$$\varepsilon_i, \mu_i, \ell_i \rightarrow \left[A^i\right] \quad ...i \neq u \tag{2.51}$$

where the tilde notation has been dropped for convenience. Note that the A-parameters of the unknown material, which will be designated as layer u, cannot be computed. The experimentally measured S-parameters of the system are then converted into A-parameters using (2.39), namely

$$\left[S_{sys}^{exp}\right] \rightarrow \left[A_{sys}^{exp}\right] \tag{2.52}$$

Next, the unknown layer of the system is isolated by mathematically removing the known layers using the following inverse matrix multiplication

$$\begin{aligned} \left[A_{sys}^{exp}\right] &= \prod_{i=1}^{N}\left[A^{i}\right] = \left[A^{1}\right]\cdots\left[A^{u-1}\right]\left[A_{u}^{exp}\right]\left[A^{u+1}\right]\cdots\left[A^{N}\right] \\ \therefore\ \left[A_{u}^{exp}\right] &= \left(\prod_{i=u-1}^{1}\left[A^{i}\right]^{-1}\right)\left[A_{sys}^{exp}\right]\left(\prod_{i=N}^{u+1}\left[A^{i}\right]^{-1}\right) \end{aligned} \tag{2.53}$$

where N (not $N+1$) must be used due to the modified A-parameter formulation. The experimental S-parameters of the unknown layer are obtained from (2.53) with the aid of (2.38), that is

$$\left[A_{u}^{exp}\right] \rightarrow \left[S_{u}^{exp}\right] \tag{2.54}$$

As a final step, the permittivity and permeability of the unknown layer can be computed analytically (if both ε and μ are desired) or numerically (if the unknown is non-magnetic) using the knowledge of section 2.2.

2.7 General Comments and Experimental Results

2.7.1 General Comments

Now that both methods of parameter extraction have been discussed, several comments are in order. First, the method of using A-parameters for layered media is exceedingly powerful since it is valid for both TEM and TE_{10} field applicator systems. Thus, the techniques discussed in sections 2.5 and 2.6 are applicable for the commonly used coaxial, free-field, stripline and rectangular waveguide systems. The second comment is in regards to how the A-parameters were defined and referenced for the entire multi-layered system. In both extraction schemes, we were ultimately interested in obtaining an overall relationship between the forward and reverse waves immediately to

the left of the first layer and the forward and reverse waves immediately to the right of the last layer. The reason we are interested in the wave amplitudes outside the multi-layered structure is that this is where the S-parameters are accessible via measurement. Another comment is that the direct method requires an initial guess for the permittivity and permeability, whereas the deembed method does not. This can be a drawback since numerical root-search algorithm's are typically very sensitive to initial guesses. However, it will be demonstrated that the direct method must be used if sample homogeneity is to be accurately monitored. One suggestion would be to invoke the deembed method to analytically obtain an initial guess and then utilize it for implementation of the direct method. The final comment is that if the known and unknown layers are perfectly homogeneous, then the two techniques should yield identical results. In the industry environment though, samples are rarely perfectly homogeneous and thus the direct method should be exploited.

2.7.2 Experimental Results

One experimental result to discuss is the verification of the multi-layered analysis using a rectangular waveguide field applicator. Consider a non-magnetic Alumina sample having a thickness $\ell = .25$ inches. Figures 2.5 and 2.6 show the permittivity computations (real and imaginary based on S_{21} only) for the sample when it is measured independently, that is, the stand-alone measurement. Next, a multi-layered system is formed by inserting the Alumina sample between a non-magnetic piece of Teflon and Zirconium Oxide (Z_rO_2). Thus, the three-layered system has Teflon as its first layer, Alumina as the second layer (treated as the unknown) and Z_rO_2 as the third layer. It will

be assumed, from previous measurements, that the known properties for Teflon and Z_rO_2 are $\varepsilon_r^{tef} = 2.09 - j0.001$, $\ell_{tef} = 0.126 in.$ and $\varepsilon_r^{Z_r} = 3.81 - j0.015$, $\ell_{Z_r} = .114 in.$, respectively. Figures 2.5 and 2.6 show the extracted permittivity values for the Alumina layer if the direct method is used (based on S_{21} only). In addition, the uncorrected values for the Alumina layer are also shown when the known layers are ignored. It is evident that the direct method does indeed accurately account for the layered environment. The results are erroneous if the extraction method is not utilized. For example, Figure 2.6 falsely shows that the Alumina sample is highly lossy when the Teflon and Z_rO_2 layers are blatantly ignored.

The other significant result to discuss is the advantage that the direct method has over the deembed method for monitoring sample homogeneity. Suppose we construct a two-layer system using the above mentioned Teflon, Z_rO_2 and Alumina materials. Layer *1* will consist of the Teflon and Z_rO_2 samples and will be treated as the unknown layer. Layer *2* is comprised of the Alumina sample and will be assumed to have the known properties $\varepsilon_r = 9.65$, $\ell = .25 in.$ Layer *1* has been made inhomogeneous on purpose to see whether both techniques can detect this inhomogeneity. Figures 2.7 and 2.8 show the results of the direct method of parameter extraction for the real and imaginary parts of the computed permittivity based on S_{11} (for the forward direction) and S_{22} (for the reverse direction). Similarly, Figures 2.9 and 2.10 show the results of the deembed method of parameter extraction. The direct method clearly reveals that the unknown layer must be inhomogeneous since the S_{11} (forward) and S_{22} (reverse) measurements are drastically different. In comparison, the deembed method shows

virtually no difference between forward and reverse measurements, even though it is known that layer *1* was intentionally made inhomogeneous. Thus, although the direct method requires an initial guess, it has a clear advantage over the deembed method for detecting sample inhomogeneities. It should be noted that this issue of monitoring for sample inhomogeneity is important in the industry environment since it frequently occurs due to the limitations of the various methods of sample preparation.

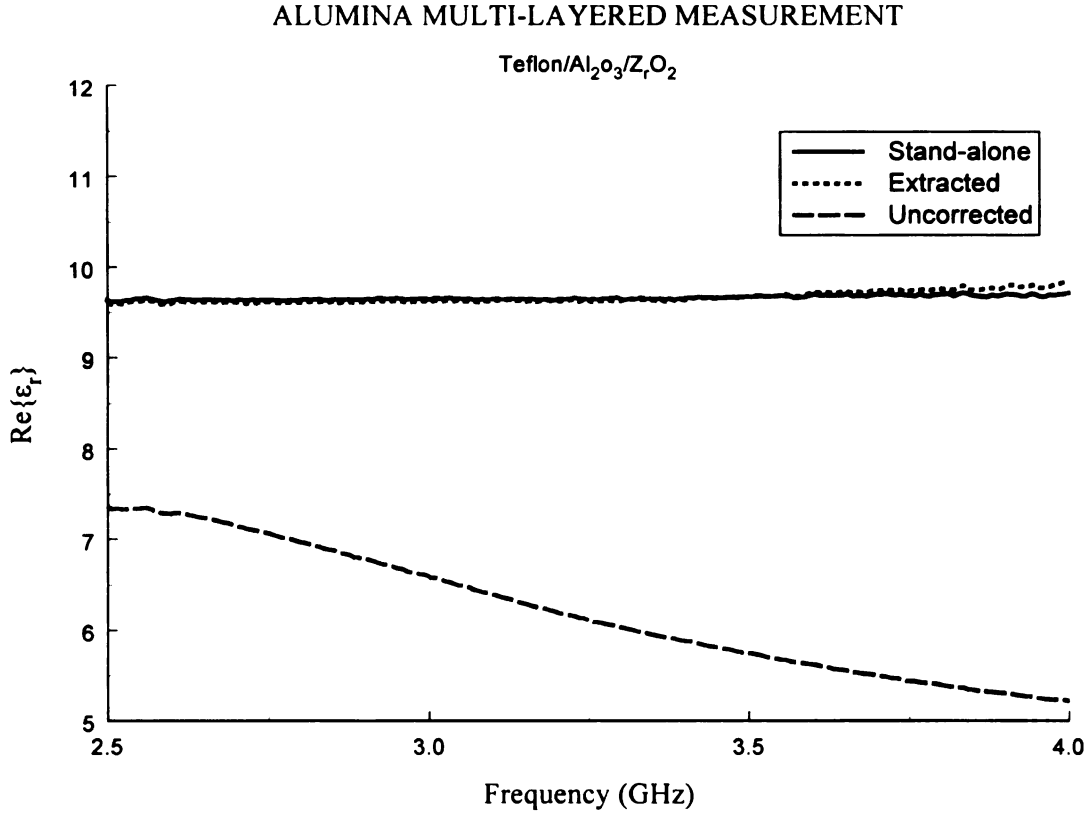

Figure 2.5 Verification of layered analysis for $\mathrm{Re}\{\varepsilon_r\}$ using an Alumina sample.

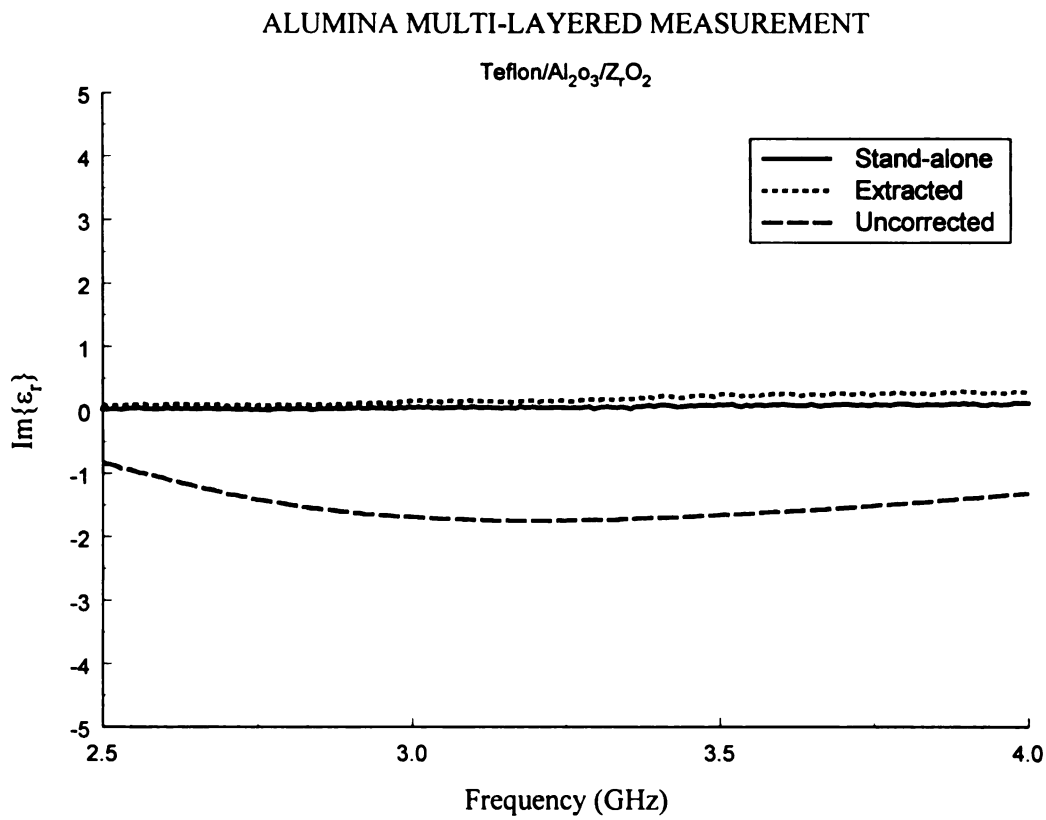

Figure 2.6 Verification of layered analysis for $\mathrm{Im}\{\varepsilon_r\}$ using an Alumina sample.

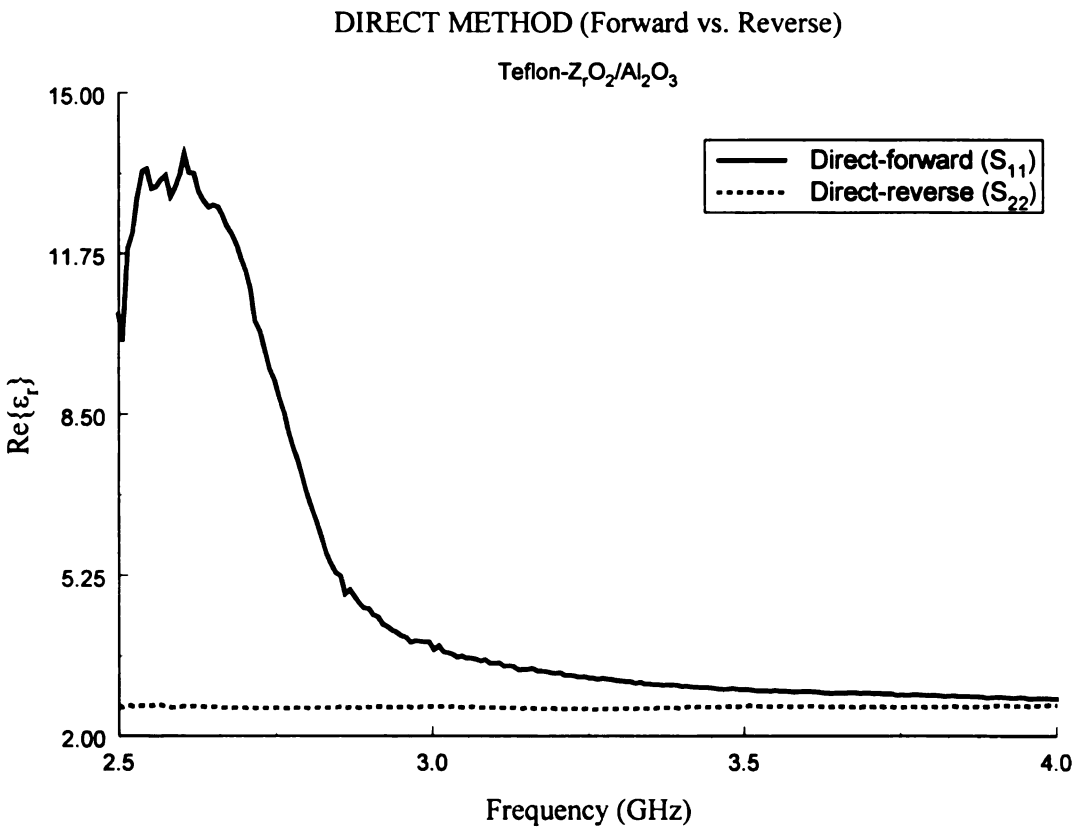

Figure 2.7 Homogeneity interrogation of $\mathrm{Re}\{\varepsilon_r\}$ via direct method.

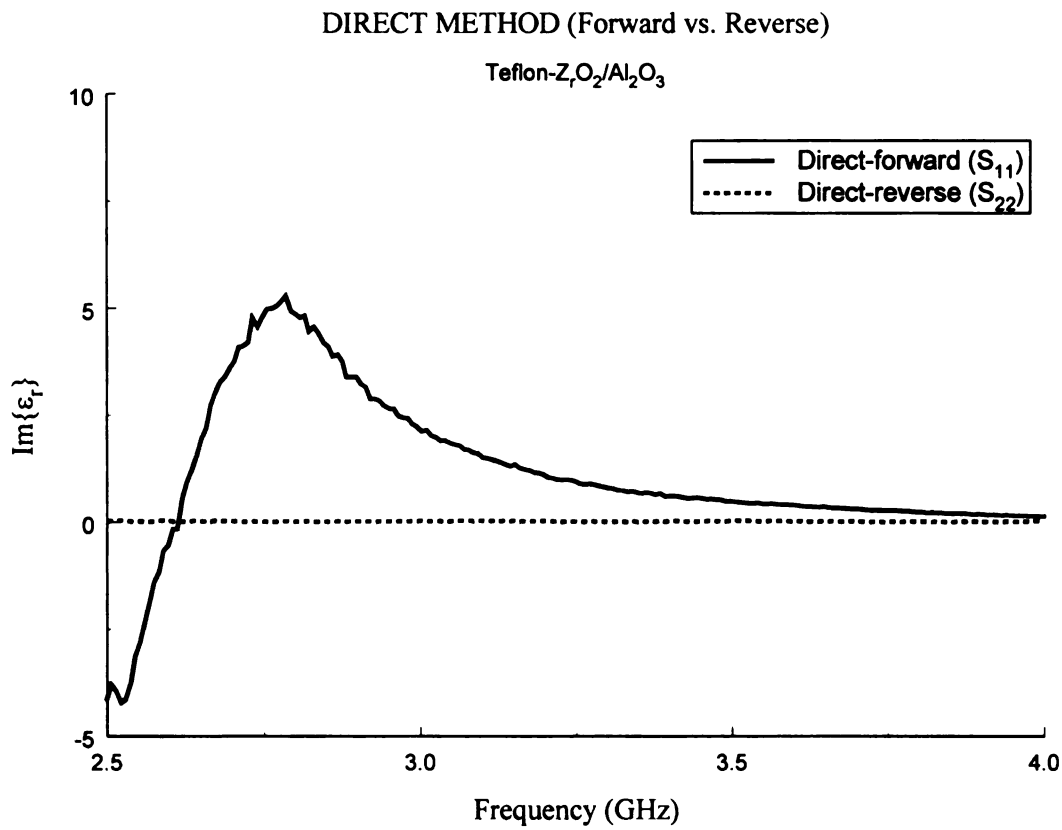

Figure 2.8 Homogeneity interrogation of $\mathrm{Im}\{\varepsilon_r\}$ via direct method.

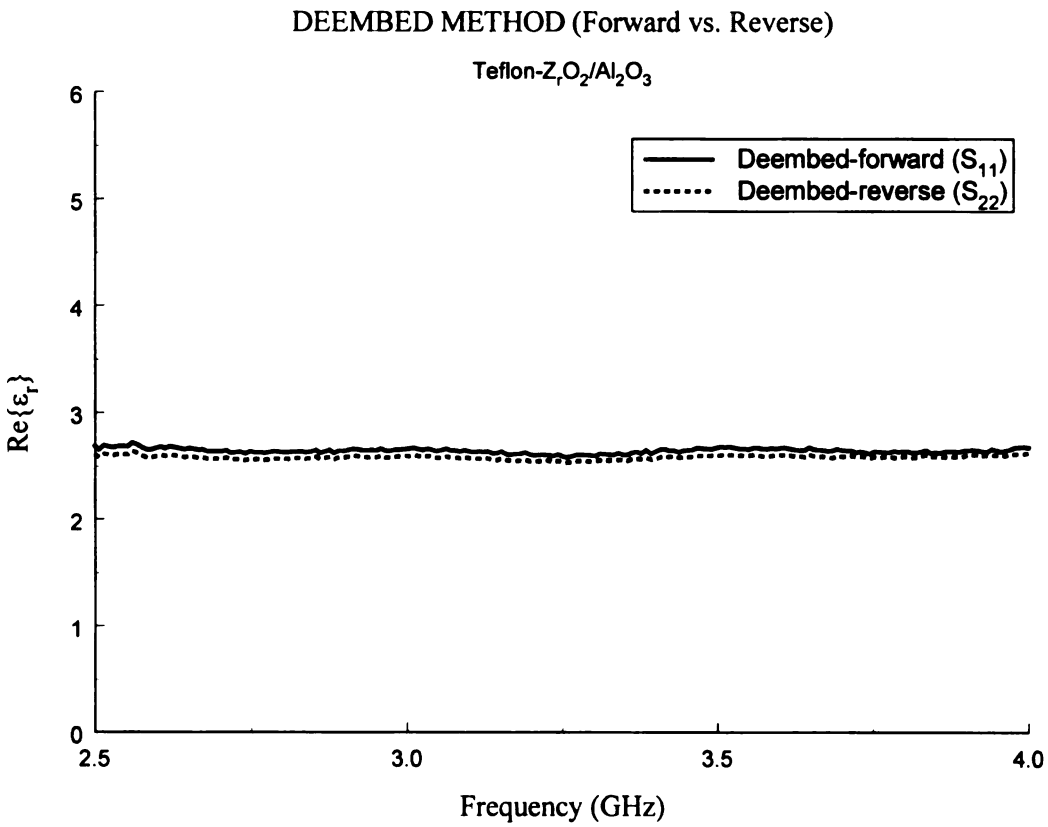

Figure 2.9 Homogeneity interrogation of $\mathrm{Re}\{\varepsilon_r\}$ via deembed method.

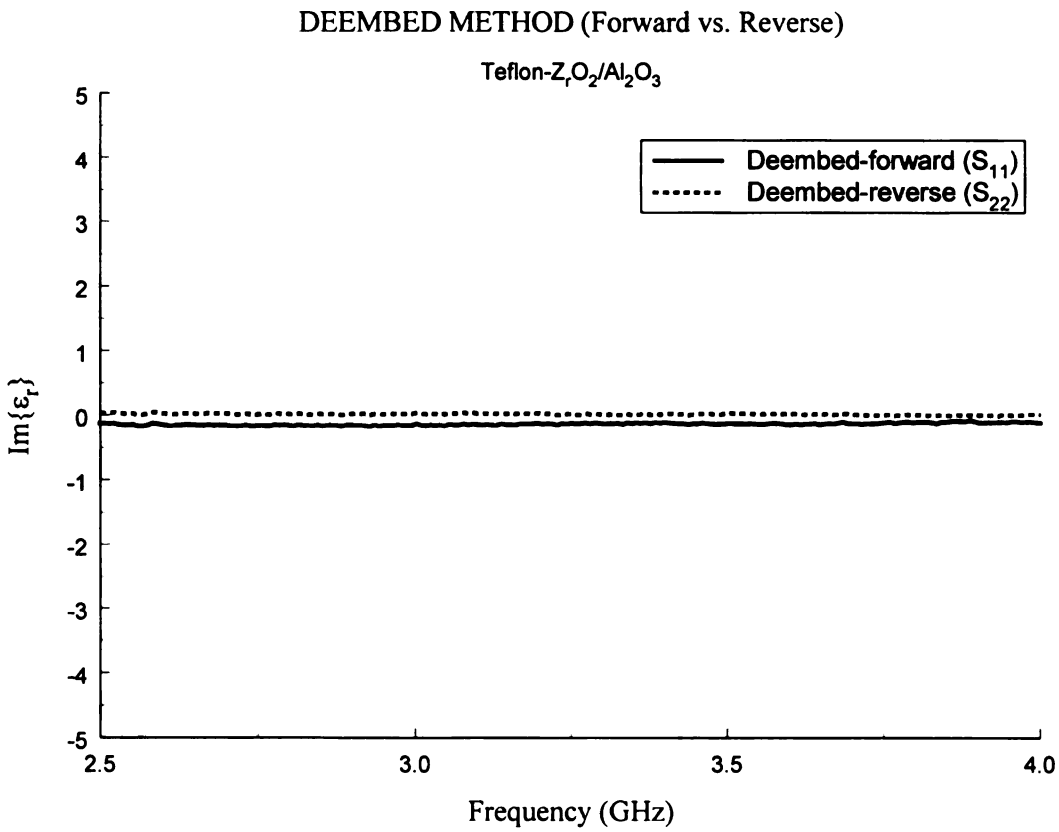

Figure 2.10 Homogeneity interrogation of $\mathrm{Im}\{\varepsilon_r\}$ via deembed method.

Chapter 3

ANALYSIS OF SAMPLE-TO-WALL GAPS IN RECTANGULAR WAVEGUIDE MATERIAL CHARACTERIZATION MEASUREMENTS

3.1 Introduction

In rectangular waveguide material characterization measurements, gaps commonly occur between the sample and waveguide walls as a result of imprecise machining of the sample. These gaps are exacerbated in high temperature measurements due to the differing thermal rates of expansion for the waveguide and sample materials. These gaps can influence the accuracy of measured constitutive parameters because higher order modes are excited, resulting in a shift of the ideal TE_{10} mode propagation constant and changes in the ideal wave impedance and interfacial reflection and transmission coefficients.

Sample-to-wall gaps will be analyzed in this chapter by regarding the waveguide as inhomogeneously filled in the cross-sectional plane with *LSM* and *LSE* propagation modes supported in the sample/gap region [3]. The longitudinal section magnetic (*LSM*) modes accommodate bottom/top gap geometries, whereas longitudinal section electric (*LSE*) modes accommodate left/right sample-to-wall gaps. Characteristic equations for the corresponding propagation constants will be derived and solved numerically to determine shifts from the ideal TE_{10} propagation constant of a uniformly-filled guide. A modal analysis is utilized to obtain (under small gap conditions) approximate expressions for the wave impedance and interfacial reflection and

transmission coefficients. This is done by considering a single TE_{10} mode incident upon, and reflected from, the sample and only a single LSM or LSE mode inside the sample region. Approximate expressions for the scattering parameters are also obtained using wave matrices. Theoretical and experimental results will be given and discussed.

3.2 Review of a Uniformly-Filled Rectangular Waveguide

Consider a rectangular waveguide, having width a and height b, operating in its principal TE_{10} mode and uniformly filled in the cross-sectional dimensions by a planar sample having thickness ℓ (it is assumed that the sample is linear, homogeneous and isotropic). If the scattering parameters S_{11}^{exp} and S_{21}^{exp} are experimentally measured, then the following scheme is utilized for computing the relative permittivity and permeability (ε_r, μ_r) of the sample. First, an initial guess for ε_r and μ_r is provided. Next, the propagation constants in the free-space (γ_0) and sample regions (γ) are computed using

$$\gamma_0 = \sqrt{k_c^2 - k_0^2} \quad , \quad \gamma = \sqrt{k_c^2 - k^2} \tag{3.1}$$

where

$$k_0 = \omega\sqrt{\varepsilon_0\mu_0} = \frac{\omega}{c} \quad , \quad k = k_0\sqrt{\varepsilon_r\mu_r} \quad , \quad k_c = \frac{\pi}{a} \tag{3.2}$$

The wave impedance in the free-space (Z_0) and sample regions (Z) are determined next, followed by the interfacial reflection coefficient (R) and one-way phase delay and attenuation term (P)

$$Z_0 = \frac{j\omega\mu_0}{\gamma_0} \quad , \quad Z = \frac{j\omega\mu_0\mu_r}{\gamma} \tag{3.3}$$

$$R = \frac{Z - Z_0}{Z + Z_0} \quad , \quad P = e^{-\gamma \ell} \tag{3.4}$$

The final step is to calculate the theoretical S-parameters and compare them with the experimentally measured values, that is

$$S_{11}^{thy} = \frac{R(1-P^2)}{1-R^2P^2} \quad , \quad S_{21}^{thy} = \frac{P(1-R^2)}{1-R^2P^2} \tag{3.5}$$

$$\begin{aligned} S_{11}^{thy}(\omega, \varepsilon_r, \mu_r) - S_{11}^{exp}(\omega) = 0 \\ S_{21}^{thy}(\omega, \varepsilon_r, \mu_r) - S_{21}^{exp}(\omega) = 0 \end{aligned} \tag{3.6}$$

The parameters ε_r and μ_r are iterated using a two-dimensional root search algorithm (such as Newton's method) until (3.6) is satisfied within the desired/specified accuracy. If the sample is non-magnetic, then $\mu_r = 1$ and ε_r can be computed using the following

$$S_{11}^{thy}(\omega, \varepsilon_r) - S_{11}^{exp}(\omega) = 0 \quad or \quad S_{21}^{thy}(\omega, \varepsilon_r) - S_{21}^{exp}(\omega) = 0 \tag{3.7}$$

The procedure for computing ε_r and μ_r when gaps are accommodated is similar except that the expressions for γ, Z, R and P must be modified (as will be demonstrated).

3.3 LSM Mode Analysis for Bottom/Top Gaps

3.3.1 Geometry

The geometry for the bottom/top gap analysis is depicted in Figure 3.1. The spacing of the bottom gap in region 1 is d_1 and the spacing of the top gap in region 3 is d_2. Both gap regions are assumed to have constitutive parameters (ε_0, μ_0). The height of the sample in region 2 is t_1 and has constitutive parameters (ε_r, μ_r). The width and height of the rectangular waveguide are a and b, respectively. The thickness of the sample along the z-axis is ℓ. The waveguide walls are assumed to be perfectly

conducting.

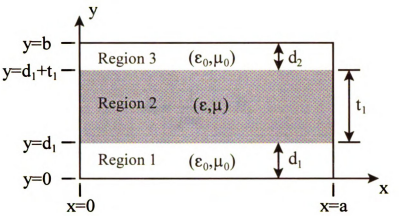

Figure 3.1 Cross-sectional geometry for bottom/top gap analysis.

3.3.2 Hertzian Potential Generating Function and EM Field Components

An electric-type Hertz potential having only a $\hat{y}$-component is sufficient to generate all EM field components (i.e., *LSM* modes) necessary for satisfying boundary conditions, that is

$$\vec{\pi}_i^e = \hat{y}\pi_{iy}^e(x,y)e^{-\gamma_{lsm}z} = \hat{y}f_i(x)g_i(y)e^{-\gamma_{lsm}z} \tag{3.8}$$

for a forward traveling wave in the i^{th} region, where it is assumed that propagation is along the z-axis. Note that this particular choice is justified by the uniqueness theorem. Also, it is common knowledge [3] that the propagation constant γ_{lsm} in each region must be identical, thus having a subscript i on γ_{lsm} is not required). Since it is assumed that no sources exist in the sample or gap regions, the electric-type Hertz potential satisfies the source-free Helmholtz wave equation

$$\nabla^2\vec{\pi}_i^e + k_i^2\vec{\pi}_i^e = 0 \tag{3.9}$$

where $k_1 = k_3 = k_0$ and $k_2 = k$. The EM field components satisfy the well-known relations (see Appendix A for details)

$$\vec{H}_i = j\omega\varepsilon_i \nabla \times \vec{\pi}_i^e \tag{3.10}$$

$$\vec{E}_i = \frac{1}{j\omega\varepsilon_i} \nabla \times \vec{H}_i \tag{3.11}$$

Substitution of (3.8) into (3.10) and (3.11) leads to the following field components

$$\vec{H}_i = j\omega\varepsilon_i \left[\hat{x}\gamma_{lsm} f_i(x) + \hat{z} \frac{\partial f_i(x)}{\partial x} \right] g_i(y) e^{-\gamma_{lsm} z} \tag{3.12}$$

$$\begin{aligned} \vec{E}_i = \Bigg\{ & \hat{x} \frac{\partial f_i(x)}{\partial x} \frac{\partial g_i(y)}{\partial y} - \hat{y} \left[\frac{\partial^2 f_i(x)}{\partial x^2} + \gamma_{lsm}^2 f_i(x) \right] g_i(y) \\ & - \hat{z}\gamma_{lsm} f_i(x) \frac{\partial g_i(y)}{\partial y} \Bigg\} e^{-\gamma_{lsm} z} \end{aligned} \tag{3.13}$$

Note, equation (3.12) reveals that $\vec{H}$ only has components in the longitudinal $x-z$ plane, hence the *LSM* terminology. The above wave equation and field components are utilized in the development of the characteristic equation for propagation constant γ_{lsm} in the next section.

3.3.3 Identification of the *LSM* Mode Characteristic Equation for γ_{lsm}

The *LSM* mode characteristic equation for γ_{lsm} can be identified by solving the wave equation in the gap and sample regions and enforcing boundary conditions at the waveguide walls and air/dielectric interfaces. Substitution of (3.8) into (3.9) and dividing by $f_i(x)g_i(y)e^{-\gamma_{lsm} z}$ leads to the familiar separation of variables result

$$\frac{1}{f_i(x)}\frac{\partial^2 f_i(x)}{\partial x^2}+\frac{1}{g_i(y)}\frac{\partial^2 g_i(y)}{\partial y^2}=-(\gamma_{lsm}^2+k_i^2) \tag{3.14}$$

Equation (3.14) can only be satisfied if the first and second terms are constants, that is

$$\frac{1}{f_i(x)}\frac{\partial^2 f_i(x)}{\partial x^2}=-k_{ix}^2 \tag{3.15}$$

$$\frac{1}{g_i(y)}\frac{\partial^2 g_i(y)}{\partial y^2}=-k_{iy}^2 \tag{3.16}$$

where the constraint equation is

$$k_{ix}^2+k_{iy}^2=\gamma_{lsm}^2+k_i^2 \tag{3.17}$$

Equations (3.15) and (3.16) are ordinary differential equations which have the following well-known solutions

$$f_i(x)=A_i\sin k_{ix}x+B_i\cos k_{ix}x \tag{3.18}$$

$$g_i(y)=C_i\sin k_{iy}y+D_i\cos k_{iy}y \tag{3.19}$$

It will be shown that $f_i(x)$ is identical in each region but $g_i(y)$ is not. Therefore, it is mathematically convenient to introduce appropriate shift factors in the definition of $g_i(y)$ as follows

$$g_1(y)=C_1\sin hy+D_1\cos hy \quad ...0<y<d_1 \tag{3.20}$$

$$g_2(y)=C_2\sin l(y-d_1)+D_2\cos l(y-d_1) \quad ...d_1<y<d_1+t_1 \tag{3.21}$$

$$g_3(y)=C_3\sin h(b-y)+D_3\cos h(b-y) \quad ...d_1+t_1<y<b \tag{3.22}$$

where the wavenumbers along the y direction are

$$k_{1y}=k_{3y}=h \quad , \quad k_{2y}=l \tag{3.23}$$

Boundary conditions on $\vec{E}$ and $\vec{H}$ can now be implemented with the aid of (3.12)

and (3.13). The tangential electric field at $x = 0, a$ (for all y, z) must be zero, thus

$$E_{i\alpha}(0, y, z) = 0 \ , \ E_{i\alpha}(a, y, z) = 0 \ \ldots \alpha = y, z \tag{3.24}$$

Substitution of (3.13) into (3.24) produces the following condition

$$f_i(x)\big|_{x=0,a} = 0 \tag{3.25}$$

The tangential electric field at $y = 0, b$ (for all x, z) must be zero, that is

$$E_{1\alpha}(x, 0, z) = 0 \ , \ E_{3\alpha}(x, b, z) = 0 \ \ldots \alpha = x, z \tag{3.26}$$

Substitution of (3.13) into (3.26) results in the general relations

$$\left.\frac{\partial g_1(y)}{\partial y}\right|_{y=0} = 0 \quad , \quad \left.\frac{\partial g_3(y)}{\partial y}\right|_{y=b} = 0 \tag{3.27}$$

The tangential electric field must be continuous at $y = d_1, d_1 + t_1$ (for all x, z), thus

$$E_{1\alpha}(x, d_1, z) = E_{2\alpha}(x, d_1, z) \ , \ E_{2\alpha}(x, d_1 + t_1, z) = E_{3\alpha}(x, d_1 + t_1, z) \ \ldots \alpha = x, z \tag{3.28}$$

Inserting (3.13) into (3.28) produces the following

$$\left.\frac{\partial g_1(y)}{\partial y}\right|_{y=d_1} = \left.\frac{\partial g_2(y)}{\partial y}\right|_{y=d_1} \quad , \quad \left.\frac{\partial g_2(y)}{\partial y}\right|_{y=d_1+t_1} = \left.\frac{\partial g_3(y)}{\partial y}\right|_{y=d_1+t_1} \tag{3.29}$$

$$f_1(x) = f_2(x) = f_3(x) = f(x) = A \sin k_x x + B \cos k_x x \tag{3.30}$$

Equation (3.30) physically requires that the phase velocity along the x direction must be the same in the sample and gap regions for boundary conditions to be satisfied (same applies for propagation along the z direction since γ_{lsm} is the same in each region). The final boundary condition is that the magnetic field must be continuous at $y = d_1, d_1 + t_1$ (for all x, z), thus

$$H_{1\alpha}(x, d_1, z) = H_{2\alpha}(x, d_1, z) \ , \ H_{2\alpha}(x, d_1 + t_1, z) = H_{3\alpha}(x, d_1 + t_1, z) \ \ldots \alpha = x, z \tag{3.31}$$

Substitution of (3.12) into (3.31) leads to

$$g_1(d_1) = \varepsilon_r g_2(d_1) \quad , \quad \varepsilon_r g_2(d_1 + t_1) = g_3(d_1 + t_1) \tag{3.32}$$

The *LSM* mode characteristic equation is obtained by inserting (3.20)-(3.22) and (3.30) into the above various relations. First, substitution of (3.30) into (3.25) produces the result

$$f(x) = A \sin k_x x = A \sin(m\pi x / a) \quad ...m = 1,2,3,... \tag{3.33}$$

where

$$k_x = \frac{m\pi}{a} \tag{3.34}$$

is the same in the sample and gap regions. If the coefficient A is absorbed into the coefficients of $g_i(y)$, then $f(x)$ can be written as

$$f(x) = \sin(m\pi x / a) \quad ...m = 1,2,3,... \tag{3.35}$$

Note that $f(x) = 0$ when $m = 0$ and is therefore of no interest since it leads to a trivial solution. Substitution of (3.20) and (3.22) into (3.27) leads to

$$\frac{\partial g_1(0)}{\partial y} = 0 \quad \Rightarrow \quad C_1 = 0 \qquad \therefore \; g_1(y) = D_1 \cos hy \tag{3.36}$$

$$\frac{\partial g_3(b)}{\partial y} = 0 \quad \Rightarrow \quad C_3 = 0 \qquad \therefore \; g_3(y) = D_3 \cos h(b - y) \tag{3.37}$$

Inserting (3.36) and (3.21) into the first relation of (3.29) gives

$$\left.\frac{\partial g_1(y)}{\partial y}\right|_{y=d_1} = \left.\frac{\partial g_2(y)}{\partial y}\right|_{y=d_1} \quad \Rightarrow \quad -D_1 h \sin h d_1 = C_2 l \tag{3.38}$$

Solving (3.38) for C_2 allows $g_2(y)$ to be written as

$$g_2(y) = -D_1 \frac{h}{l} \sin h d_1 \sin l(y - d_1) + D_2 \cos l(y - d_1) \tag{3.39}$$

Substitution of (3.39) and (3.37) into the second relation of (3.29) results in

$$\left.\frac{\partial g_2(y)}{\partial y}\right|_{y=d_1+t_1} = \left.\frac{\partial g_3(y)}{\partial y}\right|_{y=d_1+t_1} \Rightarrow -D_1 h \sin hd_1 \cos lt_1 - D_2 l \sin lt_1 = D_3 h \sin hd_2 \quad (3.40)$$

Solving (3.40) for D_3 and inserting this result into (3.37) leads to the following expression for $g_3(y)$

$$g_3(y) = -\frac{D_1 h \sin hd_1 \cos lt_1 + D_2 l \sin lt_1}{h \sin hd_2} \cos h(b-y) \quad (3.41)$$

Substitution of (3.36) and (3.39) into the first condition of (3.32) gives

$$g_1(d_1) = \varepsilon_r g_2(d_1) \Rightarrow D_1 \cos hd_1 = \varepsilon_r D_2 \quad \therefore D_2 = D_1 \frac{\cos hd_1}{\varepsilon_r} \quad (3.42)$$

Insertion of (3.42) into (3.39) and (3.41) leads to

$$g_2(y) = D_1 \left[\frac{1}{\varepsilon_r} \cos hd_1 \cos l(y-d_1) - \frac{h}{l} \sin hd_1 \sin l(y-d_1) \right] \quad (3.43)$$

$$g_3(y) = -D_1 \frac{h \sin hd_1 \cos lt_1 + \frac{l}{\varepsilon_r} \cos hd_1 \sin lt_1}{h \sin hd_2} \cos h(b-y) \quad (3.44)$$

As a final step, (3.43) and (3.44) are substituted into the second relation of (3.32), giving

$$\cos hd_1 \cos lt_1 - \frac{\varepsilon_r h}{l} \sin hd_1 \sin lt_1 = -\frac{h \sin hd_1 \cos lt_1 + \frac{l}{\varepsilon_r} \cos hd_1 \sin lt_1}{h \sin hd_2} \cos hd_2 \quad (3.45)$$

Multiplying (3.45) by the factor $\varepsilon_r h \sin hd_2$ and using the trigonometric identity $\sin hd_1 \cos hd_2 + \cos hd_1 \sin hd_2 = \sin h(d_1 + d_2)$ produces the characteristic equation

$$\left(l \cos hd_1 \cos hd_2 - \frac{\varepsilon_r^2 h^2}{l} \sin hd_1 \sin hd_2 \right) \sin lt_1 + \varepsilon_r h \sin h(d_1 + d_2) \cos lt_1 = 0 \quad (3.46)$$

where, upon using (3.17), (3.23) and (3.34), the wavenumbers h and l are

$$h = \sqrt{\gamma_{lsm}^2 + k_0^2 - (m\pi/a)^2} \quad , \quad l = \sqrt{\gamma_{lsm}^2 + k^2 - (m\pi/a)^2} \quad (3.47)$$

Since $h = h(\gamma_{lsm})$ and $l = l(\gamma_{lsm})$, equation (3.46) constitutes a transcendental equation for γ_{lsm} which must be solved numerically. An infinite number of solutions exist for the LSM mode characteristic equation (i.e., $n = 1,2,3,...$). The gap geometry, dimensions of the waveguide and the frequency of operation all determine whether a mode is propagating ($\gamma_{lsm} = j\beta_{lsm}$) or evanescent ($\gamma_{lsm} = \alpha_{lsm}$). If the sample is lossy, no true cutoff exists and all the modes will be propagation modes (however, the modes that exist above the frequency of operation will decay rapidly). Note that, for the mn^{th} LSM mode, the indices m and n give a measure of the field variation along the x and y directions, respectively. Also note that when $d_1, d_2 \to 0$ ($\Rightarrow t_1 \to b$), equation (3.46) simplifies to $\sin lb = 0 \Rightarrow l = \tilde{n}\pi / b$ for $\tilde{n} = 0,1,2,....$ This, of course, is a well-known result of guided wave theory.

3.3.4 Perturbation Theory for Lowest-Order LSM Mode Propagation Constant

It was mentioned in the previous section that an infinite number of roots exist for the characteristic equation for γ_{lsm}. If the gaps between the sample and waveguide walls are small compared to the dimensions of the waveguide (and frequency of operation), then the lowest-order (i.e., LSM_{11}) mode propagation constant should be dominant (the higher-order mode propagation constants will lead to waves that are highly evanescent). It should also be anticipated that this propagation constant will only be slightly perturbed from the ideal TE_{10} propagation constant (γ) for a guide uniformly filled with the sample material, that is

$$\gamma_{lsm}^2 \approx \gamma^2 + \delta\gamma_{lsm}^2 \tag{3.48}$$

where

$$\gamma^2 = (\pi / a)^2 - k^2 \tag{3.49}$$

Since the algorithm for finding the various roots of (3.46) is sensitive to the initial guess, the perturbation expression in (3.48) will be utilized to obtain an accurate initial guess for γ_{lsm}. Note, the perturbation $\gamma_{lsm}^2 \approx \gamma^2 + \delta\gamma_{lsm}^2$ is used instead of $\gamma_{lsm} \approx \gamma + \delta\gamma_{lsm}$ since the wavenumbers in (3.47) depend on γ_{lsm}^2 and not γ_{lsm}.

A perturbation formula for $\delta\gamma_{lsm}^2$ can be obtained by first substituting (3.48) and (3.49) into (3.47), resulting in the following expressions for h^2 and l^2 (for $m = 1$)

$$h^2 = k_0^2 - k^2 + \delta\gamma_{lsm}^2 = h_u^2 + h_p^2 \tag{3.50}$$

$$l^2 = \delta\gamma_{lsm}^2 \tag{3.51}$$

where

$$h_u^2 = k_0^2 - k^2 \quad , \quad h_p^2 = \delta\gamma_{lsm}^2 \tag{3.52}$$

Next, the Taylor series expansions for $\sin x$ and $\cos x$, that is

$$\sin x \approx x \ , \ \cos x \approx 1 - \frac{x^2}{2} \quad \ldots x \ll 1 \tag{3.53}$$

are utilized in (3.46), leading to the following simplifications (assuming that hd_1, hd_2 and lt_1 are small compared to 1)

$$l \cos hd_1 \cos hd_2 \sin lt_1 \approx l^2 t_1 \left(1 - \frac{h^2 d_1^2}{2}\right)\left(1 - \frac{h^2 d_2^2}{2}\right) \tag{3.54}$$

$$l \cos hd_1 \cos hd_2 \sin lt_1 \approx C\delta\gamma_{lsm}^2 \quad , \quad C = t_1 \left(1 - \frac{h_u^2 d_1^2}{2}\right)\left(1 - \frac{h_u^2 d_2^2}{2}\right) \tag{3.55}$$

$$-\frac{\varepsilon_r^2 h^2}{l}\sin hd_1 \sin hd_2 \sin lt_1 \approx -d_1 d_2 t_1 \varepsilon_r^2 h^4 \approx -d_1 d_2 t_1 \varepsilon_r^2 h_u^4 - 2d_1 d_2 t_1 \varepsilon_r^2 h_u^2 h_p^2 \quad (3.56)$$

$$-\frac{\varepsilon_r^2 h^2}{l}\sin hd_1 \sin hd_2 \sin lt_1 \approx -A + D\delta\gamma_{lsm}^2 \qquad (3.57)$$
$$A = d_1 d_2 t_1 \varepsilon_r^2 h_u^4 \ , \ D = -2d_1 d_2 t_1 \varepsilon_r^2 h_u^2$$

$$\varepsilon_r h \sin h(d_1 + d_2)\cos lt_1 \approx \varepsilon_r h^2 (d_1 + d_2)\left(1 - \frac{l^2 t_1^2}{2}\right)$$
$$\approx \varepsilon_r (d_1 + d_2) h_u^2 + \varepsilon_r (d_1 + d_2)\left(1 - \frac{h_u^2 t_1^2}{2}\right)\delta\gamma_{lsm}^2 \qquad (3.58)$$

$$\therefore \quad \varepsilon_r h \sin h(d_1 + d_2)\cos lt_1 \approx -B + E\delta\gamma_{lsm}^2$$
$$B = -\varepsilon_r (d_1 + d_2) h_u^2 \ , \ E = \varepsilon_r (d_1 + d_2)\left(1 - \frac{h_u^2 t_1^2}{2}\right) \qquad (3.59)$$

Substitution of (3.55), (3.57) and (3.59) into (3.46) leads to the desired result

$$-(A + B) + (C + D + E)\delta\gamma_{lsm}^2 = 0 \quad \Rightarrow \quad \delta\gamma_{lsm}^2 = \frac{A + B}{C + D + E} \qquad (3.60)$$

$$\gamma_{lsm}^{guess} \approx \sqrt{\gamma^2 + \delta\gamma_{lsm}^2} \qquad (3.61)$$

The result of (3.61) is used as the initial guess in the algorithm for finding the lowest-order root of (3.46). The reader is reminded that this perturbation result is only valid if the gaps are small. Note that lt_1 is always much smaller than unity since $l = \delta\gamma_{lsm}$, thus the Taylor series expansions in (3.53) are always valid. This is not necessarily the case for hd_1 and hd_2. However, h can be broken into an unperturbed and perturbed portion and the sin and cos angle formulas invoked. It can be shown (although algebraically tedious) that this leads to a better approximation to $\delta\gamma_{lsm}^2$, and hence a more accurate initial guess.

Now that we have developed a scheme for computing the propagation constant γ_{lsm}, we can compute the one-way propagation term P by using the second term of (3.4) with γ replaced by γ_{lsm}. This expression is not exact, but offers a good approximation if the gaps are small. However, experience shows that a more adequate model for the interfacial reflection and transmission coefficient R,T and wave impedance Z can be developed by using mode matching, as will be discussed in the following section. Once these expressions have been found, the general technique of section 3.2 can be invoked for the material characterization process.

3.3.5 Approximate Expressions for Scattering Parameters Using Mode Matching

The objective of this section is to obtain expressions for the scattering parameters S_{11}^{lsm} and S_{21}^{lsm}. Approximate formulas can be obtained using wave matrices if the interfacial reflection and transmission coefficients are computed at the front (R_{lsm}, T_{lsm}) and back ($\tilde{R}_{lsm}, \tilde{T}_{lsm}$) sample interfaces. The front sample surface is comprised of an air/dielectric interface, whereas the back sample surface is a dielectric/air interface. Expressions for R_{lsm}, T_{lsm} and $\tilde{R}_{lsm}, \tilde{T}_{lsm}$ will be found using mode matching. An approximate expression for the equivalent wave impedance in the region $0 < z < \ell$ will also be obtained using the above analysis.

A general formulation for computing the reflection and transmission coefficients at an air/dielectric interface is as follows. First, assume that only a single mode is incident upon the interface and N modes are reflected and transmitted. Thus, the total tangential fields for $z < 0$ and $z > 0$ can be written as

$$\left.\begin{aligned}\vec{E}_{1t} &= a_1^+\vec{e}_1 e^{-\gamma_1 z} + \sum_{n=1}^{N} a_n^-\vec{e}_n e^{\gamma_n z} \\ \vec{H}_{1t} &= a_1^+\vec{h}_1 e^{-\gamma_1 z} - \sum_{n=1}^{N} a_n^-\vec{h}_n e^{\gamma_n z}\end{aligned}\right\} \quad \ldots z<0 \tag{3.62}$$

$$\left.\begin{aligned}\vec{E}_{2t} &= \sum_{n=1}^{N} b_n^+\vec{e}_n^{lsm} e^{-\gamma_n^{lsm} z} \\ \vec{H}_{2t} &= \sum_{n=1}^{N} b_n^+\vec{h}_n^{lsm} e^{-\gamma_n^{lsm} z}\end{aligned}\right\} \quad \ldots z>0 \tag{3.63}$$

where $\vec{e}_n, \vec{h}_n, \vec{e}_n^{lsm}, \vec{h}_n^{lsm}$ are the normal modes for the electric and magnetic fields in the air and dielectric regions. Enforcing continuity at the $z=0$ interface leads to

$$a_1^+\vec{e}_1 + \sum_{n=1}^{N} a_n^-\vec{e}_n = \sum_{n=1}^{N} b_n^+\vec{e}_n^{lsm} \tag{3.64}$$

$$a_1^+\vec{h}_1 - \sum_{n=1}^{N} a_n^-\vec{h}_n = \sum_{n=1}^{N} b_n^+\vec{h}_n^{lsm} \tag{3.65}$$

If the above equations are divided by a_1^+ and the operators

$$\int_{CS} \vec{e}_j \cdot \{\} ds \ , \ \int_{CS} \vec{h}_j \cdot \{\} ds \ \ldots j = 1, \ldots, N \tag{3.66}$$

are applied to (3.64) and (3.65), respectively, then the following relations prevail

$$\int_{CS} \vec{e}_j \cdot \vec{e}_1 ds + \sum_{n=1}^{N} R_n \int_{CS} \vec{e}_j \cdot \vec{e}_n ds = \sum_{n=1}^{N} T_n \int_{CS} \vec{e}_j \cdot \vec{e}_n^{lsm} ds \ \ldots j = 1, \ldots, N \tag{3.67}$$

$$\int_{CS} \vec{h}_j \cdot \vec{h}_1 ds - \sum_{n=1}^{N} R_n \int_{CS} \vec{h}_j \cdot \vec{h}_n ds = \sum_{n=1}^{N} T_n \int_{CS} \vec{h}_j \cdot \vec{h}_n^{lsm} ds \ \ldots j = 1, \ldots, N \tag{3.68}$$

where

$$R_n = \frac{a_n^-}{a_1^+} \ , \ T_n = \frac{b_n^+}{a_1^+} \ , \ R_{lsm} = R_1 \ , \ T_{lsm} = T_1 \tag{3.69}$$

It will be assumed that the normal modes are normalized in the following manner

$$\int_{CS} \vec{e}_j \cdot \vec{e}_n ds = \delta_{jn} = \begin{cases} 1 & \ldots n = j \\ 0 & \ldots n \neq j \end{cases} \quad , \quad \int_{CS} \vec{h}_j \cdot \vec{h}_n ds = C_{jn}\delta_{jn} = \begin{cases} C_{jj} & \ldots n = j \\ 0 & \ldots n \neq j \end{cases} \tag{3.70}$$

Thus, equations (3.67) and (3.68) may be written

$$\delta_{j1} + R_j = \sum_{n=1}^{N} M_{jn} T_n \quad \ldots j = 1, \ldots, N \tag{3.71}$$

$$C_{11}\delta_{j1} - C_{jj} R_j = \sum_{n=1}^{N} N_{jn} T_n \quad \ldots j = 1, \ldots, N \tag{3.72}$$

where

$$M_{jn} = \int_{CS} \vec{e}_j \cdot \vec{e}_n^{lsm} ds \quad , \quad N_{jn} = \int_{CS} \vec{h}_j \cdot \vec{h}_n^{lsm} ds \tag{3.73}$$

The factors δ_{j1} and $C_{11}\delta_{j1}$ are the matrix forcing terms, thus (3.71) and (3.72) can be more suitably written as

$$\left.\begin{aligned} R_j - \sum_{n=1}^{N} M_{jn} T_n &= -\delta_{j1} \\ C_{jj} R_j + \sum_{n=1}^{N} N_{jn} T_n &= C_{11}\delta_{j1} \end{aligned}\right\} \ldots for \ j = 1, \ldots, N \tag{3.74}$$

or in partitioned matrix form

$$\begin{bmatrix} I & -M \\ C & N \end{bmatrix} \begin{bmatrix} R \\ T \end{bmatrix} = \begin{bmatrix} B_1 \\ B_2 \end{bmatrix} \tag{3.75}$$

where I is the $N \times N$ identity matrix, C is a $N \times N$ diagonal matrix with elements C_{jj}, M and N are $N \times N$ matrices with elements M_{jn}, N_{jn} and R, T, B_1, B_2 are $N \times 1$ column vectors given by

$$[R]=\begin{bmatrix} R_1 \\ \vdots \\ R_N \end{bmatrix} \quad , \quad [T]=\begin{bmatrix} T_1 \\ \vdots \\ T_N \end{bmatrix} \quad , \quad [B_1]=\begin{bmatrix} -1 \\ 0 \\ \vdots \end{bmatrix} \quad , \quad [B_2]=\begin{bmatrix} C_{11} \\ 0 \\ \vdots \end{bmatrix} \tag{3.76}$$

Note that the expected result of $R_n, T_n = 0$ for $n \neq 1$ when $d_1, d_2 \to 0$. That is, coupling to higher-order modes disappears when the gaps are removed.

In a similar manner, a general formulation for computing $\tilde{R}_{lsm}, \tilde{T}_{lsm}$ can be found by considering a dominant propagating mode incident upon a dielectric/air interface. The total tangential fields in the dielectric ($z < 0$) and air ($z > 0$) regions are

$$\left.\begin{aligned} \vec{E}_{1t} &= \tilde{a}_1^+ \vec{e}_1^{lsm} e^{-\gamma_1^{lsm} z} + \sum_{n=1}^{N} \tilde{a}_n^- \vec{e}_n^{lsm} e^{\gamma_n^{lsm} z} \\ \vec{H}_{1t} &= \tilde{a}_1^+ \vec{h}_1^{lsm} e^{-\gamma_1^{lsm} z} - \sum_{n=1}^{N} \tilde{a}_n^- \vec{h}_n^{lsm} e^{\gamma_n^{lsm} z} \end{aligned}\right\} \ldots z < 0 \tag{3.77}$$

$$\left.\begin{aligned} \vec{E}_{2t} &= \sum_{n=1}^{N} \tilde{b}_n^+ \vec{e}_n e^{-\gamma_n z} \\ \vec{H}_{2t} &= \sum_{n=1}^{N} \tilde{b}_n^+ \vec{h}_n e^{-\gamma_n z} \end{aligned}\right\} \ldots z > 0 \tag{3.78}$$

Enforcing continuity at the $z = 0$ dielectric/air interface leads to

$$\tilde{a}_1^+ \vec{e}_1^{lsm} + \sum_{n=1}^{N} \tilde{a}_n^- \vec{e}_n^{lsm} = \sum_{n=1}^{N} \tilde{b}_n^+ \vec{e}_n \tag{3.79}$$

$$\tilde{a}_1^+ \vec{h}_1^{lsm} - \sum_{n=1}^{N} \tilde{a}_n^- \vec{h}_n^{lsm} = \sum_{n=1}^{N} \tilde{b}_n^+ \vec{h}_n \tag{3.80}$$

Dividing the above equations by $\tilde{a}_1^+$, and using a similar set of steps as in the previous paragraph, produces the result

$$\begin{bmatrix} M & -I \\ N & C \end{bmatrix} \begin{bmatrix} \tilde{R} \\ \tilde{T} \end{bmatrix} = \begin{bmatrix} \tilde{B}_1 \\ \tilde{B}_2 \end{bmatrix} \tag{3.81}$$

where $\tilde{R}_n = \tilde{a}_n^- / \tilde{a}_1^+$, $\tilde{T}_n = \tilde{b}_n^+ / \tilde{a}_1^+$, $\tilde{R}_{lsm} = \tilde{R}_1$, $\tilde{T}_{lsm} = \tilde{T}_1$ and

$$\left[\tilde{R}\right] = \begin{bmatrix} \tilde{R}_1 \\ \vdots \\ \tilde{R}_N \end{bmatrix} \quad , \quad \left[\tilde{T}\right] = \begin{bmatrix} \tilde{T}_1 \\ \vdots \\ \tilde{T}_N \end{bmatrix} \quad , \quad \left[\tilde{B}_1\right] = -\begin{bmatrix} M_{11} \\ \vdots \\ M_{N1} \end{bmatrix} \quad , \quad \left[\tilde{B}_2\right] = \begin{bmatrix} N_{11} \\ \vdots \\ N_{N1} \end{bmatrix} \tag{3.82}$$

As a specific example, consider a single incident, reflected and transmitted wave (i.e., $N = 1$). If the incident wave is the TE_{10} dominant mode, then the well known tangential fields in the region $z < 0$ are

$$\left.\begin{aligned} \vec{E}_{1t}(x,z) &= a_1^+ \vec{e}_1(x) e^{-\gamma_1 z} + a_1^- \vec{e}_1(x) e^{\gamma_1 z} \\ \vec{H}_{1t}(x,z) &= a_1^+ \vec{h}_1(x) e^{-\gamma_1 z} - a_1^- \vec{h}_1(x) e^{\gamma_1 z} \end{aligned}\right\} \quad ...z < 0 \tag{3.83}$$

where

$$\vec{e}_1 = \hat{y}\sqrt{\frac{2}{ab}}\sin\frac{\pi x}{a} \quad , \quad \vec{h}_1 = -\hat{x}\frac{1}{Z_0}\sqrt{\frac{2}{ab}}\sin\frac{\pi x}{a} \quad , \quad \gamma_1 = \sqrt{(\pi/a)^2 - k_0^2} \tag{3.84}$$

The tangential fields in the region $z > 0$ for the lowest-order LSM mode (i.e., the LSM_{11} mode), upon examination of section 3.3.2-3.3.3, are

$$\left.\begin{aligned} \vec{E}_{2t}(x,y,z) &= b_1^+ \vec{e}_1^{lsm}(x,y) e^{-\gamma_1^{lsm} z} \\ \vec{H}_{2t}(x,y,z) &= b_1^+ \vec{h}_1^{lsm}(x,y) e^{-\gamma_1^{lsm} z} \end{aligned}\right\} \quad ...z > 0 \tag{3.85}$$

where

$$\begin{aligned} b_1^+ &= \frac{D_1}{\varepsilon_r}\sqrt{\frac{ab}{2}}\left[\frac{\pi^2}{a^2} - \left(\gamma_1^{lsm}\right)^2\right] \\ \vec{e}_1^{lsm} &= \hat{y}\sqrt{\frac{2}{ab}}\sin\frac{\pi x}{a} g_1^{lsm}(y) \quad , \quad \vec{h}_1^{lsm} = -\hat{x}\frac{1}{Z_1^{lsm}(y)}\sqrt{\frac{2}{ab}}\sin\frac{\pi x}{a} g_1^{lsm}(y) \end{aligned} \tag{3.86}$$

$$Z_1^{lsm}(y) = \frac{(\gamma_1^{lsm})^2 - (\pi/a)^2}{j\omega\varepsilon(y)\gamma_1^{lsm}} \quad , \quad \varepsilon(y) = \begin{cases} \varepsilon_0 & ...gap\ region \\ \varepsilon & ...sample\ region \end{cases} \tag{3.87}$$

$$g_1^{lsm} = \begin{cases} \varepsilon_r \cos h_1 y \quad ...0 < y < d_1 \\ \cos h_1 d_1 \cos l_1 (y - d_1) - \dfrac{\varepsilon_r h_1}{l_1} \sin h_1 d_1 \sin l_1 (y - d_1) \quad ...d_1 < y < d_1 + t_1 \\ -\dfrac{\varepsilon_r h_1 \sin h_1 d_1 \cos l_1 t_1 + l_1 \cos h_1 d_1 \sin l_1 t_1}{h_1 \sin h_1 d_2} \cos h_1 (b - y) \quad ...d_1 + t_1 < y < b \end{cases} \tag{3.88}$$

$$h_1 = \sqrt{(\gamma_1^{lsm})^2 + k_0^2 - (\pi / a)^2} \quad , \quad l_1 = \sqrt{(\gamma_1^{lsm})^2 + k^2 - (\pi / a)^2} \tag{3.89}$$

The matrix equation (3.75), for this special case, reduces to

$$\begin{bmatrix} 1 & -M_{11} \\ C_{11} & N_{11} \end{bmatrix} \begin{bmatrix} R_1 \\ T_1 \end{bmatrix} = \begin{bmatrix} -1 \\ C_{11} \end{bmatrix} \tag{3.90}$$

where

$$C_{11} = \int_{CS} \vec{h}_1 \cdot \vec{h}_1 ds = \frac{1}{Z_0^2} \tag{3.91}$$

$$M_{11} = \int_{CS} \vec{e}_1 \cdot \vec{e}_1^{lsm} ds = \frac{1}{b} \int_0^b g_1^{lsm}(y) dy = A \tag{3.92}$$

$$N_{11} = \int_{CS} \vec{h}_1 \cdot \vec{h}_1^{lsm} ds = \frac{1}{bZ_0} \int_0^b \frac{g_1^{lsm}(y)}{Z_1^{lsm}(y)} dy = \frac{1}{Z_0 Z_{lsm}^{eff}} \tag{3.93}$$

The solution to (3.90) is

$$R_1 = R_{lsm} = \frac{Z_{lsm}^{eq} - Z_0}{Z_{lsm}^{eq} + Z_0} \quad , \quad T_1 = T_{lsm} = \frac{1}{A}(1 + R_{lsm}) \quad , \quad Z_{lsm}^{eq} = A Z_{lsm}^{eff} \tag{3.94}$$

Note that the following expected result occurs when $d_1, d_2 \to 0$, namely

$$R_1 = \frac{Z - Z_0}{Z + Z_0} \quad , \quad T_1 = 1 + R_1 \quad , \quad Z_{lsm}^{eq} = A \cdot Z_{lsm}^{eff} = 1 \cdot Z = Z \tag{3.95}$$

It should be noted that the relations in (3.94) are approximate for several reasons. First, the fields in the region $z < 0$ are independent of the variable y, whereas the fields

in the region $z > 0$ are functions of y. Secondly, the x-directed tangential electric field for the LSM_{11} mode has been ignored (i.e., assumed to be negligibly small). Finally, and most importantly, the expressions are approximate since the modal expansion of the reflected and transmitted fields has been truncated to a single mode.

In a similar manner, the interfacial reflection and transmission coefficients $\tilde{R}_{lsm}, \tilde{T}_{lsm}$ at the dielectric/air interface are found by considering a single LSM mode incident upon, and reflected from, the interface and a single TE_{10} mode transmitted into the air region. The result, with the aid of (3.81), is

$$\tilde{R}_{lsm} = -R_{lsm} \quad , \quad \tilde{T}_{lsm} = A(1+\tilde{R}_{lsm}) = A(1-R_{lsm}) \tag{3.96}$$

If the sample region has length ℓ, then an application of the wave-matrix approach of chapter 2 leads to the desired scattering parameter expressions

$$S_{11}^{lsm} = \frac{R_{lsm}(1-P_{lsm}^2)}{1-R_{lsm}^2 P_{lsm}^2} \quad , \quad S_{21}^{lsm} = \frac{P_{lsm}(1-R_{lsm}^2)}{1-R_{lsm}^2 P_{lsm}^2} \tag{3.97}$$

where

$$P_{lsm} = e^{-\gamma_1^{lsm}\ell} \tag{3.98}$$

Of course, these scattering parameters are only approximate since R_{lsm}, T_{lsm} and P_{lsm} are not exact.

3.4 LSE Mode Analysis for Left/Right Gaps

3.4.1 Geometry

Figure 3.2 shows the cross-sectional dimensions of a sample inserted into a rectangular waveguide having left/right gaps. The spacing of the left gap in region 1 is

d_3 and the right gap spacing in region 3 is d_4. Both gap regions are assumed to have constitutive parameters (ε_0, μ_0). The width of the sample in region 2 is t_2 and has the electromagnetic properties (ε_r, μ_r). The width and height of the rectangular waveguide are a and b. The sample has a thickness ℓ and the walls of the waveguide are assumed to be perfectly conducting.

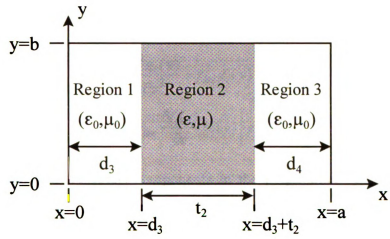

Figure 3.2 Cross-sectional geometry for left/right gap analysis.

3.4.2 Hertzian Potential Generating Function and EM Field Components

The following magnetic-type Hertz potential is sufficient to generate all EM field components necessary for satisfying boundary conditions for the left/right gap geometry

$$\vec{\pi}_i^h = \hat{x}\pi_{iy}^h(x,y)e^{-\gamma_{iwz}z} = \hat{x}f_i(x)g_i(y)e^{-\gamma_{iwz}z} \tag{3.99}$$

where the Hertz potential satisfies the source-free Helmholtz wave equation

$$\nabla^2\vec{\pi}_i^h + k_i^2\vec{\pi}_i^h = 0 \tag{3.100}$$

with $k_1 = k_3 = k_0$ and $k_2 = k$. For magnetic-type Hertz potentials, the EM field

components satisfy the relations

$$\vec{E}_i = -j\omega\mu_i \nabla \times \vec{\pi}_i^h \tag{3.101}$$

$$\vec{H}_i = -\frac{1}{j\omega\mu_i} \nabla \times \vec{E}_i \tag{3.102}$$

Substitution of (3.99) into (3.101) and (3.102) leads to the following field components

$$\vec{E}_i = j\omega\mu_i f_i(x)\left[\hat{y}\gamma_{lse} g_i(y) + \hat{z}\frac{\partial g_i(y)}{\partial y}\right] e^{-\gamma_{lse} z} \tag{3.103}$$

$$\begin{aligned}\vec{H}_i = \Bigg\{ & -\hat{x} f_i(x)\left[\frac{\partial^2 g_i(y)}{\partial y^2} + \gamma_{lse}^2 g_i(y)\right] + \hat{y}\frac{\partial f_i(x)}{\partial x}\frac{\partial g_i(y)}{\partial y} \\ & -\hat{z}\gamma_{lse}\frac{\partial f_i(x)}{\partial x} g_i(y)\Bigg\} e^{-\gamma_{lse} z}\end{aligned} \tag{3.104}$$

Note, the electric field only has components in the longitudinal $y-z$ plane (i.e., the plane parallel to the gap-sample interface) and are therefore called *LSE* modes.

3.4.3 Identification of the *LSE* Mode Characteristic Equation for γ_{lse}

The form of $f_i(x)$ and $g_i(y)$ for the magnetic-type Hertz potential, determined by solving (3.100), is

$$f_1(x) = A_1 \sin px + B_1 \cos px \quad \ldots 0 < x < d_3 \tag{3.105}$$

$$f_2(x) = A_2 \sin q(x-d_3) + B_2 \cos q(x-d_3) \quad \ldots d_3 < x < d_3 + t_2 \tag{3.106}$$

$$f_3(x) = A_3 \sin p(a-x) + B_3 \cos p(a-x) \quad \ldots d_3 + t_2 < x < a \tag{3.107}$$

$$g_i(y) = C_i \sin k_{iy} y + D_i \cos k_{iy} y \tag{3.108}$$

where the constraint equation and wavenumbers along the x direction are given by

$$k_{ix}^2 + k_{iy}^2 = \gamma_{lse}^2 + k_i^2 \tag{3.109}$$

$$k_{1x} = k_{3x} = p \quad , \quad k_{2x} = q \tag{3.110}$$

The following boundary conditions for $f_i(x)$ and $g_i(y)$ prevail

$$\vec{E}_{tang}(x,0,z) = \vec{E}_{tang}(x,b,z) = 0 \;\Rightarrow\; \left.\frac{\partial g_i(y)}{\partial y}\right|_{y=0,b} = 0 \tag{3.111}$$

$$\vec{E}_{tang}(0,y,z) = \vec{E}_{tang}(a,y,z) = 0 \;\Rightarrow\; f_1(0) = 0 \;,\; f_3(a) = 0 \tag{3.112}$$

$$\vec{E}_{tang}(d_3^-,y,z) = \vec{E}_{tang}(d_3^+,y,z) \;\Rightarrow\; f_1(d_3) = \mu_r f_2(d_3) \tag{3.113}$$

$$\vec{E}_{tang}(d_3 + t_2^-,y,z) = \vec{E}_{tang}(d_3 + t_2^+,y,z) \;\Rightarrow\; \mu_r f_2(d_3 + t_2) = f_3(d_3 + t_2) \tag{3.114}$$

$$\vec{H}_{tang}(d_3^-,y,z) = \vec{H}_{tang}(d_3^+,y,z) \;\Rightarrow\; \left.\frac{\partial f_1(x)}{\partial x}\right|_{x=d_3} = \left.\frac{\partial f_2(x)}{\partial x}\right|_{x=d_3} \tag{3.115}$$

$$\vec{H}_{tang}(d_3 + t_2^-,y,z) = \vec{H}_{tang}(d_3 + t_2^+,y,z) \;\Rightarrow\; \left.\frac{\partial f_2(x)}{\partial x}\right|_{x=d_3+t_2} = \left.\frac{\partial f_3(x)}{\partial x}\right|_{x=d_3+t_2} \tag{3.116}$$

In addition, the relations in (3.113)-(3.116) also require that

$$g_1(y) = g_2(y) = g_3(y) = g(y) = C\sin k_y y + D\cos k_y y \tag{3.117}$$

The *LSE* characteristic equation is identified by substituting (3.105)-(3.107) and (3.117) into the above boundary conditions. The result is

$$\left.\frac{\partial g_i(y)}{\partial y}\right|_{y=0,b} = 0 \;\Rightarrow\; g(y) = \cos k_y y = \cos\frac{n\pi y}{b} \;\ldots n = 0,1,2,\ldots \tag{3.118}$$

$$f_1(0) = 0 \;\Rightarrow\; B_1 = 0 \qquad \therefore\; f_1(x) = A_1 \sin px \tag{3.119}$$

$$f_3(a) = 0 \;\Rightarrow\; B_3 = 0 \qquad \therefore\; f_3(x) = A_3 \sin p(a-x) \tag{3.120}$$

$$f_1(d_3) = \mu_r f_2(d_3) \;\Rightarrow\; A_1 \sin pd_3 = \mu_r B_2 \;\Rightarrow\; B_2 = A_1 \frac{\sin pd_3}{\mu_r} \tag{3.121}$$

$$f_2(x) = A_2 \sin q(x-d_3) + A_1 \frac{\sin pd_3}{\mu_r}\cos q(x-d_3) \tag{3.122}$$

$$\mu_r f_2(d_3+t_2) = f_3(d_3+t_2) \;\Rightarrow$$
$$\mu_r\left(A_2\sin qt_2 + A_1\frac{\sin pd_3}{\mu_r}\cos qt_2\right) = A_3\sin pd_4 \tag{3.123}$$

$$f_3(x) = \frac{\mu_r}{\sin pd_4}\left(A_2\sin qt_2 + A_1\frac{\sin pd_3}{\mu_r}\cos qt_2\right)\sin p(a-x) \tag{3.124}$$

$$\left.\frac{\partial f_1(x)}{\partial x}\right|_{x=d_3} = \left.\frac{\partial f_2(x)}{\partial x}\right|_{x=d_3} \Rightarrow A_1 p\cos pd_3 = A_2 q \Rightarrow A_2 = A_1\frac{p\cos pd_3}{q} \tag{3.125}$$

$$f_2(x) = A_1\left[\frac{p}{q}\cos pd_3\sin q(x-d_3) + \frac{1}{\mu_r}\sin pd_3\cos q(x-d_3)\right] \tag{3.126}$$

$$f_3(x) = A_1\frac{\mu_r}{\sin pd_4}\left(\frac{p}{q}\cos pd_3\sin qt_2 + \frac{1}{\mu_r}\sin pd_3\cos qt_2\right)\sin p(a-x) \tag{3.127}$$

$$\left.\frac{\partial f_2(x)}{\partial x}\right|_{x=d_3+t_2} = \left.\frac{\partial f_3(x)}{\partial x}\right|_{x=d_3+t_2} \Rightarrow \tag{3.128}$$

$$p\cos pd_3\cos qt_2 - \frac{q}{\mu_r}\sin pd_3\sin qt_2 =$$
$$-\frac{p\mu_r\cos pd_4}{\sin pd_4}\left(\frac{p}{q}\cos pd_3\sin qt_2 + \frac{1}{\mu_r}\sin pd_3\cos qt_2\right) \tag{3.129}$$

Multiplying (3.129) by the factor $q\sin pd_4 / p\mu_r$ and using the trigonometric identity $\sin p(d_3+d_4) = \sin pd_3\cos pd_4 + \cos pd_3\sin pd_4$ leads to the following *LSE* mode characteristic equation

$$\left(p\cos pd_3\cos pd_4 - \frac{q^2}{p\mu_r^2}\sin pd_3\sin pd_4\right)\sin qt_2$$
$$+\frac{q}{\mu_r}\sin p(d_3+d_4)\cos qt_2 = 0 \tag{3.130}$$

where

$$p = \sqrt{\gamma_{lse}^2 + k_0^2 - (n\pi/b)^2} \quad , \quad q = \sqrt{\gamma_{lse}^2 + k^2 - (n\pi/b)^2} \tag{3.131}$$

The above eigenvalue equation has an infinite number ($m = 1,2,3,...$) of roots for γ_{lse} and must be solved numerically. Note that (3.130) implies that $q = m\pi / a$ when $d_3, d_4 \to 0$, as expected.

3.4.4 Perturbation Theory for Lowest-Order *LSE* Mode Propagation Constant

An initial guess for the lowest-order *LSE* (i.e., the LSE_{10}) mode propagation constant can be obtained using the perturbation approximation

$$\gamma_{lse}^2 \approx \gamma^2 + \delta\gamma_{lse}^2 \quad , \quad \gamma^2 = (\pi / a)^2 - k^2 \tag{3.132}$$

Substitution of (3.132) into (3.131) leads to the following binomial approximations for p and q

$$p = p_u + p_p \quad , \quad q = q_u + q_p \tag{3.133}$$

where

$$p_u = (\gamma^2 + k_0^2)^{1/2} \quad , \quad p_p = \frac{\delta\gamma_{lse}^2}{2p_u} \quad , \quad q_u = \frac{\pi}{a} \quad , \quad q_p = \frac{\delta\gamma_{lse}^2}{2q_u} \tag{3.134}$$

Steps analogous to those in section 3.3.4 lead to the result

$$\gamma_{lse}^{guess} \approx \sqrt{\gamma^2 + \delta\gamma_{lse}^2} \quad , \quad \delta\gamma_{lse}^2 = \frac{A + B + C}{D + E + F} \tag{3.135}$$

where

$$\begin{aligned} A &= -p_u q_u t_2 \left(1 - \frac{p_u^2 d_3^2}{2}\right)\left(1 - \frac{p_u^2 d_4^2}{2}\right) = -p_u q_u t_2 C_1 C_2 \\ B &= d_3 d_4 t_2 p_u q_u^3 / \mu_r^2 \quad , \quad C = -\frac{p_u q_u (d_3 + d_4)}{\mu_r}\left(1 - \frac{q_u^2 t_2^2}{2}\right) \end{aligned} \tag{3.136}$$

$$D = \frac{t_2}{2}\left[\frac{p_u}{q_u}C_1C_2 - p_u q_u d_4^2 C_1 + C_2\left(1 - \frac{3p_u^2 d_3^2}{2}\right)\right]$$

$$E = -\frac{d_3 d_4 t_2 q_u}{2\mu_r^2}\left(3 + \frac{q_u^2}{p_u}\right) \tag{3.137}$$

$$F = \frac{p_u q_u (d_3 + d_4)}{2\mu_r}\left[\left(\frac{1}{p_u^2} + \frac{1}{q_u^2}\right)\left(1 - \frac{q_u^2 t_2^2}{2}\right) - t_2^2\right]$$

3.4.5 Approximate Expressions for Scattering Parameters Using Mode Matching

It can be shown by a set of steps similar to those in section 3.3.5, that the approximate scattering parameters for the left/right gap geometry are (for $N = 1$)

$$S_{11}^{lse} = \frac{R_{lse}(1 - P_{lse}^2)}{1 - R_{lse}^2 P_{lse}^2} \quad , \quad S_{21}^{lse} = \frac{P_{lse}(1 - R_{lse}^2)}{1 - R_{lse}^2 P_{lse}^2} \tag{3.138}$$

These scattering parameters are found using the wave matrix formulation which requires the computation of the interfacial reflection and transmission coefficients R_{lse}, T_{lse} at the front sample interface and $\tilde{R}_{lse}, \tilde{T}_{lse}$ at the back sample interface. As in section 3.3.5, the above coefficients can be computed using (3.75) and (3.81), except that M_{jn}, N_{jn} are given by

$$M_{jn} = \int_{CS} \vec{e}_j \cdot \vec{e}_n^{lse} ds \quad , \quad N_{jn} = \int_{CS} \vec{h}_j \cdot \vec{h}_n^{lse} ds \tag{3.139}$$

As a specific example, when $N = 1$, the matrix equation for the air/dielectric interface reduces to (3.90). The tangential fields in the region $z < 0$ are given by (3.83)-(3.84) and the tangential fields in the region $z > 0$, with the aid of sections 3.4.2-3.4.3, are

$$\left.\begin{aligned}\vec{E}_{2t}(x,y,z) &= b_1^+ \vec{e}_1^{lse}(x,y)e^{-\gamma_1^{lse}z} \\ \vec{H}_{2t}(x,y,z) &= b_1^+ \vec{h}_1^{lse}(x,y)e^{-\gamma_1^{lse}z}\end{aligned}\right\} \quad ...z>0 \tag{3.140}$$

where

$$b_1^+ = A_1 j\omega\mu_0\mu_r\gamma_1^{lse}\frac{p}{q}\sqrt{\frac{ab}{2}} \tag{3.141}$$

$$\vec{e}_1^{lse}(x) = \hat{y}\sqrt{\frac{2}{ab}}f_1^{lse}(x) \quad , \quad \vec{h}_1^{lse}(x) = -\hat{x}\frac{1}{Z_1^{lse}(x)}\sqrt{\frac{2}{ab}}f_1^{lse}(x) \tag{3.142}$$

$$f_1^{lse}(x) = \mu_r(x)\tilde{f}_1^{lse}(x) \quad , \quad \mu_r(x) = \begin{cases} 1 & ...gap\ region \\ \mu_r & ...sample\ region \end{cases} \tag{3.143}$$

$$\tilde{f}_1^{lse} = \begin{cases} \dfrac{q_1 \sin p_1 x}{p_1\mu_r} & ...0<x<d_3 \\ \dfrac{\cos p_1 d_3 \sin q_1(x-d_3)}{\mu_r} + \dfrac{q_1 \sin p_1 d_3 \cos q_1(x-d_3)}{p_1\mu_r^2} & ...d_3<x<d_3+t_2 \\ \dfrac{\sin p_1(a-x)}{\sin p_1 d_4}\left(\cos p_1 d_3 \sin q_1 t_2 + \dfrac{q_1 \sin p_1 d_3 \cos q_1 t_2}{p_1\mu_r}\right) & ...d_3+t_2<x<a \end{cases} \tag{3.144}$$

$$Z_1^{lse}(x) = \frac{j\omega\mu(x)}{\gamma_1^{lse}} \quad , \quad \mu(x) = \mu_0\mu_r(x) \tag{3.145}$$

The factor C_{11} is given by (3.91) and the matrix elements M_{11} and N_{11} are

$$M_{11} = \int_{CS} \vec{e}_1 \cdot \vec{e}_1^{lse} ds = \frac{2}{a}\int_0^a \sin(\pi x/a) f_1^{lse}(x)dx = B \tag{3.146}$$

$$N_{11} = \int_{CS} \vec{h}_1 \cdot \vec{h}_1^{lse} ds = \frac{2}{aZ_0}\int_0^a \frac{\sin(\pi x/a) f_1^{lse}(x)}{Z_1^{lse}(x)}dx = \frac{1}{Z_0 Z_{lse}^{eff}} \tag{3.147}$$

Therefore, the solution to (3.90) is

$$R_1 = R_{lse} = \frac{Z_{lse}^{eq} - Z_0}{Z_{lse}^{eq} + Z_0} \quad , \quad T_1 = T_{lse} = \frac{1}{B}(1+R_{lse}) \quad , \quad Z_{lse}^{eq} = BZ_{lse}^{eff} \tag{3.148}$$

Similarly, the solution for $\tilde{R}_{lse}$ and $\tilde{T}_{lse}$ at the dielectric/air interface is

$$\tilde{R}_{lse} = -R_{lse} \quad , \quad \tilde{T}_{lse} = B(1+\tilde{R}_{lse}) = B(1-R_{lse}) \tag{3.149}$$

An application of the wave-matrix procedure leads to the desired result (3.138) where

$$P_{lse} = e^{-\gamma_1^{lse}\ell} \tag{3.150}$$

Note, since $\tilde{R}_{lse} = -R_{lse}$ and $T_{lse}\tilde{T}_{lse} = 1 - R_{lse}^2$, the wave-matrix procedure leads to the result in (3.138). However, for the case $N > 1$, these relations may not be valid and the general wave-matrix result must be used, that is

$$S_{11} = \frac{R + \tilde{R}P^2}{1 + R\tilde{R}P^2} \quad , \quad S_{21} = \frac{PT\tilde{T}}{1 + R\tilde{R}P^2} \tag{3.151}$$

$$S_{22} = -\frac{\tilde{R} + RP^2}{1 + R\tilde{R}P^2} \quad , \quad S_{12} = \frac{P(1-R^2)(1-\tilde{R}^2)}{T\tilde{T}(1 + R\tilde{R}P^2)} \tag{3.152}$$

where $R, T, \tilde{R}, \tilde{T}$ are representative of the LSM or LSE interfacial reflection and transmission coefficients at the front and back sample planes and P is equal to $e^{-\gamma_{lsm}}$ or $e^{-\gamma_{lse}}$. One can see that, when $\tilde{R} = -R$ and $T\tilde{T} = 1 - R^2$, the anticipated scattering parameters are obtained.

3.5 Experimental Results

The gap analysis measurements for an Alumina (Al_2O_3) sample are discussed in this section in order to verify the theoretical development in the preceding sections. In the top/bottom gap measurements, an Alumina sample having length $\ell = 0.05$ inches was initially machined to accurately fit into an ideal X-band waveguide having a width of $a = 0.9$ inches and height of $b = 0.4$ inches. The permittivity of this sample was

computed using the ideal procedure in section 3.2. Next, the sample was machined so that the height was reduced by *0.0008* inches (i.e., 0.8 mils). Thus, the height of the sample was reduced from *0.4* inches to *0.3992* inches. Note, the width of the sample (*0.9* inches) was not altered. The sample was then reinserted into the waveguide and it was noted that there was a 0.5 mil gap at the bottom and a 0.3 mil top gap. The permittivity was then determined with and without implementing the gap correction (for $N=1$) of section 3.3. Figures 3.3 ($\mathrm{Re}\{\varepsilon_r\}$ vs. freq.) and 3.4 ($\mathrm{Im}\{\varepsilon_r\}$ vs. freq.) clearly show the validity of the gap analysis. The sample was then removed, machined to a height of *0.3981* inches and inserted back into the waveguide. Again, the permittivity was computed with and without gap correction and subsequently compared to the ideal case. Figure 3.5 shows that the analysis of section 3.3 mitigates the gap error. In addition, Figure 3.6 demonstrates the effects of a *2.9* mil gap. In this case, the gap correction accommodates an error of approximately *5%*.

Figure 3.7 reveals that left/right gaps do not significantly alter permittivity measurements of non-magnetic materials. Although the left and right gaps were *17.5* mils, the difference between the gap and no-gap correction was negligible. This is an anticipated result since the electric field is exceedingly small near the walls at $x=0,a$. It is anticipated that the permeability profile of a magnetic material would be significantly altered by the presence of left/right gaps.

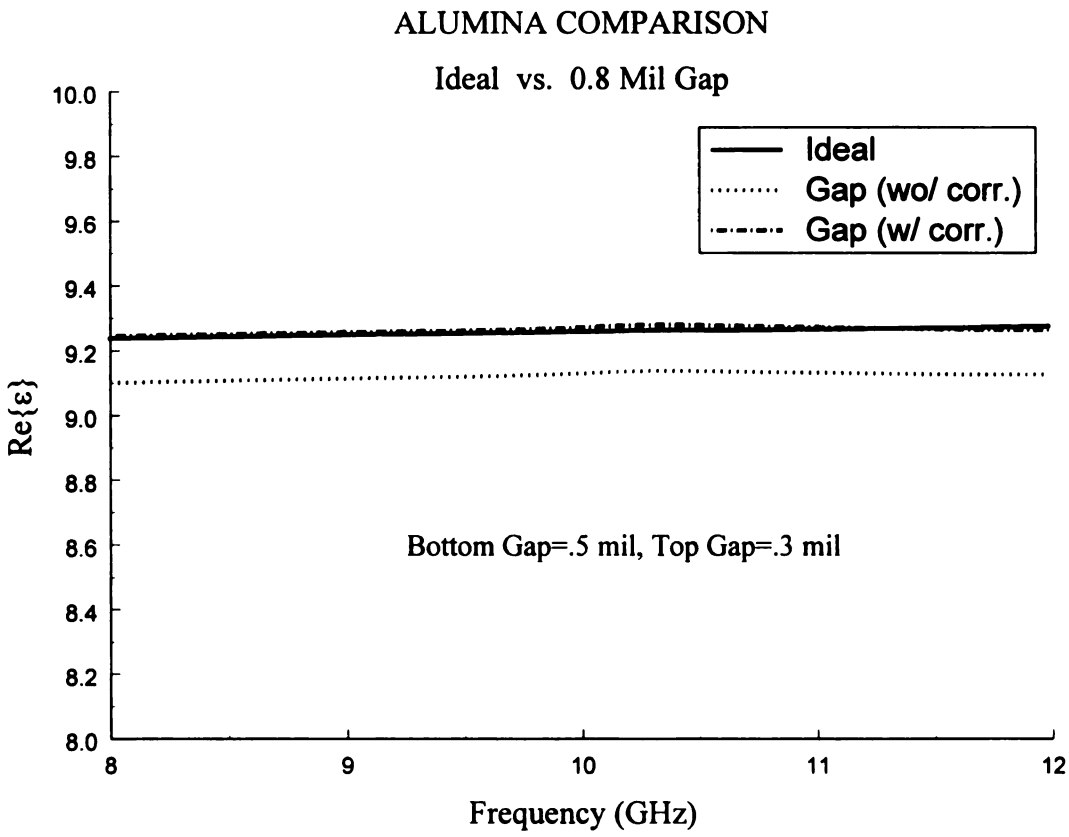

Figure 3.3 Experimental results of a *0.8* mil top/bottom gap for $\mathrm{Re}\{\varepsilon_r\}$.

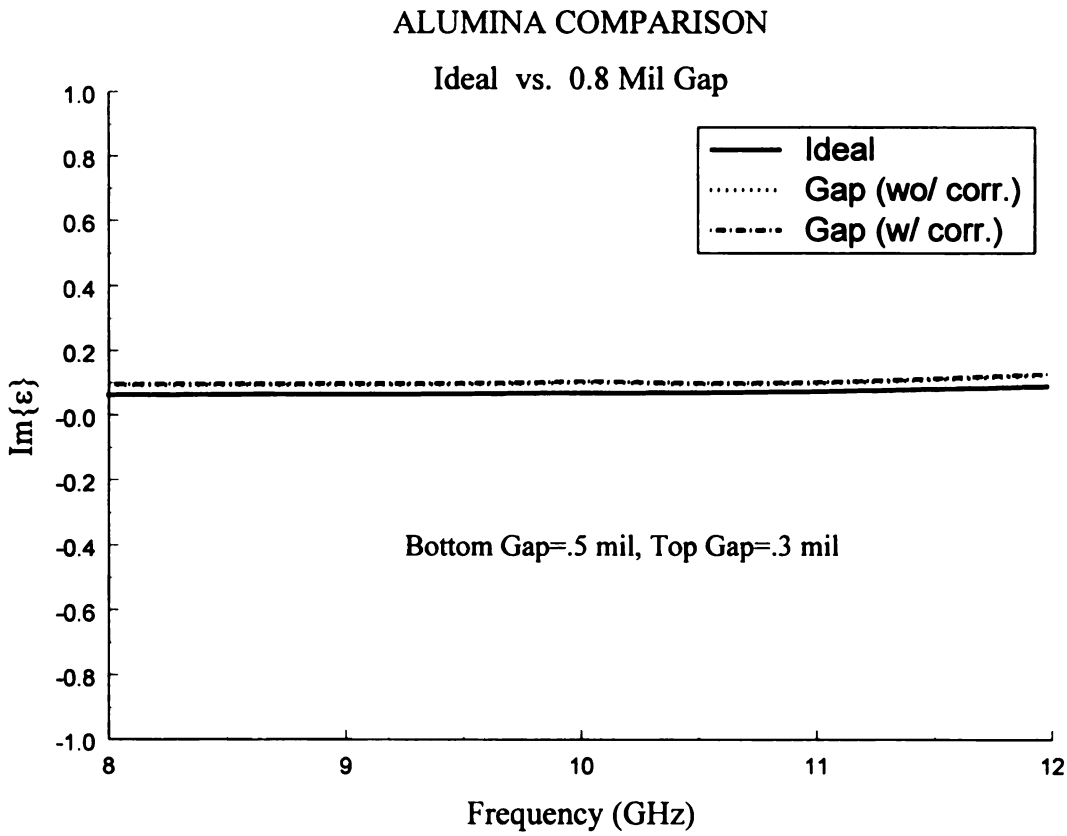

Figure 3.4 Experimental results of a *0.8* mil top/bottom gap for $\mathrm{Im}\{\varepsilon_r\}$.

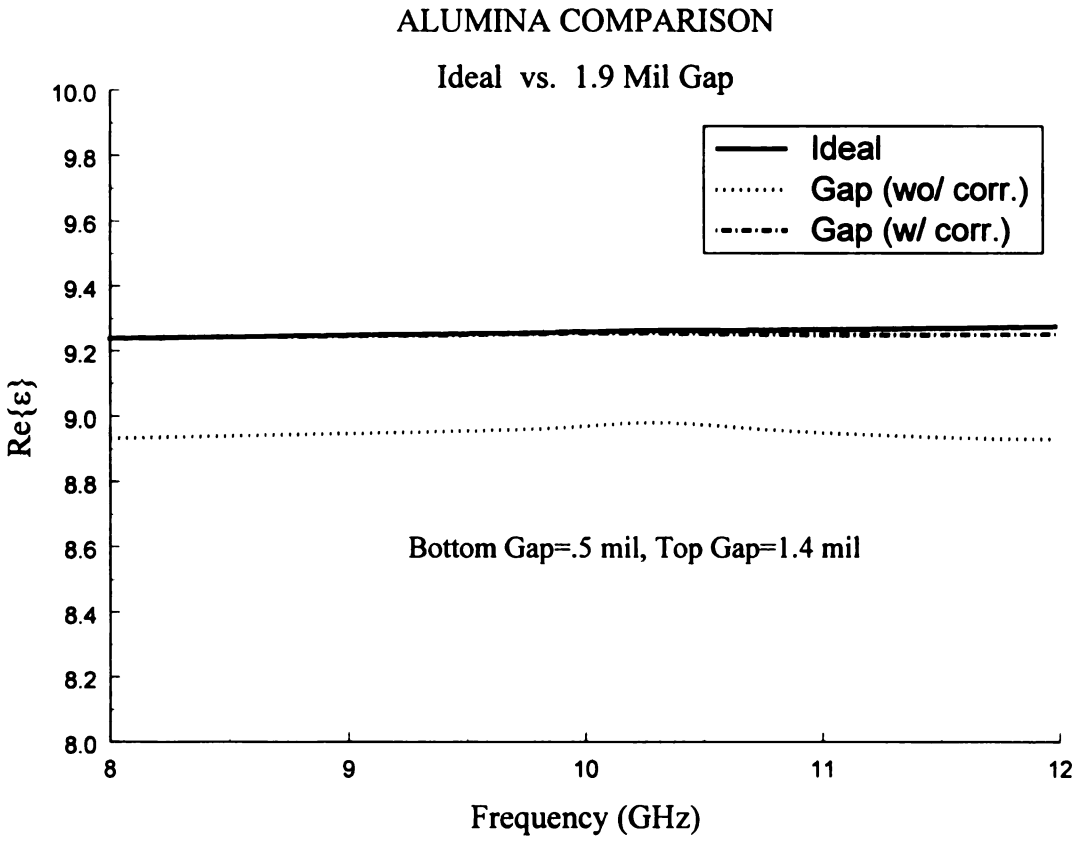

Figure 3.5 Experimental results of a *1.9* mil top/bottom gap for $\mathrm{Re}\{\varepsilon_r\}$.

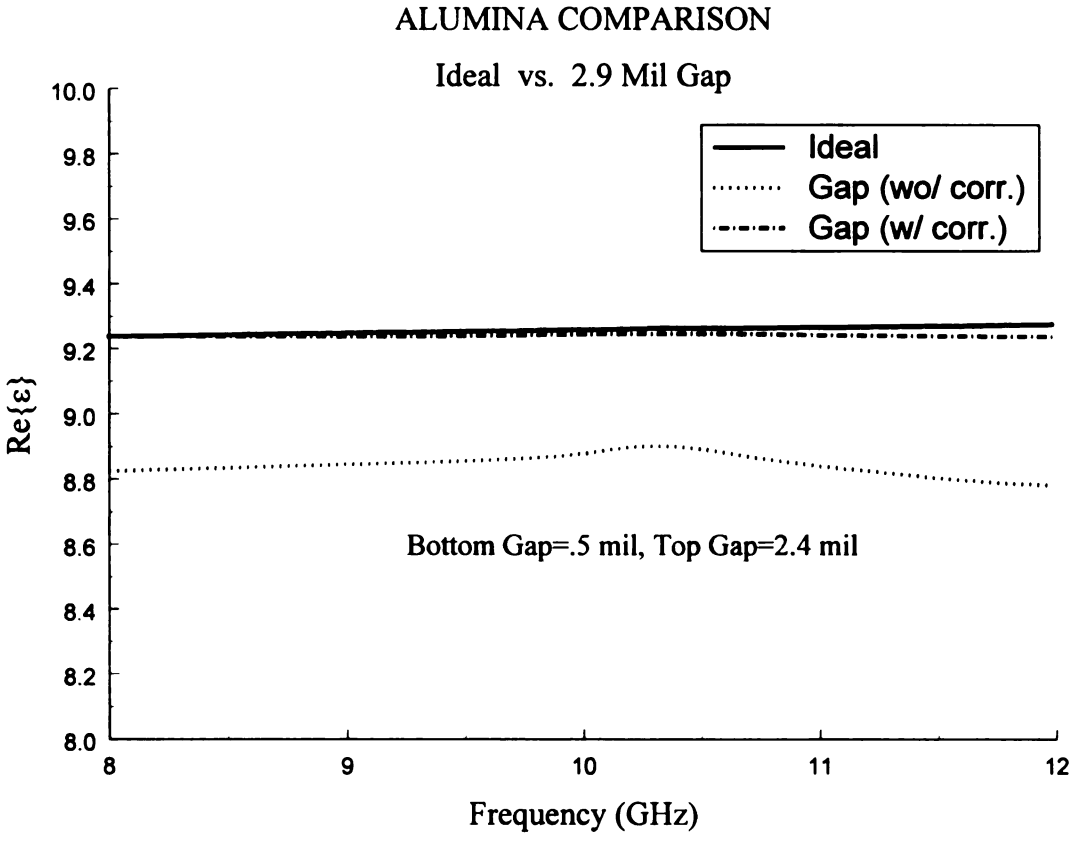

Figure 3.6 Experimental results of a *2.9* mil top/bottom gap for $\mathrm{Re}\{\varepsilon_r\}$.

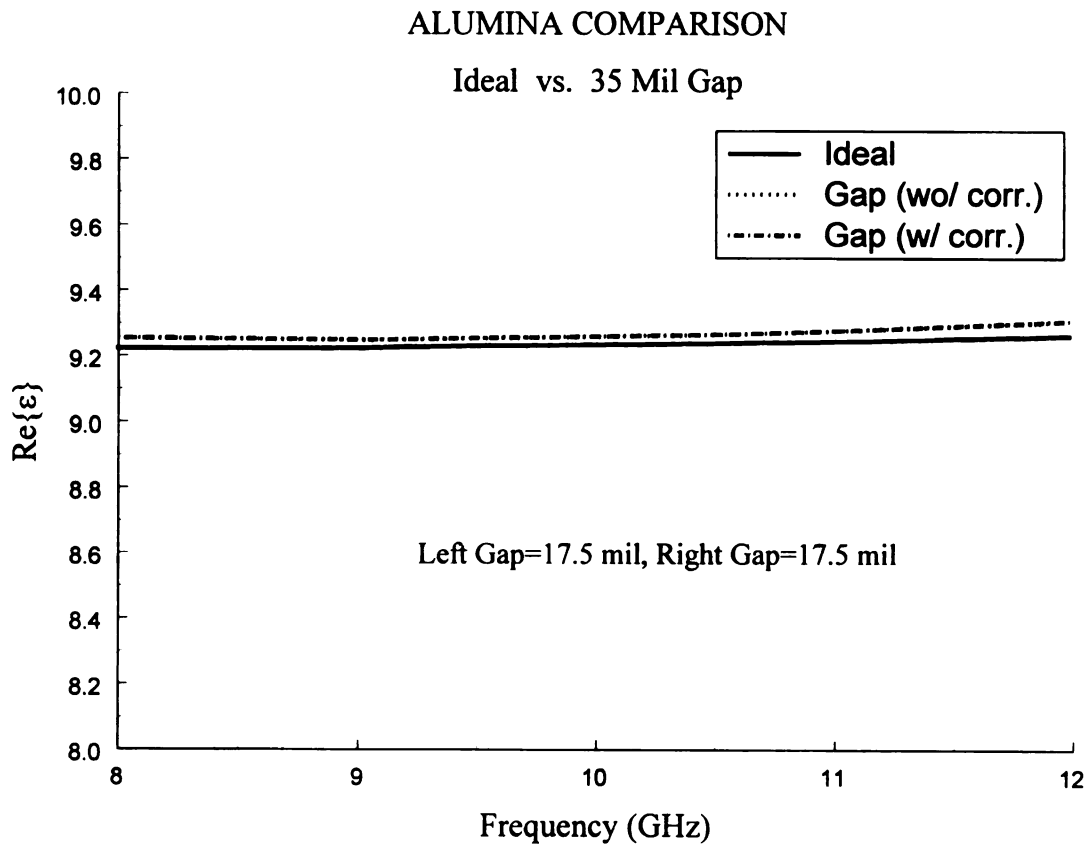

Figure 3.7 Experimental results of a *35* mil left/right gap for $\mathrm{Re}\{\varepsilon_r\}$.

Chapter 4

ACCOMMODATION OF WALL LOSS IN RECTANGULAR WAVEGUIDE MATERIAL CHARACTERIZATION MEASUREMENTS

4.1 Introduction

Imperfectly conducting walls can influence the accuracy of measured constitutive parameters in rectangular waveguide material characterization measurements. Wall loss effects become significant in the presence of materials having large permittivities or permeabilities and in high-temperature applications in which the waveguide material has relatively poor conductivity. The finite conductivity induces mode conversion and results in a shift of the ideal TE_{10} mode propagation constant.

Wall loss effects can be accounted for using a coupled-mode perturbation theory (specialized to single-mode operation) which is based upon an impedance boundary condition at the imperfectly-conducting waveguide walls. The result is a complex correction to the ideal TE_{10} propagation constant. Experimental results will be given and a comparison will be made with the standard power-loss method of attenuation correction.

4.2 Review of Attenuation Correction for the Ideal TE_{10} Propagation Constant

An expression for the conductor loss attenuation correction α_c to the ideal TE_{10} mode propagation constant can be obtained by considering the rate of decrease of power propagated along a finitely conducting line [17]. If the power at $z = 0$ is P_0, then at z it

is $P_z(z) = P_0 e^{-2\alpha_c z}$. Consequently, the conservation of energy requires

$$P_l(z) = -\frac{dP_z(z)}{dz} = 2\alpha_c P_z(z) \quad \Rightarrow \quad \alpha_c = \frac{P_l(z)}{2P_z(z)} = \frac{P_l(z=0)}{2P_z(z=0)} = \frac{P_{l0}}{2P_0} \tag{4.1}$$

where P_{l0} is the power loss/unit length at $z = 0$ due to finite conductivity and P_0 is the total axial power transport at $z = 0$. That is, the power loss along the line is equal to the rate of decrease of the power propagated along the line.

If the conductor loss is small, the fields will not be substantially perturbed from their loss-free values. Thus, an approximate expression for α_c can be obtained by using the known fields of the loss-free case. Finite (i.e., good) conductors exhibit a surface impedance (see appendix D)

$$Z_c = R_c + jX_c = (1+j)\sqrt{\frac{\omega\mu_c}{2\sigma_c}} \tag{4.2}$$

and the tangential fields satisfy the boundary condition

$$\vec{E}_{tang} = Z_c \hat{n} \times \vec{H}_{tang} = Z_c \vec{K} \tag{4.3}$$

Therefore, the power loss/unit length (i.e., the power transported normally into the conducting surface/unit length) can be written

$$\begin{aligned} P_{l0} &= -\frac{1}{2}\int_{CS} \mathrm{Re}\left\{\vec{E}_{tang} \times \vec{H}^*_{tang} \cdot \hat{n}\right\} dS = \frac{1}{2}\int_C \int_0^1 \mathrm{Re}\left\{\vec{E}_{tang} \cdot \hat{n} \times \vec{H}^*_{tang}\right\} dz dl \\ \therefore \quad P_{l0} &= \frac{R_c}{2}\int_C \left|\vec{K}\right|^2 dl = \frac{R_c}{2}\int_C \left|\hat{n} \times \vec{H}_{tang}\right|^2 dl = \frac{R_c}{2}\int_C \left|\vec{H}_{tang}\right|^2 dl \end{aligned} \tag{4.4}$$

where C is the periphery around the waveguide, $\hat{n}$ is the unit outward normal pointing from the conductor into the guiding region and $\vec{E}_{tang}, \vec{H}_{tang}$ are the unperturbed TE_{10} tangential fields relative to the conducting surface at location $z = 0$. The total axial

power transport at $z = 0$ is

$$P_0 = \frac{1}{2}\int_{CS} \mathrm{Re}\left\{\vec{E}_t \times \vec{H}_t^* \cdot \hat{z}\right\} dS = \frac{R_{10}}{2}\int_0^a\int_0^b \left|\hat{z} \times \vec{H}_t\right|^2 dxdy = \frac{R_{10}}{2}\int_0^a\int_0^b \left|\vec{H}_t\right|^2 dxdy \qquad (4.5)$$

where $\vec{E}_t, \vec{H}_t$ are the unperturbed TE_{10} transverse electromagnetic fields at $z = 0$, $R_{10} = \mathrm{Re}\{Z_{10}\} = \mathrm{Re}\{j\omega\mu/\gamma_{10}\}$ is the real part of the TE_{10} wave impedance with $\gamma_{10} = \sqrt{(\pi/a)^2 - k^2}$ and $\vec{E}_t = -Z_{10}\hat{z} \times \vec{H}_t$ is the relationship between the transverse field components.

The well-known unperturbed fields for the TE_{10} mode at $z = 0$ are

$$\begin{aligned} \vec{E} &= \hat{y}A\sin\frac{\pi x}{a} \\ \vec{H} &= -\hat{x}\frac{A}{Z_{10}}\sin\frac{\pi x}{a} - \hat{z}A\frac{\pi/a}{j\omega\mu}\cos\frac{\pi x}{a} \end{aligned} \qquad (4.6)$$

The power loss/unit length at $z = 0$ for the TE_{10} mode can therefore be written

$$P_{l0} = \frac{R_c}{2}\int_C \left|\vec{H}_{tang}\right|^2 dl = \frac{R_c}{2}\int_{\sum_{n=1}^4 C_n} \left|\vec{H}_{tang}\right|^2 dl \qquad (4.7)$$

where

$$\frac{R_c}{2}\int_{C_1} \left|\vec{H}_{tang}\right|^2 dl = \frac{R_c}{2}\int_0^a (H_x H_x^* + H_z H_z^*)\Big|_{y,z=0} dx = \frac{R_c}{2}\frac{AA^*}{\omega^2\mu\mu^*}\left(\frac{a}{2}\gamma_{10}\gamma_{10}^* + \frac{\pi^2}{2a}\right) \qquad (4.8)$$

$$\frac{R_c}{2}\int_{C_2} \left|\vec{H}_{tang}\right|^2 dl = \frac{R_c}{2}\int_0^b H_z H_z^*\Big|_{x=a,z=0} dy = \frac{R_c}{2}\frac{AA^*}{\omega^2\mu\mu^*}\left(b\frac{\pi^2}{a^2}\right) \qquad (4.9)$$

$$\frac{R_c}{2}\int_{C_3} \left|\vec{H}_{tang}\right|^2 dl = \frac{R_c}{2}\int_0^a (H_x H_x^* + H_z H_z^*)\Big|_{y=b,z=0} dx = \frac{R_c}{2}\frac{AA^*}{\omega^2\mu\mu^*}\left(\frac{a}{2}\gamma_{10}\gamma_{10}^* + \frac{\pi^2}{2a}\right) \qquad (4.10)$$

$$\frac{R_c}{2}\int_{C_4}\left|\vec{H}_{tang}\right|^2 dl = \frac{R_c}{2}\int_0^b H_z H_z^*\Big|_{x,z=0} dy = \frac{R_c}{2}\frac{AA^*}{\omega^2\mu\mu^*}\left(b\frac{\pi^2}{a^2}\right) \tag{4.11}$$

Therefore, the power loss/unit length is

$$P_{l0} = R_c\frac{AA^*}{\omega^2\mu\mu^*}\left(\frac{a}{2}\gamma_{10}\gamma_{10}^* + \frac{\pi^2}{2a} + b\frac{\pi^2}{a^2}\right) \tag{4.12}$$

The total axial power transport at $z = 0$ is

$$P_0 = \frac{R_{10}}{2}\int_0^a\int_0^b\left|\vec{H}_t\right|^2 dxdy = \frac{R_{10}}{2}\int_0^a\int_0^b H_x H_x^*\Big|_{z=0} dxdy = R_{10}\frac{AA^*}{\omega^2\mu\mu^*}\left(\frac{ab}{4}\gamma_{10}\gamma_{10}^*\right) \tag{4.13}$$

Thus, the attenuation constant due to conductor loss will be

$$\alpha_c = \frac{P_{l0}}{2P_0} = \frac{R_c\left(\frac{a}{2}\gamma_{10}\gamma_{10}^* + \frac{\pi^2}{2a} + b\frac{\pi^2}{a^2}\right)}{R_{10}\left(\frac{ab}{2}\gamma_{10}\gamma_{10}^*\right)} \tag{4.14}$$

which is in agreement with Collin [17] when the material medium inside the guide is lossless.

The overall perturbed propagation constant γ can therefore be written as

$$\gamma = \gamma_{10} + \alpha_c \tag{4.15}$$

Note that the power-loss method only results in a real correction to the ideal TE_{10} mode propagation constant. It will be shown in the following sections that a coupled-mode perturbation theory can be utilized to obtain a complex correction to the ideal propagation constant.

4.3 Accommodation of Wall Loss Using a Coupled-Mode Perturbation Theory

4.3.1 EM Field in Terms of the Transverse Electric Field

A guide with lossy walls will support hybrid modes, that is, the modes of propagation are combinations of TE and TM modes. Therefore, both h_z (the generating function for the TE modes) and e_z (the generating function for the TM modes) are involved. This combination is required to generate all field components necessary for satisfying boundary conditions. However, it can be shown that the transverse field $\vec{e}$ (or $\vec{h}$) alone is sufficient to generate all field components necessary for implementing boundary conditions.

Consider the electric and magnetic fields of a hybrid mode with propagation constant γ, namely

$$\vec{E} = \vec{e}(\vec{\rho})e^{-\gamma z} + \hat{z}e_z(\vec{\rho})e^{-\gamma z} \tag{4.16}$$

$$\vec{H} = \vec{h}(\vec{\rho})e^{-\gamma z} + \hat{z}h_z(\vec{\rho})e^{-\gamma z} \tag{4.17}$$

where $\vec{e}, \vec{h}$ are transverse fields, e_z, h_z are longitudinal fields and $\vec{\rho} = \hat{x}x + \hat{y}y$. Since $\nabla \cdot \vec{E} = (\nabla_t + \hat{z}\partial/\partial z) \cdot \vec{E} = 0$ in a source-free simple medium, we obtain the following longitudinal electric field component

$$e_z = \frac{1}{\gamma}\nabla_t \cdot \vec{e} \tag{4.18}$$

where $\nabla_t = \hat{x}\partial/\partial x + \hat{y}\partial/\partial y$. Substitution of (4.16) and (4.17) into Faraday's law, equating transverse and longitudinal field components and using the vector identity $\nabla_t \times \hat{z}e_z = -\hat{z} \times \nabla_t e_z$ in conjunction with (4.18) leads to the following result for the magnetic field components

$$\vec{h} = \frac{1}{j\omega\mu\gamma}\hat{z} \times \left(\nabla_t \nabla_t \cdot \vec{e} + \gamma^2 \vec{e}\right) \tag{4.19}$$

$$h_z = -\frac{1}{j\omega\mu}\hat{z}\cdot\nabla_t \times \vec{e} \tag{4.20}$$

Equations (4.18)-(4.20) show that all field components can indeed be generated by $\vec{e}$. In addition, the field $\vec{E}$ satisfies the Helmholtz equation $\nabla^2\vec{E} + k^2\vec{E} = 0$, which separates into the transverse and longitudinal wave equations given by

$$\nabla_t^2\vec{e} + (\gamma^2 + k^2)\vec{e} = 0 \tag{4.21}$$

$$\nabla_t^2 e_z + (\gamma^2 + k^2)e_z = 0 \tag{4.22}$$

4.3.2 Impedance Boundary Conditions on $\vec{E}$ in Terms of Transverse Field $\vec{e}$

The coupled-mode perturbation theory requires boundary conditions on the tangential components of $\vec{E}$ at the surface of the imperfectly-conducting waveguide walls based on $\vec{e}$ alone. If $\hat{n}$ is the unit normal pointing from the conductor into the guiding region, $\hat{\tau}$ is the unit tangent in the transverse plane and $\hat{z}$ is the unit tangent along the axial direction (where $\hat{\tau}\times\hat{n} = \hat{z}$ as shown in Figure 4.1), then the tangential boundary conditions can be found by investigating the relations $\hat{\tau}\cdot\vec{E}_{tang}$ and $\hat{z}\cdot\vec{E}_{tang}$. Note, of course, that $\hat{\tau}\cdot\vec{E}_{tang} = \hat{\tau}\cdot\vec{e}e^{-\gamma z}$ will have a transverse component only and $\hat{z}\cdot\vec{E}_{tang} = e_z e^{-\gamma z}$ will have only an axial (i.e., longitudinal) component.

The first boundary condition on $\vec{e}$ can be obtained by taking the dot product of $\hat{\tau}$ and equation (4.3), noting that $\hat{\tau}\cdot\hat{n}\times\vec{H}_{tang} = \hat{\tau}\times\hat{n}\cdot\vec{H}_{tang} = \hat{z}\cdot\vec{H}_{tang} = h_z e^{-\gamma z}$ and using the result from (4.20), leading to

$$\hat{\tau}\cdot\vec{E}_{tang} = Z_c\hat{\tau}\cdot\hat{n}\times\vec{H}_{tang} \quad\Rightarrow\quad \hat{\tau}\cdot\vec{e} = -\frac{Z_c}{j\omega\mu}\hat{z}\cdot\nabla_t\times\vec{e} \tag{4.23}$$

The second boundary condition on $\vec{e}$ is obtained by dotting $\hat{z}$ into (4.3). The left-hand side of this relation, with the aid of (4.18), is

$$\hat{z}\cdot\vec{E}_{tang} = e_z e^{-\gamma z} = \frac{1}{\gamma}\nabla_t\cdot\vec{e}e^{-\gamma z} \tag{4.24}$$

The right-hand side of $\hat{z}$ dotted into (4.3) is

$$Z_c\hat{z}\cdot\hat{n}\times\vec{H}_{tang} = Z_c\hat{z}\times\hat{n}\cdot\vec{H}_{tang} = -Z_c\hat{\tau}\cdot\vec{H}_{tang} = -Z_c\hat{\tau}\cdot\vec{h}e^{-\gamma z} \tag{4.25}$$

Substitution of (4.19) into (4.25) gives

$$\begin{aligned} -Z_c\hat{\tau}\cdot\vec{h}e^{-\gamma z} &= -\frac{Z_c}{j\omega\mu\gamma}\hat{\tau}\cdot\hat{z}\times\left(\nabla_t\nabla_t\cdot\vec{e}+\gamma^2\vec{e}\right)e^{-\gamma z} \\ = -\frac{Z_c}{j\omega\mu\gamma}\hat{\tau}\times\hat{z}\cdot\left(\nabla_t\nabla_t\cdot\vec{e}+\gamma^2\vec{e}\right)e^{-\gamma z} &= \frac{Z_c}{j\omega\mu\gamma}\hat{n}\cdot\left(\nabla_t\nabla_t\cdot\vec{e}+\gamma^2\vec{e}\right)e^{-\gamma z} \end{aligned} \tag{4.26}$$

since $\hat{\tau}\times\hat{z} = -\hat{n}$. Using the identity $\nabla_t\nabla_t\cdot\vec{e} = \nabla_t\times\nabla_t\times\vec{e}+\nabla_t^2\vec{e}$ and (4.21) allows (4.26) to be written as

$$Z_c\hat{z}\cdot\hat{n}\times\vec{H}_{tang} = -Z_c\hat{\tau}\cdot\vec{h}e^{-\gamma z} = \frac{Z_c}{j\omega\mu\gamma}\hat{n}\cdot\left(\nabla_t\times\nabla_t\times\vec{e}-k^2\vec{e}\right)e^{-\gamma z} \tag{4.27}$$

Thus, the second boundary condition on $\vec{e}$ is

$$\hat{z}\cdot\vec{E}_{tang} = Z_c\hat{z}\cdot\hat{n}\times\vec{H}_{tang} \quad\Rightarrow\quad \nabla_t\cdot\vec{e} = \frac{Z_c}{j\omega\mu}\hat{n}\cdot\left(\nabla_t\times\nabla_t\times\vec{e}-k^2\vec{e}\right) \tag{4.28}$$

Note, when the walls are perfectly conducting, $Z_c = 0$ (since $\sigma_c\to\infty$) and the boundary conditions of (4.23) and (4.28) simplify to the expected well-known result

$$\left.\begin{aligned}\hat{\tau}\cdot\vec{e} &= 0\\ \nabla_t\cdot\vec{e} = \gamma e_z &= 0\end{aligned}\right\} \text{ or } \hat{n}\times\vec{e} = 0 \ \ldots \textit{for } \sigma_c\to\infty \tag{4.29}$$

4.3.3 Coupled-Mode Perturbation Theory

The next step in the analysis is to expand $\vec{e}$ in terms of the normal mode

functions for the same guide with perfectly-conducting walls, that is

$$\vec{e} = \sum_{n=1}^{\infty} a_n \vec{e}_n \tag{4.30}$$

The sum is extended over all the TE and TM modes, a_n is an unknown amplitude coefficient and $\vec{e}_n$ is the transverse electric field for a given mode in the lossless (i.e., ideal) guide which satisfies the wave equation

$$\nabla_t^2 \vec{e}_n + (\Gamma_n^2 + k^2)\vec{e}_n = 0 \tag{4.31}$$

where Γ_n is the ideal-mode propagation constant. It will be assumed that the normal mode functions $\vec{e}_n$ have been normalized in the following manner

$$\int_{CS} \vec{e}_j . \vec{e}_n dS = \delta_{jn} = \begin{cases} 1 & \ldots n = j \\ 0 & \ldots n \neq j \end{cases} \tag{4.32}$$

Hence, the mode functions form an orthonormal set. Note, $\vec{e}_j$ satisfies a wave equation similar to (4.31), that is

$$\nabla_t^2 \vec{e}_j + (\Gamma_j^2 + k^2)\vec{e}_j = 0 \tag{4.33}$$

The unknown amplitude coefficients are given by

$$a_n = \int_{CS} \vec{e} \cdot \vec{e}_n dS \tag{4.34}$$

where $\vec{e}$ is the actual transverse electric field in the lossy guide and $\vec{e}_n$ is the transverse electric field of the n^{th} mode in the ideal lossless guide. This result is obtained by dotting $\vec{e}_j$ into equation (4.30), integrating over the guide cross-section and using (4.32).

The coefficients a_n and hybrid-mode propagation constant γ can be determined in the following manner. First, scalar multiply (4.21) by $\vec{e}_j$ and (4.33) by $\vec{e}$, subtract the

two resulting equations and integrate over the guide cross section. This leads to

$$(\gamma^2 - \Gamma_j^2) \int_{CS} \vec{e} \cdot \vec{e}_j dS = (\gamma^2 - \Gamma_j^2) a_j = \int_{CS} (\vec{e} \cdot \nabla_t^2 \vec{e}_j - \vec{e}_j \cdot \nabla_t^2 \vec{e}) dS \tag{4.35}$$

The surface integral on the right-hand side of (4.35) can be converted into a contour integral using the vector relation [3]

$$\begin{aligned} &\int_{CS} (\vec{B} \cdot \nabla_t^2 \vec{A} - \vec{A} \cdot \nabla_t^2 \vec{B}) dS \\ &= \oint_C [(\hat{n} \times \vec{A}) \cdot (\nabla_t \times \vec{B}) + \hat{n} \times (\nabla_t \times \vec{A}) \cdot \vec{B} + (\hat{n} \cdot \vec{A}) \nabla_t \cdot \vec{B} - (\hat{n} \cdot \vec{B}) \nabla_t \cdot \vec{A}] dl \end{aligned} \tag{4.36}$$

where $\hat{n}$ is the unit normal pointing from the conductor boundary into the guiding region. Letting $\vec{A} = \vec{e}_j$ and $\vec{B} = \vec{e}$ in (4.36) allows (4.35) to be written as

$$(\gamma^2 - \Gamma_j^2) a_j = \oint_C [(\hat{n} \times \vec{e}_j) \cdot (\nabla_t \times \vec{e}) + \hat{n} \times (\nabla_t \times \vec{e}_j) \cdot \vec{e} + (\hat{n} \cdot \vec{e}_j) \nabla_t \cdot \vec{e} - (\hat{n} \cdot \vec{e}) \nabla_t \cdot \vec{e}_j] dl \tag{4.37}$$

The tangential electric field components for the lossless guide are zero on the boundary, that is

$$\hat{n} \times \vec{e}_j = 0 \quad , \quad e_{zj} = \frac{1}{\Gamma_j} \nabla_t \cdot \vec{e}_j = 0 \tag{4.38}$$

and equation (4.37) therefore simplifies to

$$(\gamma^2 - \Gamma_j^2) a_j = \oint_C [\hat{n} \times (\nabla_t \times \vec{e}_j) \cdot \vec{e} + (\hat{n} \cdot \vec{e}_j) \nabla_t \cdot \vec{e}] dl \tag{4.39}$$

An expression for the first term of the contour integral in (4.39) can be found by using the relation $\nabla_t \times \vec{e}_j = -\hat{z} j\omega\mu h_{zj}$ (from Faraday's law) and equation (4.23). This produces, with the aid of $\hat{n} \times \hat{z} = \hat{\tau}$, the result

$$\hat{n} \times (\nabla_t \times \vec{e}_j) \cdot \vec{e} = -j\omega\mu h_{zj} \hat{\tau} \cdot \vec{e} = Z_c h_{zj} \hat{z} \cdot (\nabla_t \times \vec{e}) = -\frac{Z_c}{j\omega\mu} (\nabla_t \times \vec{e}_j) \cdot (\nabla_t \times \vec{e}) \tag{4.40}$$

The final step involves the substitution of (4.40), (4.28) and (4.30) into (4.39), leading to

$$(\gamma^2-\Gamma_j^2)a_j=-\frac{Z_c}{j\omega\mu}\oint_C[(\nabla_t\times\vec{e}_j)\cdot(\nabla_t\times\vec{e})-(\hat{n}\cdot\vec{e}_j)(\hat{n}\cdot\nabla_t\times\nabla_t\times\vec{e}-k^2\hat{n}\cdot\vec{e})]dl \quad (4.41)$$

$$\therefore\quad (\gamma^2-\Gamma_j^2)a_j=-\frac{Z_c}{j\omega\mu}\sum_{n=1}^{\infty}a_n\oint_C[(\nabla_t\times\vec{e}_j)\cdot(\nabla_t\times\vec{e}_n) -(\hat{n}\cdot\vec{e}_j)(\hat{n}\cdot\nabla_t\times\nabla_t\times\vec{e}_n-k^2\hat{n}\cdot\vec{e}_n)]dl \quad ...j=1,2,3,... \quad (4.42)$$

Equation (4.42) can be cast into the following matrix form

$$[M][a]=[0] \quad (4.43)$$

where

$$M_{jn}=\frac{Z_c}{j\omega\mu}\oint_C[(\nabla_t\times\vec{e}_j)\cdot(\nabla_t\times\vec{e}_n)-(\hat{n}\cdot\vec{e}_j)(\hat{n}\cdot\nabla_t\times\nabla_t\times\vec{e}_n-k^2\hat{n}\cdot\vec{e}_n)]dl \quad ...j\neq n \quad (4.44)$$

$$M_{jj}=\gamma^2-\Gamma_j^2+\frac{Z_c}{j\omega\mu}\oint_C[(\nabla_t\times\vec{e}_j)\cdot(\nabla_t\times\vec{e}_j)-(\hat{n}\cdot\vec{e}_j)(\hat{n}\cdot\nabla_t\times\nabla_t\times\vec{e}_j-k^2\hat{n}\cdot\vec{e}_j)]dl \quad (4.45)$$

$$[a]=\begin{bmatrix}a_1\\a_2\\\vdots\end{bmatrix} \quad (4.46)$$

Note, when the walls become perfectly conducting (i.e., $Z_c=0$), equation (4.42) implies that $\gamma^2=\Gamma_j^2$ as expected.

The above result represents an infinite set of equations for the unknown coefficients a_n. An examination of (4.43) shows that a solution for the a_n exists only if the determinant vanishes. This leads to a characteristic equation that has an infinite number of roots for γ^2, which corresponds with the infinite number of hybrid modes that may exist in the lossy guide. For each root of γ^2, a set of coefficients a_n is obtained, and it is these coefficients that determine the field configuration of the particular hybrid

mode.

4.3.4 Complex Correction to the Ideal TE_{10} Mode Propagation Constant

In practice, the expansion in (4.30) must be truncated in order to obtain a finite number of equations. Equation (4.42) reveals that all the coefficients are small except those for which $\gamma^2 \approx \Gamma_j^2$, thus an approximate expression for γ^2 can be found by including only a single mode in the expansion. Since we are interested in how the propagation constant of the TE_{10} mode is perturbed, this suggests making the following choice

$$\vec{e}_j = \vec{e}_n = \vec{e}_1 = \hat{y}\sqrt{\frac{2}{ab}}\sin\frac{\pi x}{a} \quad , \quad \Gamma_1 = \gamma_{10} = \sqrt{(\pi/a)^2 - k^2} \tag{4.47}$$

where $\vec{e}_1$ and Γ_1 are the ideal TE_{10} transverse electric field and propagation constant, respectively. For this single-mode case, equation (4.43) reduces to

$$M_{11}a_1 = 0 \quad \Rightarrow \quad M_{11} = 0 \tag{4.48}$$

Substitution of (4.45) into (4.48) leads to the following approximate expression for the hybrid-mode propagation constant

$$\gamma^2 \approx \gamma_{10}^2 + \delta\gamma^2 \tag{4.49}$$

where the complex correction $\delta\gamma^2$ to the ideal TE_{10} propagation constant γ_{10}^2 is given by

$$\delta\gamma^2 = -\frac{Z_c}{j\omega\mu}\oint_C [(\nabla_t \times \vec{e}_1)\cdot(\nabla_t \times \vec{e}_1) - (\hat{n}\cdot\vec{e}_1)(\hat{n}\cdot\nabla_t \times \nabla_t \times \vec{e}_1 - k^2\hat{n}\cdot\vec{e}_1)]dl \tag{4.50}$$

If a rectangular guide having width a and height b is considered, then integration along the bottom (contour C_1 where $\hat{n} = \hat{y}$, $y = 0$ and $dl = dx$), right (contour C_2 where $\hat{n} = -\hat{x}$, $x = a$ and $dl = dy$), top (contour C_3 where $\hat{n} = -\hat{y}$, $y = b$ and $dl = dx$) and left

(contour C_4 where $\hat{n}=\hat{x}$, $x=0$ and $dl=dy$) boundaries leads to the following result

$$\int_{C_1}[(\nabla_t\times\vec{e}_1)\cdot(\nabla_t\times\vec{e}_1)-(\hat{n}\cdot\vec{e}_1)(\hat{n}\cdot\nabla_t\times\nabla_t\times\vec{e}_1-k^2\hat{n}\cdot\vec{e}_1)]\Big|_{y=0}dl$$
$$=\int_0^a[(\nabla_t\times\vec{e}_1)\cdot(\nabla_t\times\vec{e}_1)-(\hat{y}\cdot\vec{e}_1)(\hat{y}\cdot\nabla_t\times\nabla_t\times\vec{e}_1-k^2\hat{y}\cdot\vec{e}_1)]\Big|_{y=0}dx=\frac{k^2}{b} \tag{4.51}$$

$$\int_{C_2}[(\nabla_t\times\vec{e}_1)\cdot(\nabla_t\times\vec{e}_1)-(\hat{n}\cdot\vec{e}_1)(\hat{n}\cdot\nabla_t\times\nabla_t\times\vec{e}_1-k^2\hat{n}\cdot\vec{e}_1)]\Big|_{x=a}dl$$
$$=\int_0^b(\nabla_t\times\vec{e}_1)\cdot(\nabla_t\times\vec{e}_1)\big|_{x=a}dy=\frac{2\pi^2}{a^3} \tag{4.52}$$

$$\int_{C_3}[(\nabla_t\times\vec{e}_1)\cdot(\nabla_t\times\vec{e}_1)-(\hat{n}\cdot\vec{e}_1)(\hat{n}\cdot\nabla_t\times\nabla_t\times\vec{e}_1-k^2\hat{n}\cdot\vec{e}_1)]\Big|_{y=b}dl=\frac{k^2}{b} \tag{4.53}$$

$$\int_{C_4}[(\nabla_t\times\vec{e}_1)\cdot(\nabla_t\times\vec{e}_1)-(\hat{n}\cdot\vec{e}_1)(\hat{n}\cdot\nabla_t\times\nabla_t\times\vec{e}_1-k^2\hat{n}\cdot\vec{e}_1)]\Big|_{x=0}dl=\frac{2\pi^2}{a^3} \tag{4.54}$$

Substitution of (4.51)-(4.54) into (4.50) produces the final desired result

$$\delta\gamma^2=-\frac{Z_c}{j\omega\mu}\left(\frac{4\pi^2}{a^3}+\frac{2k^2}{b}\right) \tag{4.55}$$

$$\gamma=\sqrt{\gamma_{10}^2-\frac{Z_c}{j\omega\mu}\left(\frac{4\pi^2}{a^3}+\frac{2k^2}{b}\right)}\quad,\quad\gamma_{10}^2=\frac{\pi^2}{a^2}-k^2 \tag{4.56}$$

Note, the ideal propagation constant is recovered if the walls are lossless (i.e., $Z_c=0$).

The coupled-mode perturbation theory has several advantages over the power-loss method. First, the coupled-mode perturbation theory resulted in both an attenuation and phase constant correction to the ideal TE_{10} mode propagation constant whereas the power-loss method produced only an attenuation correction. The additional phase correction is important in material characterization measurements. Secondly, it is

observed that the attenuation correction term from the power-loss method approaches infinity at the cut-off frequency since axial power transport ceases. The more rigorous coupled-mode perturbation theory shows that infinite values of attenuation do not occur. From a physical viewpoint, the presence of finite conductivity results in a coupling between the TE and TM modes, and propagation along the guide does not stop at a particular frequency. Hence, there is finite axial power transport, resulting in finite attenuation. Lastly, the coupled-mode perturbation theory can easily accommodate attenuation due to degenerate modes while the power-loss method cannot. If two or more modes are present simultaneously, the power-loss method can be applied to each mode individually, provided the axial power transport and power loss are the sum of those contributed by each mode. That is, the power-loss method can be applied if the modes are not strongly coupled. However, strong coupling does occur when the modes are degenerate, thus the power-loss method breaks down. Mode degeneracy is inherently accounted for in the coupled-mode perturbation theory.

4.4 Experimental Results

Figures 4.2 and 4.3 show a comparison between the power-loss and coupled-mode perturbation theories for an Alumina material characterization measurement. The Alumina sample (of thickness $\ell = 0.1314\ cm$) was initially placed inside a silver-plated rectangular waveguide holder having conductivity $\sigma_c = 6.1\times10^7\ [S/m]$ and the permittivity was subsequently computed. This measurement constitutes the ideal case in Figures 4.2 and 4.3. Next, the sample was removed from the ideal silver-plated sample holder and placed into a high-temperature rectangular waveguide having a conductivity

$\sigma_c = 3\times10^5$ $[S/m]$. The scattering parameters were then measured and the permittivity computed using no wall loss correction, the power-loss method of attenuation correction and the coupled-mode theory of attenuation and phase correction. Figures 4.2 and 4.3 reveal how critical the additional phase correction can be in material characterization measurements.

The second set of measurements in Figures 4.4 and 4.5 demonstrates the sensitivity of the material characterization process on the conductivity of the waveguide holder. A high dielectric resistive-card sample (having a thickness of .004 *in.*) was placed into the silver-plated rectangular waveguide holder and the real and imaginary permittivity was computed using the conductivities of $\sigma_c = 6.1e7$, $\sigma_c = 1e4$ and $\sigma_c = 1e3$. Figures 4.4 and 4.5 show that errors on the order of 10% can occur if precise knowledge of the waveguide conductivity is not known. Thus, wall loss correction can be a critical factor in the material characterization process.

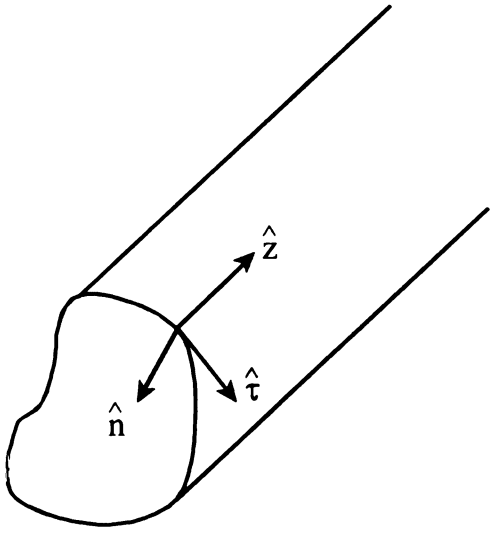

Figure 4.1 Defined unit vectors for a uniform waveguide.

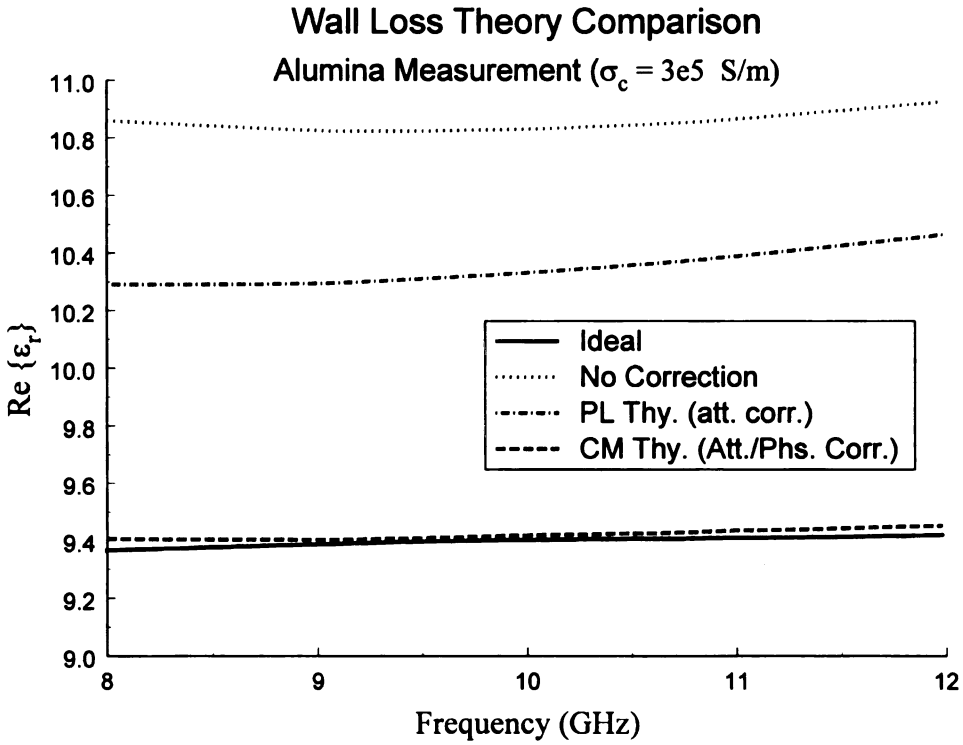

Figure 4.2 Wall loss theory comparison for $\mathrm{Re}\{\varepsilon_r\}$ using Alumina.

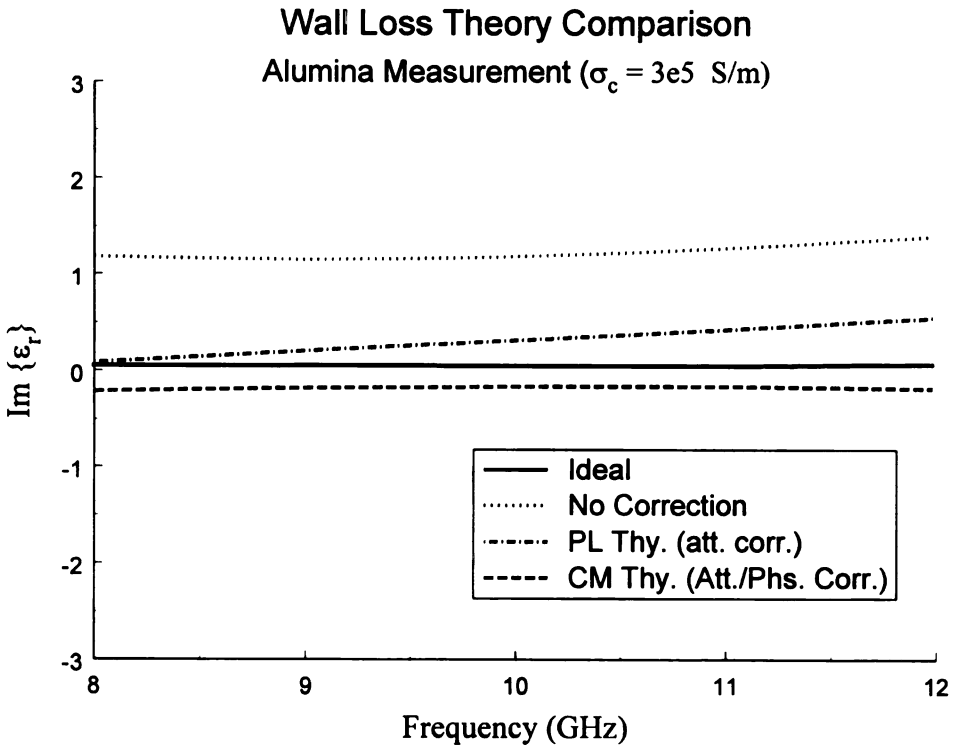

Figure 4.3 Wall loss theory comparison for Im$\{\varepsilon_r\}$ using Alumina.

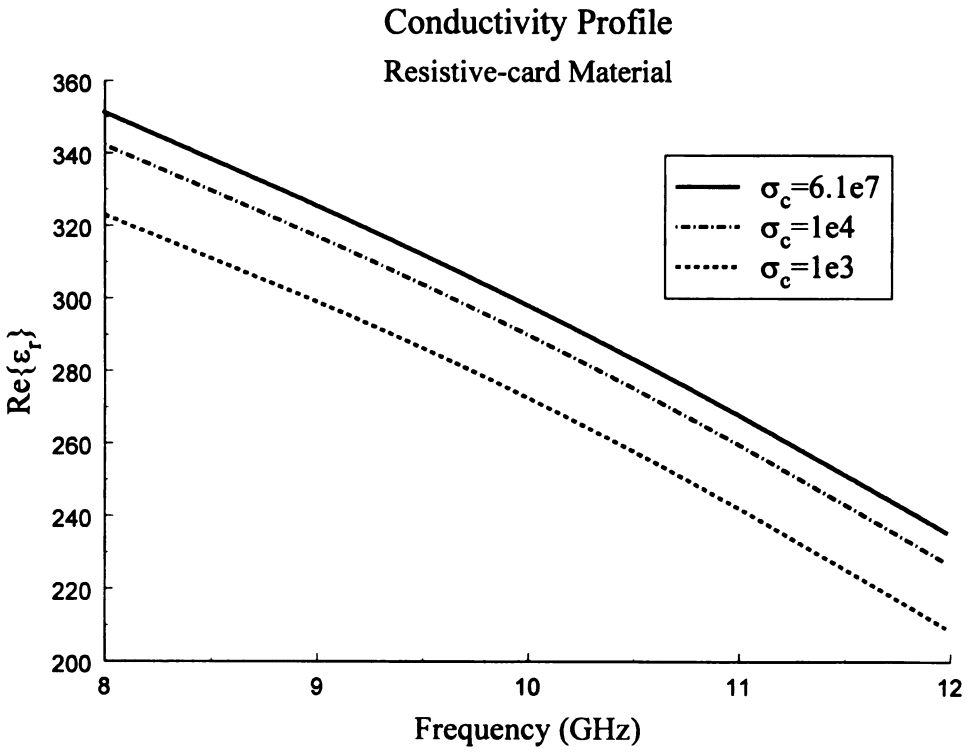

Figure 4.4 Conductivity profile of $\mathrm{Re}\{\varepsilon_r\}$ for a resistive-card material.

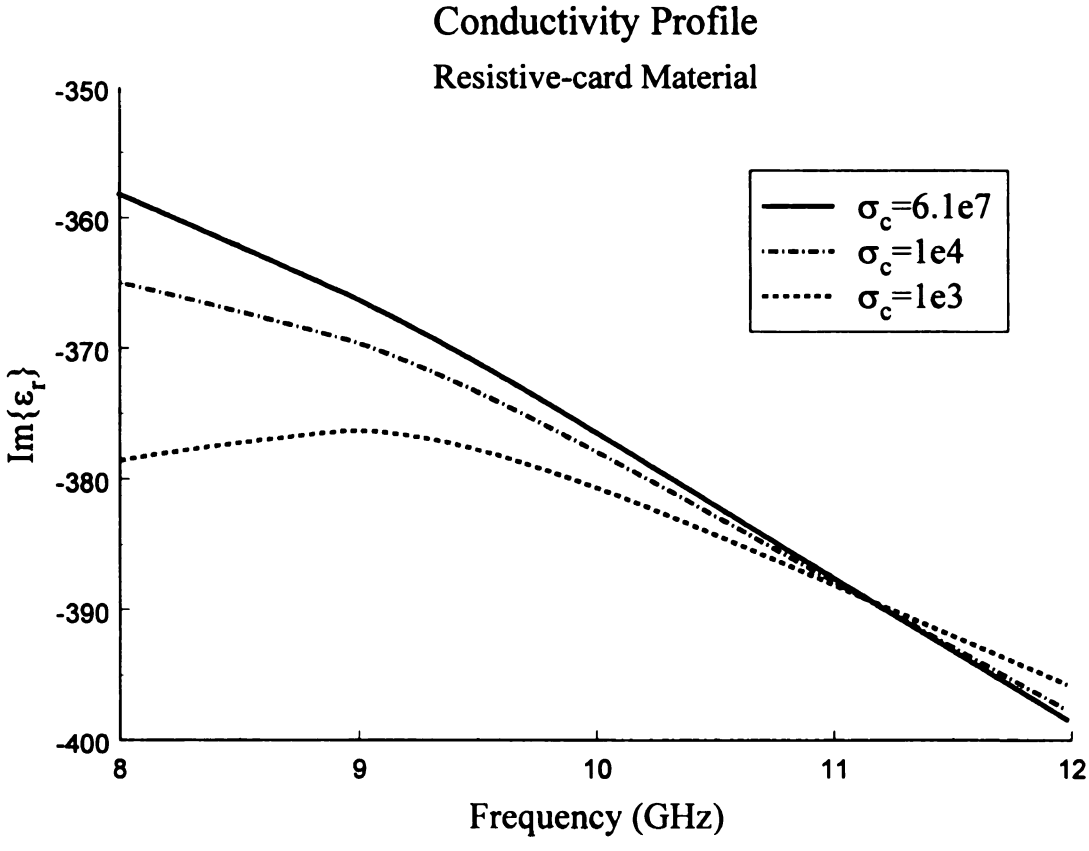

Figure 4.5 Conductivity profile of $\mathrm{Im}\{\varepsilon_r\}$ for a resistive-card material.

Chapter 5

GREEN'S FUNCTION FOR EM FIELD WITHIN AN IMPERFECTLY-CONDUCTING PARALLEL-PLATE ENVIRONMENT

5.1 Introduction

In this chapter, the Hertzian-potential and electric and magnetic-field dyadic Green's functions [30] are found for a general 3D current source immersed within an imperfectly-conducting parallel-plate environment. This analysis will be utilized in Chapter 6 to understand the effect of wall loss for a stripline field applicator. The above Green's functions will be determined using two methods. The first method consists of analyzing a symmetric slab waveguide and investigating the limiting case where the outer regions (having conductivity σ_c and permittivity $\tilde{\varepsilon}_c$) become good conductors [$\sigma_c / \omega\tilde{\varepsilon}_c \gg 1 \Rightarrow \varepsilon_c = \tilde{\varepsilon}_c(1 - j\sigma_c / \omega\tilde{\varepsilon}_c) \rightarrow -j\sigma_c / \omega$, where ε_c is the effective complex permittivity]. The second method utilizes Hertzian-potential impedance boundary conditions.

5.2 Geometrical Configuration

Figure 5.1 shows the geometry of the parallel-plate environment. Regions 1 and 3 comprise the outer portion of the structure and region 2 the inner portion. A general 3D electric current source $\vec{J}$ is immersed only within region 2. The structure (but not the current) is invariant along the x and z axis. The total height of the inner region is $2h$ and is centered about $y = 0$. The effective complex permittivities of the outer (i.e.,

cover) regions are assumed to be identical, that is, $\varepsilon_1 = \varepsilon_3 = \varepsilon_c = \tilde{\varepsilon}_c(1 - j\sigma_c / \omega\tilde{\varepsilon}_c)$, and the effective complex permittivity of the inner region is $\varepsilon_2 = \varepsilon = \tilde{\varepsilon}(1 - j\sigma / \omega\tilde{\varepsilon})$. All three regions are assumed to be non-magnetic ($\mu_1 = \mu_2 = \mu_3 = \mu_0$).

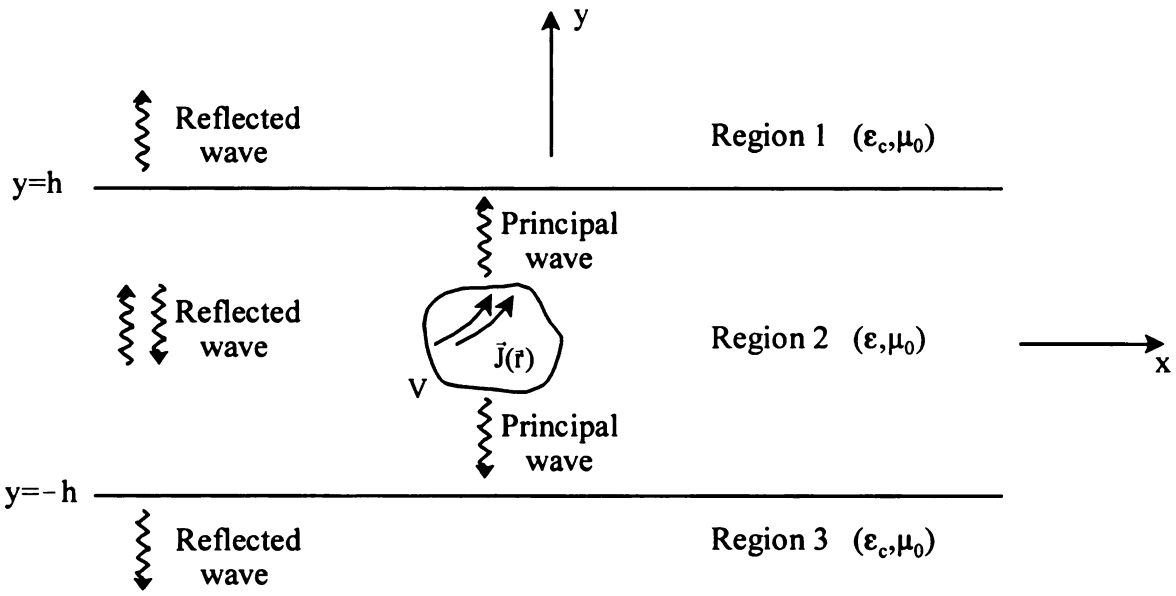

Figure 5.1 Parallel-plate environment with general 3D current $\vec{J}(\vec{r})$.

5.3 EM Fields and Helmholtz Equation for Hertzian Potential

The electric and magnetic-field dyadic Green's functions $\bar{\bar{G}}^e(\vec{r}|\vec{r}')$ and $\bar{\bar{G}}^h(\vec{r}|\vec{r}')$ can be identified by using a Hertzian potential $\vec{\pi}$ as an intermediate step (see Appendix A for further details). One reason for using a Hertzian potential is that $\bar{\bar{G}}^e$ and $\bar{\bar{G}}^h$ are more readily determined by first solving the Hertzian potential wave equation

$$\nabla^2\vec{\pi} + k^2\vec{\pi} = -\frac{\vec{J}}{j\omega\varepsilon} \tag{5.1}$$

and then computing $\vec{E}$ and $\vec{H}$ using

$$\vec{E} = k^2\vec{\pi} + \nabla(\nabla\bullet\vec{\pi}) \tag{5.2}$$

$$\vec{H} = j\omega\varepsilon\nabla\times\vec{\pi} \tag{5.3}$$

The alternative is to identify $\ddot{G}^e$ and $\ddot{G}^h$ by directly solving the wave equations for $\vec{E}$ and $\vec{H}$, that is

$$\nabla^2\vec{E} + k^2\vec{E} = j\omega\mu\vec{J} - \frac{1}{j\omega\varepsilon}\nabla(\nabla\bullet\vec{J}) \tag{5.4}$$

$$\nabla^2\vec{H} + k^2\vec{H} = -\nabla\times\vec{J} \tag{5.5}$$

The Hertzian potential approach is easier to implement since a simpler relationship exists between $\vec{\pi}$ and $\vec{J}$ in (5.1) than $\vec{E}, \vec{H}$ and $\vec{J}$ in (5.4) and (5.5).

Another motivation for using a Hertzian potential is that $\vec{\pi}$ is less singular than $\vec{E}$ or $\vec{H}$. It will be shown that this leads to, in a mathematically straight-forward manner, expressions for $\ddot{G}^e$ and $\ddot{G}^h$ that are valid both inside and outside the source region. Thus, the electric and magnetic-field dyadic Green's functions will be found by first determining $\vec{\pi}$ using (5.1) and then computing $\vec{E}$ and $\vec{H}$ from equations (5.2) and (5.3).

5.4 Spectral Representation of Principal and Scattered Waves

5.4.1 General Formulation

As mentioned in section 5.3, the solution to equation (5.1) needs to be determined. This solution can be found using the superposition of a principal wave $\vec{\pi}^p$ emanating from the source $\vec{J}$ in unbounded space (having effective complex permittivity

ε) and waves $\vec{\pi}^r$ that are reflected from the introduction of boundaries at $y = \pm h$ with the source removed (see Figure 5.1). This method is often used in the solution of differential equations, where the principal wave is called the particular solution and the reflected wave is referred to as the homogeneous (or complementary) solution. The total solution for $\vec{\pi}$ in each respective region will therefore be

$$\vec{\pi}_1 = \vec{\pi}_1^r \tag{5.6}$$

$$\vec{\pi}_2 = \vec{\pi}_2^p + \vec{\pi}_2^r \tag{5.7}$$

$$\vec{\pi}_3 = \vec{\pi}_3^r \tag{5.8}$$

where $\vec{\pi}_2^p$ and $\vec{\pi}_\beta^r$ ($\beta = 1,2,3$) satisfy the respective Hertzian potential wave equations

$$\nabla^2 \vec{\pi}_2^p + k_2^2 \vec{\pi}_2^p = -\frac{\vec{J}}{j\omega\varepsilon_2} \tag{5.9}$$

$$\nabla^2 \vec{\pi}_\beta^r + k_\beta^2 \vec{\pi}_\beta^r = 0 \tag{5.10}$$

where $k_1^2 = k_3^2 = k_c^2 = \omega^2 \varepsilon_c \mu_0$, $k_2^2 = k^2 = \omega^2 \varepsilon \mu_0$ and $\varepsilon_2 = \varepsilon$. The principal wave contributes only in the inner region since it has been assumed that $\vec{J}$ is strictly confined within region 2. Although the structure is symmetric about $y = 0$, the current is generally not, thus no mathematical simplification can be used in the analysis that follows.

Equations (5.9) and (5.10) can be decomposed into 3 scalar equations each, thus solutions must be found for the following equations

$$\nabla^2 \pi_{2\alpha}^p(\vec{r}) + k^2 \pi_{2\alpha}^p(\vec{r}) = -\frac{J_\alpha(\vec{r})}{j\omega\varepsilon} \tag{5.11}$$

$$\nabla^2 \pi_{\beta\alpha}^r(\vec{r}) + k_\beta^2 \pi_{\beta\alpha}^r(\vec{r}) = 0 \tag{5.12}$$

where $\alpha = x, y, z$ and $\beta = 1,2,3$. The Fourier transform domain method will be employed here to solve these equations. The background structure is invariant along the x and z directions, which prompts transformation on those variables using the generic 2D Fourier transform pair

$$\tilde{f}(\vec{\lambda}, y) = \int_{-\infty}^{\infty}\int_{-\infty}^{\infty} f(\vec{r}) e^{-j\vec{\lambda}\bullet\vec{r}}\, dxdz \tag{5.13}$$

$$f(\vec{r}) = \frac{1}{(2\pi)^2}\int_{-\infty}^{\infty}\int_{-\infty}^{\infty} \tilde{f}(\vec{\lambda}, y) e^{j\vec{\lambda}\bullet\vec{r}}\, d^2\lambda \tag{5.14}$$

where $\vec{\lambda} = \hat{x}\xi + \hat{z}\zeta$ $(\Rightarrow \lambda^2 = \vec{\lambda}\bullet\vec{\lambda} = \xi^2 + \zeta^2)$, $\vec{r} = \hat{x}x + \hat{y}y + \hat{z}z$ and $d^2\lambda = d\xi d\zeta$. Transformation with respect to y is avoided at this point so that boundary conditions can be enforced at $y = \pm h$. Applying the Fourier transform differentiation theorem, equations (5.11) and (5.12) become

$$\frac{\partial^2 \tilde{\pi}^p_{2\alpha}(\vec{\lambda}, y)}{\partial y^2} - p_2^2 \tilde{\pi}^p_{2\alpha}(\vec{\lambda}, y) = -\frac{\tilde{J}_\alpha(\vec{\lambda}, y)}{j\omega\varepsilon} \tag{5.15}$$

$$\frac{\partial^2 \tilde{\pi}^r_{\beta\alpha}(\vec{\lambda}, y)}{\partial y^2} - p_\beta^2 \tilde{\pi}^r_{\beta\alpha}(\vec{\lambda}, y) = 0 \tag{5.16}$$

where $p_1 = p_3 = p_c = \sqrt{\lambda^2 - k_c^2}$, $p_2 = p = \sqrt{\lambda^2 - k^2}$ with $\mathrm{Re}\{p_\beta\} > 0$ chosen and

$$\tilde{\pi}^p_{2\alpha}(\vec{\lambda}, y) = \int_{-\infty}^{\infty}\int_{-\infty}^{\infty} \pi^p_{2\alpha}(\vec{r}) e^{-j\vec{\lambda}\bullet\vec{r}}\, dxdz \tag{5.17}$$

$$\tilde{\pi}^r_{\beta\alpha}(\vec{\lambda}, y) = \int_{-\infty}^{\infty}\int_{-\infty}^{\infty} \pi^r_{\beta\alpha}(\vec{r}) e^{-j\vec{\lambda}\bullet\vec{r}}\, dxdz \tag{5.18}$$

$$\tilde{J}_\alpha(\vec{\lambda}, y) = \int_{-\infty}^{\infty}\int_{-\infty}^{\infty} J_\alpha(\vec{r}) e^{-j\vec{\lambda}\bullet\vec{r}}\, dxdz \tag{5.19}$$

The general form of the solution to equation (5.15) in the central region (i.e., region 2) and equation (5.16) in regions 1, 2 and 3 will be investigated in sections 5.4.2 and 5.4.3.

5.4.2 Principal Wave Representation

The principle wave satisfies equation (5.15) for all unbounded space (i.e., in the absence of boundaries), as dictated by the superposition method of solution. This prompts transformation on the y-variable in equation (5.15), leading to (with the aid of the differentiation theorem)

$$-\eta^2 \tilde{\tilde{\pi}}_{2\alpha}^{p}(\vec{\lambda},\eta) - p^2 \tilde{\tilde{\pi}}_{2\alpha}^{p}(\vec{\lambda},\eta) = -\frac{\tilde{\tilde{J}}_{\alpha}(\vec{\lambda},\eta)}{j\omega\varepsilon} \tag{5.20}$$

where

$$\tilde{\tilde{\pi}}_{2\alpha}^{p}(\vec{\lambda},\eta) = \int_{-\infty}^{\infty} \tilde{\pi}_{2\alpha}^{p}(\vec{\lambda},y) e^{-j\eta y} dy \tag{5.21}$$

$$\tilde{\tilde{J}}_{\alpha}(\vec{\lambda},\eta) = \int_{-\infty}^{\infty} \tilde{J}_{\alpha}(\vec{\lambda},y) e^{-j\eta y} dy \tag{5.22}$$

Solving for $\tilde{\tilde{\pi}}_{2\alpha}^{p}$ in equation (5.20) produces the result

$$\tilde{\tilde{\pi}}_{2\alpha}^{p}(\vec{\lambda},\eta) = \frac{\tilde{\tilde{J}}_{\alpha}(\vec{\lambda},\eta)/j\omega\varepsilon}{(\eta^2 + p^2)} = \frac{\tilde{\tilde{J}}_{\alpha}(\vec{\lambda},\eta)/j\omega\varepsilon}{(\eta + jp)(\eta - jp)} \tag{5.23}$$

Since $p = p(\xi,\zeta)$ is not a function of η and $\mathrm{Re}\{p\} > 0$, this implies that $\eta = \pm jp$ are simple poles in the upper and lower-half of the complex η-plane, respectively.

The inverse transform must now be taken to get back to the complex λ-plane so that the y-variable is present for implementing boundary conditions. The inverse transform is calculated using the formula

$$\tilde{\pi}_{2\alpha}^{p}(\vec{\lambda},y)=\frac{1}{2\pi}\int_{-\infty}^{\infty}\tilde{\tilde{\pi}}_{2\alpha}^{p}(\vec{\lambda},\eta)e^{j\eta y}d\eta=\frac{1}{2\pi}\int_{-\infty}^{\infty}\frac{\tilde{\tilde{J}}_{\alpha}(\vec{\lambda},\eta)/j\omega\varepsilon}{(\eta+jp)(\eta-jp)}e^{j\eta y}d\eta \tag{5.24}$$

The Fourier representation of $\tilde{\tilde{J}}_{\alpha}$ is

$$\tilde{\tilde{J}}_{\alpha}(\vec{\lambda},\eta)=\int_{-\infty}^{\infty}\tilde{J}_{\alpha}(\vec{\lambda},y')e^{-j\eta y'}dy'=\int_{y'}\tilde{J}_{\alpha}(\vec{\lambda},y')e^{-j\eta y'}dy' \tag{5.25}$$

The limits of integration in (5.25) have been truncated since $\tilde{J}_{\alpha}(\vec{\lambda},y')=0$ outside the source region. Also, y' has been used in (5.25) as the dummy integration variable instead of y so as not to confuse it with the functional y-dependence of the $e^{j\eta y}$ term in equation (5.24). Substitution of (5.25) into (5.24) and interchanging the integral signs (valid if the analysis accurately describes a real physical problem [31]) leads to

$$\tilde{\pi}_{2\alpha}^{p}(\vec{\lambda},y)=\int_{y'}\tilde{G}_{2}^{p}(\vec{\lambda};y|y')\frac{\tilde{J}_{\alpha}(\vec{\lambda},y')}{j\omega\varepsilon}dy' \tag{5.26}$$

where

$$\tilde{G}_{2}^{p}(\vec{\lambda};y|y')=\tilde{G}_{2}^{p}(\vec{\lambda};y-y')=\frac{1}{2\pi}\int_{-\infty}^{\infty}\frac{e^{j\eta(y-y')}}{(\eta+jp)(\eta-jp)}d\eta \tag{5.27}$$

is the spectral-domain principal wave Hertzian-potential Green's function. Equation (5.27) may be evaluated using Cauchy's Integral Theorem. The result is (see Appendix B for details)

$$\tilde{G}_{2}^{p}(\vec{\lambda};y|y')=\tilde{G}_{2}^{p}(\vec{\lambda};y-y')=\frac{e^{-p|y-y'|}}{2p} \tag{5.28}$$

The representation of the principle wave in the complex λ-plane is therefore

$$\tilde{\pi}_{2\alpha}^{p}(\vec{\lambda},y)=\int_{y'}\frac{e^{-p|y-y'|}}{2p}\frac{\tilde{J}_{\alpha}(\vec{\lambda},y')}{j\omega\varepsilon}dy' \tag{5.29}$$

where y is the field point, y' is the source point and p is the spectral-domain propagation factor.

5.4.3 Reflected Wave Representation

The spectral-domain representation of the reflected waves for each region is obtained from (5.16). The well-known solution of this second-order partial differential equation is

$$\tilde{\pi}^r_{\beta\alpha}(\vec{\lambda}, y) = W^+_{\beta\alpha}(\vec{\lambda})e^{-p_\beta y} + W^-_{\beta\alpha}(\vec{\lambda})e^{p_\beta y} \tag{5.30}$$

where $W^{\pm}_{\beta\alpha}$ are the complex amplitude coefficients of the up and down-going reflected waves, respectively.

5.4.4 Total Wave Representation

The spectral-domain representation of the total waves in each region is obtained by superposing the results from the previous sections. This leads to the following

$$\tilde{\pi}_{1\alpha} = \tilde{\pi}^r_{1\alpha} = W^+_{1\alpha}e^{-p_c y} + W^-_{1\alpha}e^{p_c y} \quad ...h < y < \infty \tag{5.31}$$

$$\tilde{\pi}_{2\alpha} = \tilde{\pi}^p_{2\alpha} + \tilde{\pi}^r_{2\alpha} = \int_{y'} \frac{e^{-p|y-y'|}}{2p} \frac{\tilde{J}_\alpha}{j\omega\varepsilon} dy' + W^+_{2\alpha}e^{-py} + W^-_{2\alpha}e^{py} \quad ...-h < y < h \tag{5.32}$$

$$\tilde{\pi}_{3\alpha} = \tilde{\pi}^r_{3\alpha} = W^+_{3\alpha}e^{-p_c y} + W^-_{3\alpha}e^{p_c y} \quad ...-\infty < y < -h \tag{5.33}$$

where the functional dependence in the above equations has been dropped for notational convenience. Note that

$$|y - y'| = \begin{cases} y - y' & ...y > y' \\ y' - y & ...y < y' \end{cases} \tag{5.34}$$

thus, equation (5.32) may be written (for the purpose of implementing boundary conditions) as

$$\tilde{\pi}_{2\alpha} = V_\alpha^+ e^{-py} + W_{2\alpha}^+ e^{-py} + W_{2\alpha}^- e^{py} \quad \ldots y' < y < h \tag{5.35}$$

$$\tilde{\pi}_{2\alpha} = V_\alpha^- e^{py} + W_{2\alpha}^+ e^{-py} + W_{2\alpha}^- e^{py} \quad \ldots -h < y < y' \tag{5.36}$$

where

$$V_\alpha^\pm = V_\alpha^\pm(\vec{\lambda}) = \int_{y'} \frac{e^{\pm p(\vec{\lambda})y'}}{2p(\vec{\lambda})} \frac{\tilde{J}_\alpha(\vec{\lambda}, y')}{j\omega\varepsilon} dy' \tag{5.37}$$

are associated with up and down-going waves launched from the source.

It is observed in equations (5.31)-(5.33) that there are 18 unknown spectral-domain coefficients, thus 18 boundary conditions must be enforced to guarantee a unique solution. These spectral coefficients, $W_{\beta\alpha}^\pm$, will be determined in the following sections using the two methods discussed in section 5.1.

5.5 Computation of Spectral Coefficients from Limit of Highly-Conducting Case

5.5.1 Introduction

One approach that will be used to determine the spectral coefficients $W_{\beta\alpha}^\pm$ for the imperfectly-conducting parallel-plate environment of Figure 5.1 is to first consider the solution to a symmetric dielectric slab waveguide and then look at the limit where the outer dielectrics become good conductors. If $\varepsilon_c = \tilde{\varepsilon}_c(1 - j\sigma_c / \omega\tilde{\varepsilon}_c)$ is the effective complex permittivity of the outer (i.e., cover) regions, then the appropriate specialization is that $\varepsilon_c \to -j\sigma_c / \omega$ if $\sigma_c / \omega\tilde{\varepsilon}_c \gg 1$ (i.e., if the conduction current dominates over the displacement current in regions 1 and 3).

The solution to the above symmetric slab waveguide can be found by enforcing the following spectral-domain radiation and boundary conditions (see Appendix C)

$$\tilde{\pi}_{1\alpha}(\vec{\lambda}, y \to \infty) = \tilde{\pi}_{3\alpha}(\vec{\lambda}, y \to -\infty) = 0 \ \ldots \alpha = x, y, z \tag{5.38}$$

$$\varepsilon_c \tilde{\pi}_{1\alpha}(\vec{\lambda}, h) = \varepsilon \tilde{\pi}_{2\alpha}(\vec{\lambda}, h) \ \ldots \alpha = x, z \tag{5.39}$$

$$\varepsilon \tilde{\pi}_{2\alpha}(\vec{\lambda}, -h) = \varepsilon_c \tilde{\pi}_{3\alpha}(\vec{\lambda}, -h) \ \ldots \alpha = x, z \tag{5.40}$$

$$\varepsilon_c \frac{\partial \tilde{\pi}_{1\alpha}(\vec{\lambda}, h)}{\partial y} = \varepsilon \frac{\partial \tilde{\pi}_{2\alpha}(\vec{\lambda}, h)}{\partial y} \ \ldots \alpha = x, z \tag{5.41}$$

$$\varepsilon \frac{\partial \tilde{\pi}_{2\alpha}(\vec{\lambda}, -h)}{\partial y} = \varepsilon_c \frac{\partial \tilde{\pi}_{3\alpha}(\vec{\lambda}, -h)}{\partial y} \ \ldots \alpha = x, z \tag{5.42}$$

$$\varepsilon_c \tilde{\pi}_{1y}(\vec{\lambda}, h) = \varepsilon \tilde{\pi}_{2y}(\vec{\lambda}, h) \tag{5.43}$$

$$\varepsilon \tilde{\pi}_{2y}(\vec{\lambda}, -h) = \varepsilon_c \tilde{\pi}_{3y}(\vec{\lambda}, -h) \tag{5.44}$$

$$\frac{\partial \tilde{\pi}_{1y}(\vec{\lambda}, h)}{\partial y} - \frac{\partial \tilde{\pi}_{2y}(\vec{\lambda}, h)}{\partial y} = [1 - (\varepsilon / \varepsilon_c)]\left[j\xi \tilde{\pi}_{2x}(\vec{\lambda}, h) + j\zeta \tilde{\pi}_{2z}(\vec{\lambda}, h) \right] \tag{5.45}$$

$$\frac{\partial \tilde{\pi}_{2y}(\vec{\lambda}, -h)}{\partial y} - \frac{\partial \tilde{\pi}_{3y}(\vec{\lambda}, -h)}{\partial y} = [1 - (\varepsilon_c / \varepsilon)]\left[j\xi \tilde{\pi}_{3x}(\vec{\lambda}, -h) + j\zeta \tilde{\pi}_{3z}(\vec{\lambda}, -h) \right] \tag{5.46}$$

Equation (5.38) represents the radiation conditions. Equations (5.39)-(5.42) are tangential boundary conditions, (5.43)-(5.44) are normal boundary conditions and (5.45)-(5.46) are mixed/coupled boundary conditions. Since (5.45) and (5.46) are coupled boundary conditions (i.e., contain both tangential and normal components), this suggests enforcing boundary conditions in a specified order. The easiest and first boundary condition that will be implemented is (5.38). Equations (5.39)-(5.42), the tangential boundary conditions, are enforced next, followed by the normal boundary conditions (5.43) and (5.44). The coupled boundary conditions (5.45) and (5.46), which are the

most difficult to implement, are enforced in the final step. Note, there are 18 boundary conditions as required.

5.5.2 Radiation Conditions

The radiation conditions in (5.38) are the easiest to implement and lead to the following result when applied to (5.31) and (5.33)

$$\tilde{\pi}_{1\alpha}(\vec{\lambda}, y \to \infty) = 0 \quad \Rightarrow \quad W_{1\alpha}^{-} = 0 \;\; ...\alpha = x, y, z \tag{5.47}$$

$$\tilde{\pi}_{3\alpha}(\vec{\lambda}, y \to -\infty) = 0 \quad \Rightarrow \quad W_{3\alpha}^{+} = 0 \;\; ...\alpha = x, y, z \tag{5.48}$$

since $\mathrm{Re}\{p_c\} > 0$ (a result of the medium being assumed to be lossy, i.e., $\mathrm{Im}\{k_c\} < 0$). Therefore, the spectral representation of the Hertz potential consists of only an up-going reflected wave in region 1 and only a down-going reflected wave in region 3 (as shown in Figure 5.1), that is

$$\tilde{\pi}_{1\alpha} = \tilde{\pi}_{1\alpha}^{r} = W_{1\alpha}^{+} e^{-p_c y} \quad ...h < y < \infty \quad (\alpha = x, y, z) \tag{5.49}$$

$$\tilde{\pi}_{3\alpha} = \tilde{\pi}_{3\alpha}^{r} = W_{3\alpha}^{-} e^{p_c y} \quad ...-\infty < y < -h \quad (\alpha = x, y, z) \tag{5.50}$$

5.5.3 Tangential Boundary Conditions

The first tangential boundary condition (at the $y = h$ interface) is enforced by substituting (5.49) and (5.35) into (5.39). This leads to the following expression

$$\varepsilon_c W_{1\alpha}^{+} e^{-p_c h} = \varepsilon \left(V_{\alpha}^{+} e^{-ph} + W_{2\alpha}^{+} e^{-ph} + W_{2\alpha}^{-} e^{ph} \right) \;\; ...\alpha = x, z \tag{5.51}$$

Solving (5.51) for $W_{1\alpha}^{+}$ leads to

$$W_{1\alpha}^{+} = \frac{\varepsilon}{\varepsilon_c} e^{p_c h} \left(V_{\alpha}^{+} e^{-ph} + W_{2\alpha}^{+} e^{-ph} + W_{2\alpha}^{-} e^{ph} \right) \;\; ...\alpha = x, z \tag{5.52}$$

Therefore, upon substitution of (5.52) into (5.49), the spectral-domain representation for $\tilde{\pi}_{1\alpha}$ becomes

$$\tilde{\pi}_{1\alpha} = \frac{\varepsilon}{\varepsilon_c} e^{-p_c(y-h)} \left(V_\alpha^+ e^{-ph} + W_{2\alpha}^+ e^{-ph} + W_{2\alpha}^- e^{ph} \right) \quad ...\alpha = x, z \tag{5.53}$$

The second tangential boundary condition (at the $y = -h$ interface) is implemented through the substitution of (5.36) and (5.50) into equation (5.40). The result is

$$W_{3\alpha}^- = \frac{\varepsilon}{\varepsilon_c} e^{p_c h} \left(V_\alpha^- e^{-ph} + W_{2\alpha}^+ e^{ph} + W_{2\alpha}^- e^{-ph} \right) \quad ...\alpha = x, z \tag{5.54}$$

$$\tilde{\pi}_{3\alpha} = W_{3\alpha}^- e^{p_c y} = \frac{\varepsilon}{\varepsilon_c} e^{p_c(y+h)} \left(V_\alpha^- e^{-ph} + W_{2\alpha}^+ e^{ph} + W_{2\alpha}^- e^{-ph} \right) \quad ...\alpha = x, z \tag{5.55}$$

Substitution of (5.53) and (5.35) into the third tangential boundary condition (5.41) leads to

$$p_c \left(V_\alpha^+ e^{-ph} + W_{2\alpha}^+ e^{-ph} + W_{2\alpha}^- e^{ph} \right) = p \left(V_\alpha^+ e^{-ph} + W_{2\alpha}^+ e^{-ph} - W_{2\alpha}^- e^{ph} \right) \quad ...\alpha = x, z \tag{5.56}$$

Solving (5.56) in terms of $W_{2\alpha}^-$ gives

$$W_{2\alpha}^- = -R e^{-2ph} \left(V_\alpha^+ + W_{2\alpha}^+ \right) \quad ...\alpha = x, z \tag{5.57}$$

where

$$R = \frac{p_c - p}{p_c + p} \tag{5.58}$$

is the interfacial reflection coefficient. The last tangential boundary condition is implemented by substituting (5.36) and (5.55) into (5.42), producing the result

$$p \left(V_\alpha^- e^{-ph} - W_{2\alpha}^+ e^{ph} + W_{2\alpha}^- e^{-ph} \right) = p_c \left(V_\alpha^- e^{-ph} + W_{2\alpha}^+ e^{ph} + W_{2\alpha}^- e^{-ph} \right) \quad ...\alpha = x, z \tag{5.59}$$

Solving (5.59) in terms of $W_{2\alpha}^-$ gives

$$W_{2\alpha}^{-} = -V_{\alpha}^{-} - \frac{e^{2ph}}{R} W_{2\alpha}^{+} \quad ...\alpha = x, z \tag{5.60}$$

The spectral coefficient $W_{2\alpha}^{+}$ can now be explicitly determined (for $\alpha = x, z$) by equating (5.57) and (5.60). The result is

$$W_{2\alpha}^{+} = \frac{R^2 e^{-4ph} V_{\alpha}^{+} - R e^{-2ph} V_{\alpha}^{-}}{1 - R^2 e^{-4ph}} \quad ...\alpha = x, z \tag{5.61}$$

The spectral coefficient $W_{2\alpha}^{-}$ is found by substituting (5.61) into either (5.57) or (5.60), leading to

$$W_{2\alpha}^{-} = \frac{R^2 e^{-4ph} V_{\alpha}^{-} - R e^{-2ph} V_{\alpha}^{+}}{1 - R^2 e^{-4ph}} \quad ...\alpha = x, z \tag{5.62}$$

Those familiar with guided wave theory will note that the denominator of equations (5.61) and (5.62) can be factored into the form $1 - R^2 e^{-4ph} = (1 + R e^{-2ph})(1 - R e^{-2ph})$. This is significant because the eigenvalue equation $1 \pm R e^{-2ph} = 0$ identifies the expected poles of the even/odd TE surface-wave modes of a symmetric slab waveguide. A more detailed discussion will be provided later.

5.5.4 Normal Boundary Conditions

The first normal-component boundary condition is implemented by substituting (5.49) and (5.35) into relation (5.43), leading to

$$W_{1y}^{+} = \frac{\varepsilon}{\varepsilon_c} e^{p_c h} \left(V_y^{+} e^{-ph} + W_{2y}^{+} e^{-ph} + W_{2y}^{-} e^{ph} \right) \tag{5.63}$$

$$\tilde{\pi}_{1y} = \frac{\varepsilon}{\varepsilon_c} e^{-p_c (y-h)} \left(V_y^{+} e^{-ph} + W_{2y}^{+} e^{-ph} + W_{2y}^{-} e^{ph} \right) \tag{5.64}$$

Similarly, substitution of (5.36) and (5.50) into the second normal boundary condition (5.44) produces the result

$$W_{3y}^{-} = \frac{\varepsilon}{\varepsilon_c} e^{p_c h}\left(V_y^{-} e^{-ph} + W_{2y}^{+} e^{ph} + W_{2y}^{-} e^{-ph}\right) \tag{5.65}$$

$$\tilde{\pi}_{3y} = W_{3y}^{-} e^{p_c y} = \frac{\varepsilon}{\varepsilon_c} e^{p_c (y+h)}\left(V_y^{-} e^{-ph} + W_{2y}^{+} e^{ph} + W_{2y}^{-} e^{-ph}\right) \tag{5.66}$$

5.5.5 Mixed/Coupled Boundary Conditions

The final two remaining spectral coefficients, W_{2y}^{+} and W_{2y}^{-}, can be determined from the coupled boundary conditions. Inserting (5.64) and (5.35) into (5.45) gives

$$\begin{aligned} &-p_c \frac{\varepsilon}{\varepsilon_c}\left(V_y^{+} e^{-ph} + W_{2y}^{+} e^{-ph} + W_{2y}^{-} e^{ph}\right) + \\ &p\left(V_y^{+} e^{-ph} + W_{2y}^{+} e^{-ph} - W_{2y}^{-} e^{ph}\right) = A\left(1 - \frac{\varepsilon}{\varepsilon_c}\right) \end{aligned} \tag{5.67}$$

where

$$\begin{aligned} &A = j\xi A_x + j\zeta A_z = \\ &j\xi\left(V_x^{+} e^{-ph} + W_{2x}^{+} e^{-ph} + W_{2x}^{-} e^{ph}\right) + j\zeta\left(V_z^{+} e^{-ph} + W_{2z}^{+} e^{-ph} + W_{2z}^{-} e^{ph}\right) \end{aligned} \tag{5.68}$$

Solving (5.67) for W_{2y}^{-} and letting $N^2 = \varepsilon / \varepsilon_c$ leads to

$$W_{2y}^{-} = -\bar{R} e^{-2ph} V_y^{+} - \bar{R} e^{-2ph} W_{2y}^{+} + \frac{e^{-ph}(N^2 - 1)}{p_c N^2 + p} A \tag{5.69}$$

where

$$\bar{R} = \frac{p_c N^2 - p}{p_c N^2 + p} \tag{5.70}$$

is the interfacial reflection coefficient. The expression in (5.70) occurs in the analysis of a current source in the presence of a half-plane where $p_c N^2 + p = 0$ identifies Zenneck surface-wave poles. It will be shown later that Zenneck surface waves do not exist for the parallel-plate environment.

Substitution of (5.36) and (5.66) into the second coupled boundary condition (5.46) gives

$$\begin{aligned} &p\left(V_y^- e^{-ph} - W_{2y}^+ e^{ph} + W_{2y}^- e^{-ph}\right) - \\ &p_c \frac{\varepsilon}{\varepsilon_c}\left(V_y^- e^{-ph} + W_{2y}^+ e^{ph} + W_{2y}^- e^{-ph}\right) = B\left(\frac{\varepsilon}{\varepsilon_c} - 1\right) \end{aligned} \tag{5.71}$$

where

$$\begin{aligned} &B = j\xi B_x + j\zeta B_z = \\ &j\xi\left(V_x^- e^{-ph} + W_{2x}^+ e^{ph} + W_{2x}^- e^{-ph}\right) + j\zeta\left(V_z^- e^{-ph} + W_{2z}^+ e^{ph} + W_{2z}^- e^{-ph}\right) \end{aligned} \tag{5.72}$$

The solution of (5.71) in terms of W_{2y}^- is

$$W_{2y}^- = -V_y^- - \frac{e^{2ph}}{\bar{R}} W_{2y}^+ + \frac{e^{ph}(1-N^2)}{p_c N^2 - p} B \tag{5.73}$$

The spectral coefficient W_{2y}^+ is explicitly determined by equating (5.69) and (5.73). The result is

$$W_{2y}^+ = \frac{\bar{R}^2 e^{-4ph} V_y^+ - \bar{R} e^{-2ph} V_y^- + \dfrac{\bar{R} e^{-3ph}(1-N^2)A}{p_c N^2 + p} + \dfrac{\bar{R} e^{-ph}(1-N^2)B}{p_c N^2 - p}}{1 - \bar{R}^2 e^{-4ph}} \tag{5.74}$$

Substitution of (5.74) into either (5.69) or (5.73) leads to the following expression for the spectral coefficient W_{2y}^-

$$W_{2y}^{-}=\frac{\bar{R}^2e^{-4ph}V_y^{-}-\bar{R}e^{-2ph}V_y^{+}-\dfrac{e^{-ph}(1-N^2)A}{p_cN^2+p}-\dfrac{\bar{R}^2e^{-3ph}(1-N^2)B}{p_cN^2-p}}{1-\bar{R}^2e^{-4ph}} \tag{5.75}$$

The spectral coefficient W_{2y}^{+} can be cast into a more physically meaningful form (as will be shown later) via substitution of (5.61), (5.62), (5.68) and (5.72) into (5.74). The result is, after some algebraic effort,

$$W_{2y}^{+}=W_{2yx}^{+}+W_{2yy}^{+}+W_{2yz}^{+} \tag{5.76}$$

where

$$W_{2yx}^{+}=\frac{\dfrac{\bar{R}e^{-3ph}(1-N^2)j\xi A_x}{p_cN^2+p}+\dfrac{\bar{R}e^{-ph}(1-N^2)j\xi B_x}{p_cN^2-p}}{1-\bar{R}^2e^{-4ph}}=\frac{C_{yx}^{++}e^{-4ph}V_x^{+}-C_{yx}^{+-}e^{-2ph}V_x^{-}}{(1-R^2e^{-4ph})(1-\bar{R}^2e^{-4ph})} \tag{5.77}$$

$$W_{2yy}^{+}=\frac{\bar{R}^2e^{-4ph}V_y^{+}-\bar{R}e^{-2ph}V_y^{-}}{1-\bar{R}^2e^{-4ph}} \tag{5.78}$$

$$W_{2yz}^{+}=\frac{\dfrac{\bar{R}e^{-3ph}(1-N^2)j\zeta A_z}{p_cN^2+p}+\dfrac{\bar{R}e^{-ph}(1-N^2)j\zeta B_z}{p_cN^2-p}}{1-\bar{R}^2e^{-4ph}}=\frac{C_{yz}^{++}e^{-4ph}V_z^{+}-C_{yz}^{+-}e^{-2ph}V_z^{-}}{(1-R^2e^{-4ph})(1-\bar{R}^2e^{-4ph})} \tag{5.79}$$

$$\begin{aligned}C_{yx}^{++}&=j\xi\frac{\bar{R}(1-N^2)(1-R)(1-R/\bar{R})}{p_cN^2+p}\\ C_{yx}^{+-}&=j\xi\frac{\bar{R}(1-N^2)(1-R)(Re^{-4ph}-1/\bar{R})}{p_cN^2+p}\end{aligned} \tag{5.80}$$

$$\begin{aligned}C_{yz}^{++}&=j\zeta\frac{\bar{R}(1-N^2)(1-R)(1-R/\bar{R})}{p_cN^2+p}\\ C_{yz}^{+-}&=j\zeta\frac{\bar{R}(1-N^2)(1-R)(Re^{-4ph}-1/\bar{R})}{p_cN^2+p}\end{aligned} \tag{5.81}$$

Similarly, substitution of (5.61), (5.62), (5.68) and (5.72) into (5.75) leads to the following expression for W_{2y}^{-}

$$W_{2y}^{-} = W_{2yx}^{-} + W_{2yy}^{-} + W_{2yz}^{-} \tag{5.82}$$

where

$$W_{2yx}^{-} = -\frac{\dfrac{e^{-ph}(1-N^2)j\xi A_x}{p_c N^2 + p} + \dfrac{\bar{R}^2 e^{-3ph}(1-N^2)j\xi B_x}{p_c N^2 - p}}{1-\bar{R}^2 e^{-4ph}} = \frac{C_{yx}^{--} e^{-4ph} V_x^{-} - C_{yx}^{-+} e^{-2ph} V_x^{+}}{(1-R^2 e^{-4ph})(1-\bar{R}^2 e^{-4ph})} \tag{5.83}$$

$$W_{2yy}^{-} = \frac{\bar{R}^2 e^{-4ph} V_y^{-} - \bar{R} e^{-2ph} V_y^{+}}{1-\bar{R}^2 e^{-4ph}} \tag{5.84}$$

$$W_{2yz}^{-} = -\frac{\dfrac{e^{-ph}(1-N^2)j\zeta A_z}{p_c N^2 + p} + \dfrac{\bar{R}^2 e^{-3ph}(1-N^2)j\zeta B_z}{p_c N^2 - p}}{1-\bar{R}^2 e^{-4ph}} = \frac{C_{yz}^{--} e^{-4ph} V_z^{-} - C_{yz}^{-+} e^{-2ph} V_z^{+}}{(1-R^2 e^{-4ph})(1-\bar{R}^2 e^{-4ph})} \tag{5.85}$$

$$C_{yx}^{--} = -C_{yx}^{++} \;,\; C_{yx}^{-+} = -C_{yx}^{+-} \tag{5.86}$$

$$C_{yz}^{--} = -C_{yz}^{++} \;,\; C_{yz}^{-+} = -C_{yz}^{+-} \tag{5.87}$$

5.5.6 Limiting Case $\varepsilon_c \to -j\sigma_c/\omega$

The limiting case of when the outer dielectrics become good conductors is discussed in this section. Only the spectral coefficients $W_{2\alpha}^{\pm}$ will be examined since we are specifically interested in the Green's function for the central region. If the outer regions are good conductors, then the following relation prevails

$$\varepsilon_c = \tilde{\varepsilon}_c - j\frac{\sigma_c}{\omega} \approx -j\frac{\sigma_c}{\omega} \tag{5.88}$$

since $\sigma_c \gg \omega\tilde{\varepsilon}_c$ (i.e., the conduction current dominates over the displacement current). The tangential coefficients $W_{2\alpha}^{\pm}$ $(\alpha = x, z)$ for the symmetric slab waveguide, repeated here for convenience, are

$$W_{2\alpha}^{\pm} = \frac{R^2 e^{-4ph} V_{\alpha}^{\pm} - R e^{-2ph} V_{\alpha}^{\mp}}{1 - R^2 e^{-4ph}} \quad ...\alpha = x, z \tag{5.89}$$

where

$$R = \frac{p_c - p}{p_c + p} \tag{5.90}$$

If (5.88) is inserted into (5.90), then the interfacial reflection coefficient R reduces to the following expression

$$R = \frac{\sigma_c Z_c - p}{\sigma_c Z_c + p} = \frac{1 - p/\sigma_c Z_c}{1 + p/\sigma_c Z_c} \tag{5.91}$$

since (see Appendix D)

$$\begin{aligned} \lim_{\varepsilon_c \to -j\frac{\sigma_c}{\omega}} p_c &= \lim_{\varepsilon_c \to -j\frac{\sigma_c}{\omega}} \sqrt{\lambda^2 - k_c^2} \approx \lim_{\varepsilon_c \to -j\frac{\sigma_c}{\omega}} \sqrt{-k_c^2} = \lim_{\varepsilon_c \to -j\frac{\sigma_c}{\omega}} \sqrt{-\omega^2 \varepsilon_c \mu_0} \\ \therefore \quad \lim_{\varepsilon_c \to -j\frac{\sigma_c}{\omega}} p_c &= \sqrt{j\omega\sigma_c \mu_0} = \sigma_c \sqrt{\frac{j\omega\mu_0}{\sigma_c}} = \sigma_c Z_c \end{aligned} \tag{5.92}$$

where it has been assumed that $k_c^2 \gg \lambda^2$ (when λ becomes large in the inversion integral the contribution to $\vec{\pi}$ approaches zero due to the Riemann-Lebesgue lemma [26]). Therefore, the tangential spectral coefficients in region 2 are given by (5.89) where the interfacial reflection coefficient R is now given by (5.91).

The normal spectral coefficients in region 2 for the symmetric slab waveguide are given by equations (5.76)-(5.87). If $\varepsilon_c \to -j\sigma_c/\omega$ then, using (5.92) and $N^2 = \varepsilon/\varepsilon_c$, the following relations are established

$$\lim_{\varepsilon_c \to -j\frac{\sigma_c}{\omega}} N^2 = \lim_{\varepsilon_c \to -j\frac{\sigma_c}{\omega}} \frac{\varepsilon}{\varepsilon_c} = \frac{j\omega\varepsilon}{\sigma_c} \to 0 \tag{5.93}$$

$$\lim_{\varepsilon_c \to -j\frac{\sigma_c}{\omega}} p_c N^2 = \sigma_c Z_c \frac{j\omega\varepsilon}{\sigma_c} = j\omega\varepsilon Z_c \tag{5.94}$$

$$\lim_{\varepsilon_c \to -j\frac{\sigma_c}{\omega}} \bar{R} = \lim_{\varepsilon_c \to -j\frac{\sigma_c}{\omega}} \frac{p_c N^2 - p}{p_c N^2 + p} = \frac{j\omega\varepsilon Z_c - p}{j\omega\varepsilon Z_c + p} = -\frac{1 - j\omega\varepsilon Z_c / p}{1 + j\omega\varepsilon Z_c / p} \tag{5.95}$$

since $\sigma_c \gg \omega\varepsilon$ is assumed in (5.93). Note that $Z_c \propto 1/\sqrt{\sigma_c}$ whereas $N^2 \propto 1/\sigma_c$, that is, terms on the order of $1/\sqrt{\sigma_c}$ are kept, while terms on the order of $1/\sigma_c$ are neglected. Substitution of (5.92)-(5.95) into (5.80), (5.81), (5.86) and (5.87) leads to

$$\begin{aligned} C_{yx}^{++} &= -C_{yx}^{--} = j\xi \frac{\bar{R}(1-R)(1-R/\bar{R})}{j\omega\varepsilon Z_c + p} \\ C_{yx}^{+-} &= -C_{yx}^{-+} = j\xi \frac{\bar{R}(1-R)(Re^{-4ph} - 1/\bar{R})}{j\omega\varepsilon Z_c + p} \end{aligned} \tag{5.96}$$

$$\begin{aligned} C_{yz}^{++} &= -C_{yz}^{--} = j\zeta \frac{\bar{R}(1-R)(1-R/\bar{R})}{j\omega\varepsilon Z_c + p} \\ C_{yz}^{+-} &= -C_{yz}^{-+} = j\zeta \frac{\bar{R}(1-R)(Re^{-4ph} - 1/\bar{R})}{j\omega\varepsilon Z_c + p} \end{aligned} \tag{5.97}$$

where R and $\bar{R}$ are given by (5.91) and (5.95), respectively. The second method for determining the spectral coefficients is presented next and will be compared to the above limiting case.

5.6 Computation of Spectral Coefficients Using Impedance Boundary Conditions

5.6.1 Introduction

The second method for computing the spectral coefficients is based on the spectral-domain electric-type Hertzian-potential impedance boundary conditions (see Appendix D for details)

$$\tilde{\pi}_{2\alpha}(\vec{\lambda},h) = -\frac{1}{\sigma_c Z_c}\frac{\partial \tilde{\pi}_{2\alpha}(\vec{\lambda},h)}{\partial y} \quad ...\alpha = x,z \tag{5.98}$$

$$\tilde{\pi}_{2\alpha}(\vec{\lambda},-h) = \frac{1}{\sigma_c Z_c}\frac{\partial \tilde{\pi}_{2\alpha}(\vec{\lambda},-h)}{\partial y} \quad ...\alpha = x,z \tag{5.99}$$

$$\frac{\partial \tilde{\pi}_{2y}(\vec{\lambda},h)}{\partial y} = -j\omega\varepsilon Z_c \tilde{\pi}_{2y}(\vec{\lambda},h) - j\xi\tilde{\pi}_{2x}(\vec{\lambda},h) - j\zeta\tilde{\pi}_{2z}(\vec{\lambda},h) \tag{5.100}$$

$$\frac{\partial \tilde{\pi}_{2y}(\vec{\lambda},-h)}{\partial y} = j\omega\varepsilon Z_c \tilde{\pi}_{2y}(\vec{\lambda},-h) - j\xi\tilde{\pi}_{2x}(\vec{\lambda},-h) - j\zeta\tilde{\pi}_{2z}(\vec{\lambda},-h) \tag{5.101}$$

Equations (5.98) and (5.99) are tangential boundary conditions, equations (5.100) and (5.101) are coupled boundary conditions and $Z_c = (1+j)\sqrt{\omega\mu_0 / 2\sigma_c}$ is the intrinsic impedance of the imperfect conductors. The radiation conditions are built into the impedance boundary conditions and therefore do not appear here as they did in section 5.5.1. In addition, computation of the spectral coefficients in the conducting regions is not required since the tangential coefficients are essentially accounted for through the intrinsic impedance Z_c and the normal coefficients are zero (refer to Appendix D). Thus, there are only 6 spectral coefficients, $W_{2\alpha}^{\pm}$ for $\alpha = x,y,z$, that must be computed in comparison with the 18 required for the more complicated method in section 5.5.

5.6.2 Geometry

The geometry that depicts the Hertzian-potential impedance boundary condition approach is shown in Figure 5.2. The top and bottom conductors have a conductivity of σ_c and permeability μ_0, or equivalently, an intrinsic impedance of Z_c. Region 2 is the central/material region and has an effective complex permittivity ε and permeability μ_0.

The reflected waves in the conductors are not shown since they do not need to be computed, as previously mentioned. The unit vector $\hat{n}$ points out of the conductor and into the material region.

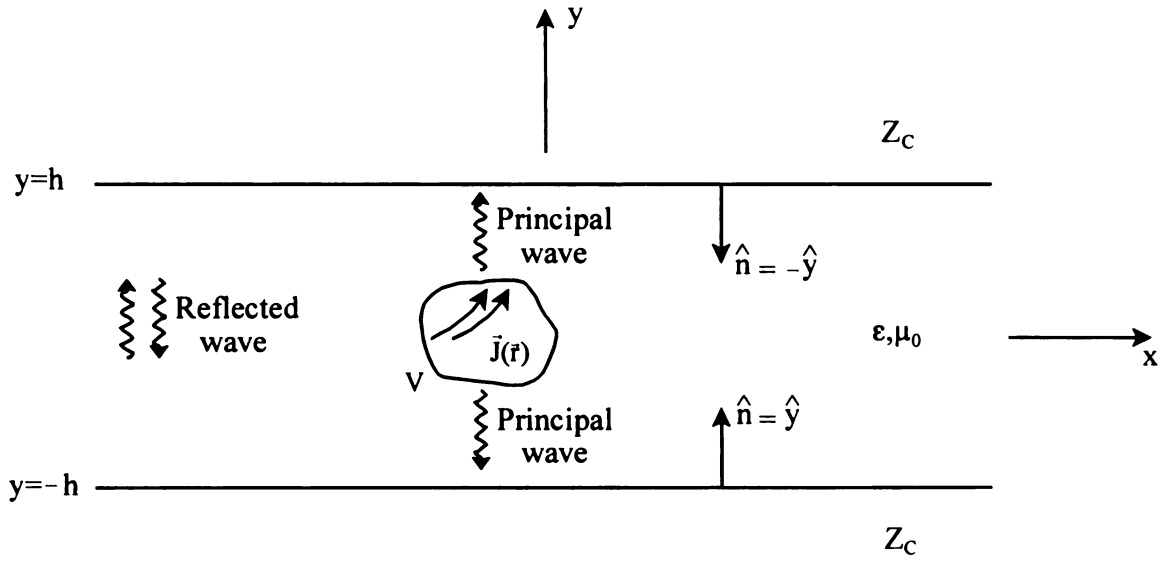

Figure 5.2 Parallel-plate environment for impedance boundary condition analysis.

5.6.3 Tangential Impedance Boundary Conditions

The first tangential impedance boundary condition (at the $y = h$ interface) is enforced by substituting (5.35) into (5.98). This leads to the following expression

$$V_\alpha^+ e^{-ph} + W_{2\alpha}^+ e^{-ph} + W_{2\alpha}^- e^{ph} = \frac{p}{\sigma_c Z_c}\left(V_\alpha^+ e^{-ph} + W_{2\alpha}^+ e^{-ph} - W_{2\alpha}^- e^{ph}\right) \quad ...\alpha = x, z \qquad (5.102)$$

Solving (5.102) in terms of $W_{2\alpha}^-$ leads to

$$W_{2\alpha}^- = -R\, e^{-2ph}\left(V_\alpha^+ + W_{2\alpha}^+\right) \quad ...\alpha = x, z \qquad (5.103)$$

where the interfacial reflection coefficient R is given by

$$R = \frac{\sigma_c Z_c - p}{\sigma_c Z_c + p} = \frac{1 - p/\sigma_c Z_c}{1 + p/\sigma_c Z_c} \tag{5.104}$$

Substitution of (5.36) into the second impedance boundary condition (5.99) gives

$$V_\alpha^- e^{-ph} + W_{2\alpha}^+ e^{ph} + W_{2\alpha}^- e^{-ph} = \frac{p}{\sigma_c Z_c}\left(V_\alpha^- e^{-ph} - W_{2\alpha}^+ e^{ph} + W_{2\alpha}^- e^{-ph}\right) \quad ...\alpha = x, z \tag{5.105}$$

Solving (5.105) in terms of $W_{2\alpha}^-$ leads to

$$W_{2\alpha}^- = -V_\alpha^- - \frac{e^{2ph}}{R} W_{2\alpha}^+ \quad ...\alpha = x, z \tag{5.106}$$

The spectral coefficient $W_{2\alpha}^+$ can now be explicitly determined (for $\alpha = x, z$) by equating (5.103) and (5.106). The result is

$$W_{2\alpha}^+ = \frac{R^2 e^{-4ph} V_\alpha^+ - R e^{-2ph} V_\alpha^-}{1 - R^2 e^{-4ph}} \quad ...\alpha = x, z \tag{5.107}$$

The spectral coefficient $W_{2\alpha}^-$ is found by substituting (5.107) into either (5.103) or (5.106), leading to

$$W_{2\alpha}^- = \frac{R^2 e^{-4ph} V_\alpha^- - R e^{-2ph} V_\alpha^+}{1 - R^2 e^{-4ph}} \quad ...\alpha = x, z \tag{5.108}$$

Note that (5.107), (5.108) and (5.104) are in agreement with (5.89) and (5.91).

5.6.4 Coupled Impedance Boundary Conditions

The first coupled impedance boundary condition is implemented by inserting (5.35) into (5.100). This results in the following relation

$$p\left(V_y^+ e^{-ph} + W_{2y}^+ e^{-ph} - W_{2y}^- e^{ph}\right) = j\omega\varepsilon Z_c \left(V_y^+ e^{-ph} + W_{2y}^+ e^{-ph} + W_{2y}^- e^{ph}\right) + A \tag{5.109}$$

where A is given by (5.68). Solving (5.109) for W_{2y}^- leads to

$$W_{2y}^{-} = -\bar{R}e^{-2ph}V_y^{+} - \bar{R}e^{-2ph}W_{2y}^{+} - \frac{e^{-ph}A}{j\omega\varepsilon Z_c + p} \tag{5.110}$$

where the interfacial reflection coefficient $\bar{R}$ is given by

$$\bar{R} = \frac{j\omega\varepsilon Z_c - p}{j\omega\varepsilon Z_c + p} = -\frac{1 - j\omega\varepsilon Z_c / p}{1 + j\omega\varepsilon Z_c / p} \tag{5.111}$$

Substitution of (5.36) into the second coupled impedance boundary condition (5.101) produces the result

$$p\left(V_y^{-}e^{-ph} - W_{2y}^{+}e^{ph} + W_{2y}^{-}e^{-ph}\right) = j\omega\varepsilon Z_c\left(V_y^{-}e^{-ph} + W_{2y}^{+}e^{ph} + W_{2y}^{-}e^{-ph}\right) - B \tag{5.112}$$

where B is given by (5.72). Solving (5.112) for W_{2y}^{-} leads to

$$W_{2y}^{-} = -V_y^{-} - \frac{e^{2ph}}{\bar{R}}W_{2y}^{+} + \frac{e^{ph}B}{j\omega\varepsilon Z_c - p} \tag{5.113}$$

The spectral coefficient W_{2y}^{+} is explicitly determined by equating (5.110) and (5.113). The result is

$$W_{2y}^{+} = \frac{\bar{R}^2e^{-4ph}V_y^{+} - \bar{R}e^{-2ph}V_y^{-} + \dfrac{\bar{R}e^{-3ph}A}{j\omega\varepsilon Z_c + p} + \dfrac{\bar{R}e^{-ph}B}{j\omega\varepsilon Z_c - p}}{1 - \bar{R}^2e^{-4ph}} \tag{5.114}$$

Substitution of (5.114) into either (5.110) or (5.113) leads to the following expression for the spectral coefficient W_{2y}^{-}

$$W_{2y}^{-} = \frac{\bar{R}^2e^{-4ph}V_y^{-} - \bar{R}e^{-2ph}V_y^{+} - \dfrac{e^{-ph}A}{j\omega\varepsilon Z_c + p} - \dfrac{\bar{R}^2e^{-3ph}B}{j\omega\varepsilon Z_c - p}}{1 - \bar{R}^2e^{-4ph}} \tag{5.115}$$

The spectral coefficient W_{2y}^{+} can be cast into a more physically meaningful form via substitution of (5.107), (5.108), (5.68) and (5.72) into (5.114). The result is, after some algebraic effort,

$$W_{2y}^{+} = W_{2yx}^{+} + W_{2yy}^{+} + W_{2yz}^{+} \tag{5.116}$$

where

$$W_{2yx}^{+} = \frac{\dfrac{\bar{R}\,e^{-3ph} j\xi A_x}{j\omega\varepsilon Z_c + p} + \dfrac{\bar{R}\,e^{-ph} j\xi B_x}{j\omega\varepsilon Z_c - p}}{1 - \bar{R}^2 e^{-4ph}} = \frac{C_{yx}^{++} e^{-4ph} V_x^{+} - C_{yx}^{+-} e^{-2ph} V_x^{-}}{(1 - R^2 e^{-4ph})(1 - \bar{R}^2 e^{-4ph})} \tag{5.117}$$

$$W_{2yy}^{+} = \frac{\bar{R}^2 e^{-4ph} V_y^{+} - \bar{R}\,e^{-2ph} V_y^{-}}{1 - \bar{R}^2 e^{-4ph}} \tag{5.118}$$

$$W_{2yz}^{+} = \frac{\dfrac{\bar{R}\,e^{-3ph} j\zeta A_z}{j\omega\varepsilon Z_c + p} + \dfrac{\bar{R}\,e^{-ph} j\zeta B_z}{j\omega\varepsilon Z_c - p}}{1 - \bar{R}^2 e^{-4ph}} = \frac{C_{yz}^{++} e^{-4ph} V_z^{+} - C_{yz}^{+-} e^{-2ph} V_z^{-}}{(1 - R^2 e^{-4ph})(1 - \bar{R}^2 e^{-4ph})} \tag{5.119}$$

$$C_{yx}^{++} = j\xi \frac{\bar{R}(1-R)(1-R/\bar{R})}{j\omega\varepsilon Z_c + p} \quad , \quad C_{yx}^{+-} = j\xi \frac{\bar{R}(1-R)(R e^{-4ph} - 1/\bar{R})}{j\omega\varepsilon Z_c + p} \tag{5.120}$$

$$C_{yz}^{++} = j\zeta \frac{\bar{R}(1-R)(1-R/\bar{R})}{j\omega\varepsilon Z_c + p} \quad , \quad C_{yz}^{+-} = j\zeta \frac{\bar{R}(1-R)(R e^{-4ph} - 1/\bar{R})}{j\omega\varepsilon Z_c + p} \tag{5.121}$$

Note that equations (5.120)-(5.121) are in agreement with the limiting case (5.96)-(5.97). Similarly, substitution of (5.107), (5.108), (5.68) and (5.72) into (5.115) leads to the following expression for W_{2y}^{-}

$$W_{2y}^{-} = W_{2yx}^{-} + W_{2yy}^{-} + W_{2yz}^{-} \tag{5.122}$$

where

$$W_{2yx}^{-} = -\frac{\dfrac{e^{-ph} j\xi A_x}{j\omega\varepsilon Z_c + p} + \dfrac{\bar{R}^2 e^{-3ph} j\xi B_x}{j\omega\varepsilon Z_c - p}}{1 - \bar{R}^2 e^{-4ph}} = \frac{C_{yx}^{--} e^{-4ph} V_x^{-} - C_{yx}^{-+} e^{-2ph} V_x^{+}}{(1 - R^2 e^{-4ph})(1 - \bar{R}^2 e^{-4ph})} \tag{5.123}$$

$$W_{2yy}^{-} = \frac{\bar{R}^2 e^{-4ph} V_y^{-} - \bar{R}\,e^{-2ph} V_y^{+}}{1 - \bar{R}^2 e^{-4ph}} \tag{5.124}$$

$$W_{2yz}^{-}=-\frac{\dfrac{e^{-ph}j\zeta A_z}{j\omega\varepsilon Z_c+p}+\dfrac{\bar{R}^2e^{-3ph}j\zeta B_z}{j\omega\varepsilon Z_c-p}}{1-\bar{R}^2e^{-4ph}}=\frac{C_{yz}^{--}e^{-4ph}V_z^{-}-C_{yz}^{-+}e^{-2ph}V_z^{+}}{(1-R^2e^{-4ph})(1-\bar{R}^2e^{-4ph})} \tag{5.125}$$

$$C_{yx}^{--}=-C_{yx}^{++}\ ,\ C_{yx}^{-+}=-C_{yx}^{+-} \tag{5.126}$$

$$C_{yz}^{--}=-C_{yz}^{++}\ ,\ C_{yz}^{-+}=-C_{yz}^{+-} \tag{5.127}$$

Equations (5.126)-(5.127) are also in agreement with the limiting case (5.96)-(5.97). Now that the spectral coefficients have been found (using the method in section 5.5 or 5.6), the Hertzian-potential dyadic Green's function can be identified.

5.7 Hertzian-Potential Dyadic Green's Function

The Hertzian-potential dyadic Green's function $\ddot{\tilde{G}}(\vec{r}|\vec{r}')$ can be identified by initially examining the tangential and normal components $\tilde{\pi}_{2x},\tilde{\pi}_{2z}$ and $\tilde{\pi}_{2y}$. Substitution of (5.28), (5.37), (5.61) and (5.62) into (5.32) leads to the following result for the tangential components

$$\tilde{\pi}_{2\alpha}(\vec{\lambda},y)=\int_{y'}\left[\tilde{G}^{p}(\vec{\lambda};y-y')+\tilde{G}_{\alpha\alpha}^{r}(\vec{\lambda};y,y')\right]\frac{\tilde{J}_{\alpha}(\vec{\lambda},y')}{j\omega\varepsilon}dy'\ \ ...\alpha=x,z \tag{5.128}$$

where the spectral-domain principal and reflected Green's functions are

$$\tilde{G}^{p}(\vec{\lambda};y-y')=\tilde{G}_{2}^{p}(\vec{\lambda};y-y')=\frac{e^{-p|y-y'|}}{2p} \tag{5.129}$$

$$\tilde{G}_{\alpha\alpha}^{r}(\vec{\lambda};y,y')=\frac{R^2e^{-p\phi_1}-Re^{-p\phi_2}+R^2e^{-p\phi_3}-Re^{-p\phi_4}}{2p(1-R^2e^{-4ph})}\ \ ...\alpha=x,z \tag{5.130}$$

$$\phi_1=\phi_1(y,y')=4h+y-y' \tag{5.131}$$

$$\phi_2=\phi_2(y,y')=2h+y+y' \tag{5.132}$$

$$\phi_3 = \phi_3(y, y') = 4h - y + y' \tag{5.133}$$

$$\phi_4 = \phi_4(y, y') = 2h - y - y' \tag{5.134}$$

where $\phi_i(y, y')$ are associated with phase-delay distances. Substitution of (5.28), (5.37), (5.76)-(5.79) and (5.82)-(5.85) into (5.32) leads to the following result for the normal component

$$\begin{aligned}\tilde{\pi}_{2y}(\vec{\lambda}, y) = &\int_{y'}\left[\tilde{G}^p(\vec{\lambda}; y - y') + \tilde{G}^r_{yy}(\vec{\lambda}; y, y')\right]\frac{\tilde{J}_y(\vec{\lambda}, y')}{j\omega\varepsilon}dy' + \\ &\int_{y'}\tilde{G}^r_{yx}(\vec{\lambda}; y, y')\frac{\tilde{J}_x(\vec{\lambda}, y')}{j\omega\varepsilon}dy' + \int_{y'}\tilde{G}^r_{yz}(\vec{\lambda}; y, y')\frac{\tilde{J}_z(\vec{\lambda}, y')}{j\omega\varepsilon}dy'\end{aligned} \tag{5.135}$$

where

$$\tilde{G}^r_{y\alpha}(\vec{\lambda}; y, y') = \frac{C^{++}_{y\alpha}e^{-p\phi_1} - C^{+-}_{y\alpha}e^{-p\phi_2} + C^{-+}_{y\alpha}e^{-p\phi_3} - C^{--}_{y\alpha}e^{-p\phi_4}}{2p(1 - R^2e^{-4ph})(1 - \bar{R}^2e^{-4ph})} \quad ...\alpha = x, z \tag{5.136}$$

$$\tilde{G}^r_{yy}(\vec{\lambda}; y, y') = \frac{\bar{R}^2e^{-p\phi_1} - \bar{R}e^{-p\phi_2} + \bar{R}^2e^{-p\phi_3} - \bar{R}e^{-p\phi_4}}{2p(1 - \bar{R}^2e^{-4ph})} \tag{5.137}$$

The spectral-domain Hertzian-potential dyadic Green's function $\bar{\bar{\tilde{G}}}(\vec{\lambda}; y, y')$ is revealed by using the above results and writing the spectral-domain Hertzian potential for region 2 in vector form, leading to

$$\bar{\bar{\tilde{\pi}}}_2(\vec{\lambda}, y) = \int_{y'}\bar{\bar{\tilde{G}}}(\vec{\lambda}; y, y') \cdot \frac{\bar{\bar{J}}(\vec{\lambda}, y')}{j\omega\varepsilon}dy' \tag{5.138}$$

where

$$\bar{\bar{\tilde{G}}}(\vec{\lambda}; y, y') = \bar{\bar{\tilde{G}}}^p(\vec{\lambda}; y - y') + \bar{\bar{\tilde{G}}}^r(\vec{\lambda}; y, y') \tag{5.139}$$

$$\bar{\bar{\tilde{G}}}^p(\vec{\lambda}; y - y') = \bar{\bar{I}}\tilde{G}^p = \hat{x}\tilde{G}^p\hat{x} + \hat{y}\tilde{G}^p\hat{y} + \hat{z}\tilde{G}^p\hat{z} \tag{5.140}$$

$$\tilde{\bar{G}}^r(\vec{\lambda};y,y') = \hat{x}\tilde{G}^r_{xx}\hat{x} + \hat{y}\tilde{G}^r_{yx}\hat{x} + \hat{y}\tilde{G}^r_{yy}\hat{y} + \hat{y}\tilde{G}^r_{yz}\hat{z} + \hat{z}\tilde{G}^r_{zz}\hat{z} \tag{5.141}$$

The Hertzian-potential dyadic Green's function is identified by using the following Fourier transform relations

$$\vec{\pi}_2(\vec{r}) = \frac{1}{(2\pi)^2}\int_{-\infty}^{\infty}\int_{-\infty}^{\infty}\tilde{\vec{\pi}}_2(\vec{\lambda},y)e^{j\vec{\lambda}\cdot\vec{r}}d^2\lambda \tag{5.142}$$

$$\tilde{\vec{J}}(\vec{\lambda},y') = \int_{-\infty}^{\infty}\int_{-\infty}^{\infty}\vec{J}(\vec{r}')e^{-j\vec{\lambda}\cdot\vec{r}'}dx'dz' = \int_{x'}\int_{z'}\vec{J}(\vec{r}')e^{-j\vec{\lambda}\cdot\vec{r}'}dx'dz' \tag{5.143}$$

Substitution of (5.138) into (5.142) and using (5.143) leads to the following expression

$$\vec{\pi}_2(\vec{r}) = \int_{V'}\bar{\bar{G}}(\vec{r}|\vec{r}')\cdot\frac{\vec{J}(r')}{j\omega\varepsilon}dV' = \int_{V'}\left[\bar{\bar{G}}^p(\vec{r}-\vec{r}') + \bar{\bar{G}}^r(\vec{r}|\vec{r}')\right]\cdot\frac{\vec{J}(r')}{j\omega\varepsilon}dV' \tag{5.144}$$

where the Hertzian-potential dyadic Green's function is

$$\bar{\bar{G}}(\vec{r}|\vec{r}') = \frac{1}{(2\pi)^2}\int_{-\infty}^{\infty}\int_{-\infty}^{\infty}\tilde{\bar{G}}(\vec{\lambda};y,y')e^{j\vec{\lambda}\cdot(\vec{r}-\vec{r}')}d^2\lambda \tag{5.145}$$

5.8 Physical Observations and Limiting Cases

5.8.1 Introduction

In section 5.8, some observations will be made to ensure the physical reasonableness of the above analysis. In addition, a couple limiting cases will be investigated to see if the above theory reduces to expected (i.e., well-known) results. First, the terms $1-R^2e^{-4ph}$ and $1-\bar{R}^2e^{-4ph}$ will be examined to show that they lead to the anticipated *TE* and *TM* modes of a symmetric slab waveguide. Next, the terms like those in equation (5.130) will be identified as waves interacting with the conducting

boundaries. The limiting cases when the conductors become perfect ($\sigma_c \to \infty$) and when the top imperfectly-conducting plate is removed will also be investigated.

5.8.2 Symmetric-Slab Waveguide Modes

The characteristic equation $1 - R^2 e^{-4ph} = 0$ can be shown to identify the *TE* surface-wave modes of a symmetric slab waveguide in the following manner. Multiplying the above equation by e^{2ph} and factoring gives

$$e^{2ph} - R^2 e^{-2ph} = 0 \;\Rightarrow\; (e^{ph} + Re^{-ph})(e^{ph} - Re^{-ph}) = 0 \tag{5.146}$$

Setting each term in (5.146) equal to zero and using (5.58) leads to the following set of characteristic equations

$$e^{ph} + Re^{-ph} = 0 \;\Rightarrow\; (p_c + p)e^{ph} + (p_c - p)e^{-ph} = 0 \tag{5.147}$$

$$e^{ph} - Re^{-ph} = 0 \;\Rightarrow\; (p_c + p)e^{ph} - (p_c - p)e^{-ph} = 0 \tag{5.148}$$

Equations (5.147) and (5.148), after being multiplying by $1/2$ (for convenience), can be grouped as follows

$$p_c \frac{e^{ph} + e^{-ph}}{2} + p \frac{e^{ph} - e^{-ph}}{2} = 0 \;\Rightarrow\; p_c \cosh ph + p \sinh ph = 0 \tag{5.149}$$

$$p_c \frac{e^{ph} - e^{-ph}}{2} + p \frac{e^{ph} + e^{-ph}}{2} = 0 \;\Rightarrow\; p_c \sinh ph + p \cosh ph = 0 \tag{5.150}$$

The eigenvalue equations in (5.149) and (5.150) are well-known [26], [32], [33]. They identify the even and odd *TE* surface-wave modes since they are even and odd in p, respectively. A similar analysis shows that $1 - \bar{R}^2 e^{-4ph} = 0$ leads to the well-known [26], [32], [33] even and odd TM surface-wave mode eigenvalue equations

$$p_c N^2 \cosh ph + p \sinh ph = 0 \tag{5.151}$$

$$p_c N^2 \sinh ph + p \cosh ph = 0 \tag{5.152}$$

5.8.3 Wave Interaction Between Source and Field Points

In this section, the terms of equations (5.129) and (5.130) will be examined for physical insight. Consider the geometry in Figure 5.3. Wave 0 travels from the source point y' directly to the field point y and traverses a distance $y - y'$. Hence, wave 0 is associated with the principal wave of (5.129). Wave 1, which experiences two interfacial reflections and travels a distance $4h + y - y'$, is associated with the first term in (5.130). Wave 2 is associated with the second term of (5.130) since it experiences only one interfacial reflection and travels a distance $2h + y + y'$. A similar discussion shows that waves 3 and 4 are associated with the third and fourth terms of (5.130). Note that waves $1-4$ experience reflection from the top $(y = h)$ and/or bottom $(y = -h)$ conductors and thus are associated with the reflected Green's function.

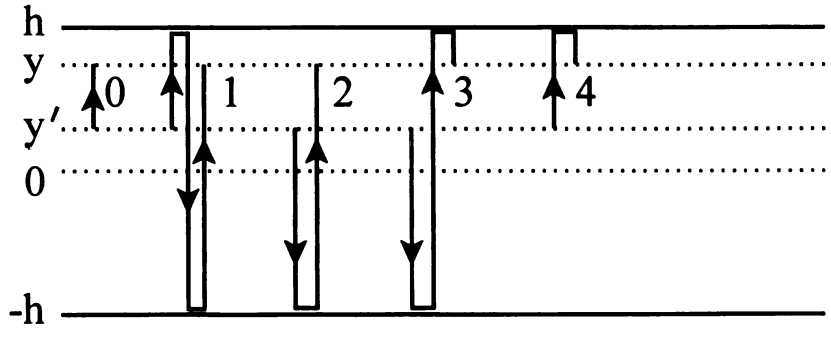

Figure 5.3 Wave interaction between source and field points.

5.8.4 Limiting Case for a Perfect Conductor

If the conductors become perfect ($\sigma_c \to \infty$), equations (5.130), (5.136) and (5.137) reduce to the correct/known result [34]

$$\tilde{G}^r_{\alpha\alpha}(\vec{\lambda}; y, y') = \frac{e^{-p\phi_1} - e^{-p\phi_2} + e^{-p\phi_3} - e^{-p\phi_4}}{2p(1-e^{-4ph})} \quad ...\alpha = x, z \tag{5.153}$$

$$\tilde{G}^r_{y\alpha}(\vec{\lambda}; y, y') = 0 \quad ...\alpha = x, z \tag{5.154}$$

$$\tilde{G}^r_{yy}(\vec{\lambda}; y, y') = \frac{e^{-p\phi_1} + e^{-p\phi_2} + e^{-p\phi_3} + e^{-p\phi_4}}{2p(1-e^{-4ph})} \tag{5.155}$$

since

$$\lim_{\sigma_c \to \infty} R = 1 \quad , \quad \lim_{\sigma_c \to \infty} \bar{R} = -1 \tag{5.156}$$

5.8.5 Limiting Case for a Source Over an Imperfectly-Conducting Half Space

Another known case is the problem in which a current source is situated over an imperfectly-conducting half-space [3], [25], [27]. In the parallel plate environment of Figure 5.1 (or 5.2), the half-space geometry can be achieved if the top plate is removed. However, if h is allowed to approach infinity in Figure 5.1, both plates would reside out to infinity since the top plate is at h and the bottom plate is at $-h$. This difficulty can be avoided if the structure is shifted upwards by a distance h so that the bottom plate is located at 0 and the top plate at $2h$. The geometrical shift can be accomplished mathematically using the following change of variables

$$\bar{y} = y + h \quad \Rightarrow \quad y = \bar{y} - h \tag{5.157}$$

$$\bar{y}' = y' + h \quad \Rightarrow \quad y' = \bar{y}' - h \tag{5.158}$$

Substitution of (5.157) and (5.158) into equations (5.129)-(5.134), (5.136), (5.137) and taking the limit as $h \to \infty$ leads to the following known result

$$\tilde{G}^p(\vec{\lambda}; \bar{y} - \bar{y}') = \frac{e^{-p|\bar{y}-\bar{y}'|}}{2p} \tag{5.159}$$

$$\tilde{G}^r_{\alpha\alpha}(\vec{\lambda}; \bar{y}, \bar{y}') = -\frac{R e^{-p(\bar{y}+\bar{y}')}}{2p} \quad ...\alpha = x, z \tag{5.160}$$

$$\tilde{G}^r_{y\alpha}(\vec{\lambda}; \bar{y}, \bar{y}') = -\frac{C^{+-}_{y\alpha} e^{-p(\bar{y}+\bar{y}')}}{2p} \quad ...\alpha = x, z \tag{5.161}$$

$$\tilde{G}^r_{yy}(\vec{\lambda}; \bar{y}, \bar{y}') = -\frac{\bar{R} e^{-p(\bar{y}+\bar{y}')}}{2p} = -\frac{(p_c N^2 - p) e^{-p(\bar{y}+\bar{y}')}}{2p(p_c N^2 + p)} \tag{5.162}$$

Of course, the working variables y, y' can be recovered by a second change of variables $y = \bar{y}, y' = \bar{y}'$. Equation (5.159) constitutes the principal-wave contribution directly from the source to the point of observation. Equations (5.160)-(5.162) are the reflected waves that emanate downward from the source, experience reflection at the half-space boundary, and travel upwards to the observation point. The reader familiar with guided wave theory will recognize the familiar Zenneck surface-wave [26] contribution in (5.162), for example. A Zenneck wave doesn't exist in the parallel plate environment since the factor $p_c N^2 + p$ doesn't explicitly occur in the denominator of (5.130), (5.136) or (5.137).

5.9 Electric Field Dyadic Green's Function

5.9.1 Introduction

The electric field dyadic Green's function can be identified by examining the following relation for the electric field, that is

$$\vec{E} = k^2\vec{\pi} + \nabla\nabla\cdot\vec{\pi} \tag{5.163}$$

It is convenient to break (5.163) into two parts, a principal and scattered part, where

$$\vec{E} = \vec{E}^p + \vec{E}^r = \int_{V'} \ddot{G}^e(\vec{r}|\vec{r}')\cdot\vec{J}(\vec{r}')dV' = \int_{V'}\left[\ddot{G}^{ep}(\vec{r}-\vec{r}') + \ddot{G}^{er}(\vec{r}|\vec{r}')\right]\cdot\vec{J}(\vec{r}')dV' \tag{5.164}$$

$$\vec{E}^p = k^2\vec{\pi}^p + \nabla\nabla\cdot\vec{\pi}^p = \int_{V'} \ddot{G}^{ep}(\vec{r}-\vec{r}')\cdot\vec{J}(\vec{r}')dV' \tag{5.165}$$

$$\vec{E}^r = k^2\vec{\pi}^r + \nabla\nabla\cdot\vec{\pi}^r = \int_{V'} \ddot{G}^{er}(\vec{r}|\vec{r}')\cdot\vec{J}(\vec{r}')dV' \tag{5.166}$$

It must be mentioned that no mathematical difficulties arise if the $\nabla\nabla\cdot$ operator is applied in the computation of $\vec{E}^r$ in (5.166) since the integrand of $\vec{\pi}^r$ is well behaved. This is not the case in (5.165), as discussed by [35]-[38]. Recall that

$$\vec{\pi}^p = \vec{\pi}_2^p(\vec{r}) = \int_{V'} \ddot{G}^p(\vec{r}-\vec{r}')\cdot\frac{\vec{J}(r')}{j\omega\varepsilon}dV' \tag{5.167}$$

where

$$\ddot{G}^p(\vec{r}-\vec{r}') = \frac{1}{(2\pi)^2}\int_{-\infty}^{\infty}\int_{-\infty}^{\infty}\ddot{I}\frac{e^{-p|y-y'|}}{2p}e^{j\vec{\lambda}\cdot(\vec{r}-\vec{r}')}d^2\lambda \tag{5.168}$$

A simple passing of the $\nabla\nabla\cdot$ (more precisely, the $\partial^2/\partial y^2$) operator through the integral term in (5.167) is not allowed in this case since the integral would become singular due to the absolute value term $|y-y'|$. In order to carefully handle this source point singularity, integration over y' must be broken into two parts as follows

$$\int_{y'} = \lim_{\delta\to 0^+}\left[\int_{-h}^{y-\delta} + \int_{y+\delta}^{h}\right] = PV\int_{y'} \tag{5.169}$$

and is known as evaluating the integral in a Cauchy Principle Value sense. However, this can be done only if the excluded portion doesn't contribute, that is

$$\lim_{\delta\to 0^+}\int_{y-\delta}^{y+\delta}\left[\frac{1}{(2\pi)^2}\int_{-\infty}^{\infty}\int_{-\infty}^{\infty}\vec{I}\frac{e^{-p|y-y'|}}{2p}e^{j\vec{\lambda}\cdot(\vec{r}-\vec{r}')}d^2\lambda\right]\cdot\frac{\vec{J}(r')}{j\omega\varepsilon}dy'=0 \qquad (5.170)$$

Since the integrand in (5.170) is continuous, the contribution from the excluded part is indeed zero and the integral in (5.167) can be evaluated in the Cauchy Principle Value sense, namely

$$\vec{\pi}^p = PV\int_{V'}\vec{\bar{G}}^p(\vec{r}-\vec{r}')\cdot\frac{\vec{J}(r')}{j\omega\varepsilon}dV' = \int_{x'}\int_{z'}\left[PV\int_{y'}\vec{\bar{G}}^p(\vec{r}-\vec{r}')\cdot\frac{\vec{J}(r')}{j\omega\varepsilon}dy'\right]dx'dz' \quad (5.171)$$

Note, any differential operator involving x or z can be freely passed through the volume integral in (5.167) since the integrand is well behaved in those variables. Also, since the integrand is continuous, Leibnitz's rule for differentiation guarantees that the $\partial/\partial y$ operator can also be freely passed through the volume integral. It will be demonstrated (via Leibnitz's rule) that, because the limits of integration in (5.171) depend on y and the integrand becomes discontinuous after one differentiation with respect to y, the $\partial^2/\partial y^2$ operator introduces an additional term that would be absent if it were simply passed through. Note, the PV notation will be assumed but dropped for convenience.

5.9.2 Principal Electric Field Dyadic Green's Function

The principal electric field dyadic Green's function can be identified by inserting (5.167) into (5.165), resulting in the following

$$\vec{E}^p = \frac{1}{j\omega\varepsilon}\int_{V'}\left(\hat{x}k^2G^p\hat{x}+\hat{y}k^2G^p\hat{y}+\hat{z}k^2G^p\hat{z}\right)\cdot\vec{J}dV' +$$
$$\frac{1}{j\omega\varepsilon}\int_{V'}\left(\hat{x}\frac{\partial^2G^p}{\partial x^2}\hat{x}+\hat{x}\frac{\partial^2G^p}{\partial x\partial y}\hat{y}+\hat{x}\frac{\partial^2G^p}{\partial x\partial z}\hat{z}\right)\cdot\vec{J}dV' +$$
$$\frac{1}{j\omega\varepsilon}\int_{V'}\left(\hat{y}\frac{\partial^2G^p}{\partial y\partial x}\hat{x}+\hat{y}\frac{\partial^2G^p}{\partial y\partial z}\hat{z}\right)\cdot\vec{J}dV' + \frac{1}{j\omega\varepsilon}\frac{\partial^2}{\partial y^2}\int_{V'}\hat{y}G^p\hat{y}\cdot\vec{J}dV' + \tag{5.172}$$
$$\frac{1}{j\omega\varepsilon}\int_{V'}\left(\hat{z}\frac{\partial^2G^p}{\partial z\partial x}\hat{x}+\hat{z}\frac{\partial^2G^p}{\partial z\partial y}\hat{y}+\hat{z}\frac{\partial^2G^p}{\partial z^2}\hat{z}\right)\cdot\vec{J}dV'$$

Leibnitz's rule for differentiation is [39]

$$\frac{\partial}{\partial y}\int_{a(y)}^{b(y)} f(y,y')dy' = \int_{a(y)}^{b(y)}\frac{\partial f(y,y')}{\partial y}dy' + f[y,b(y)]\frac{\partial b(y)}{\partial y} - f[y,a(y)]\frac{\partial a(y)}{\partial y} \tag{5.173}$$

and when applied to the $\partial^2/\partial y^2$ term in (5.172) produces the following results

$$\frac{\partial^2}{\partial y^2}\int_{V'}\hat{y}G^p\hat{y}\cdot\vec{J}dV' = \int_{x'}\int_{z'}\left[\frac{\partial}{\partial y}\int_{y'}\hat{y}\frac{\partial G^p}{\partial y}\hat{y}\cdot\vec{J}dy'\right]dx'dz' \tag{5.174}$$

$$\frac{\partial}{\partial y}\int_{y'}\hat{y}\frac{\partial G^p}{\partial y}\hat{y}\cdot\vec{J}dy' = \lim_{\delta\to 0^+}\frac{\partial}{\partial y}\left[\int_{-h}^{y-\delta}\hat{y}\frac{\partial G^p}{\partial y}\hat{y}\cdot\vec{J}dy' + \int_{y+\delta}^{h}\hat{y}\frac{\partial G^p}{\partial y}\hat{y}\cdot\vec{J}dy'\right] \tag{5.175}$$

where

$$\frac{\partial G^p}{\partial y} = \frac{\partial G^p(\vec{r}-\vec{r}')}{\partial y} = -\frac{1}{(2\pi)^2}\int_{-\infty}^{\infty}\int_{-\infty}^{\infty} p\,\mathrm{sgn}(y-y')\tilde{G}^p(\vec{\lambda};y-y')e^{j\vec{\lambda}\cdot(\vec{r}-\vec{r}')}d^2\lambda \tag{5.176}$$

The right-hand side of (5.175) leads to, with the aid of (5.173)

$$\lim_{\delta\to 0^+}\frac{\partial}{\partial y}\int_{-h}^{y-\delta}\hat{y}\frac{\partial G^p}{\partial y}\hat{y}\cdot\vec{J}dy' = \int_{-h}^{y-\delta}\hat{y}\frac{\partial^2 G^p}{\partial y^2}\hat{y}\cdot\vec{J}dy' - \hat{y}\frac{1}{2}\delta(\vec{\rho}-\vec{\rho}')\hat{y}\cdot\vec{J}(\vec{\rho}',y) \tag{5.177}$$

$$\lim_{\delta\to 0^+}\frac{\partial}{\partial y}\int_{y+\delta}^{h}\hat{y}\frac{\partial G^p}{\partial y}\hat{y}\cdot\vec{J}dy' = \int_{y+\delta}^{h}\hat{y}\frac{\partial^2 G^p}{\partial y^2}\hat{y}\cdot\vec{J}dy' - \hat{y}\frac{1}{2}\delta(\vec{\rho}-\vec{\rho}')\hat{y}\cdot\vec{J}(\vec{\rho}',y) \tag{5.178}$$

where the generalized function identity [23], [40]

$$\delta(\vec{\rho}-\vec{\rho}')=\frac{1}{(2\pi)^2}\int_{-\infty}^{\infty}\int_{-\infty}^{\infty}e^{j\vec{\lambda}\cdot(\vec{r}-\vec{r}')}d^2\lambda \tag{5.179}$$

has been used. Therefore, it is concluded that

$$\frac{\partial^2}{\partial y^2}\int_{V'}\hat{y}G^p\hat{y}\cdot\vec{J}dV'=\int_{V'}\hat{y}\left[\frac{\partial^2 G^p(\vec{r}-\vec{r}')}{\partial y^2}-\delta(\vec{r}-\vec{r}')\right]\hat{y}\cdot\vec{J}dV' \tag{5.180}$$

The principal electric field dyadic Green's function can be deduced by combining the results of (5.180) and (5.172), leading to

$$\begin{aligned}\bar{\bar{G}}^{ep}&=\hat{x}G^{ep}_{xx}\hat{x}+\hat{x}G^{ep}_{xy}\hat{y}+\hat{x}G^{ep}_{xz}\hat{z}+\\ &\hat{y}G^{ep}_{yx}\hat{x}+\hat{y}G^{ep}_{yy}\hat{y}+\hat{y}G^{ep}_{yz}\hat{z}+\hat{z}G^{ep}_{zx}\hat{x}+\hat{z}G^{ep}_{zy}\hat{y}+\hat{z}G^{ep}_{zz}\hat{z}\end{aligned} \tag{5.181}$$

where

$$G^{ep}_{xx}=\frac{1}{j\omega\varepsilon}\left(k^2G^p+\frac{\partial^2G^p}{\partial x^2}\right),\ G^{ep}_{xy}=\frac{1}{j\omega\varepsilon}\frac{\partial^2G^p}{\partial x\partial y},\ G^{ep}_{xz}=\frac{1}{j\omega\varepsilon}\frac{\partial^2G^p}{\partial x\partial z} \tag{5.182}$$

$$\begin{aligned}G^{ep}_{yx}&=\frac{1}{j\omega\varepsilon}\frac{\partial^2G^p}{\partial y\partial x},\ G^{ep}_{yz}=\frac{1}{j\omega\varepsilon}\frac{\partial^2G^p}{\partial y\partial z}\\ G^{ep}_{yy}&=\frac{1}{j\omega\varepsilon}\left[k^2G^p+\frac{\partial^2G^p}{\partial y^2}-\delta(\vec{r}-\vec{r}')\right]\end{aligned} \tag{5.183}$$

$$G^{ep}_{zx}=\frac{1}{j\omega\varepsilon}\frac{\partial^2G^p}{\partial z\partial x},\ G^{ep}_{zy}=\frac{1}{j\omega\varepsilon}\frac{\partial^2G^p}{\partial z\partial y},\ G^{ep}_{zz}=\frac{1}{j\omega\varepsilon}\left(k^2G^p+\frac{\partial^2G^p}{\partial z^2}\right) \tag{5.184}$$

$$\frac{\partial^2G^p}{\partial x^2}=-\frac{1}{(2\pi)^2}\int_{-\infty}^{\infty}\int_{-\infty}^{\infty}\xi^2\tilde{G}^pe^{j\vec{\lambda}\cdot(\vec{r}-\vec{r}')}d^2\lambda \tag{5.185}$$

$$\frac{\partial^2G^p}{\partial x\partial y}=\frac{\partial^2G^p}{\partial y\partial x}=-\frac{1}{(2\pi)^2}\int_{-\infty}^{\infty}\int_{-\infty}^{\infty}j\xi p\,\mathrm{sgn}(y-y')\tilde{G}^pe^{j\vec{\lambda}\cdot(\vec{r}-\vec{r}')}d^2\lambda \tag{5.186}$$

$$\frac{\partial^2 G^p}{\partial x \partial z} = \frac{\partial^2 G^p}{\partial z \partial x} = -\frac{1}{(2\pi)^2} \int_{-\infty}^{\infty} \int_{-\infty}^{\infty} \xi\zeta \tilde{G}^p e^{j\vec{\lambda}\cdot(\vec{r}-\vec{r}')} d^2\lambda \tag{5.187}$$

$$\frac{\partial^2 G^p}{\partial y \partial z} = \frac{\partial^2 G^p}{\partial z \partial y} = -\frac{1}{(2\pi)^2} \int_{-\infty}^{\infty} \int_{-\infty}^{\infty} j\zeta\, p\, \mathrm{sgn}(y-y') \tilde{G}^p e^{j\vec{\lambda}\cdot(\vec{r}-\vec{r}')} d^2\lambda \tag{5.188}$$

$$\frac{\partial^2 G^p}{\partial y^2} = \frac{1}{(2\pi)^2} \int_{-\infty}^{\infty} \int_{-\infty}^{\infty} p^2 \tilde{G}^p e^{j\vec{\lambda}\cdot(\vec{r}-\vec{r}')} d^2\lambda \tag{5.189}$$

$$\frac{\partial^2 G^p}{\partial z^2} = -\frac{1}{(2\pi)^2} \int_{-\infty}^{\infty} \int_{-\infty}^{\infty} \zeta^2 \tilde{G}^p e^{j\vec{\lambda}\cdot(\vec{r}-\vec{r}')} d^2\lambda \tag{5.190}$$

$$G^p = \frac{1}{(2\pi)^2} \int_{-\infty}^{\infty} \int_{-\infty}^{\infty} \tilde{G}^p e^{j\vec{\lambda}\cdot(\vec{r}-\vec{r}')} d^2\lambda \quad , \quad \tilde{G}^p = \tilde{G}^p(\vec{\lambda}; y-y') = \frac{e^{-p|y-y'|}}{2p} \tag{5.191}$$

5.9.3 Reflected Electric Field Dyadic Green's Function

In an analogous set of steps as in section 5.9.2, the reflected electric field dyadic Green's function can be identified by inserting the expression for $\vec{\pi}^r$ into (5.166). The result is

$$\begin{aligned} \bar{\bar{G}}^{er} &= \hat{x}G^{er}_{xx}\hat{x} + \hat{x}G^{er}_{xy}\hat{y} + \hat{x}G^{er}_{xz}\hat{z} + \\ &\hat{y}G^{er}_{yx}\hat{x} + \hat{y}G^{er}_{yy}\hat{y} + \hat{y}G^{er}_{yz}\hat{z} + \hat{z}G^{er}_{zx}\hat{x} + \hat{z}G^{er}_{zy}\hat{y} + \hat{z}G^{er}_{zz}\hat{z} \end{aligned} \tag{5.192}$$

where

$$G^{er}_{xx} = \frac{1}{j\omega\varepsilon}\left(k^2 G^r_{xx} + \frac{\partial^2 G^r_{xx}}{\partial x^2} + \frac{\partial^2 G^r_{yx}}{\partial x \partial y}\right) \tag{5.193}$$

$$G^{er}_{xy} = \frac{1}{j\omega\varepsilon}\frac{\partial^2 G^r_{yy}}{\partial x \partial y} \quad , \quad G^{er}_{xz} = \frac{1}{j\omega\varepsilon}\left(\frac{\partial^2 G^r_{yz}}{\partial x \partial y} + \frac{\partial^2 G^r_{zz}}{\partial x \partial z}\right) \tag{5.194}$$

$$G_{yx}^{er} = \frac{1}{j\omega\varepsilon}\left(k^2 G_{yx}^{r} + \frac{\partial^2 G_{yx}^{r}}{\partial y^2} + \frac{\partial^2 G_{xx}^{r}}{\partial y \partial x}\right) \tag{5.195}$$

$$G_{yy}^{er} = \frac{1}{j\omega\varepsilon}\left(k^2 G_{yy}^{r} + \frac{\partial^2 G_{yy}^{r}}{\partial y^2}\right) \quad , \quad G_{yz}^{er} = \frac{1}{j\omega\varepsilon}\left(k^2 G_{yz}^{r} + \frac{\partial^2 G_{yz}^{r}}{\partial y^2} + \frac{\partial^2 G_{zz}^{r}}{\partial y \partial z}\right) \tag{5.196}$$

$$G_{zx}^{er} = \frac{1}{j\omega\varepsilon}\left(\frac{\partial^2 G_{xx}^{r}}{\partial z \partial x} + \frac{\partial^2 G_{yx}^{r}}{\partial z \partial y}\right) \quad , \quad G_{zy}^{er} = \frac{1}{j\omega\varepsilon}\frac{\partial^2 G_{yy}^{r}}{\partial z \partial y} \tag{5.197}$$

$$G_{zz}^{er} = \frac{1}{j\omega\varepsilon}\left(k^2 G_{zz}^{r} + \frac{\partial^2 G_{zz}^{r}}{\partial z^2} + \frac{\partial^2 G_{yz}^{r}}{\partial z \partial y}\right) \tag{5.198}$$

$$\frac{\partial^2 G_{xx}^{r}}{\partial x^2} = -\frac{1}{(2\pi)^2}\int_{-\infty}^{\infty}\int_{-\infty}^{\infty} \xi^2 \tilde{G}_{xx}^{r} e^{j\vec{\lambda}\cdot(\vec{r}-\vec{r}')} d^2\lambda \tag{5.199}$$

$$\frac{\partial^2 G_{y\alpha}^{r}}{\partial x \partial y} = \frac{1}{(2\pi)^2}\int_{-\infty}^{\infty}\int_{-\infty}^{\infty} j\xi \frac{\partial \tilde{G}_{y\alpha}^{r}}{\partial y} e^{j\vec{\lambda}\cdot(\vec{r}-\vec{r}')} d^2\lambda \quad ...\alpha = x, y, z \tag{5.200}$$

$$\frac{\partial \tilde{G}_{y\alpha}^{r}}{\partial y} = -\frac{C_{y\alpha}^{++}e^{-p\phi_1} - C_{y\alpha}^{+-}e^{-p\phi_2} - C_{y\alpha}^{--}e^{-p\phi_3} + C_{y\alpha}^{-+}e^{-p\phi_4}}{2(1-R^2e^{-4ph})(1-\bar{R}^2e^{-4ph})} \quad ...\alpha = x, z \tag{5.201}$$

$$\frac{\partial \tilde{G}_{yy}^{r}}{\partial y} = -\frac{\bar{R}^2 e^{-p\phi_1} - \bar{R}\, e^{-p\phi_2} - \bar{R}^2 e^{-p\phi_3} + \bar{R}\, e^{-p\phi_4}}{2(1-\bar{R}^2e^{-4ph})} \tag{5.202}$$

$$\frac{\partial^2 G_{zz}^{r}}{\partial x \partial z} = -\frac{1}{(2\pi)^2}\int_{-\infty}^{\infty}\int_{-\infty}^{\infty} \xi\zeta \tilde{G}_{zz}^{r} e^{j\vec{\lambda}\cdot(\vec{r}-\vec{r}')} d^2\lambda \tag{5.203}$$

$$\frac{\partial^2 G_{y\alpha}^{r}}{\partial y^2} = \frac{1}{(2\pi)^2}\int_{-\infty}^{\infty}\int_{-\infty}^{\infty} p^2 \tilde{G}_{y\alpha}^{r} e^{j\vec{\lambda}\cdot(\vec{r}-\vec{r}')} d^2\lambda \quad ...\alpha = x, y, z \tag{5.204}$$

$$\frac{\partial^2 G_{xx}^{r}}{\partial y \partial x} = \frac{1}{(2\pi)^2}\int_{-\infty}^{\infty}\int_{-\infty}^{\infty} j\xi \frac{\partial \tilde{G}_{xx}^{r}}{\partial y} e^{j\vec{\lambda}\cdot(\vec{r}-\vec{r}')} d^2\lambda \tag{5.205}$$

$$\frac{\partial^2 G^r_{zz}}{\partial y \partial z} = \frac{1}{(2\pi)^2} \int_{-\infty}^{\infty} \int_{-\infty}^{\infty} j\zeta \frac{\partial \tilde{G}^r_{zz}}{\partial y} e^{j\vec{\lambda}\cdot(\vec{r}-\vec{r}')} d^2\lambda \tag{5.206}$$

$$\frac{\partial \tilde{G}^r_{\alpha\alpha}}{\partial y} = -\frac{R^2 e^{-p\phi_1} - Re^{-p\phi_2} - R^2 e^{-p\phi_3} + Re^{-p\phi_4}}{2(1-R^2 e^{-4ph})} \quad ...\alpha = x, z \tag{5.207}$$

$$\frac{\partial^2 G^r_{xx}}{\partial z \partial x} = -\frac{1}{(2\pi)^2} \int_{-\infty}^{\infty} \int_{-\infty}^{\infty} \xi\zeta \tilde{G}^r_{xx} e^{j\vec{\lambda}\cdot(\vec{r}-\vec{r}')} d^2\lambda \tag{5.208}$$

$$\frac{\partial^2 G^r_{y\alpha}}{\partial z \partial y} = \frac{1}{(2\pi)^2} \int_{-\infty}^{\infty} \int_{-\infty}^{\infty} j\zeta \frac{\partial \tilde{G}^r_{y\alpha}}{\partial y} e^{j\vec{\lambda}\cdot(\vec{r}-\vec{r}')} d^2\lambda \quad ...\alpha = x, y, z \tag{5.209}$$

$$\frac{\partial^2 G^r_{zz}}{\partial z^2} = -\frac{1}{(2\pi)^2} \int_{-\infty}^{\infty} \int_{-\infty}^{\infty} \zeta^2 \tilde{G}^r_{zz} e^{j\vec{\lambda}\cdot(\vec{r}-\vec{r}')} d^2\lambda \tag{5.210}$$

5.10 Magnetic Field Dyadic Green's Function

The principal and reflected magnetic field dyadic Green's functions are found by substituting $\vec{\pi}^p$ and $\vec{\pi}^r$ into the expression for $\vec{H}$, that is

$$\vec{H}^p = j\omega\varepsilon \nabla \times \vec{\pi}^p = \int_{V'} \tilde{\vec{G}}^{hp}(\vec{r}-\vec{r}') \cdot \vec{J}(\vec{r}') dV' \tag{5.211}$$

$$\vec{H}^r = j\omega\varepsilon \nabla \times \vec{\pi}^r = \int_{V'} \tilde{\vec{G}}^{hr}(\vec{r}|\vec{r}') \cdot \vec{J}(\vec{r}') dV' \tag{5.212}$$

The principal and reflected Green's functions, $\tilde{\vec{G}}^{hp}$ and $\tilde{\vec{G}}^{hr}$, for the magnetic field are (the minor details are left for the enjoyment of the reader)

$$\tilde{\vec{G}}^{hp} = \hat{x}G^{hp}_{xy}\hat{y} + \hat{x}G^{hp}_{xz}\hat{z} + \hat{y}G^{hp}_{yx}\hat{x} + \hat{y}G^{hp}_{yz}\hat{z} + \hat{z}G^{hp}_{zx}\hat{x} + \hat{z}G^{hp}_{zy}\hat{y} \tag{5.213}$$

$$G^{hp}_{xy} = -G^{hp}_{yx} = -\frac{\partial G^p}{\partial z} = -\frac{1}{(2\pi)^2} \int_{-\infty}^{\infty} \int_{-\infty}^{\infty} j\zeta \tilde{G}^p e^{j\vec{\lambda}\cdot(\vec{r}-\vec{r}')} d^2\lambda \tag{5.214}$$

$$G_{xz}^{hp} = -G_{zx}^{hp} = \frac{\partial G^p}{\partial y} = -\frac{1}{(2\pi)^2}\int_{-\infty}^{\infty}\int_{-\infty}^{\infty} p\,\mathrm{sgn}(y-y')\tilde{G}^p e^{j\vec{\lambda}\cdot(\vec{r}-\vec{r}')}d^2\lambda \qquad (5.215)$$

$$G_{yz}^{hp} = -G_{zy}^{hp} = -\frac{\partial G^p}{\partial x} = -\frac{1}{(2\pi)^2}\int_{-\infty}^{\infty}\int_{-\infty}^{\infty} j\xi\tilde{G}^p e^{j\vec{\lambda}\cdot(\vec{r}-\vec{r}')}d^2\lambda \qquad (5.216)$$

$$\tilde{\bar{G}}^{hr} = \hat{x}G_{xx}^{hr}\hat{x} + \hat{x}G_{xy}^{hr}\hat{y} + \hat{x}G_{xz}^{hr}\hat{z} + \hat{y}G_{yx}^{hr}\hat{x} + \hat{y}G_{yz}^{hr}\hat{z} + \hat{z}G_{zx}^{hr}\hat{x} + \hat{z}G_{zy}^{hr}\hat{y} + \hat{z}G_{zz}^{hr}\hat{z} \qquad (5.217)$$

$$G_{xx}^{hr} = -\frac{\partial G_{yx}^r}{\partial z}\ ,\ G_{xy}^{hr} = -\frac{\partial G_{yy}^r}{\partial z}\ ,\ G_{xz}^{hr} = \frac{\partial G_{zz}^r}{\partial y} - \frac{\partial G_{yz}^r}{\partial z} \qquad (5.218)$$

$$G_{yx}^{hr} = \frac{\partial G_{xx}^r}{\partial z}\ ,\ G_{yz}^{hr} = -\frac{\partial G_{zz}^r}{\partial x} \qquad (5.219)$$

$$G_{zx}^{hr} = \frac{\partial G_{yx}^r}{\partial x} - \frac{\partial G_{xx}^r}{\partial y}\ ,\ G_{zy}^{hr} = \frac{\partial G_{yy}^r}{\partial x}\ ,\ G_{zz}^{hr} = \frac{\partial G_{yz}^r}{\partial x} \qquad (5.220)$$

$$\frac{\partial G_{y\alpha}^r}{\partial z} = \frac{1}{(2\pi)^2}\int_{-\infty}^{\infty}\int_{-\infty}^{\infty} j\zeta\tilde{G}_{y\alpha}^r e^{j\vec{\lambda}\cdot(\vec{r}-\vec{r}')}d^2\lambda \ \ldots\alpha = x, y, z \qquad (5.221)$$

$$\frac{\partial G_{\alpha\alpha}^r}{\partial y} = \frac{1}{(2\pi)^2}\int_{-\infty}^{\infty}\int_{-\infty}^{\infty} \frac{\partial\tilde{G}_{\alpha\alpha}^r}{\partial y} e^{j\vec{\lambda}\cdot(\vec{r}-\vec{r}')}d^2\lambda \ \ldots\alpha = x, z \qquad (5.222)$$

$$\frac{\partial G_{xx}^r}{\partial z} = \frac{1}{(2\pi)^2}\int_{-\infty}^{\infty}\int_{-\infty}^{\infty} j\zeta\tilde{G}_{xx}^r e^{j\vec{\lambda}\cdot(\vec{r}-\vec{r}')}d^2\lambda \qquad (5.223)$$

$$\frac{\partial G_{zz}^r}{\partial x} = \frac{1}{(2\pi)^2}\int_{-\infty}^{\infty}\int_{-\infty}^{\infty} j\xi\tilde{G}_{zz}^r e^{j\vec{\lambda}\cdot(\vec{r}-\vec{r}')}d^2\lambda \qquad (5.224)$$

$$\frac{\partial G_{y\alpha}^r}{\partial x} = \frac{1}{(2\pi)^2}\int_{-\infty}^{\infty}\int_{-\infty}^{\infty} j\xi\tilde{G}_{y\alpha}^r e^{j\vec{\lambda}\cdot(\vec{r}-\vec{r}')}d^2\lambda \ \ldots\alpha = x, y, z \qquad (5.225)$$

Chapter 6

ANALYSIS OF A LOSSY STRIPLINE FIELD APPLICATOR

6.1 Introduction

The analysis of an imperfectly-conducting strip transmission line [41]-[44] symmetrically located between two imperfectly-conducting plates is considered in this chapter. Specifically, the effect that the lossy conductors have on the principal (i.e., dominant) discrete-mode propagation constant and respective surface current will be investigated. Understanding the nature of the principal mode is fundamental to the material characterization process (as well as to many other applications), and thus provides motivation for this study.

The first step in the analysis is to specialize the general 3D current source of chapter 5 to an infinitely-long strip surface current symmetrically located between imperfectly-conducting plates. Next, an EFIE (electric field integral equation) is developed by satisfying an impedance boundary condition on the strip conductor. As a final step, the EFIE is solved using a MoM (method of moments) technique and the principal-mode propagation constant and corresponding surface current distribution are subsequently identified.

6.2 Geometry

The geometry of the lossy stripline field applicator is shown in Figure 6.1. The structure is comprised of two imperfectly-conducting plates located at $y = \pm h$ and an

imperfect strip conductor located in the center at $y = 0$. The top and bottom plates are assumed to be infinite in length along the x, z directions and have properties (σ_c, Z_c). The infinitesimally-thin center strip of width $2a$ has properties (σ_s, Z_s) and is assumed to be infinite in length along the z direction. The center strip is embedded in a non-magnetic material characterized by the material parameters (ε, μ_0).

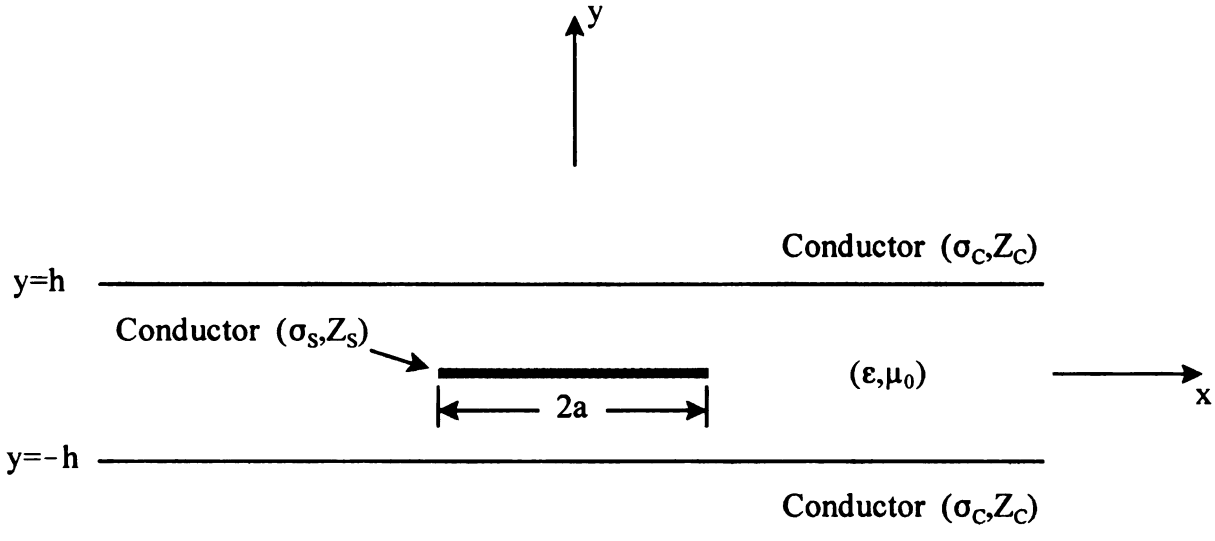

Figure 6.1 Cross-sectional geometry of the lossy stripline field applicator.

6.3 Development of the Lossy Stripline EFIE

The EFIE for the discrete-mode propagation constants of the stripline field applicator is obtained by first introducing an excitatory current $\vec{J}^i$ into the stripline environment that maintains an electric field $\vec{E}^i$. This impressed field will induce a surface current $\vec{K}$ on the strip conductor that subsequently maintains a scattered field given by

$$\vec{E}^s(\vec{r}) = \int_{S'} \ddot{G}^e(\vec{r}|\vec{r}') \cdot \vec{K}(\vec{r}')dV' = \int_{-a}^{a}\int_{-\infty}^{\infty} \ddot{G}^e(x,y|x',0;z-z') \cdot \vec{K}(x',z')dx'dz' \qquad (6.1)$$

where $\ddot{G}^e$ is the electric-field dyadic Green's function developed in chapter 5. The source $\vec{K}$ for the scattered field is confined to $y'=0$ and is invariant along the z direction, thus $\ddot{G}^e = \ddot{G}^e(x,y|x',y'=0;z-z')$. In addition, $\vec{K}$ will only be a function of x and z and will have no normal component (since the strip conductor is infinitesimally thin), that is

$$\vec{K}(\vec{r}) = \hat{x}K_x(x,z) + \hat{z}K_z(x,z) \qquad (6.2)$$

As a last step, the EFIE for the lossy stripline is developed by invoking the following impedance boundary condition on the imperfect strip conductor

$$\lim_{y\to 0} \hat{t} \cdot \left[\vec{E} = Z_s \vec{K}\right] \quad ...\forall\ x,z \in S \qquad (6.3)$$

where S is the surface of the strip conductor, $\hat{t} = \hat{x},\hat{z}$ is the unit tangent vector and $\vec{E}$ is the total field

$$\vec{E} = \vec{E}^i + \vec{E}^s \qquad (6.4)$$

The limit as $y \to 0$ must be used for convergence reasons and will be discussed shortly. Substitution of (6.4) and (6.1) into (6.3) produces the EFIE result

$$\lim_{y\to 0} \hat{t} \cdot \left[\int_{-a}^{a}\int_{-\infty}^{\infty} \ddot{G}^e(x,y|x',0;z-z') \cdot \vec{K}(x',z')dx'dz' - Z_s\vec{K}(x,z) = -\vec{E}^i(\vec{r})\right] \qquad (6.5)$$

The above equation is actually a pair of coupled EFIE's (coupled Fredholm equations of the second kind) since it must hold for $\hat{t} = \hat{x}$ and $\hat{z}$. Due to the form of $\ddot{G}^e$, the limit cannot be interchanged with the integral in (6.5) since this would render it divergent.

However, the MoM technique will strengthen the convergence of the integral and the limit can then be freely passed through, as will be shown in the next section.

Since the structure is invariant along the z-direction, it becomes computationally advantageous (and necessary) to transform (6.5) on the z-variable invoking the following transform pair

$$\begin{aligned} f(\vec{\rho},\zeta) &= \int_{-\infty}^{\infty} F(\vec{\rho},z)e^{-j\zeta z}dz \\ F(\vec{\rho},z) &= \frac{1}{2\pi}\int_{-\infty}^{\infty} f(\vec{\rho},\zeta)e^{j\zeta z}d\zeta \end{aligned} \tag{6.6}$$

with $\vec{\rho} = \hat{x}x + \hat{y}y$. The result, with the aid of the convolution theorem, is

$$\lim_{y\to 0}\hat{t}\cdot\left[\int_{-a}^{a}\vec{g}^{e}(x,y|x',0;\zeta)\cdot\vec{k}(x',\zeta)dx' - Z_s\vec{k}(x,\zeta) = -\vec{e}^{i}(\vec{\rho},\zeta)\right] \ldots\forall\ x\in C \tag{6.7}$$

where C is the periphery of the strip conductor ($-a < x < a$). Equation (6.7) represents the EFIE in the axial Fourier transform domain (i.e., the complex ζ domain), the solution of which, leads to the p^{th} discrete-mode propagation constant ζ_p. It can be shown [45] that near simple poles for the propagation constant ζ_p, the spectral-domain current has the following behavior (for a wave traveling in the $\pm z$ direction)

$$\lim_{\zeta\to\mp\zeta_p}\vec{k}(x,\zeta)\approx\frac{\vec{k}_p(x)}{\zeta\pm\zeta_p} \tag{6.8}$$

where $\vec{k}_p$ is the eigenmode current associated with the p^{th} discrete propagation mode. Substitution of (6.8) into (6.7) leads to

$$\lim_{\substack{y\to 0\\ \zeta\to\mp\zeta_p}}\hat{t}\cdot\left[\int_{-a}^{a}\vec{g}^{e}(x,y|x',0;\zeta)\cdot\frac{\vec{k}_p(x')}{\zeta\pm\zeta_p}dx' - Z_s\frac{\vec{k}_p(x)}{\zeta\pm\zeta_p} = -\vec{e}^{i}(\vec{\rho},\zeta)\right] \tag{6.9}$$

or equivalently

$$\lim_{\substack{y\to 0\\ \zeta\to\mp\zeta_p}} \hat{t}\cdot\left[\int_{-a}^{a}\vec{\bar{g}}^{e}(x,y|x',0;\zeta)\cdot\vec{k}_p(x')dx' - Z_s\vec{k}_p(x) = -(\zeta\pm\zeta_p)\vec{e}^{\,i}(\vec{\rho},\zeta)\right] \tag{6.10}$$

The impressed field $\vec{e}^{\,i}$ remains analytic near the pole singularity $\mp\zeta_p$ since, by its very nature, is independent of and cannot be influenced by the guiding structure. Therefore, near pole singularities $\zeta\to\mp\zeta_p$, equation (6.10) reduces to

$$\lim_{y\to 0}\hat{t}\cdot\left[\int_{-a}^{a}\vec{\bar{g}}^{e}(x,y|x',0;\mp\zeta_p)\cdot\vec{k}_p(x')dx' - Z_s\vec{k}_p(x) = 0\right] \tag{6.11}$$

Decomposition into $\hat{x}$ and $\hat{z}$ components leads to

$$\int_{-a}^{a}\left[g^{e}_{xx}(x,y|x',0)k_x(x') + g^{e}_{xz}(x,y|x',0)k_z(x')\right]dx' - Z_s k_x(x) = 0 \tag{6.12}$$

$$\int_{-a}^{a}\left[g^{e}_{zx}(x,y|x',0)k_x(x') + g^{e}_{zz}(x,y|x',0)k_z(x')\right]dx' - Z_s k_z(x) = 0 \tag{6.13}$$

where the limit and ζ notation, as well as the subscript on $\vec{k}_p$, has been dropped for convenience. Equations (6.12) and (6.13) constitute the fundamental pair of coupled EFIE's for determination of the p^{th} discrete-mode propagation constant $\mp\zeta_p$ and eigenmode current $\vec{k}_p$.

The axial-transform expressions for $g^{e}_{\alpha\beta}$ $(\alpha,\beta = x,z)$ can be identified using chapter 5. The result is (using the relation $\xi C^{\pm\pm}_{yz} = \zeta C^{\pm\pm}_{yx}$ and $\tilde{G}^{r}_{xx} = \tilde{G}^{r}_{zz}$ in the expression for C_{zx})

$$g^{e}_{\alpha\beta}(x,y|x',0) = g^{ep}_{\alpha\beta}(x,y|x',0) + g^{er}_{\alpha\beta}(x,y|x',0) = \int_{-\infty}^{\infty} C_{\alpha\beta} e^{j\xi(x-x')} d\xi \tag{6.14}$$

$$C_{\alpha\beta}(\xi,y,\zeta) = C^{p}_{\alpha\beta}(\xi,y,\zeta) + C^{r}_{\alpha\beta}(\xi,y,\zeta) \tag{6.15}$$

$$C^{p}_{xx} = \frac{k^2-\xi^2}{j2\pi\omega\varepsilon}\frac{e^{-p|y|}}{2p} \tag{6.16}$$

$$C^{r}_{xx} = \frac{1}{j2\pi\omega\varepsilon}\left[(k^2-\xi^2)\tilde{G}^{r}_{xx}(y|y'=0) + j\xi\frac{\partial\tilde{G}^{r}_{yx}(y|y'=0)}{\partial y}\right] \tag{6.17}$$

$$C^{p}_{xz} = C^{p}_{zx} = -\frac{\xi\zeta}{j2\pi\omega\varepsilon}\frac{e^{-p|y|}}{2p} \tag{6.18}$$

$$C^{r}_{xz} = C^{r}_{zx} = -\frac{1}{j2\pi\omega\varepsilon}\left[\xi\zeta\tilde{G}^{r}_{zz}(y|y'=0) - j\xi\frac{\partial\tilde{G}^{r}_{yz}(y|y'=0)}{\partial y}\right] \tag{6.19}$$

$$C^{p}_{zz} = \frac{k^2-\zeta^2}{j2\pi\omega\varepsilon}\frac{e^{-p|y|}}{2p} \tag{6.20}$$

$$C^{r}_{zz} = \frac{1}{j2\pi\omega\varepsilon}\left[(k^2-\zeta^2)\tilde{G}^{r}_{zz}(y|y'=0) + j\zeta\frac{\partial\tilde{G}^{r}_{yz}(y|y'=0)}{\partial y}\right] \tag{6.21}$$

Equations (6.12) and (6.13), upon using (6.14) and interchanging the spatial and spectral integrals, may therefore be written in the following form

$$\int_{-\infty}^{\infty} d\xi e^{j\xi x}\int_{-a}^{a}\left[C_{xx}k_x(x') + C_{xz}k_z(x')\right]e^{-j\xi x'}dx' - Z_s k_x(x) = 0 \tag{6.22}$$

$$\int_{-\infty}^{\infty} d\xi e^{j\xi x}\int_{-a}^{a}\left[C_{zx}k_x(x') + C_{zz}k_z(x')\right]e^{-j\xi x'}dx' - Z_s k_z(x) = 0 \tag{6.23}$$

6.4 MoM Solution for the Lossy Stripline EFIE

6.4.1 General Formulation

The dual EFIE's in (6.22) and (6.23) can be solved using a MoM technique. The first step is to expand the unknown currents using appropriate basis functions $e_{\beta n}(x)$ with complex amplitude $a_{\beta n}$, that is

$$k_\beta(x) = \sum_{n=1}^{N_\beta} a_{\beta n} e_{\beta n}(x) \quad ...\beta = x, z \tag{6.24}$$

Insertion of (6.24) into (6.22)-(6.23) and interchanging the summation with the spatial and spectral integrals leads to

$$\sum_{n=1}^{N_x} a_{xn}\left[\int_{-\infty}^{\infty} C_{xx} g_{xn} e^{j\xi x} d\xi - Z_s e_{xn}(x)\right] + \sum_{n=1}^{N_z} a_{zn}\left[\int_{-\infty}^{\infty} C_{xz} g_{zn} e^{j\xi x} d\xi\right] = 0 \tag{6.25}$$

$$\sum_{n=1}^{N_x} a_{xn}\left[\int_{-\infty}^{\infty} C_{zx} g_{xn} e^{j\xi x} d\xi\right] + \sum_{n=1}^{N_z} a_{zn}\left[\int_{-\infty}^{\infty} C_{zz} g_{zn} e^{j\xi x} d\xi - Z_s e_{zn}(x)\right] = 0 \tag{6.26}$$

where (since x' is a dummy integration variable)

$$g_{\beta n} = g_{\beta n}(\xi) = \int_{-a}^{a} e_{\beta n}(x') e^{-j\xi x'} dx' = \int_{-a}^{a} e_{\beta n}(x) e^{-j\xi x} dx \quad ...\beta = x, z \tag{6.27}$$

The second critical step in the MoM solution is to apply the following testing operator to (6.25) and (6.26), namely

$$\int_{-a}^{a} t_{\alpha m}(x)\{\cdot\}\, dx \quad ...m = 1,..., N_x + N_z \quad ; \alpha = x, z \tag{6.28}$$

where $t_{\alpha m}(x)$ is an appropriate testing function and $\alpha = x, z$ when applied to the x, z component equation, respectively. The result, after interchanging the testing operator integral with the sum and spectral integrals, is

$$\sum_{n=1}^{N_x} a_{xn}\left[\int_{-\infty}^{\infty} C_{xx} f_{xm} g_{xn} d\xi + D_{xx}^{mn}\right] + \sum_{n=1}^{N_z} a_{zn}\left[\int_{-\infty}^{\infty} C_{xz} f_{xm} g_{zn} d\xi\right] = 0 \qquad (6.29)$$

$$\sum_{n=1}^{N_x} a_{xn}\left[\int_{-\infty}^{\infty} C_{zx} f_{zm} g_{xn} d\xi\right] + \sum_{n=1}^{N_z} a_{zn}\left[\int_{-\infty}^{\infty} C_{zz} f_{zm} g_{zn} d\xi + D_{zz}^{mn}\right] = 0 \qquad (6.30)$$

or in matrix form

$$\left.\begin{aligned} \sum_{n=1}^{N_x} A_{xx}^{mn} a_{xn} + \sum_{n=1}^{N_z} A_{xz}^{mn} a_{zn} = 0 \\ \sum_{n=1}^{N_x} A_{zx}^{mn} a_{xn} + \sum_{n=1}^{N_z} A_{zz}^{mn} a_{zn} = 0 \end{aligned}\right\} \ldots m = 1, \ldots, N_x + N_z \qquad (6.31)$$

where

$$A_{\alpha\beta}^{mn} = \lim_{y \to 0} \int_{-\infty}^{\infty} C_{\alpha\beta} f_{\alpha m} g_{\beta n} d\xi + D_{\alpha\alpha}^{mn} \delta_{\alpha\beta} \quad \ldots \alpha, \beta = x, z \qquad (6.32)$$

$$f_{\alpha m} = f_{\alpha m}(\xi) = \int_{-a}^{a} t_{\alpha m}(x) e^{j\xi x} dx \quad \ldots \alpha = x, z \qquad (6.33)$$

$$D_{\alpha\alpha}^{mn} = -Z_s \int_{-a}^{a} t_{\alpha m}(x) e_{\alpha n}(x) dx \quad , \quad \delta_{\alpha\beta} = \begin{cases} 1 & \ldots \alpha = \beta \\ 0 & \ldots \alpha \neq \beta \end{cases} \qquad (6.34)$$

The choice of expansion and testing functions is usually strongly influenced by physical and mathematical considerations. From a physical standpoint, the expansion functions should closely model the behavior of the unknown currents so that only a few expansion functions are required to efficiently obtain accurate results. In addition, a prudent choice of expansion and testing functions will allow the integrals in (6.27), (6.33) and (6.34) to be computed in closed form. Although obtaining closed-form integrals is not absolutely necessary, it does significantly reduce computational effort and therefore increases numerical efficiency.

The stripline considered in this chapter can support both even and odd modes (about the variable x) due to its symmetry. This, of course, has implications on the choice of expansion and testing functions. Even and odd modes are typically classified relative to the longitudinal current $k_z(x)$. If $k_z(x)$ is even(odd), then the particular mode supported is classified as even(odd). Consequently, $k_x(x)$ must be odd(even) and ρ_s must be even(odd) since the axial transform continuity equation is

$$\tilde{\nabla} \cdot \vec{k} = \frac{\partial k_x}{\partial x} + j\zeta k_z = -j\omega\rho_s \tag{6.35}$$

Thus, when choosing testing and expansion functions for even modes, one should select even functions to represent e_{zn}, t_{zn} and odd functions to represent e_{xn}, t_{xn}. Similarly, for odd modes, e_{zn}, t_{zn} must be odd and e_{xn}, t_{xn} will consequently have to be even. In addition, the axial and transverse surface currents have the following well-known behavior [46], [47] near the edges of the infinitesimally-thin strip conductor

$$k_x \propto \rho^{1/2} \quad , \quad k_z \propto \rho^{-1/2} \tag{6.36}$$

where ρ is the radial distance from the edge. Accordingly, one should select expansion functions that closely model this edge behavior. It is known [45] that the principal mode (which is the only mode being investigated in this chapter) is even. However, an MoM formulation for both even and odd modes will be given below for the sake of completeness.

6.4.2 Even-Mode MoM Formulation for Lossy Stripline

A common choice of expansion and testing functions employed when considering lossless structures (known as Galerkin's method [29]) for even modes is

$$e_{xn}(x) = t_{xn}(x) = T_{2n+1}(x/a)\sqrt{1-(x/a)^2} \tag{6.37}$$

$$e_{zn}(x) = t_{zn}(x) = \frac{T_{2n}(x/a)}{\sqrt{1-(x/a)^2}} \tag{6.38}$$

where $T_n(x)$ are Chebyshev polynomials [48], [49] of the first kind (see Appendix E for an overview of Chebyshev polynomials). Note that Chebyshev polynomials of odd/even order are odd/even functions, as seen from the relation [50]

$$T_n(x) = (-1)^n T_n(-x) \tag{6.39}$$

Therefore, $e_{xn}(x), e_{zn}(x)$ are odd/even functions and have appropriate weighting functions, as physically required. However, there are now mathematical difficulties encountered in the lossy case that were absent in the lossless case. Namely, the integral in expression (6.34) becomes divergent for certain m, n. To see this, consider the case when $m = n = 0$, namely

$$D_{zz}^{00} = -Z_s \int_{-a}^{a} t_{z0}(x) e_{z0}(x) dx = -Z_s \int_{-a}^{a} \frac{T_0^2(x/a)}{1-(x/a)^2} dx \tag{6.40}$$

The c.o.v. (change-of-variable) $\tilde{x} = x/a$ leads to the following integral expression

$$D_{zz}^{00} = -aZ_s \int_{-1}^{1} \frac{T_0^2(\tilde{x})}{1-\tilde{x}^2} d\tilde{x} = -aZ_s \int_{-1}^{1} \frac{1}{1-\tilde{x}^2} d\tilde{x} \tag{6.41}$$

where the property $T_0(x) = 1$ has been used. The above elementary integral is known to be divergent. Therefore, Galerkin's method is no longer applicable for lossy structures and alternative expansion and testing functions must be sought.

The problem becomes tractable if Chebyshev polynomials of both the first and second kind are used in appropriate combinations. For even modes, the following

choices should be made for the expansion and testing functions (where $m,n=0,1,2,...$)

$$e_{xn}(x)=U_{2n+1}(x/a)\sqrt{1-(x/a)^2} \tag{6.42}$$

$$t_{xm}(x)=U_{2m+1}(x/a) \tag{6.43}$$

$$e_{zn}(x)=\frac{T_{2n}(x/a)}{\sqrt{1-(x/a)^2}} \tag{6.44}$$

$$t_{zm}(x)=T_{2m}(x/a) \tag{6.45}$$

It is important that the weight functions are contained in the expansion functions since they are representing the physical currents (and are based on the required edge condition). Then, after the expansion functions have been determined, the testing functions are conveniently chosen so that (6.34) is easily computed using known orthogonality relations.

Insertion of (6.42)-(6.45) into the corresponding relations (6.27), (6.33) and (6.34) leads to (after using the c.o.v. $\tilde{x}=x/a$ and the even/odd properties of the Chebyshev polynomials)

$$f_{xm}(\xi)=j2a\int_0^1 U_{2m+1}(\tilde{x})\sin(\xi a\tilde{x})d\tilde{x}=j2aI^o_{fxm}(\xi a) \tag{6.46}$$

$$f_{zm}(\xi)=2a\int_0^1 T_{2m}(\tilde{x})\cos(\xi a\tilde{x})d\tilde{x}=2aI^e_{fzm}(\xi a) \tag{6.47}$$

$$g_{xn}(\xi)=-j2a\int_0^1 U_{2n+1}(\tilde{x})\sqrt{1-\tilde{x}^2}\sin(\xi a\tilde{x})d\tilde{x}=-j2aI^o_{gxn}(\xi a) \tag{6.48}$$

$$g_{zn}(\xi)=2a\int_0^1 \frac{T_{2n}(\tilde{x})}{\sqrt{1-\tilde{x}^2}}\cos(\xi a\tilde{x})d\tilde{x}=2aI^e_{gzn}(\xi a) \tag{6.49}$$

$$D_{xx}^{mn} = -aZ_s \int_{-1}^{1} U_{2m+1}(\tilde{x}) U_{2n+1}(\tilde{x}) \sqrt{1-\tilde{x}^2}\, d\tilde{x} = -aZ_s I_{xmn} \tag{6.50}$$

$$D_{zz}^{mn} = -aZ_s \int_{-1}^{1} \frac{T_{2m}(\tilde{x}) T_{2n}(\tilde{x})}{\sqrt{1-\tilde{x}^2}}\, d\tilde{x} = -aZ_s I_{zmn} \tag{6.51}$$

where the superscript e,o means the resulting integral is even or odd in ξ (which can be verified by trivial inspection of the above integrals). Remarkably, Appendix E shows that the above integrals exist in closed form as desired. Thus, the above combination of expansion and testing functions adhere to the physical and mathematical stipulations.

Substitution of (6.46)-(6.51) into (6.32) results in the following expressions for the matrix elements

$$A_{xx}^{mn} = \lim_{y\to 0} 8a \int_0^{\infty} C_{xx}(\xi, y, \zeta) I_{fxm}^{o}(\xi a) I_{gxn}^{o}(\xi a) d\xi - Z_s I_{xmn} \tag{6.52}$$

$$A_{xz}^{mn} = \lim_{y\to 0} j8a \int_0^{\infty} C_{xz}(\xi, y, \zeta) I_{fxm}^{o}(\xi a) I_{gzn}^{e}(\xi a) d\xi \tag{6.53}$$

$$A_{zx}^{mn} = -\lim_{y\to 0} j8a \int_0^{\infty} C_{zx}(\xi, y, \zeta) I_{fzm}^{e}(\xi a) I_{gxn}^{o}(\xi a) d\xi \tag{6.54}$$

$$A_{zz}^{mn} = \lim_{y\to 0} 8a \int_0^{\infty} C_{zz}(\xi, y, \zeta) I_{fzm}^{e}(\xi a) I_{gzn}^{e}(\xi a) d\xi - Z_s I_{zmn} \tag{6.55}$$

since C_{xx}, C_{zz} are even in ξ and C_{xz}, C_{zx} are odd in ξ. Note that one a can be dropped because we are solving a homogeneous matrix equation. In addition, a careful examination of Chapters 5 and 6 shows that $C_{xx} \sim \xi$, $C_{xz} = C_{zx} \sim 1$ and $C_{zz} \sim 1/\xi$ as $\xi \to \infty$. Thus, with the aid of Appendix E, it can be shown that the magnitude of the integrands of $A_{\alpha\beta}$, that is $\left|I(A_{\alpha\beta})\right|$, have the following asymptotic behaviors

$$\lim_{\xi\to\infty}|I(A_{xx})|,|I(A_{xz})|\sim 1/\xi^{3/2} \quad ; \quad \lim_{\xi\to\infty}|I(A_{xz})|,|I(A_{zz})|\sim 1/\xi^{5/2} \tag{6.56}$$

The strength of this asymptotic behavior guarantees convergence and formally allows the limit to be brought inside the spectral integral in expressions (6.52)-(6.55). Therefore, the above matrix elements simplify to

$$A_{xx}^{mn} = 8a\int_0^\infty C_{xx}(\xi,\zeta)I_{fxm}^o(\xi a)I_{gxn}^o(\xi a)d\xi - Z_s I_{xmn} \tag{6.57}$$

$$A_{xz}^{mn} = j8a\int_0^\infty C_{xz}(\xi,\zeta)I_{fxm}^o(\xi a)I_{gzn}^e(\xi a)d\xi \tag{6.58}$$

$$A_{zx}^{mn} = -j8a\int_0^\infty C_{zx}(\xi,\zeta)I_{fzm}^e(\xi a)I_{gxn}^o(\xi a)d\xi \tag{6.59}$$

$$A_{zz}^{mn} = 8a\int_0^\infty C_{zz}(\xi,\zeta)I_{fzm}^e(\xi a)I_{gzn}^e(\xi a)d\xi - Z_s I_{zmn} \tag{6.60}$$

where, after some algebraic manipulation, the functions $C_{\alpha\beta}(\xi,\zeta) = C_{\alpha\beta}(\xi, y=0,\zeta)$ are

$$C_{xx}(\xi,\zeta) = \frac{1}{j4\pi\omega\varepsilon D^e}\left[\frac{A(k^2-\xi^2)}{p} + \frac{\xi^2}{\sigma_c Z_c D^h}\right] \tag{6.61}$$

$$C_{xz}(\xi,\zeta) = C_{zx}(\xi,\zeta) = -\frac{\xi\zeta}{j4\pi\omega\varepsilon D^e}\left[\frac{A}{p} - \frac{1}{\sigma_c Z_c D^h}\right] \tag{6.62}$$

$$C_{zz}(\xi,\zeta) = \frac{1}{j4\pi\omega\varepsilon D^e}\left[\frac{A(k^2-\zeta^2)}{p} + \frac{\zeta^2}{\sigma_c Z_c D^h}\right] \tag{6.63}$$

$$A = \sinh ph + \frac{p}{\sigma_c Z_c}\cosh ph \tag{6.64}$$

$$D^e = \cosh ph + \frac{p}{\sigma_c Z_c}\sinh ph \quad , \quad D^h = \cosh ph + j\frac{\omega\varepsilon Z_c}{p}\sinh ph \tag{6.65}$$

Note that the $C_{\alpha\beta}$ are all even with respect to p, hence the branch points at $\lambda = \pm k$ are removable. In addition, the above matrix elements reduce to the known lossless case [34] in the limit as $\sigma_c \to \infty$, as anticipated.

As a final note, since the Chebyshev polynomials are indexed starting from zero, the matrix equation subsequently should be written as

$$\left.\begin{aligned} \sum_{n=0}^{N_x-1} A_{xx}^{mn} a_{xn} + \sum_{n=0}^{N_z-1} A_{xz}^{mn} a_{zn} = 0 \\ \sum_{n=0}^{N_x-1} A_{zx}^{mn} a_{xn} + \sum_{n=0}^{N_z-1} A_{zz}^{mn} a_{zn} = 0 \end{aligned}\right\} \ldots m = 0,\ldots, N_x + N_z - 1 \tag{6.66}$$

This also applies to the odd-mode analysis given below.

6.4.3 Odd-Mode MoM Formulation for Lossy Stripline

In the analysis of odd modes, in which k_x is even and k_z is odd, the following choices should be made for the expansion and testing functions (where $m, n = 0, 1, 2, \ldots$)

$$e_{xn}(x) = U_{2n}(x/a)\sqrt{1-(x/a)^2} \tag{6.67}$$

$$t_{xm}(x) = U_{2m}(x/a) \tag{6.68}$$

$$e_{zn}(x) = \frac{T_{2n+1}(x/a)}{\sqrt{1-(x/a)^2}} \tag{6.69}$$

$$t_{zm}(x) = T_{2m+1}(x/a) \tag{6.70}$$

In this case, the matrix elements are

$$A_{xx}^{mn} = 8a \int_0^\infty C_{xx}(\xi,\zeta)\tilde{I}_{fxm}^{e}(\xi a)\tilde{I}_{gxn}^{e}(\xi a)d\xi - Z_s \tilde{I}_{xmn} \tag{6.71}$$

$$A_{xz}^{mn} = -j8a\int_0^\infty C_{xz}(\xi,\zeta)\tilde{I}_{fxm}^{e}(\xi a)\tilde{I}_{gzn}^{o}(\xi a)d\xi \tag{6.72}$$

$$A_{zx}^{mn} = j8a\int_0^\infty C_{zx}(\xi,\zeta)\tilde{I}_{fzm}^{o}(\xi a)\tilde{I}_{gxn}^{e}(\xi a)d\xi \tag{6.73}$$

$$A_{zz}^{mn} = 8a\int_0^\infty C_{zz}(\xi,\zeta)\tilde{I}_{fzm}^{o}(\xi a)\tilde{I}_{gzn}^{o}(\xi a)d\xi - Z_s\tilde{I}_{zmn} \tag{6.74}$$

where

$$\tilde{I}_{fxm}^{e}(\xi a) = \int_0^1 U_{2m}(\tilde{x})\cos(\xi a\tilde{x})d\tilde{x} \tag{6.75}$$

$$\tilde{I}_{fzm}^{o}(\xi a) = \int_0^1 T_{2m+1}(\tilde{x})\sin(\xi a\tilde{x})d\tilde{x} \tag{6.76}$$

$$\tilde{I}_{gxn}^{e}(\xi a) = \int_0^1 U_{2n}(\tilde{x})\sqrt{1-\tilde{x}^2}\cos(\xi a\tilde{x})d\tilde{x} \tag{6.77}$$

$$\tilde{I}_{gzn}^{o}(\xi a) = \int_0^1 \frac{T_{2n+1}(\tilde{x})}{\sqrt{1-\tilde{x}^2}}\sin(\xi a\tilde{x})d\tilde{x} \tag{6.78}$$

$$\tilde{I}_{xmn} = \int_{-1}^1 U_{2m}(\tilde{x})U_{2n}(\tilde{x})\sqrt{1-\tilde{x}^2}\,d\tilde{x} \tag{6.79}$$

$$\tilde{I}_{zmn} = \int_{-1}^1 \frac{T_{2m+1}(\tilde{x})T_{2n+1}(\tilde{x})}{\sqrt{1-\tilde{x}^2}}\,d\tilde{x} \tag{6.80}$$

6.4.4 Quasi-TEM Characteristic Impedance

A quasi-TEM (transverse electromagnetic) characteristic impedance for the even principal mode can be identified for the imperfectly-conducting stripline by assuming

that the transverse current k_x is negligible in comparison with the longitudinal current k_z (Section 6.5 will show that this is indeed the case), or equivalently

$$k_x \approx 0 \quad \Rightarrow \quad \vec{K} \approx \hat{z} k_z \quad ...quasi-TEM\ approximation \tag{6.81}$$

Under these conditions, a unique characteristic impedance can be identified in the transverse plane of the stripline field applicator (since $k_x = 0$ implies that no longitudinal magnetic field is produced to cause an additional EMF) given by

$$z_0 = \pm \frac{v(z)}{i(z)} \quad ...-\infty < z < \infty \quad \Rightarrow \quad Z_0 = \pm \frac{V(\zeta)}{I(\zeta)} \tag{6.82}$$

where $V(\zeta)$ and $I(\zeta)$ are the axial transform voltage and current of a single traveling wave (only single-traveling waves will be supported on the stripline structure since it is assumed to be infinite in extent along the guiding axis). The plus sign should be used if the observation point is to the right of the source point (i.e., for a forward traveling wave) and the minus sign if the observation point is to the left of the source point (i.e., for a reverse traveling wave). Since this impedance holds true for all z, the expressions for V and I can be formulated in the axial Fourier transform domain using the following standard TEM definitions of voltage and current

$$V(\zeta) = -\int_{-}^{+} \vec{e}(\vec{\rho},\zeta) \cdot \overrightarrow{dl} \quad , \quad I(\zeta) = \oint_{C} \vec{k}(x,\zeta) \cdot \overrightarrow{d\tau} \tag{6.83}$$

Since voltage is independent of path in the transverse plane, the integration contour (from the center conductor to the ground plane) for the computation of V can be conveniently chosen along $x = 0$, thus $\overrightarrow{dl} = \hat{y} dy$. The displacement vector $\overrightarrow{d\tau}$ equals $\hat{z} dx$ since current flows along the longitudinal direction and is confined within the strip and ground planes. When the center strip is positively charged and the ground planes

negatively charged, then V and I take the following form

$$V(\zeta) = \int_0^h e_y(0,y,\zeta)dy \quad , \quad I(\zeta) = \int_{-a}^{a} k_z(x,\zeta)dx \tag{6.84}$$

Note that e_y is the $\hat{y}$ component of the total electric field, that is

$$e_y(0,y,\zeta) = e_y^i(0,y,\zeta) + e_y^s(0,y,\zeta) \tag{6.85}$$

where e_y^i is the impressed electric field and e_y^s is the scattered electric field given by (with the aid of Chapters 5 and 6)

$$e_y^s(0,y,\zeta) = \hat{y} \cdot \int_{-a}^{a} \vec{g}^e(0,y|x',0;\zeta) \cdot \vec{k}(x')dx' = \int_{-a}^{a} g_{yz}^e(0,y|x',0;\zeta) \cdot k_z(x')dx' \tag{6.86}$$

Near pole singularities, as already discussed, the surface current has the following behavior (for forward/reverse traveling waves)

$$\lim_{\zeta \to \mp\zeta_p} \vec{k}(x,\zeta) \approx \frac{\vec{k}_p(x)}{\zeta \pm \zeta_p} \quad \Rightarrow \quad \lim_{\zeta \to \mp\zeta_p} k_z(x,\zeta) \approx \frac{k_{zp}(x)}{\zeta \pm \zeta_p} \tag{6.87}$$

Substitution of (6.84)-(6.87) into (6.82) and multiplying the resulting numerator and denominator by $\zeta \pm \zeta_p$ produces the following expression

$$Z_0 = \pm \lim_{\zeta \to \mp\zeta_p} \frac{\int_0^h (\zeta \pm \zeta_p) e_y^i(0,y,\zeta)dy + \int_0^h \int_{-a}^{a} g_{yz}^e(0,y|x',0;\zeta) \cdot k_{zp}(x')dx'dy}{\int_{-a}^{a} k_{zp}(x)dx} \tag{6.88}$$

The incident field, in general, remains analytic at the pole singularities since it is independent of, and cannot be influenced by, the guiding structure. Therefore, due to the limit process above, the incident field is not implicated in the computation of characteristic impedance for the discrete principal mode. Thus, in the limit as $\zeta \to \mp\zeta_p$,

the characteristic impedance takes on the following form

$$Z_0 = \pm\frac{V}{I} = \pm\frac{\int_{0}^{h}\int_{-a}^{a} g_{yz}^{e}(0,y|x',0;\mp\zeta_p)\cdot k_z(x')dx'dy}{\int_{-a}^{a} k_z(x)dx} \tag{6.89}$$

where the p subscript on k_{zp} has been dropped for notational convenience and

$$k_z(x) = \sum_{n=0}^{N_z-1} a_{zn}e_{zn}(x) \quad , \quad e_{zn}(x) = \frac{T_{2n}(x/a)}{\sqrt{1-(x/a)^2}} \tag{6.90}$$

The computation of V involves spectral integration due to the presence of g_{yz}^{e} and must therefore be handled numerically. However, an analytical expression for I exists and can be identified as follows. First, substitution of (6.90) into the expression for I in (6.89) leads to, with the c.o.v. $\tilde{x} = x/a$ followed by the c.o.v. $\tilde{x} = x$,

$$I = a\sum_{n=0}^{N_z-1} a_{zn}\int_{-1}^{1}\frac{T_{2n}(x)}{\sqrt{1-x^2}}dx \tag{6.91}$$

The c.o.v. $x = \cos\theta$ and the use of the relation $T_{2n}(\cos\theta) = \cos(2n\theta)$ from Appendix E leads to the following expression for the integral in (6.91), namely

$$\int_{-1}^{1}\frac{T_{2n}(x)}{\sqrt{1-x^2}}dx = \int_{0}^{\pi}\cos(2n\theta)d\theta = \begin{cases}\pi & \ldots n=0\\ 0 & \ldots n\neq 0\end{cases} \tag{6.92}$$

Therefore, upon substitution of (6.92) into (6.91), the current reduces to the simple expression

$$I = a\pi a_{z0} \tag{6.93}$$

where a_{z0} is the leading expansion coefficient for the longitudinal current k_z. In general, the computation of V will require knowledge of all the coefficients a_{zn}.

6.5 Numerical Results

In this section, numerical results of the MoM solution for the propagation constant ($\zeta = \beta - j\alpha$) and surface currents (k_x, k_z) are examined. Note, it will be assumed that $\varepsilon = \varepsilon_0$, unless specified differently. First, it is important to determine how rapidly the solution converges. Figures 6.2-6.4 show that the Chebyshev polynomials insure excellent convergence properties for the propagation constant and surface currents with only a small number of expansion and testing terms. Remarkably, only a single expansion and testing function (i.e., the Maxwellian distribution) produces very accurate results. In order to adhere to common notational convention, the following symbols will be used. Ground-plane and strip conductivity are represented by the symbols σ_g and σ_s, half-width and half-height are represented by w and t, and exponentiation is represented by the letter e or d (for example, $1\times10^6 = 1e6 = 1d6$).

Next, it is important to check whether the non-Galerkin method developed here in Chapter 6 produces the same result as the known Galerkin method [34] for the lossless case (in which k_x is identically zero and $\zeta = k$). Figure 6.5 shows that both methods produce identical results, as anticipated. In addition, the full-wave theory developed in Chapters 5-6 compares closely with the well-known perturbation theory result [3], [18], as demonstrated in Figure 6.6. Note, a perturbation and full-wave theory comparison for the phase constant β cannot be made since the perturbation theory only accommodates for attenuation. Thus, an advantage of the full-wave theory is that it corrects for both phase and attenuation (note, it was already shown in Chapter 4 that phase correction is exceedingly important in material characterization measurements).

Figures 6.7-6.10 show the effects that ground-plane and strip conductivity have on the principal-mode propagation constant. Since the surface impedance $Z_{g,s} = (1+j)\sqrt{\omega\mu_0 / 2\sigma_{g,s}}$, the resistance and inductance of the stripline increases as $\sigma_{g,s}$ decreases. Elementary transmission line theory states that the phase constant β is proportional to inductance and the attenuation constant is proportional to resistance, thus one should expect an increase in the phase and attenuation constant as the conductivity decreases. An examination of Figures 6.7-6.10 demonstrates this anticipated result. In addition, the strip conductivity has a more pronounced effect on the propagation constant, as one would expect, since the current flow is restricted to a smaller region. This causes resistance and stored magnetic energy (hence inductance) to increase, resulting in an increase of α and β. The surface impedance model also predicts an increase in the attenuation and phase constants as frequency increases. The increase in the attenuation constant α at higher frequencies is clearly evident from Figures 6.8 and 6.10. The increase in phase constant β is not as clear due to the normalization with respect to k_0. Upon multiplication of k_0, the increase of β at higher frequencies would be more clearly evident, but is more cumbersome to present in graphical form due to the exceedingly large values of β. Note, exhaustive results for a stripline having both ground-plane and strip conductor losses are not given here for the sake of brevity (perturbation theory predicts that the total attenuation is simply the sum of the two cases presented here).

Figures 6.11-6.12 reveal the effects that strip conductivity has on the surface currents k_x and k_z. Figure 6.11 demonstrates that the transverse current k_x increases as

strip conductivity σ_s decreases. This is an expected result since lower conductivities allow for more pronounced longitudinal fields in the conductor, which leads to larger longitudinal field components (which are predominantly maintained by transverse currents). Figure 6.12 shows that there is seemingly little effect on the surface current k_z, probably due to the method of surface-current normalization.

The effect that frequency has on the surface currents k_x and k_z is shown in Figures 6.13 and 6.14, respectively. The surface impedance increases as frequency increases, leading to a larger longitudinal field component, hence the increasing transverse current density in Figure 6.13 is expected. Figure 6.14 reveals that the edge singularity weakens for the longitudinal surface current k_z as frequency decreases. This is also an expected result since the edge condition is an induced EMF effect. As the frequency approaches zero, the current density should become constant across the transverse dimension of the strip.

Figures 6.15-6.16 demonstrate the effects of width/height variation. Decreasing the width increases the magnetic field concentration (leading to higher inductance) and also increases resistance. This manifests itself as increased phase and attenuation. Increasing the width/height ratio has a predictable opposite effect. Figure 6.17 shows that increasing the permittivity significantly increases the attenuation factor. This is expected since higher dielectric materials reduce fringing (due to polarization and free-charge annihilation at the dielectric/conductor interfaces) and consequently forces the surface current to be more concentrated in the ground plane. The effect on the phase constant (when normalized with respect to wavenumber k) was not so prominent and was therefore not plotted. The last plot demonstrates the effect that conductor loss has on

the quasi-TEM characteristic impedance of a stripline having dimensions $w = 25\,mm$, $t = 17.38\,mm$ at a frequency of $f = 1\,GHz$. Elementary transmission line theory for a lossless dielectric predicts that the $\mathrm{Re}\{Z_0\}$ should be positive and increasing and the $\mathrm{Im}\{Z_0\}$ negative and decreasing as conductivity decreases since

$$Z_0 = \sqrt{\frac{R + j\omega L}{G + j\omega C}} = \sqrt{\frac{R + j\omega L}{j\omega C}} = \sqrt{\frac{L}{C} - j\frac{R}{\omega C}} \tag{6.94}$$

and because the surface impedance model being utilized is

$$Z_{g,s} = R_{g,s} + jL_{g,s} = (1 + j)\sqrt{\frac{\omega\mu_0}{2\sigma_{g,s}}} \tag{6.95}$$

Figure 6.18 demonstrates this general trend.

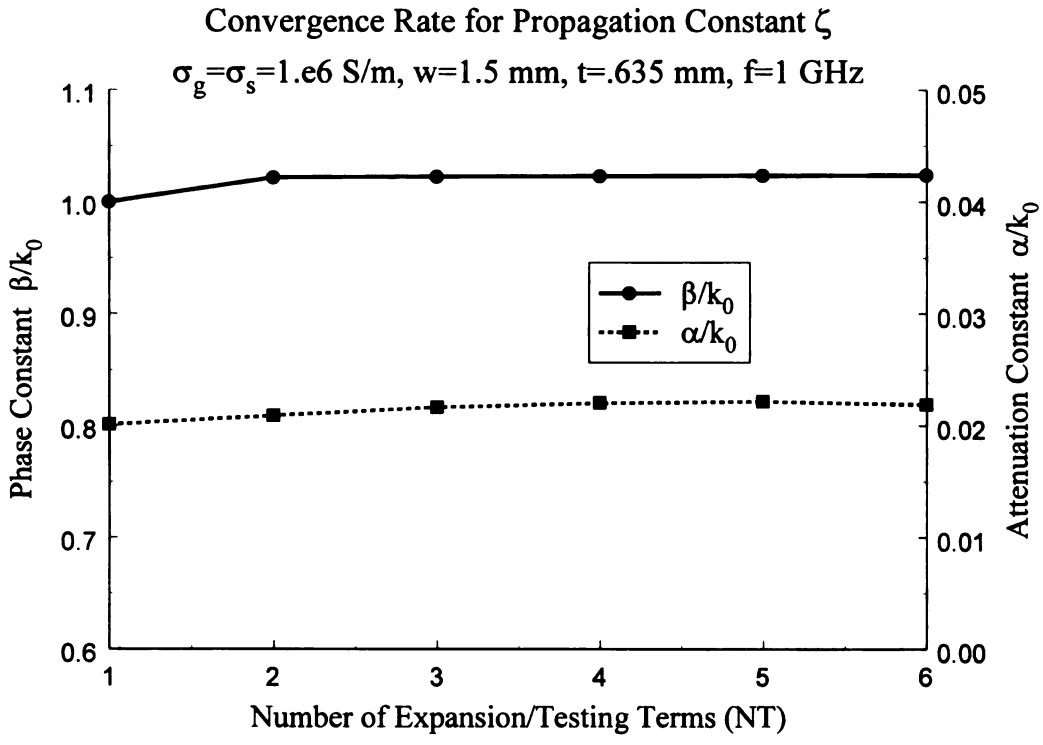

Figure 6.2 Convergence rate for propagation constant $\zeta = \beta - j\alpha$.

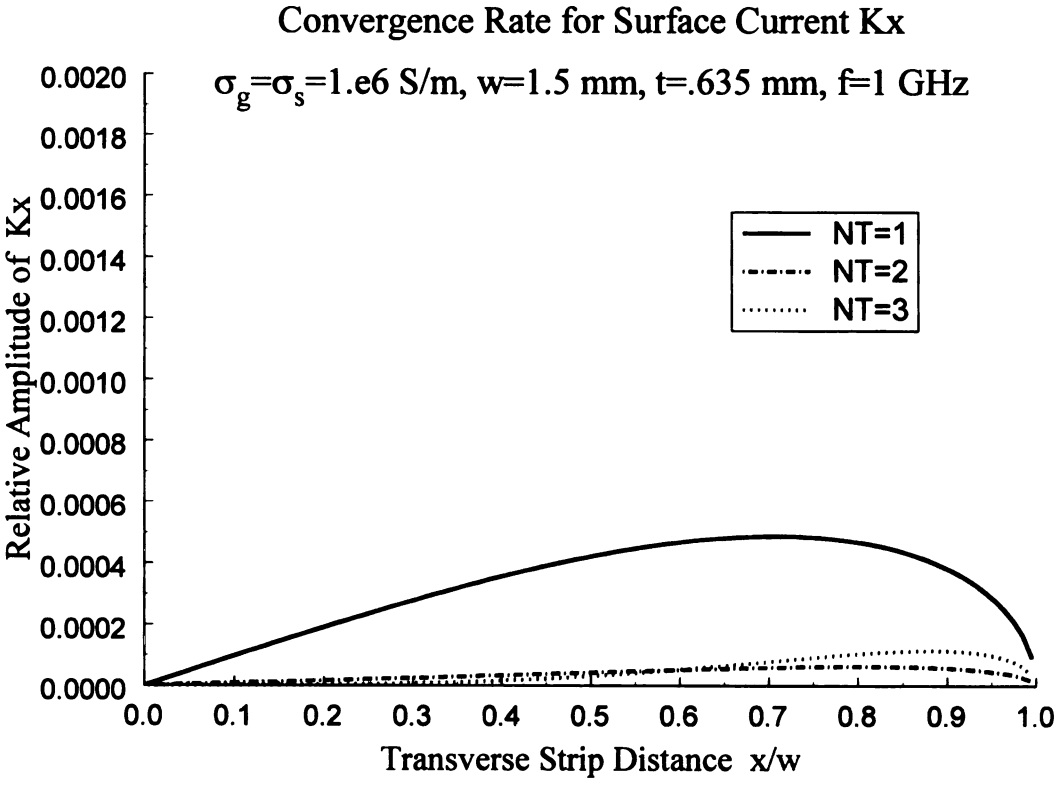

Figure 6.3 Convergence rate for surface current k_x.

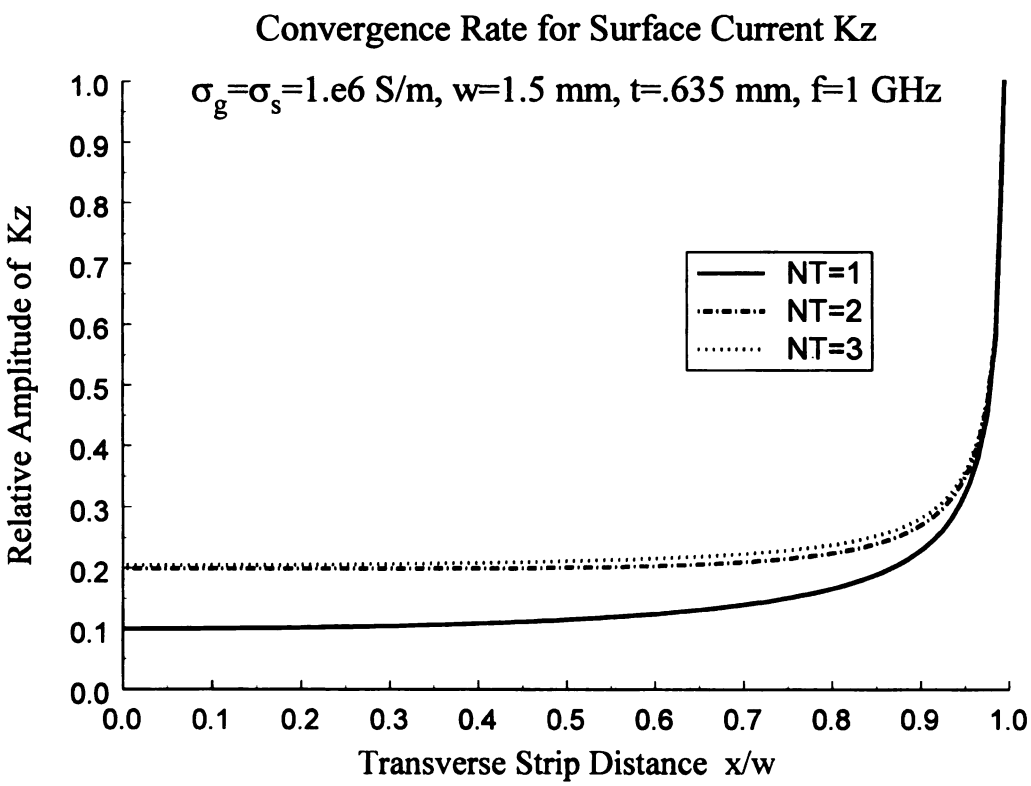

Figure 6.4 Convergence rate for surface current k_z.

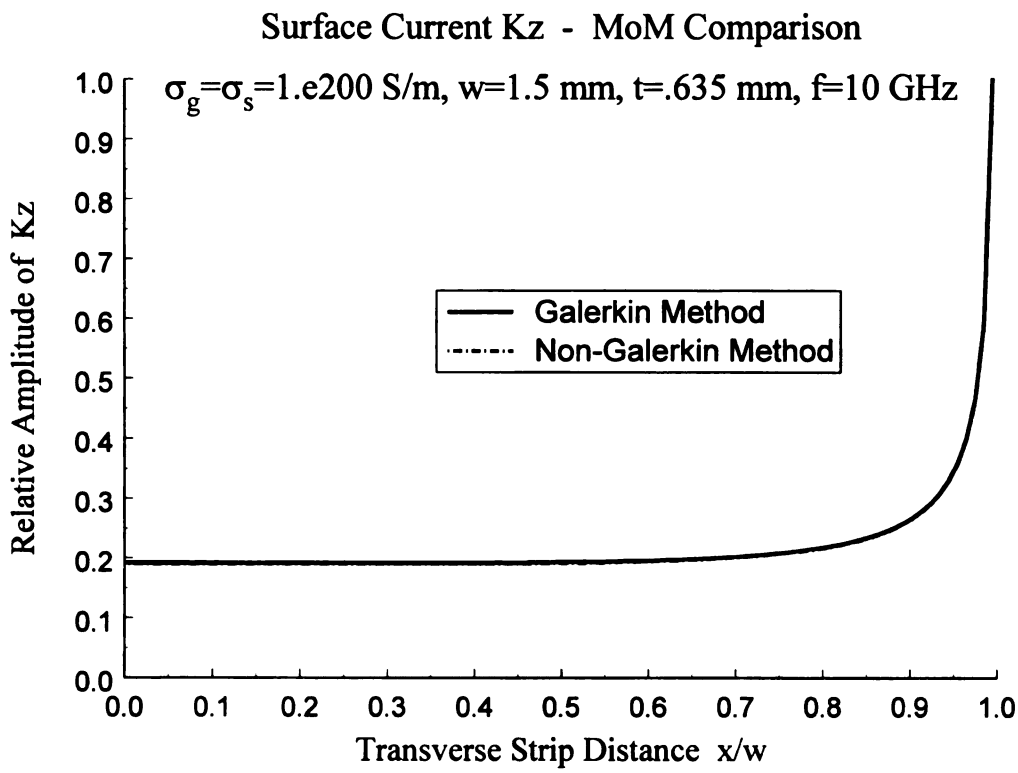

Figure 6.5 Comparison of MoM theories for surface current k_z.

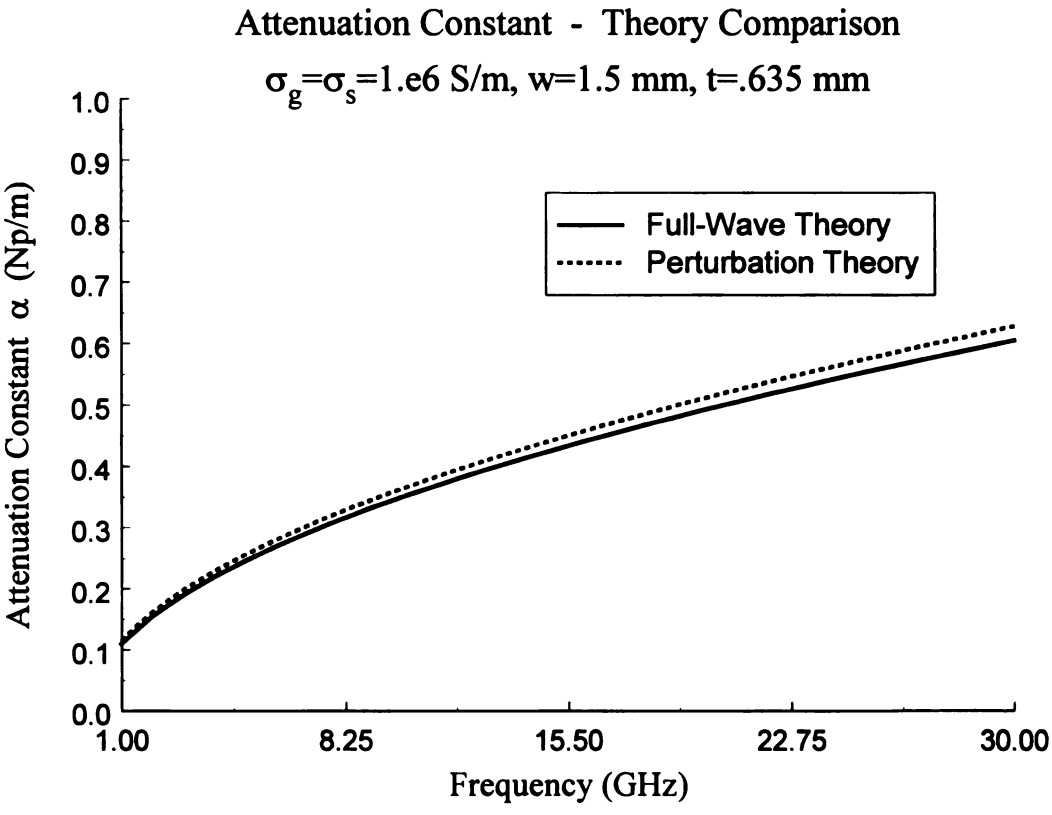

Figure 6.6 Full-wave and perturbation theory comparison for attenuation constant α.

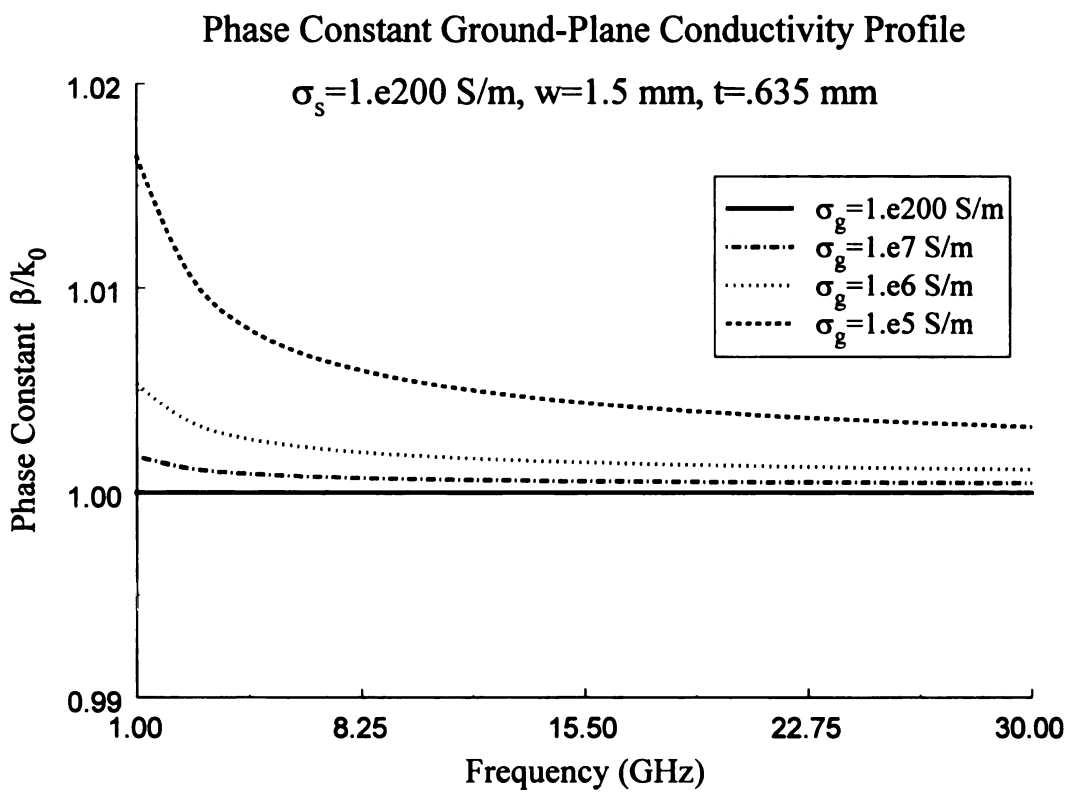

Figure 6.7 Effect of ground plane conductivity on phase constant β.

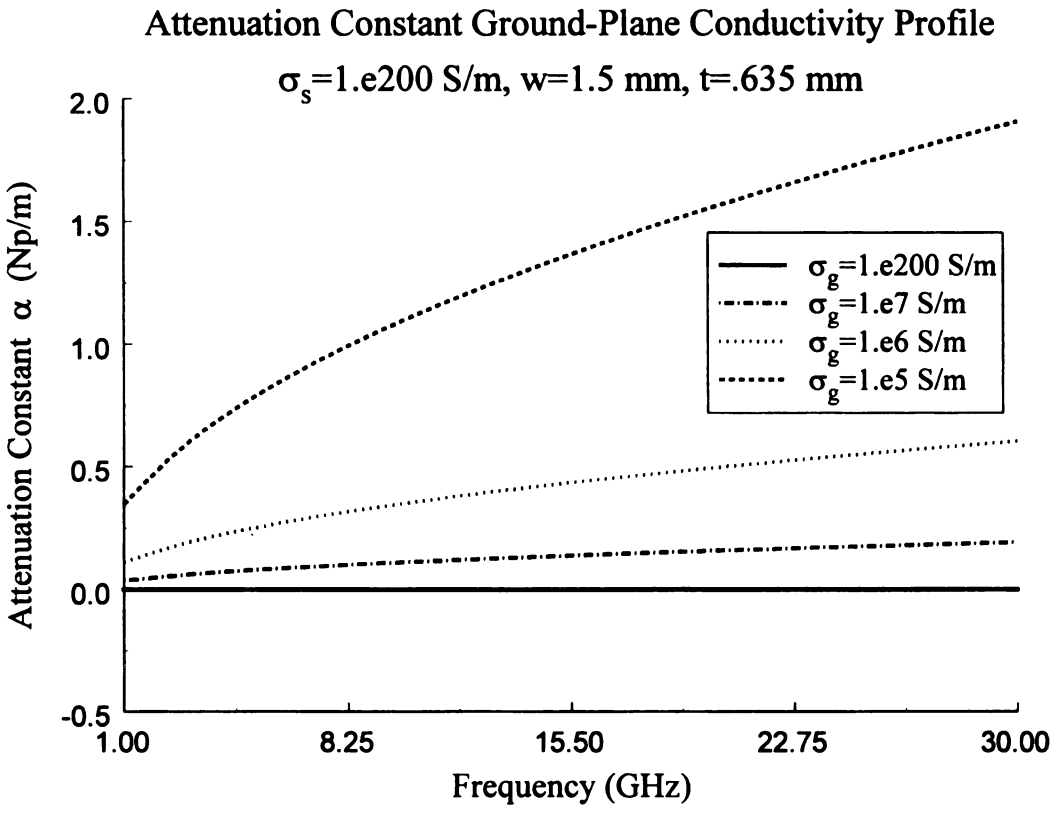

Figure 6.8 Effect of ground plane conductivity on attenuation constant α.

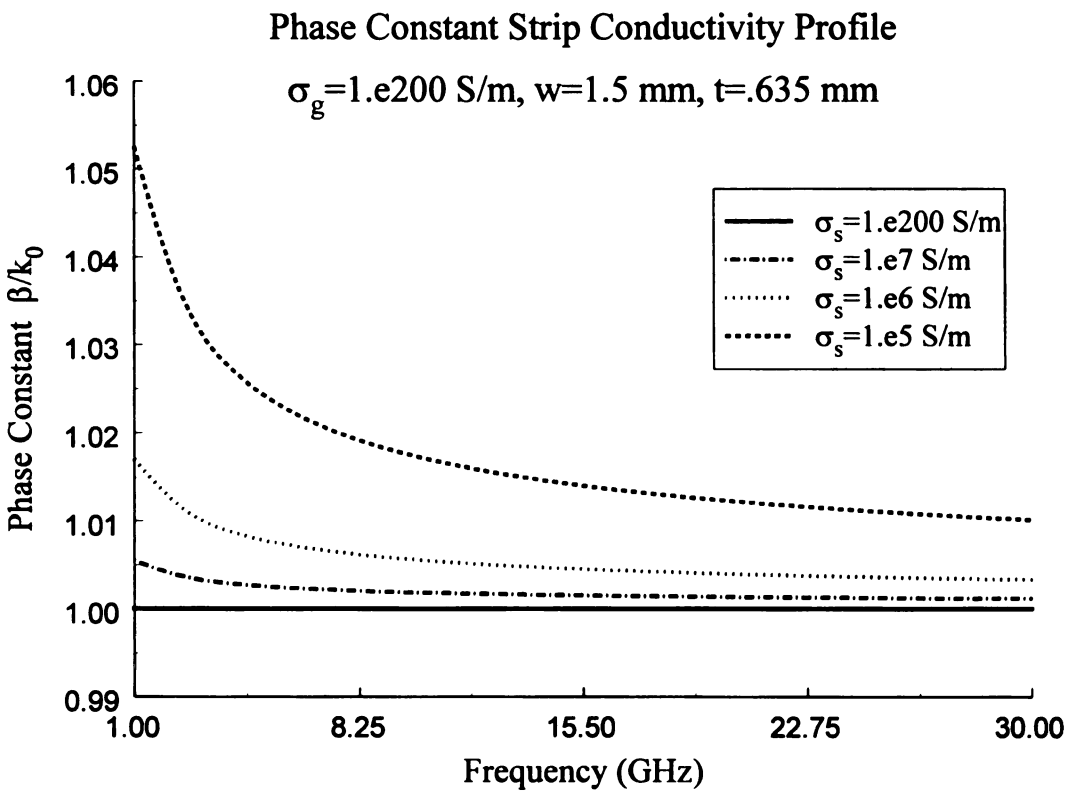

Figure 6.9 Effect of strip conductivity on phase constant β.

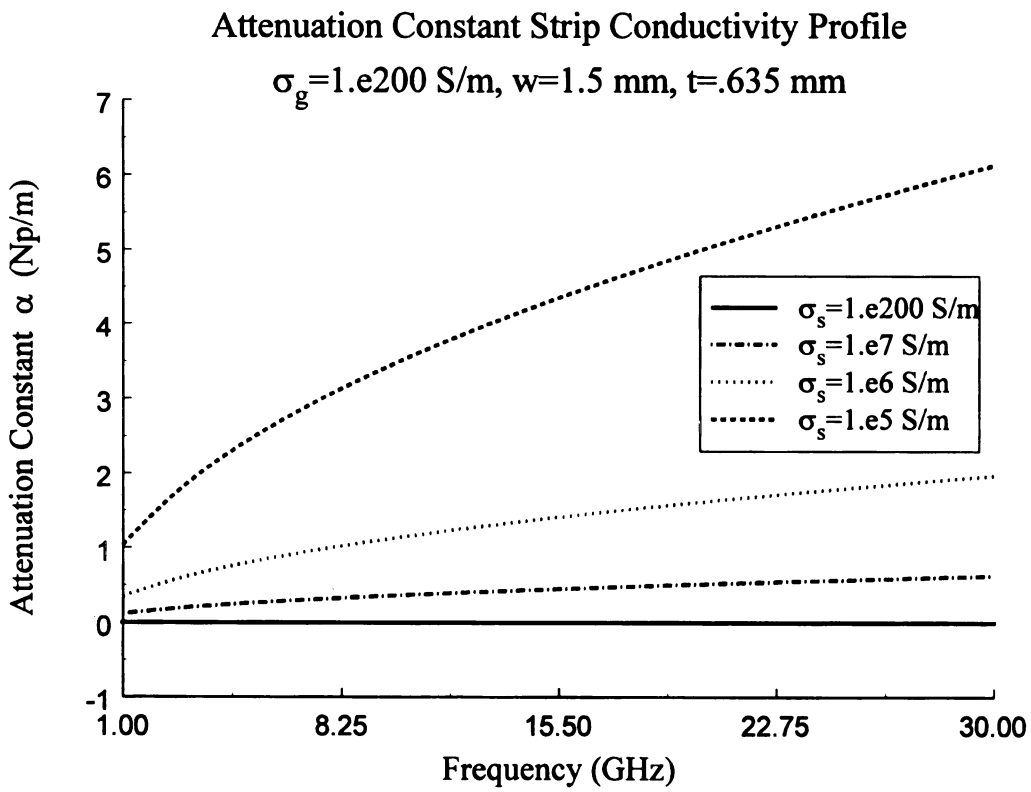

Figure 6.10 Effect of strip conductivity on attenuation constant α.

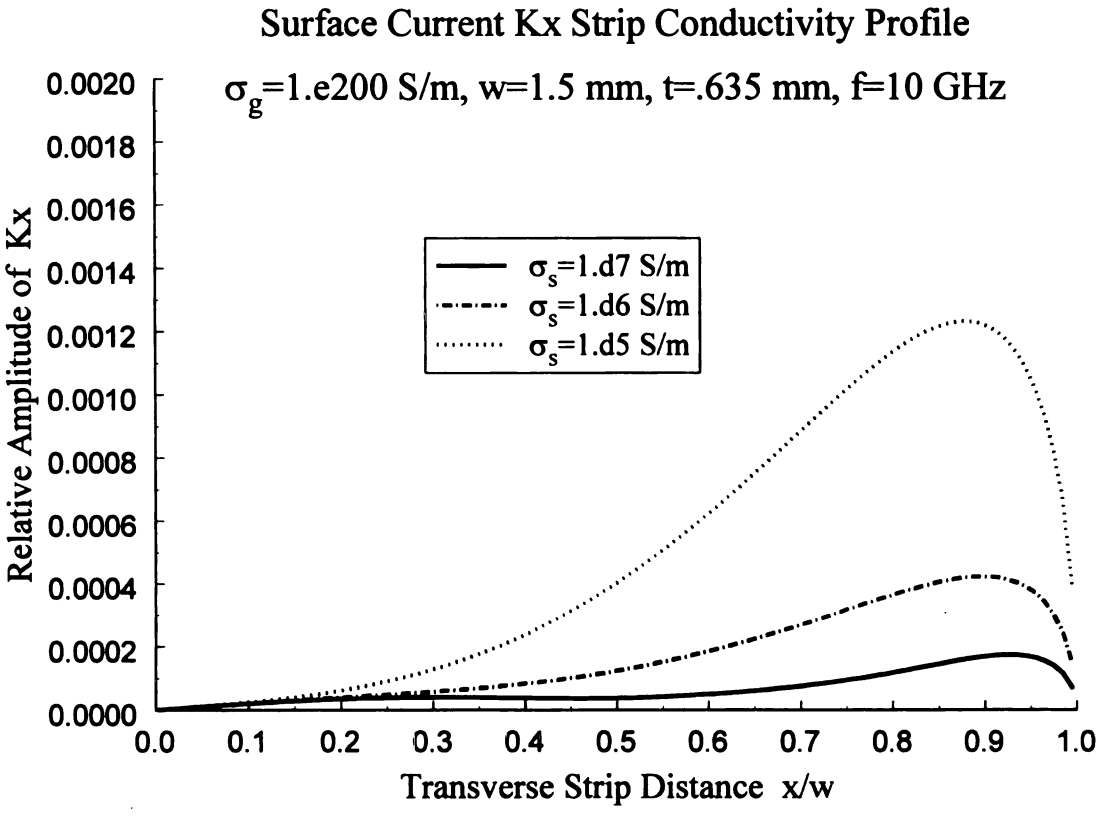

Figure 6.11 Effect of strip conductivity on surface current k_x.

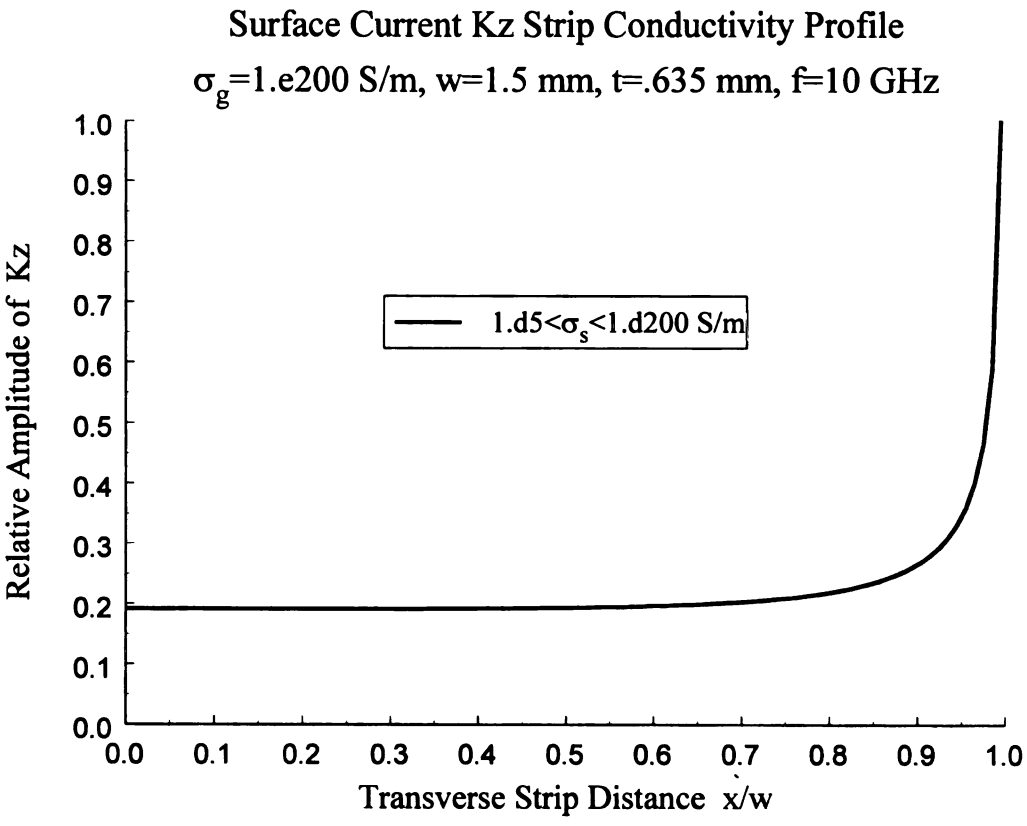

Figure 6.12 Effect of strip conductivity on surface current k_z.

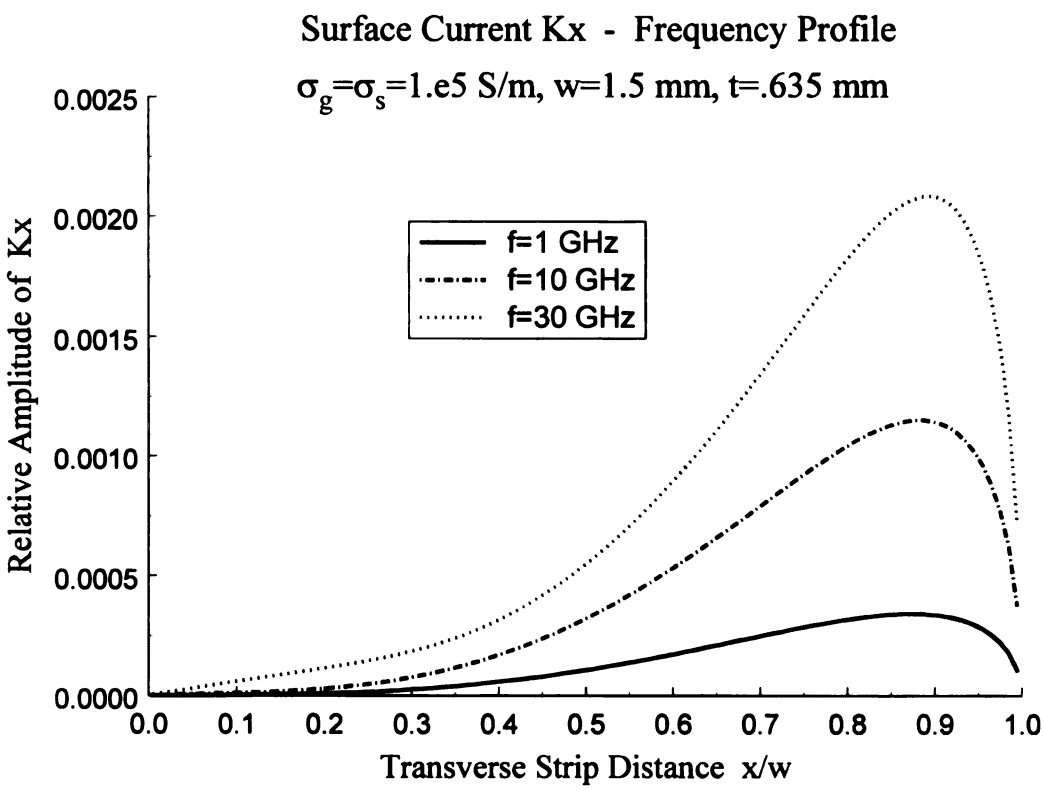

Figure 6.13 Effect of frequency on surface current k_x.

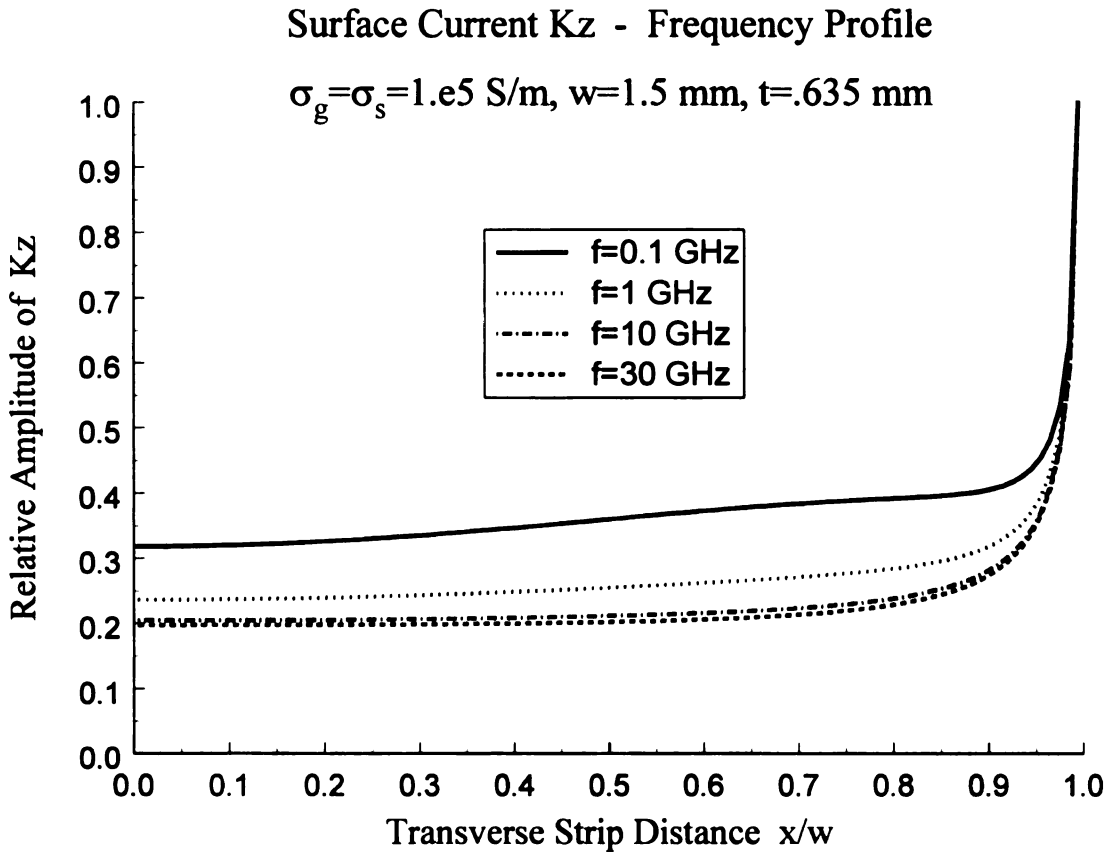

Figure 6.14 Effect of frequency on surface current k_z.

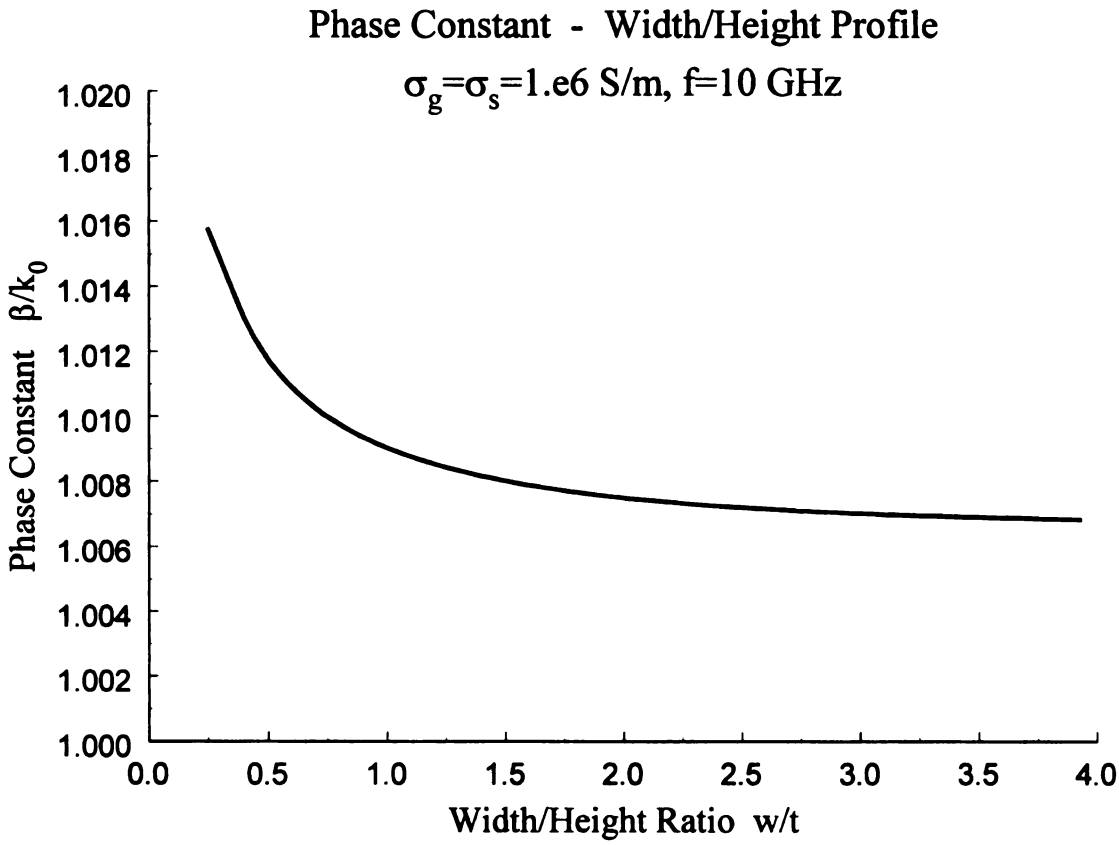

Figure 6.15 Effect of width/height ratio on phase constant β.

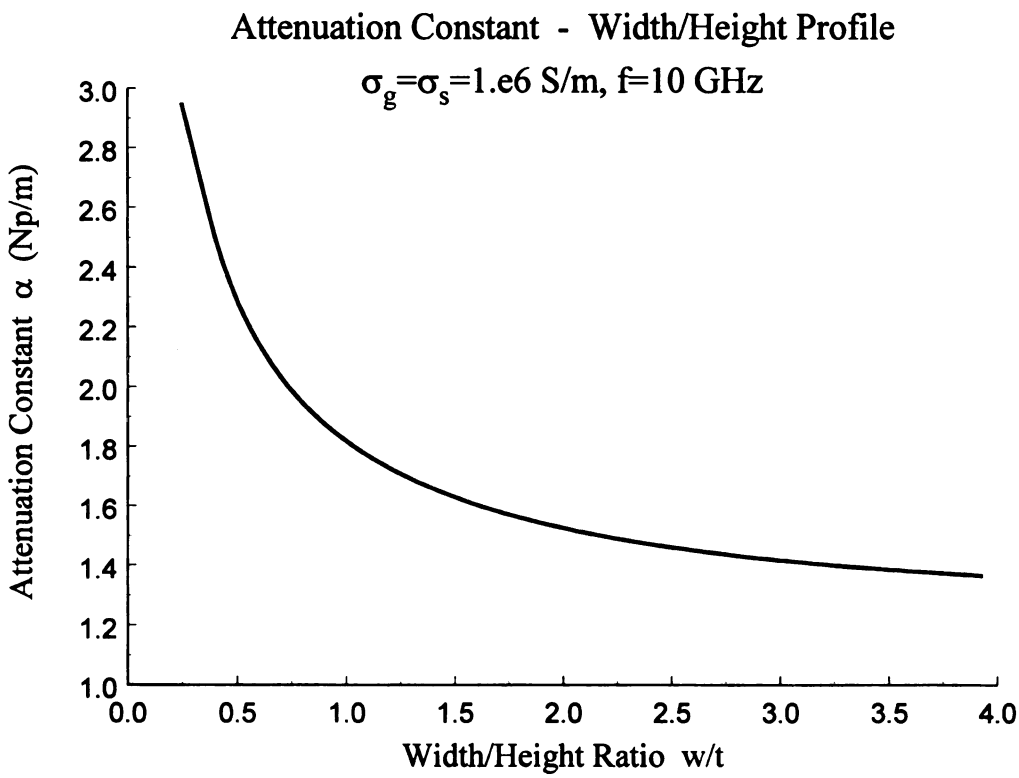

Figure 6.16 Effect of width/height ratio on attenuation constant α.

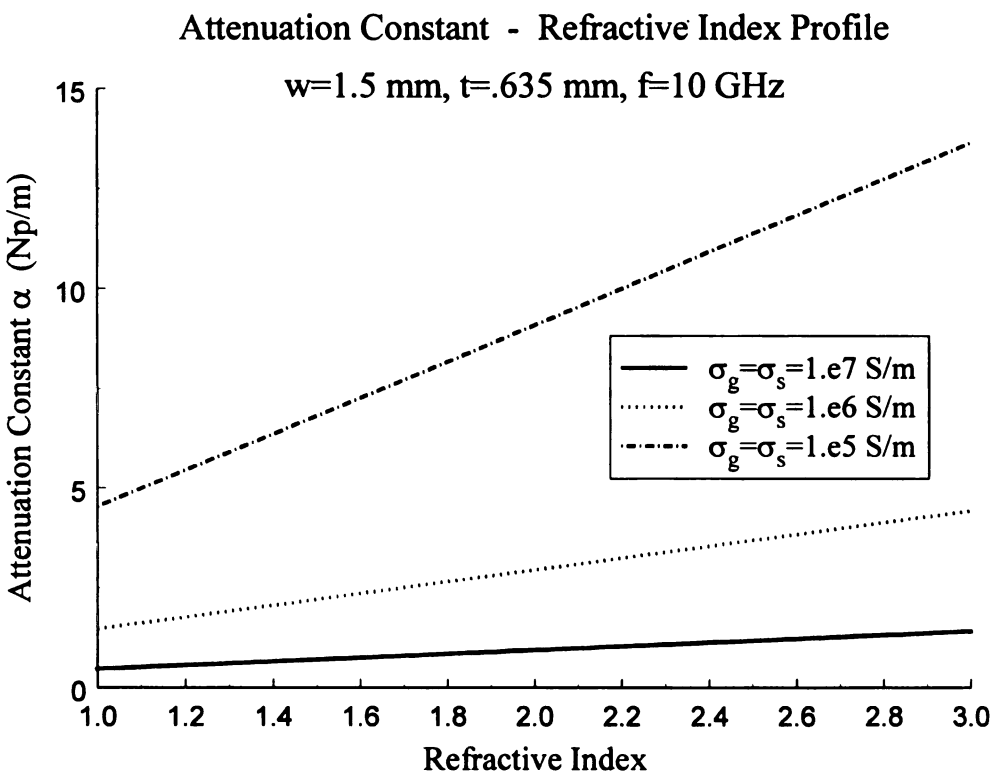

Figure 6.17 Effect of refractive index on the attenuation constant α.

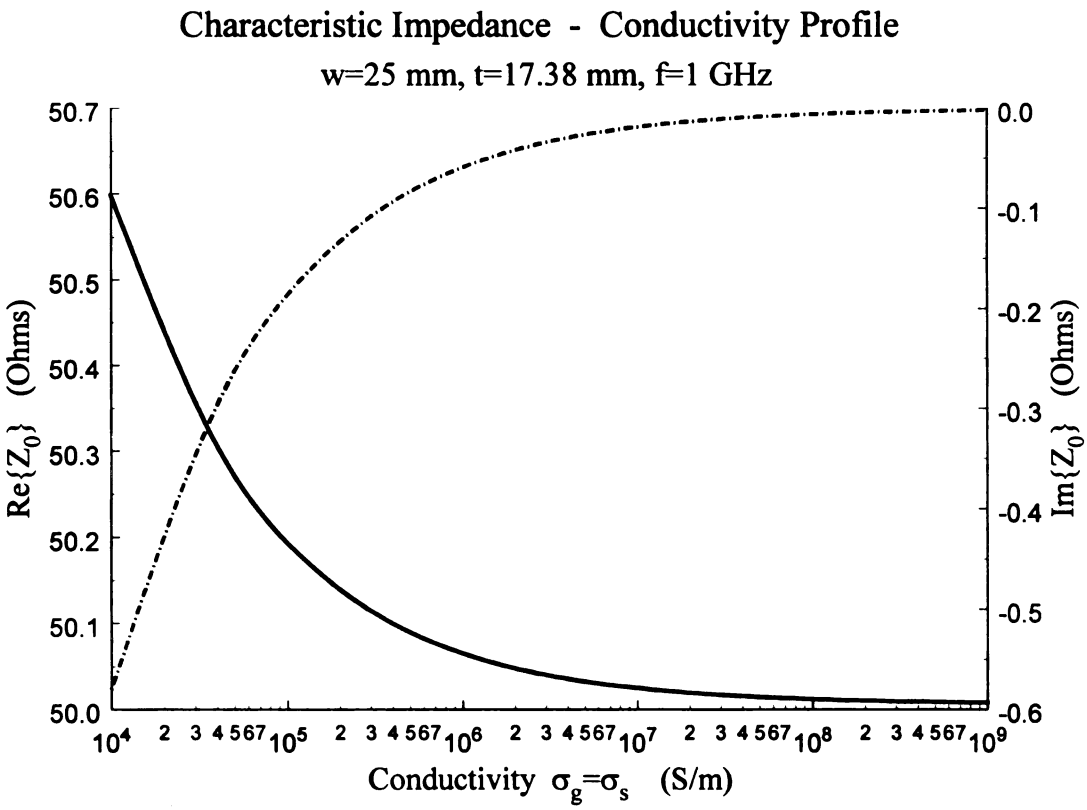

Figure 6.18 Effect of conductivity on characteristic impedance.

Chapter 7

ANALYSIS OF A LOSSY MICROSTRIP TRANSMISSION LINE HAVING AN IMPERFECTLY-CONDUCTING GROUND PLANE

7.1 Introduction

The analysis of an imperfectly-conducting microstrip transmission line [51]-[66] situated over an imperfectly-conducting ground plane will be considered in this chapter. Specifically, the effect that the lossy conductors have on the principal (i.e., dominant) discrete-mode propagation constant and respective surface current will be investigated. Understanding the nature of the principal mode is fundamental to the material characterization process (as well as other applications), and thus provides motivation for this study.

The first step in the above analysis is to (utilizing an electric-type Hertz potential) find the electric-field dyadic Green's function of the EM field for a general current source embedded in a lossy microstrip background environment. Next, an EFIE (electric field integral equation) is developed by specializing the general 3D electric current to a strip surface current located at the cover/film interface and satisfying appropriate boundary conditions on the strip conductor. As a final step, the EFIE is solved using a MoM (method of moments) technique and the principal-mode propagation constant and corresponding surface current distribution are subsequently identified.

7.2 Geometry

The microstrip background environment is depicted in Figure 7.1. The structure is comprised of two main regions located above an imperfect ground plane $(-\infty < y < -d)$ having conductivity σ_c and intrinsic impedance Z_c. The cover $(0 < y < \infty)$ and film $(-d < y < 0)$ regions have properties (ε_1, μ_0) and (ε_2, μ_0), respectively. The cover/film interface is located at $y = 0$ and the film/conductor interface is located at $y = -d$. The general 3D electric current source density $\vec{J}$ is assumed to be localized within region *1*.

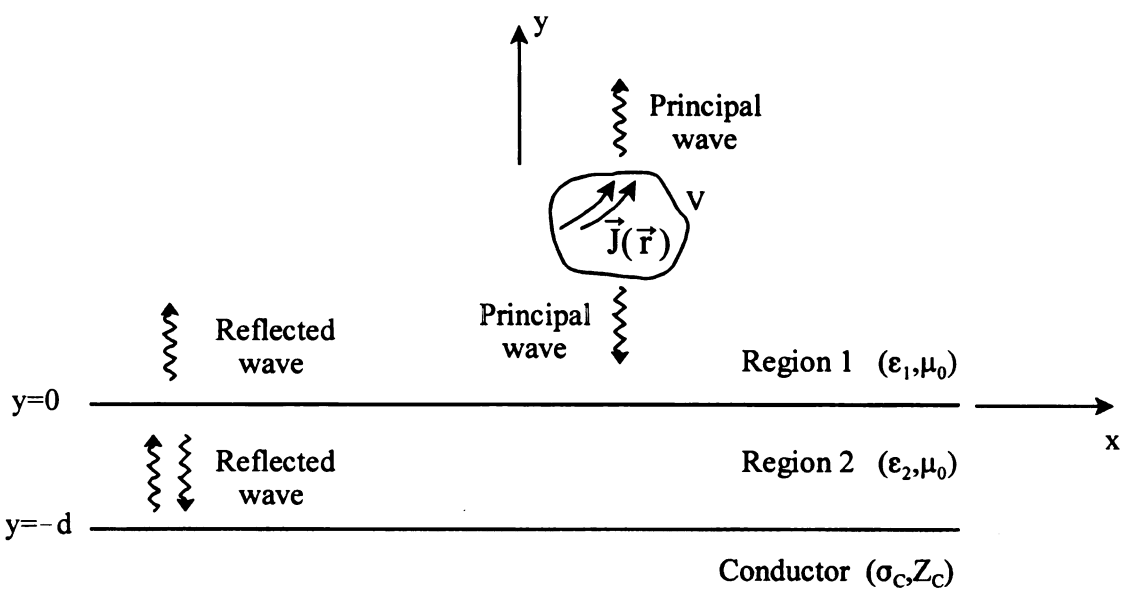

Figure 7.1 Background environment for the microstrip field applicator.

7.3 Electric-Field Dyadic Green's Function

7.3.1 General Formulation

Similar to the development in Chapter 5, an electric-type Hertz potential $\vec{\pi}$ and

the superposition method of solution can be utilized in determining the electric-field dyadic Green's function in region *1*. The total solution for $\vec{\pi}$ in each region will be

$$\vec{\pi}_1 = \vec{\pi}_1^p + \vec{\pi}_1^r \quad ...0 < y < \infty \tag{7.1}$$

$$\vec{\pi}_2 = \vec{\pi}_2^r \quad ...-d < y < 0 \tag{7.2}$$

where (for $\alpha = x, y, z$)

$$\left.\begin{aligned} \nabla^2 \pi_{1\alpha}^p + k_1^2 \pi_{1\alpha}^p &= -\frac{J_\alpha}{j\omega\varepsilon_1} \\ \nabla^2 \pi_{1\alpha}^r + k_1^2 \pi_{1\alpha}^r &= 0 \end{aligned}\right\} \quad ...0 < y < \infty \tag{7.3}$$

$$\nabla^2 \pi_{2\alpha}^r + k_2^2 \pi_{2\alpha}^r = 0 \quad ...-d < y < 0 \tag{7.4}$$

The background structure is invariant along the x and z directions, thus Fourier transformation on (7.3) and (7.4) leads to, with the aid of the transform pair of Chapter 5,

$$\left.\begin{aligned} \frac{\partial^2 \tilde{\pi}_{1\alpha}^p}{\partial y^2} - p_1^2 \tilde{\pi}_{1\alpha}^p &= -\frac{\tilde{J}_\alpha}{j\omega\varepsilon_1} \\ \frac{\partial^2 \tilde{\pi}_{1\alpha}^r}{\partial y^2} - p_1^2 \tilde{\pi}_{1\alpha}^r &= 0 \end{aligned}\right\} \quad ...0 < y < \infty \tag{7.5}$$

$$\frac{\partial^2 \tilde{\pi}_{2\alpha}^r}{\partial y^2} - p_2^2 \tilde{\pi}_{2\alpha}^r = 0 \quad ...-d < y < 0 \tag{7.6}$$

where $p_{1,2} = \sqrt{\lambda^2 - k_{1,2}^2}$ with $\mathrm{Re}\{p_{1,2}\} > 0$ chosen and $\lambda^2 = \xi^2 + \zeta^2$. The solutions of (7.5) and (7.6) in the complex λ-plane are (based on the experience of Chapter 5)

$$\tilde{\pi}_{1\alpha} = \tilde{\pi}_{1\alpha}^p + \tilde{\pi}_{1\alpha}^r = \int_{y'} \frac{e^{-p_1|y-y'|}}{2p_1} \frac{\tilde{J}_\alpha(\vec{\lambda}, y')}{j\omega\varepsilon_1} dy' + W_{1\alpha}^+ e^{-p_1 y} + W_{1\alpha}^- e^{p_1 y} \quad ...0 < y < \infty \tag{7.7}$$

or

$$\tilde{\pi}_{1\alpha} = \tilde{\pi}_{1\alpha}^p + \tilde{\pi}_{1\alpha}^r = V_\alpha^+ e^{-p_1 y} + W_{1\alpha}^+ e^{-p_1 y} + W_{1\alpha}^- e^{p_1 y} \quad ...y' < y < \infty \tag{7.8}$$

$$\tilde{\pi}_{1\alpha} = \tilde{\pi}_{1\alpha}^{p} + \tilde{\pi}_{1\alpha}^{r} = V_{\alpha}^{-} e^{p_1 y} + W_{1\alpha}^{+} e^{-p_1 y} + W_{1\alpha}^{-} e^{p_1 y} \quad ...0 < y < y' \tag{7.9}$$

and

$$\tilde{\pi}_{2\alpha} = \tilde{\pi}_{2\alpha}^{r} = W_{2\alpha}^{+} e^{-p_2 y} + W_{2\alpha}^{-} e^{p_2 y} \quad ...-d < y < 0 \tag{7.10}$$

where

$$V_{\alpha}^{\pm} = \int_{y'} \frac{e^{\pm p_1 y'}}{2p_1} \frac{\tilde{J}_{\alpha}(\vec{\lambda}, y')}{j\omega\varepsilon_1} dy' \tag{7.11}$$

The spectral coefficients $W_{1\alpha}^{\pm}, W_{2\alpha}^{\pm}$ are computed in the next section using appropriate boundary conditions.

7.3.2 Computation of Spectral Coefficients

The spectral coefficients can be computed by implementing the following boundary conditions (note, the λ dependence of the transform-domain Hertz potentials has been dropped for notational convenience)

$$\tilde{\pi}_{1\alpha}(y \to \infty) = 0 \quad ...\alpha = x, y, z \tag{7.12}$$

$$\tilde{\pi}_{1\alpha}(0) = N^2 \tilde{\pi}_{2\alpha}(0) \quad ...\alpha = x, y, z \tag{7.13}$$

$$\frac{\partial \tilde{\pi}_{1\alpha}(0)}{\partial y} = N^2 \frac{\partial \tilde{\pi}_{2\alpha}(0)}{\partial y} \quad ...\alpha = x, z \tag{7.14}$$

$$\frac{\partial \tilde{\pi}_{1y}(0)}{\partial y} - \frac{\partial \tilde{\pi}_{2y}(0)}{\partial y} = (1 - N^2)\left[j\xi\tilde{\pi}_{2x}(0) + j\zeta\tilde{\pi}_{2z}(0)\right] \tag{7.15}$$

$$\tilde{\pi}_{2\alpha}(-d) = \frac{1}{\sigma_c Z_c} \frac{\partial \tilde{\pi}_{2\alpha}(-d)}{\partial y} \quad ...\alpha = x, z \tag{7.16}$$

$$\frac{\partial \tilde{\pi}_{2y}(-d)}{\partial y} = j\omega\varepsilon_2 Z_c \tilde{\pi}_{2y}(-d) - j\xi\tilde{\pi}_{2x}(-d) - j\zeta\tilde{\pi}_{2z}(-d) \tag{7.17}$$

where the dielectric contrast and intrinsic impedance are given by

$$N^2 = \frac{\varepsilon_2}{\varepsilon_1} \quad , \quad Z_c = (1+j)\sqrt{\frac{\omega\mu_0}{2\sigma_c}} \tag{7.18}$$

Equation (7.12) is the radiation condition, equations (7.13)-(7.15) are the boundary conditions at the cover/film interface and equations (7.16)-(7.17) are the impedance boundary conditions at the surface of the imperfect (but good) conductor. As anticipated, there are 12 boundary conditions required to uniquely compute the 12 unknown spectral coefficients.

Enforcement of the radiation condition leads to the following result when applied to equation (7.8)

$$\tilde{\pi}_{1\alpha}(y \to \infty) = 0 \quad \Rightarrow \quad W_{1\alpha}^{-} = 0 \ \ldots \alpha = x, y, z \tag{7.19}$$

since $\mathrm{Re}\{p_1\} > 0$. Thus, the transform-domain Hertz potential in region *1* consists of a principal wave and only an up-going reflected wave, that is

$$\tilde{\pi}_{1\alpha} = V_{\alpha}^{+} e^{-p_1 y} + W_{1\alpha}^{+} e^{-p_1 y} \ \ldots y' < y < \infty \tag{7.20}$$

$$\tilde{\pi}_{1\alpha} = V_{\alpha}^{-} e^{p_1 y} + W_{1\alpha}^{+} e^{-p_1 y} \ \ldots 0 < y < y' \tag{7.21}$$

The tangential spectral coefficients can be computed as follows. First, insertion of (7.10) into (7.16) leads to

$$W_{2\alpha}^{+} e^{p_2 d} + W_{2\alpha}^{-} e^{-p_2 d} = -\frac{p_2}{\sigma_c Z_c}\left(W_{2\alpha}^{+} e^{p_2 d} - W_{2\alpha}^{-} e^{-p_2 d}\right) \ \ldots \alpha = x, z \tag{7.22}$$

and upon solving for $W_{2\alpha}^{+}$ gives

$$W_{2\alpha}^{+} = -R_2 e^{-2p_2 d} W_{2\alpha}^{-} \ \ldots \alpha = x, z \tag{7.23}$$

$$R_2 = \frac{\sigma_c Z_c - p_2}{\sigma_c Z_c + p_2} = \frac{1 - p_2/\sigma_c Z_c}{1 + p_2/\sigma_c Z_c} \quad , \quad \sigma_c Z_c = (1+j)\sqrt{\frac{\omega\mu_0\sigma_c}{2}} \tag{7.24}$$

Next, substitution of (7.21) and (7.10) into (7.13) and (7.14) produces the result

$$V_\alpha^- + W_{1\alpha}^+ = N^2(W_{2\alpha}^+ + W_{2\alpha}^-) \quad ...\alpha = x, y, z \tag{7.25}$$

$$p_1(V_\alpha^- - W_{1\alpha}^+) = -p_2 N^2(W_{2\alpha}^+ - W_{2\alpha}^-) \quad ...\alpha = x, z \tag{7.26}$$

Solving the above equations in terms of $W_{1\alpha}^+$ and using (7.23) gives

$$W_{1\alpha}^+ = -V_\alpha^- + N^2(1 - R_2 e^{-2p_2 d})W_{2\alpha}^- \quad ...\alpha = x, z \tag{7.27}$$

$$W_{1\alpha}^+ = V_\alpha^- - \frac{p_2}{p_1} N^2(1 + R_2 e^{-2p_2 d})W_{2\alpha}^- \quad ...\alpha = x, z \tag{7.28}$$

The spectral coefficient $W_{2\alpha}^-$ is determined by equating (7.27) and (7.28), leading to the following expression

$$W_{2\alpha}^- = T_t V_\alpha^- \quad ...\alpha = x, z \tag{7.29}$$

where the tangential transmission and interfacial reflection coefficients at the cover/film interface are

$$T_t = \frac{2p_1}{N^2(p_1 + p_2)(1 - R_1 R_2 e^{-2p_2 d})} \quad , \quad R_1 = \frac{p_1 - p_2}{p_1 + p_2} \tag{7.30}$$

Substitution of (7.29) into (7.23) and (7.27) or (7.28) identifies the remaining tangential spectral coefficients, that is

$$W_{2\alpha}^+ = -R_2 T_t e^{-2p_2 d} V_\alpha^- \quad ...\alpha = x, z \tag{7.31}$$

$$W_{1\alpha}^+ = R_t V_\alpha^- \quad ...\alpha = x, z \tag{7.32}$$

where the tangential reflection coefficient is

$$R_t = \frac{R_1 - R_2 e^{-2p_2 d}}{1 - R_1 R_2 e^{-2p_2 d}} \tag{7.33}$$

It is noted in passing that the above spectral coefficients reduce to the expected perfectly-

conducting result [45] in the limit as $\sigma_c \to \infty$.

The tangential components of the spectral-domain Hertz potential in region *1* can now be mathematically/physically identified using (7.7), (7.19) and (7.32). The result is

$$\tilde{\pi}_{1\alpha} = \tilde{\pi}_{1\alpha}^{p} + \tilde{\pi}_{1\alpha}^{r} = \int_{y'} \left[\frac{e^{-p_1|y-y'|}}{2p_1} + R_t \frac{e^{-p_1(y+y')}}{2p_1} \right] \frac{\tilde{J}_\alpha(\vec{\lambda}, y')}{j\omega\varepsilon_1} dy' \quad ...\alpha = x, z \tag{7.34}$$

The first term in (7.34) represents the principal-wave contribution that travels directly from the source point y' to the observation point y. The second term in (7.34) represents the reflected-wave contribution that travels downward from the source, gets reflected from the cover/film interface and travels upwards to the point of observation. Note, a closer examination of R_t in (7.33) reveals that the reflected-wave contribution is actually comprised of a primary reflection from the cover/film interface and a secondary reflection from the film/conductor interface. A similar picture holds for the normal component of the Hertz potential.

The normal-component spectral coefficients are determined in the following manner. First, substitution of (7.10) into (7.17) leads to

$$\begin{aligned} -p_2(W_{2y}^{+}e^{p_2 d} - W_{2y}^{-}e^{-p_2 d}) &= j\omega\varepsilon_2 Z_c(W_{2y}^{+}e^{p_2 d} + W_{2y}^{-}e^{-p_2 d}) \\ -j\xi(W_{2x}^{+}e^{p_2 d} + W_{2x}^{-}e^{-p_2 d}) - j\zeta(W_{2z}^{+}e^{p_2 d} + W_{2z}^{-}e^{-p_2 d}) & \end{aligned} \tag{7.35}$$

Solving (7.35) in terms of W_{2y}^{+} produces the result (after some algebra)

$$W_{2y}^{+} = C_{yx}e^{-2p_2 d}W_{2x}^{-} - \bar{R}_2 e^{-2p_2 d}W_{2y}^{-} + C_{yz}e^{-2p_2 d}W_{2z}^{-} \tag{7.36}$$

where the normal interfacial reflection and coupling coefficients are

$$\bar{R}_2 = \frac{j\omega\varepsilon_2 Z_c - p_2}{j\omega\varepsilon_2 Z_c + p_2} = -\frac{1 - j\omega\varepsilon_2 Z_c / p_2}{1 + j\omega\varepsilon_2 Z_c / p_2} \tag{7.37}$$

$$C_{yx} = j\xi C \quad , \quad C_{yz} = j\zeta C \quad , \quad C = \frac{1-R_2}{j\omega\varepsilon_2 Z_c + p_2} = \frac{1-R_2}{p_2(1+j\omega\varepsilon_2 Z_c / p_2)} \tag{7.38}$$

Next, the boundary condition result of (7.25) is used to express W_{1y}^{+} in terms of $W_{2y}^{\pm}$, namely

$$W_{1y}^{+} = -V_y^{-} + N^2(W_{2y}^{+} + W_{2y}^{-}) \tag{7.39}$$

Substitution of (7.36) into (7.39) gives

$$W_{1y}^{+} = -V_y^{-} + C_{yx}N^2 e^{-2p_2 d}W_{2x}^{-} + N^2(1-\bar{R}_2 e^{-2p_2 d})W_{2y}^{-} + C_{yz}N^2 e^{-2p_2 d}W_{2z}^{-} \tag{7.40}$$

The final boundary condition is enforced by substituting (7.21) and (7.10) into (7.15), leading to

$$p_1(V_y^{-} - W_{1y}^{+}) + p_2(W_{2y}^{+} - W_{2y}^{-}) = (1-N^2)\left[j\xi(W_{2x}^{+} + W_{2x}^{-}) + j\zeta(W_{2z}^{+} + W_{2z}^{-})\right] \tag{7.41}$$

Solving (7.41) for W_{1y}^{+} and using (7.23) and (7.36) gives

$$\begin{aligned} W_{1y}^{+} = V_y^{-} &+ \left[\frac{p_2 C_{yx}e^{-2p_2 d} - j\xi(1-N^2)(1-R_2 e^{-2p_2 d})}{p_1}\right]W_{2x}^{-} \\ -\frac{p_2}{p_1}(1+\bar{R}_2 e^{-2p_2 d})W_{2y}^{-} &+ \left[\frac{p_2 C_{yz}e^{-2p_2 d} - j\zeta(1-N^2)(1-R_2 e^{-2p_2 d})}{p_1}\right]W_{2z}^{-} \end{aligned} \tag{7.42}$$

Using (7.29) and equating (7.40) and (7.42) produces the following result for W_{2y}^{-} (after a little algebraic effort)

$$W_{2y}^{-} = T_n^x V_x^{-} + T_n^y V_y^{-} + T_n^z V_z^{-} \tag{7.43}$$

where the normal transmission coefficients are

$$T_n^x = -T_t\left[\frac{(p_1 N^2 - p_2)C_{yx}e^{-2p_2 d} + j\xi(1-N^2)(1-R_2 e^{-2p_2 d})}{(p_1 N^2 + p_2)(1-\bar{R}_1\bar{R}_2 e^{-2p_2 d})}\right] \tag{7.44}$$

$$T_n^y = \frac{2p_1}{(p_1N^2 + p_2)(1 - \bar{R}_1\bar{R}_2 e^{-2p_2d})} \tag{7.45}$$

$$T_n^z = -T_t\left[\frac{(p_1N^2 - p_2)C_{yz}e^{-2p_2d} + j\zeta(1-N^2)(1-R_2e^{-2p_2d})}{(p_1N^2 + p_2)(1 - \bar{R}_1\bar{R}_2 e^{-2p_2d})}\right] \tag{7.46}$$

$$\bar{R}_1 = \frac{p_1N^2 - p_2}{p_1N^2 + p_2} \tag{7.47}$$

Substitution of (7.43) into (7.36) and (7.40) or (7.42) determines, with the aid of (7.29), the remaining normal-component spectral coefficients

$$W_{2y}^+ = (C_{yx}T_t - \bar{R}_2T_n^x)e^{-2p_2d}V_x^- - \bar{R}_2e^{-2p_2d}T_n^yV_y^- + (C_{yz}T_t - \bar{R}_2T_n^z)e^{-2p_2d}V_z^- \tag{7.48}$$

$$W_{1y}^+ = R_n^xV_x^- + R_n^yV_y^- + R_n^zV_z^- \tag{7.49}$$

where

$$R_n^x = N^2\left[C_{yx}e^{-2p_2d}T_t + (1 - \bar{R}_2e^{-2p_2d})T_n^x\right] \tag{7.50}$$

$$R_n^y = N^2(1 - \bar{R}_2e^{-2p_2d})T_n^y - 1 \tag{7.51}$$

$$R_n^z = N^2\left[C_{yz}e^{-2p_2d}T_t + (1 - \bar{R}_2e^{-2p_2d})T_n^z\right] \tag{7.52}$$

The normal component of Hertz potential in the spectral domain for region *1* can therefore be identified using (7.7), (7.19) and (7.49). The result is

$$\tilde{\pi}_{1y} = \tilde{\pi}_{1y}^p + \tilde{\pi}_{1y}^r = \int_{y'}\left[\hat{y}\frac{e^{-p_1|y-y'|}}{2p_1} + \vec{R}_n\frac{e^{-p_1(y+y')}}{2p_1}\right]\cdot\frac{\vec{\tilde{J}}(\vec{\lambda}, y')}{j\omega\varepsilon_1}dy' \tag{7.53}$$

where

$$\vec{R}_n = \hat{x}R_n^x + \hat{y}R_n^y + \hat{z}R_n^z \quad , \quad \vec{\tilde{J}} = \hat{x}\tilde{J}_x + \hat{y}\tilde{J}_y + \hat{z}\tilde{J}_z \tag{7.54}$$

The first term in (7.53) is the principal-wave contribution and the second term is the reflected-wave contribution. Note, equations (7.34) and (7.53) state that the normal

component of current only couples into the normal component of potential, whereas the tangential components of current (upon interaction with the interface) couple into both the tangential and normal components of Hertz potential.

7.3.3 Identification of the Hertz Potential Dyadic Green's Function

The principal part of the spectral-domain Hertz potential in region *1* can be easily deduced from section 7.3.1 or 7.3.2, that is

$$\tilde{\pi}_{1\alpha}^{p} = \int_{y'} \tilde{G}^{p}(\vec{\lambda}, y|y') \frac{\tilde{J}_{\alpha}(\vec{\lambda}, y')}{j\omega\varepsilon_1} dy' \quad ...\alpha = x, y, z \tag{7.55}$$

where

$$\tilde{G}^{p}(\vec{\lambda}, y|y') = \tilde{G}^{p}(\vec{\lambda}, y - y') = \frac{e^{-p_1|y-y'|}}{2p_1} \tag{7.56}$$

The principal part of the spatial-domain Hertz-potential Green's function immediately follows by taking the inverse transform of (7.55), resulting in

$$\pi_{1\alpha}^{p}(\vec{r}) = \frac{1}{(2\pi)^2} \int_{-\infty}^{\infty}\int_{-\infty}^{\infty} \tilde{\pi}_{1\alpha}^{p}(\vec{\lambda}, y) e^{j\vec{\lambda}\cdot\vec{r}} d^2\lambda = \int_{V'} G^{p}(\vec{r}|\vec{r}') \frac{J_{\alpha}(\vec{r}')}{j\omega\varepsilon_1} dV' \tag{7.57}$$

where

$$G^{p}(\vec{r}|\vec{r}') = G^{p}(\vec{r} - \vec{r}') = \frac{1}{(2\pi)^2} \int_{-\infty}^{\infty}\int_{-\infty}^{\infty} \tilde{G}^{p}(\vec{\lambda}, y - y') e^{j\vec{\lambda}\cdot(\vec{r}-\vec{r}')} d^2\lambda \tag{7.58}$$

Thus, the principal Hertz-potential dyadic Green's function is identified as

$$\vec{\pi}_1^{p}(\vec{r}) = \int_{V'} \bar{\bar{G}}^{p}(\vec{r}|\vec{r}') \cdot \frac{\vec{J}(\vec{r}')}{j\omega\varepsilon_1} dV' \quad , \quad \bar{\bar{G}}^{p}(\vec{r}|\vec{r}') = \bar{\bar{I}} G^{p}(\vec{r}|\vec{r}') \tag{7.59}$$

In a similar manner, the reflected Hertz-potential dyadic Green's function is identified by

$$\vec{\pi}_1^r(\vec{r}) = \int_{V'} \bar{\bar{G}}^r(\vec{r}|\vec{r}') \cdot \frac{\vec{J}(\vec{r}')}{j\omega\varepsilon_1} dV' \tag{7.60}$$

where

$$\bar{\bar{G}}^r = \hat{x}G_{xx}^r\hat{x} + \hat{y}G_{yx}^r\hat{x} + \hat{y}G_{yy}^r\hat{y} + \hat{y}G_{yz}^r\hat{z} + \hat{z}G_{zz}^r\hat{z} \tag{7.61}$$

$$G_{\alpha\beta}^r = \frac{1}{(2\pi)^2} \int_{-\infty}^{\infty}\int_{-\infty}^{\infty} \tilde{G}_{\alpha\beta}^r(\vec{\lambda}, y|y')e^{j\vec{\lambda}\cdot(\vec{r}-\vec{r}')} d^2\lambda \quad ...\alpha,\beta = x,y,z \tag{7.62}$$

$$\tilde{G}_{\alpha\alpha}^r = R_t \frac{e^{-p_1(y+y')}}{2p_1} \quad ...\alpha = x,z \tag{7.63}$$

$$\tilde{G}_{y\alpha}^r = R_n^\alpha \frac{e^{-p_1(y+y')}}{2p_1} \quad ...\alpha = x,y,z \tag{7.64}$$

The total Hertz-potential dyadic Green's function in region *1* is therefore, by superposition

$$\bar{\bar{G}}(\vec{r}|\vec{r}') = \bar{\bar{G}}^p(\vec{r}|\vec{r}') + \bar{\bar{G}}^r(\vec{r}|\vec{r}') \tag{7.65}$$

and the total Hertz potential is

$$\vec{\pi}_1(\vec{r}) = \int_{V'} \bar{\bar{G}}(\vec{r}|\vec{r}') \cdot \frac{\vec{J}(\vec{r}')}{j\omega\varepsilon_1} dV' \tag{7.66}$$

7.3.4 Identification of the Electric-Field Dyadic Green's Function

The electric-field dyadic Green's function in region *1* is identified by using the following computation

$$\vec{E} = k_1^2\vec{\pi}_1 + \nabla\nabla\cdot\vec{\pi}_1 = \int_{V'} \bar{\bar{G}}^e(\vec{r}|\vec{r}') \cdot \vec{J}(\vec{r}')dV' \tag{7.67}$$

Of course, the field will contain a principle and reflected part, that is

$$\vec{E} = \vec{E}^p + \vec{E}^r \tag{7.68}$$

where

$$\vec{E}^p = k_1^2 \vec{\pi}_1^p + \nabla\nabla \cdot \vec{\pi}_1^p = \int_{V'} \ddot{G}^{ep}(\vec{r}|\vec{r}') \cdot \vec{J}(\vec{r}')dV' \tag{7.69}$$

$$\vec{E}^r = k_1^2 \vec{\pi}_1^r + \nabla\nabla \cdot \vec{\pi}_1^r = \int_{V'} \ddot{G}^{er}(\vec{r}|\vec{r}') \cdot \vec{J}(\vec{r}')dV' \tag{7.70}$$

The principal part of the electric-field dyadic Green's function was previously investigated in Chapter 5 and will therefore not be repeated here. Application of (7.70) leads to the following expression for the reflected part of the electric-field dyadic Green's function

$$\begin{aligned} \ddot{G}^{er} &= \hat{x}G_{xx}^{er}\hat{x} + \hat{x}G_{xy}^{er}\hat{y} + \hat{x}G_{xz}^{er}\hat{z} + \\ &\hat{y}G_{yx}^{er}\hat{x} + \hat{y}G_{yy}^{er}\hat{y} + \hat{y}G_{yz}^{er}\hat{z} + \hat{z}G_{zx}^{er}\hat{x} + \hat{z}G_{zy}^{er}\hat{y} + \hat{z}G_{zz}^{er}\hat{z} \end{aligned} \tag{7.71}$$

$$G_{xx}^{er} = \frac{1}{j\omega\varepsilon_1}\left(k_1^2 G_{xx}^r + \frac{\partial^2 G_{xx}^r}{\partial x^2} + \frac{\partial^2 G_{yx}^r}{\partial x \partial y}\right) \tag{7.72}$$

$$G_{xy}^{er} = \frac{1}{j\omega\varepsilon_1}\frac{\partial^2 G_{yy}^r}{\partial x \partial y} \quad , \quad G_{xz}^{er} = \frac{1}{j\omega\varepsilon_1}\left(\frac{\partial^2 G_{yz}^r}{\partial x \partial y} + \frac{\partial^2 G_{zz}^r}{\partial x \partial z}\right) \tag{7.73}$$

$$G_{yx}^{er} = \frac{1}{j\omega\varepsilon_1}\left(k_1^2 G_{yx}^r + \frac{\partial^2 G_{yx}^r}{\partial y^2} + \frac{\partial^2 G_{xx}^r}{\partial y \partial x}\right) \tag{7.74}$$

$$G_{yy}^{er} = \frac{1}{j\omega\varepsilon_1}\left(k_1^2 G_{yy}^r + \frac{\partial^2 G_{yy}^r}{\partial y^2}\right) \quad , \quad G_{yz}^{er} = \frac{1}{j\omega\varepsilon_1}\left(k_1^2 G_{yz}^r + \frac{\partial^2 G_{yz}^r}{\partial y^2} + \frac{\partial^2 G_{zz}^r}{\partial y \partial z}\right) \tag{7.75}$$

$$G_{zx}^{er} = \frac{1}{j\omega\varepsilon_1}\left(\frac{\partial^2 G_{xx}^r}{\partial z \partial x} + \frac{\partial^2 G_{yx}^r}{\partial z \partial y}\right) \quad , \quad G_{zy}^{er} = \frac{1}{j\omega\varepsilon_1}\frac{\partial^2 G_{yy}^r}{\partial z \partial y} \tag{7.76}$$

$$G_{zz}^{er} = \frac{1}{j\omega\varepsilon_1}\left(k_1^2 G_{zz}^r + \frac{\partial^2 G_{zz}^r}{\partial z^2} + \frac{\partial^2 G_{yz}^r}{\partial z \partial y}\right) \tag{7.77}$$

$$\frac{\partial^2 G^r_{xx}}{\partial x^2} = -\frac{1}{(2\pi)^2}\int_{-\infty}^{\infty}\int_{-\infty}^{\infty}\xi^2 \tilde{G}^r_{xx} e^{j\vec{\lambda}\cdot(\vec{r}-\vec{r}')} d^2\lambda \tag{7.78}$$

$$\frac{\partial^2 G^r_{y\alpha}}{\partial x \partial y} = \frac{1}{(2\pi)^2}\int_{-\infty}^{\infty}\int_{-\infty}^{\infty} j\xi \frac{\partial \tilde{G}^r_{y\alpha}}{\partial y} e^{j\vec{\lambda}\cdot(\vec{r}-\vec{r}')} d^2\lambda \quad ...\alpha = x, y, z \tag{7.79}$$

$$\frac{\partial \tilde{G}^r_{y\alpha}}{\partial y} = -p_1 R^{\alpha}_n \frac{e^{-p_1(y+y')}}{2p_1} = -\frac{R^{\alpha}_n}{2} e^{-p_1(y+y')} \quad ...\alpha = x, y, z \tag{7.80}$$

$$\frac{\partial^2 G^r_{\alpha\alpha}}{\partial x \partial z} = -\frac{1}{(2\pi)^2}\int_{-\infty}^{\infty}\int_{-\infty}^{\infty}\xi\zeta \tilde{G}^r_{\alpha\alpha} e^{j\vec{\lambda}\cdot(\vec{r}-\vec{r}')} d^2\lambda \quad ...\alpha = x, z \tag{7.81}$$

$$\frac{\partial^2 G^r_{y\alpha}}{\partial y^2} = \frac{1}{(2\pi)^2}\int_{-\infty}^{\infty}\int_{-\infty}^{\infty} p_1^2 \tilde{G}^r_{y\alpha} e^{j\vec{\lambda}\cdot(\vec{r}-\vec{r}')} d^2\lambda \quad ...\alpha = x, y, z \tag{7.82}$$

$$\frac{\partial^2 G^r_{xx}}{\partial y \partial x} = \frac{1}{(2\pi)^2}\int_{-\infty}^{\infty}\int_{-\infty}^{\infty} j\xi \frac{\partial \tilde{G}^r_{xx}}{\partial y} e^{j\vec{\lambda}\cdot(\vec{r}-\vec{r}')} d^2\lambda \tag{7.83}$$

$$\frac{\partial^2 G^r_{zz}}{\partial y \partial z} = \frac{1}{(2\pi)^2}\int_{-\infty}^{\infty}\int_{-\infty}^{\infty} j\zeta \frac{\partial \tilde{G}^r_{zz}}{\partial y} e^{j\vec{\lambda}\cdot(\vec{r}-\vec{r}')} d^2\lambda \tag{7.84}$$

$$\frac{\partial \tilde{G}^r_{\alpha\alpha}}{\partial y} = -p_1 R_t \frac{e^{-p_1(y+y')}}{2p_1} = -\frac{R_t}{2} e^{-p_1(y+y')} \quad ...\alpha = x, z \tag{7.85}$$

$$\frac{\partial^2 G^r_{y\alpha}}{\partial z \partial y} = \frac{1}{(2\pi)^2}\int_{-\infty}^{\infty}\int_{-\infty}^{\infty} j\zeta \frac{\partial \tilde{G}^r_{y\alpha}}{\partial y} e^{j\vec{\lambda}\cdot(\vec{r}-\vec{r}')} d^2\lambda \quad ...\alpha = x, y, z \tag{7.86}$$

$$\frac{\partial^2 G^r_{zz}}{\partial z^2} = -\frac{1}{(2\pi)^2}\int_{-\infty}^{\infty}\int_{-\infty}^{\infty}\zeta^2 \tilde{G}^r_{zz} e^{j\vec{\lambda}\cdot(\vec{r}-\vec{r}')} d^2\lambda \tag{7.87}$$

7.4 Development of the Lossy Microstrip EFIE

The EFIE for the discrete-mode propagation spectrum of the microstrip field applicator (shown in Figure 7.2) is obtained by following an analogous set of steps as in

Chapter 6. The resulting coupled EFIE's (upon suppressing the limit notation as was done in Chapter 6) are

$$\int_{-\infty}^{\infty} d\xi e^{j\xi x} \int_{-a}^{a} \left[C_{xx} k_x(x') + C_{xz} k_z(x') \right] e^{-j\xi x'} dx' - Z_s k_x(x) = 0 \tag{7.88}$$

$$\int_{-\infty}^{\infty} d\xi e^{j\xi x} \int_{-a}^{a} \left[C_{zx} k_x(x') + C_{zz} k_z(x') \right] e^{-j\xi x'} dx' - Z_s k_z(x) = 0 \tag{7.89}$$

where

$$C_{xx}(\xi, y, \zeta) = \frac{e^{-p_1 y}}{j2\pi\omega\varepsilon_1} \left[\frac{A(k_1^2 - \xi^2)}{D^h} + \xi^2 \bar{C} \right] \tag{7.90}$$

$$C_{xz}(\xi, y, \zeta) = C_{zx}(\xi, y, \zeta) = -\frac{\xi\zeta e^{-p_1 y}}{j2\pi\omega\varepsilon_1} \left(\frac{A}{D^h} - \bar{C} \right) \tag{7.91}$$

$$C_{zz}(\xi, y, \zeta) = \frac{e^{-p_1 y}}{j2\pi\omega\varepsilon_1} \left[\frac{A(k_1^2 - \zeta^2)}{D^h} + \zeta^2 \bar{C} \right] \tag{7.92}$$

$$A(\xi, \zeta) = \sinh p_2 d + \frac{p_2}{\sigma_c Z_c} \cosh p_2 d \tag{7.93}$$

$$B(\xi, \zeta) = p_1 A(N^2 - 1) \left(\cosh p_2 d + j \frac{\omega\varepsilon_2 Z_c}{p_2} \sinh p_2 d \right) \tag{7.94}$$

$$\bar{C}(\xi, \zeta) = \frac{B + (p_1 p_2 / \sigma_c Z_c)}{D^h D^e} \tag{7.95}$$

$$D^h(\xi, \zeta) = \left(p_1 + \frac{p_2^2}{\sigma_c Z_c} \right) \sinh p_2 d + p_2 \left(1 + \frac{p_1}{\sigma_c Z_c} \right) \cosh p_2 d \tag{7.96}$$

$$D^e(\xi, \zeta) = \left(p_1 N^2 + j\omega\varepsilon_2 Z_c \right) \cosh p_2 d + \left(p_2 + j \frac{\omega\varepsilon_2 Z_c p_1 N^2}{p_2} \right) \sinh p_2 d \tag{7.97}$$

Note that C_{xx}, C_{zz} are even in ξ and C_{xz}, C_{zx} are odd functions of ξ. In

addition, examination of (7.90)-(7.97) reveals that these coefficients $C_{\alpha\beta}$ are even with respect to p_2. Hence, the branch point k_2 (and associated branch cut) in p_2 is a removable singularity. The branch point k_1 in p_1 is not a removable singularity since the coefficients are not even in p_1.

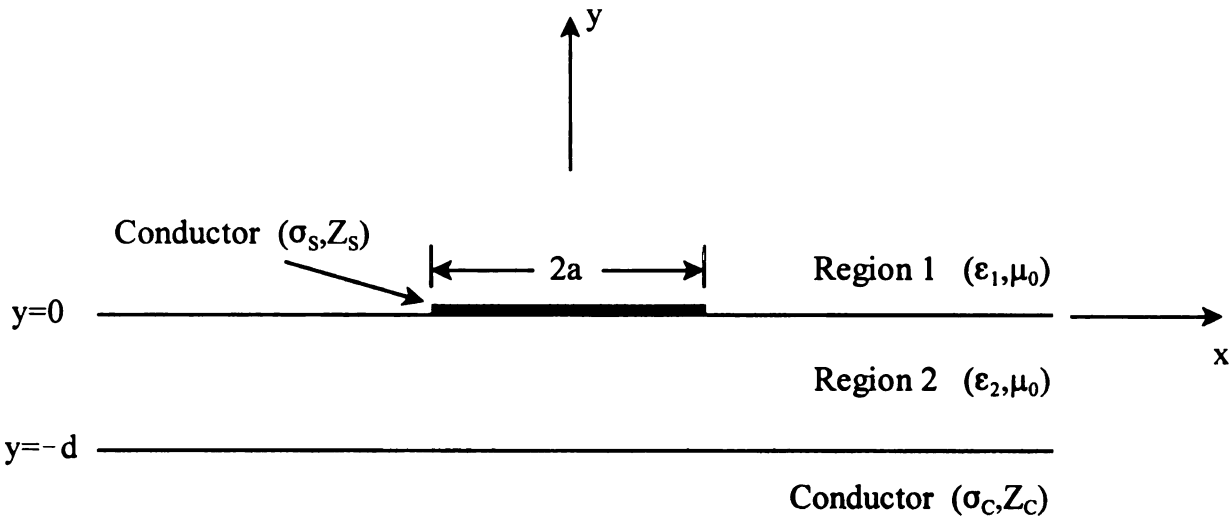

Figure 7.2 Cross-sectional geometry of the lossy microstrip field applicator.

7.5 MoM Solution for the Lossy Microstrip EFIE

The dual EFIE's in (7.88) and (7.89) can be solved using a MoM technique. Similar to Chapter 6, application of expansion and testing functions leads to the following general formulation

$$\left.\begin{aligned} \sum_{n=1}^{N_x} A_{xx}^{mn} a_{xn} + \sum_{n=1}^{N_z} A_{xz}^{mn} a_{zn} = 0 \\ \sum_{n=1}^{N_x} A_{zx}^{mn} a_{xn} + \sum_{n=1}^{N_z} A_{zz}^{mn} a_{zn} = 0 \end{aligned}\right\} \ldots m = 1,\ldots, N_x + N_z \qquad (7.98)$$

where

$$A_{\alpha\beta}^{mn} = \lim_{y\to 0^+} \int_{-\infty}^{\infty} C_{\alpha\beta} f_{\alpha m} g_{\beta n} d\xi + D_{\alpha\alpha}^{mn} \delta_{\alpha\beta} \quad ...\alpha,\beta = x,z \tag{7.99}$$

$$f_{\alpha m} = f_{\alpha m}(\xi) = \int_{-a}^{a} t_{\alpha m}(x) e^{j\xi x} dx \quad ...\alpha = x,z \tag{7.100}$$

$$g_{\alpha n} = g_{\alpha n}(\xi) = \int_{-a}^{a} e_{\alpha n}(x') e^{-j\xi x'} dx' \quad ...\alpha = x,z \tag{7.101}$$

$$D_{\alpha\alpha}^{mn} = -Z_s \int_{-a}^{a} t_{\alpha m}(x) e_{\alpha n}(x) dx \quad , \quad \delta_{\alpha\beta} = \begin{cases} 1 & ...\alpha = \beta \\ 0 & ...\alpha \neq \beta \end{cases} \tag{7.102}$$

Since the microstrip transmission line studied in this chapter exhibits symmetry, the following analysis (as in Chapter 6) prevails

$$\left.\begin{aligned} \sum_{n=0}^{N_x-1} A_{xx}^{mn} a_{xn} + \sum_{n=0}^{N_z-1} A_{xz}^{mn} a_{zn} = 0 \\ \sum_{n=0}^{N_x-1} A_{zx}^{mn} a_{xn} + \sum_{n=0}^{N_z-1} A_{zz}^{mn} a_{zn} = 0 \end{aligned}\right\} \quad ...m = 0,..., N_x + N_z - 1 \tag{7.103}$$

$$C_{xx}(\xi,\zeta) = \frac{1}{j2\pi\omega\varepsilon_1}\left[\frac{A(k_1^2 - \xi^2)}{D^h} + \xi^2 \bar{C}\right] \tag{7.104}$$

$$C_{xz}(\xi,\zeta) = C_{zx}(\xi,\zeta) = -\frac{\xi\zeta}{j2\pi\omega\varepsilon_1}\left(\frac{A}{D^h} - \bar{C}\right) \tag{7.105}$$

$$C_{zz}(\xi,\zeta) = \frac{1}{j2\pi\omega\varepsilon_1}\left[\frac{A(k_1^2 - \zeta^2)}{D^h} + \zeta^2 \bar{C}\right] \tag{7.106}$$

where, for even modes,

$$A_{xx}^{mn} = 8a \int_0^{\infty} C_{xx}(\xi,\zeta) I_{fxm}^o(\xi a) I_{gxn}^o(\xi a) d\xi - Z_s I_{xmn} \tag{7.107}$$

$$A_{xz}^{mn} = j8a\int_0^\infty C_{xz}(\xi,\zeta)I_{fxm}^{o}(\xi a)I_{gzn}^{e}(\xi a)d\xi \tag{7.108}$$

$$A_{zx}^{mn} = -j8a\int_0^\infty C_{zx}(\xi,\zeta)I_{fzm}^{e}(\xi a)I_{gxn}^{o}(\xi a)d\xi \tag{7.109}$$

$$A_{zz}^{mn} = 8a\int_0^\infty C_{zz}(\xi,\zeta)I_{fzm}^{e}(\xi a)I_{gzn}^{e}(\xi a)d\xi - Z_s I_{zmn} \tag{7.110}$$

and for odd modes

$$A_{xx}^{mn} = 8a\int_0^\infty C_{xx}(\xi,\zeta)\tilde{I}_{fxm}^{e}(\xi a)\tilde{I}_{gxn}^{e}(\xi a)d\xi - Z_s \tilde{I}_{xmn} \tag{7.111}$$

$$A_{xz}^{mn} = -j8a\int_0^\infty C_{xz}(\xi,\zeta)\tilde{I}_{fxm}^{e}(\xi a)\tilde{I}_{gzn}^{o}(\xi a)d\xi \tag{7.112}$$

$$A_{zx}^{mn} = j8a\int_0^\infty C_{zx}(\xi,\zeta)\tilde{I}_{fzm}^{o}(\xi a)\tilde{I}_{gxn}^{e}(\xi a)d\xi \tag{7.113}$$

$$A_{zz}^{mn} = 8a\int_0^\infty C_{zz}(\xi,\zeta)\tilde{I}_{fzm}^{o}(\xi a)\tilde{I}_{gzn}^{o}(\xi a)d\xi - Z_s \tilde{I}_{zmn} \tag{7.114}$$

Thus, the analytical procedure for determining the propagation constant and surface current distribution is identical to Chapter 6, except that the factors, $C_{\alpha\beta}$, are different.

7.6 Numerical Results

In this section, the numerical results for the microstrip propagation constant $\zeta = \beta - j\alpha$ and surface currents k_x and k_z will be discussed. It will be assumed that $n_1 = \sqrt{\varepsilon_{r1}} = 1$ and $n_2 = \sqrt{\varepsilon_{r2}} = 3.13$, unless specified differently. Since the convergence rates for the microstrip and stripline propagation constant and surface currents are

similar, no convergence plots will be provided. In addition, since the non-Galerkin and Galerkin microstrip MoM techniques produced identical results for the lossless scenario, no comparison plots will be supplied (as was done in Chapter 6 for the stripline field applicator).

Figure 7.3 shows that the full-wave theory developed in Chapter 7 compares reasonably well with the known perturbation theory result [3], [18]. Figures 7.4-7.7 show the effects that ground-plane and strip conductivity have on the principal-mode propagation constant. Similar to Chapter 6, the phase and attenuation constant for the microstrip increase as conductivity decreases and strip losses are more prominent, as expected. Figures 7.8-7.9 demonstrate the effects that strip conductivity has on surface current distribution. The longitudinal current is not significantly influenced by conductor loss and surprisingly, the transverse surface current decreases as conductivity decreases (this is opposite to the behavior of the transverse current for the stripline device). However, since the microstrip supports hybrid modes, this behavior may be anticipated. Finally, Figures 7.10-7.11 reveal the effect of frequency on the transverse and longitudinal surface current densities.

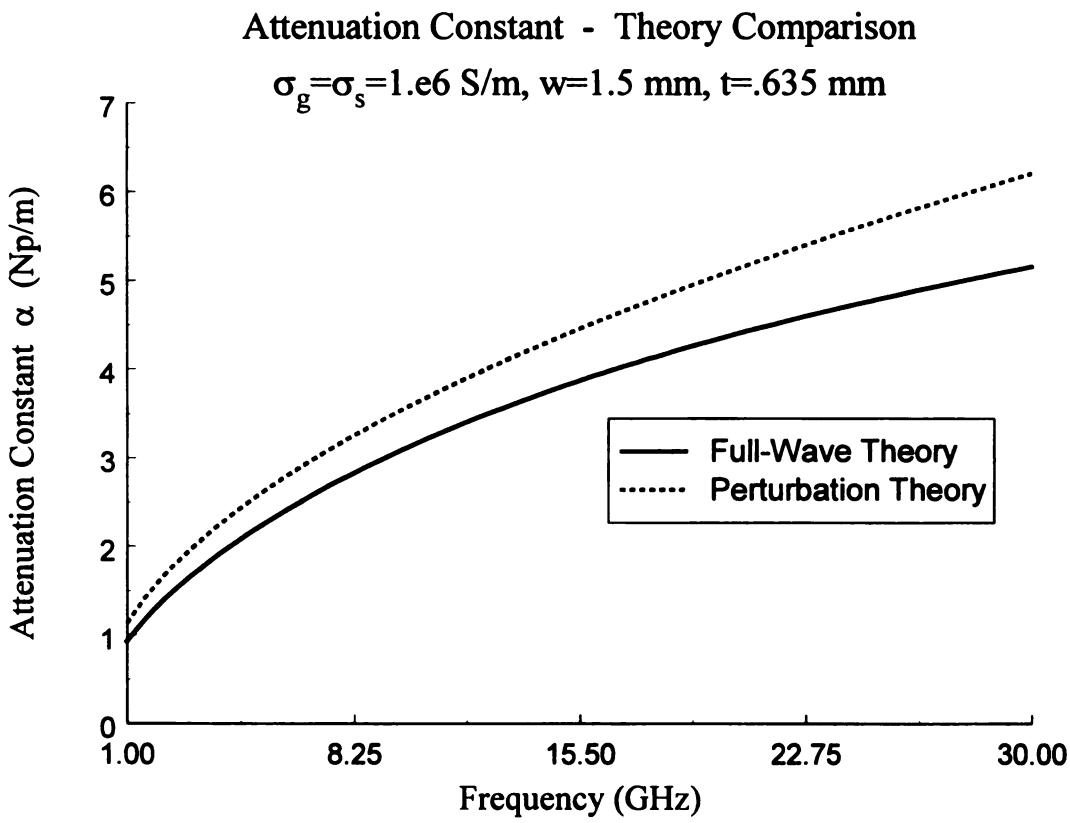

Figure 7.3 Full-wave and perturbation theory comparison for attenuation constant α.

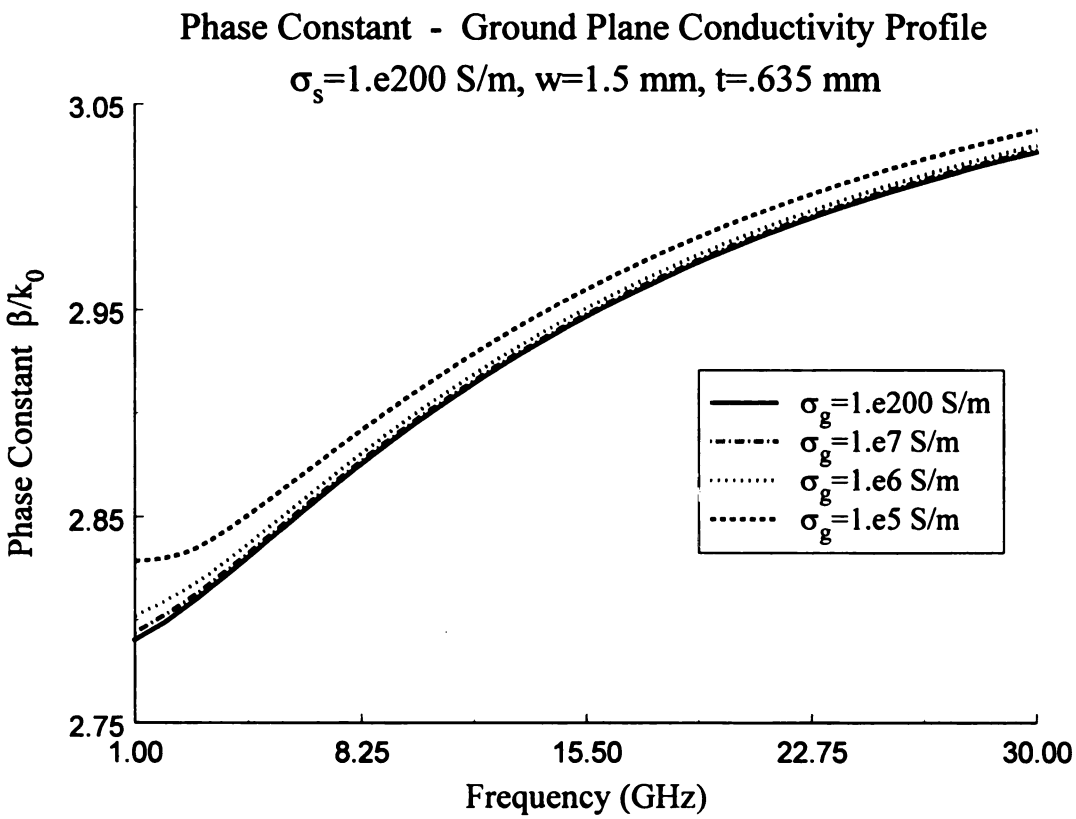

Figure 7.4 Effect of ground plane conductivity on phase constant β.

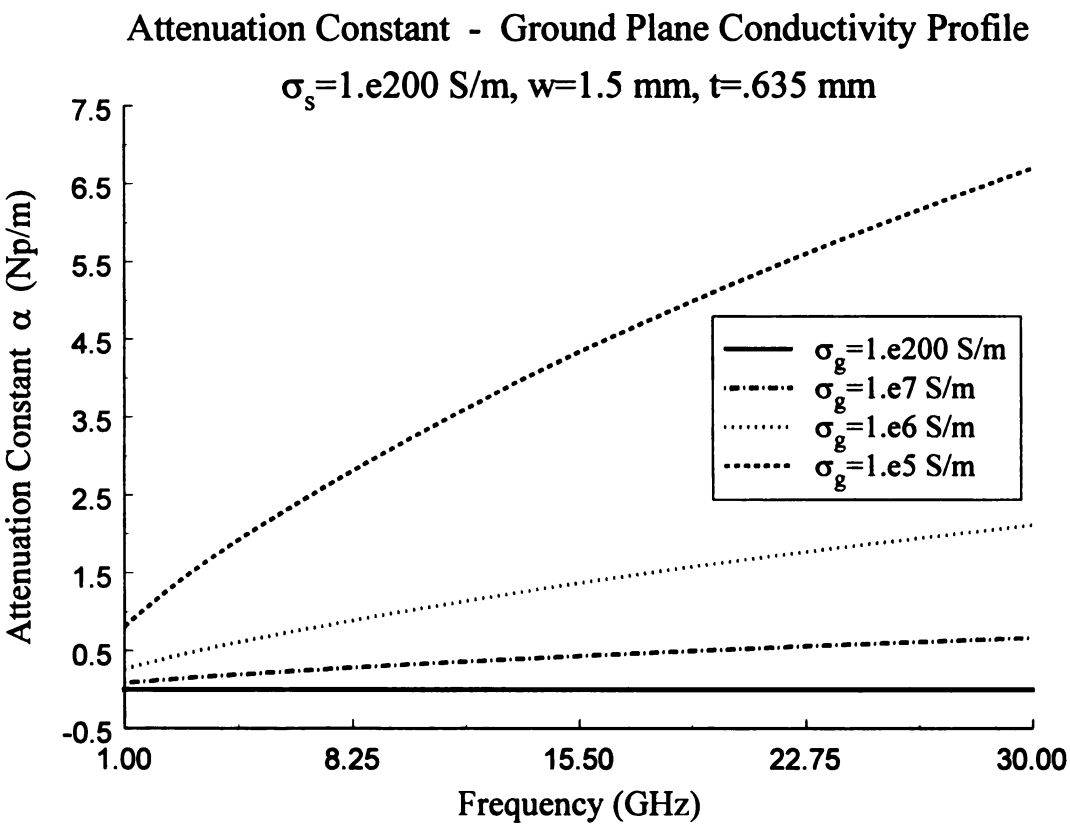

Figure 7.5 Effect of ground plane conductivity on attenuation constant α.

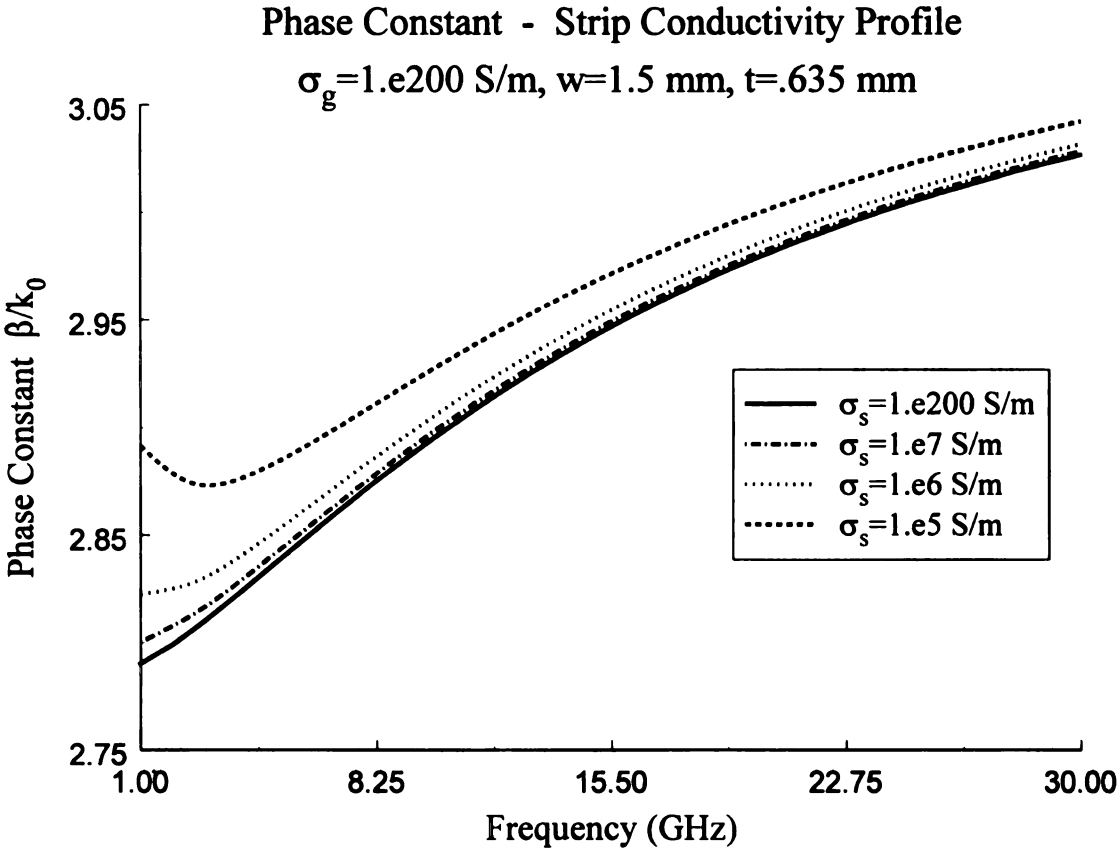

Figure 7.6 Effect of strip conductivity on phase constant β.

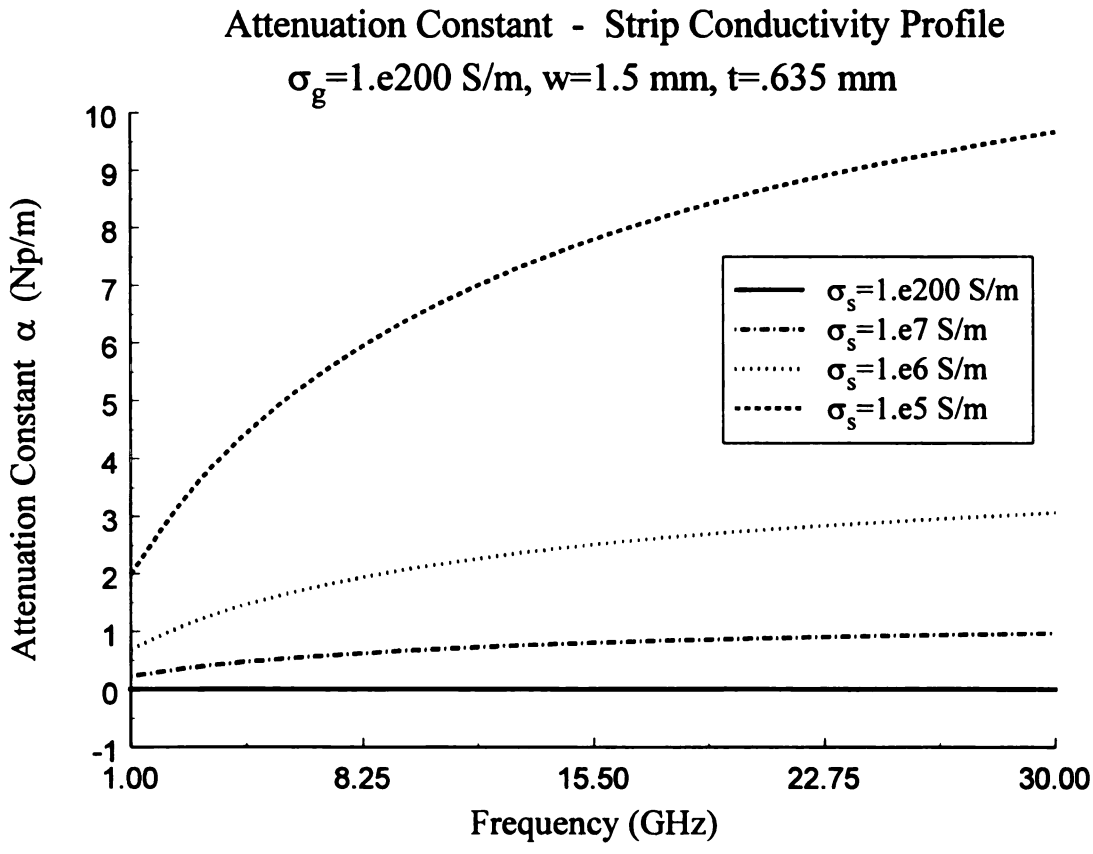

Figure 7.7 Effect of strip conductivity on attenuation constant α.

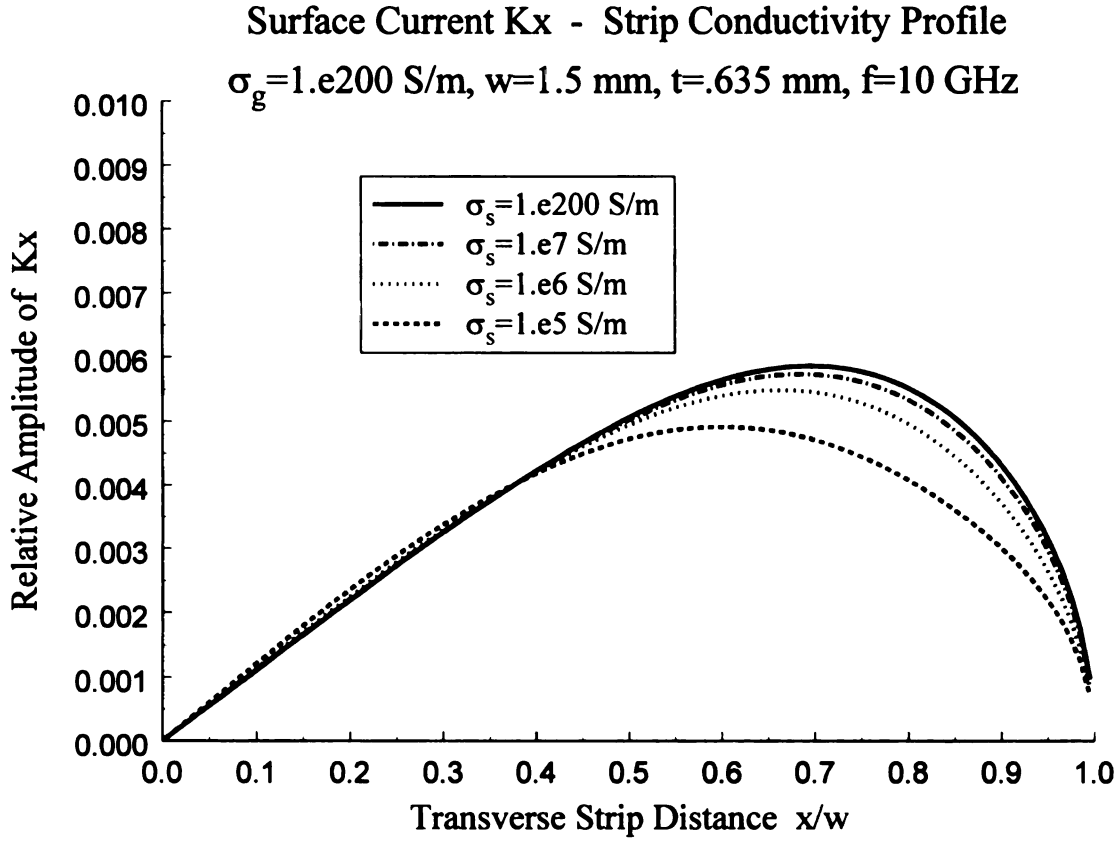

Figure 7.8 Effect of strip conductivity on surface current k_x.

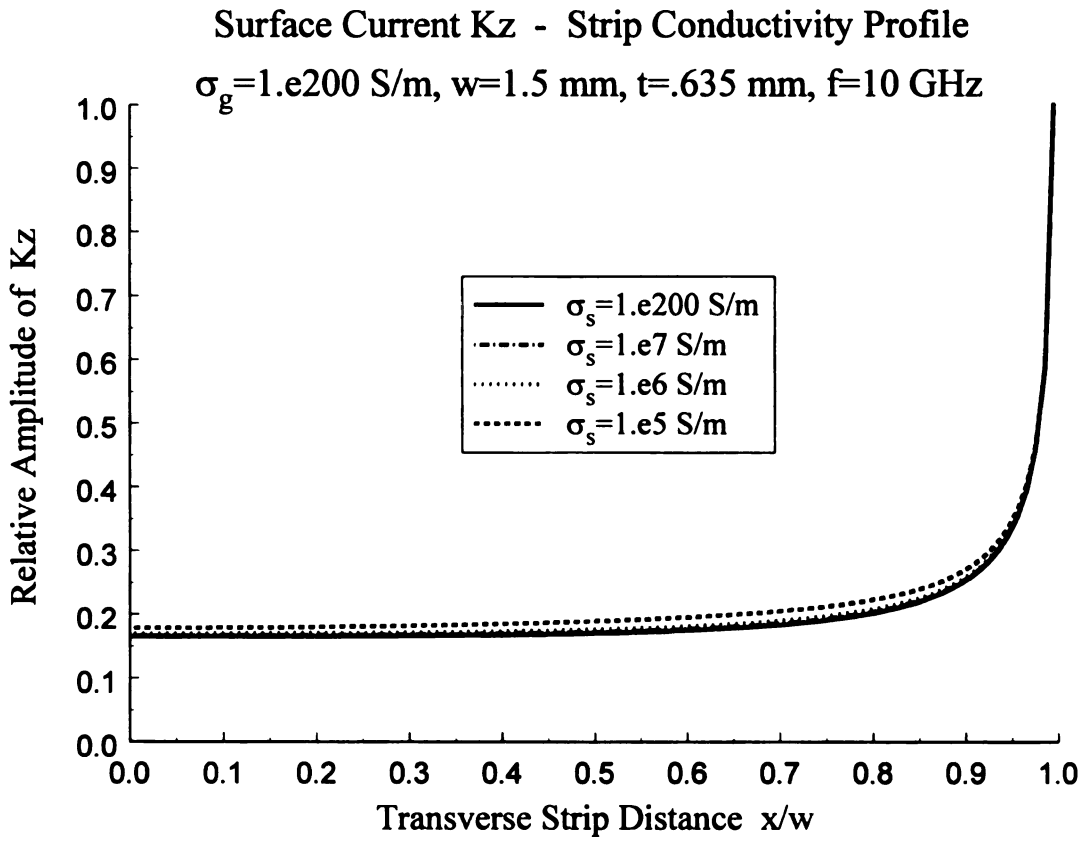

Figure 7.9 Effect of strip conductivity on surface current k_z.

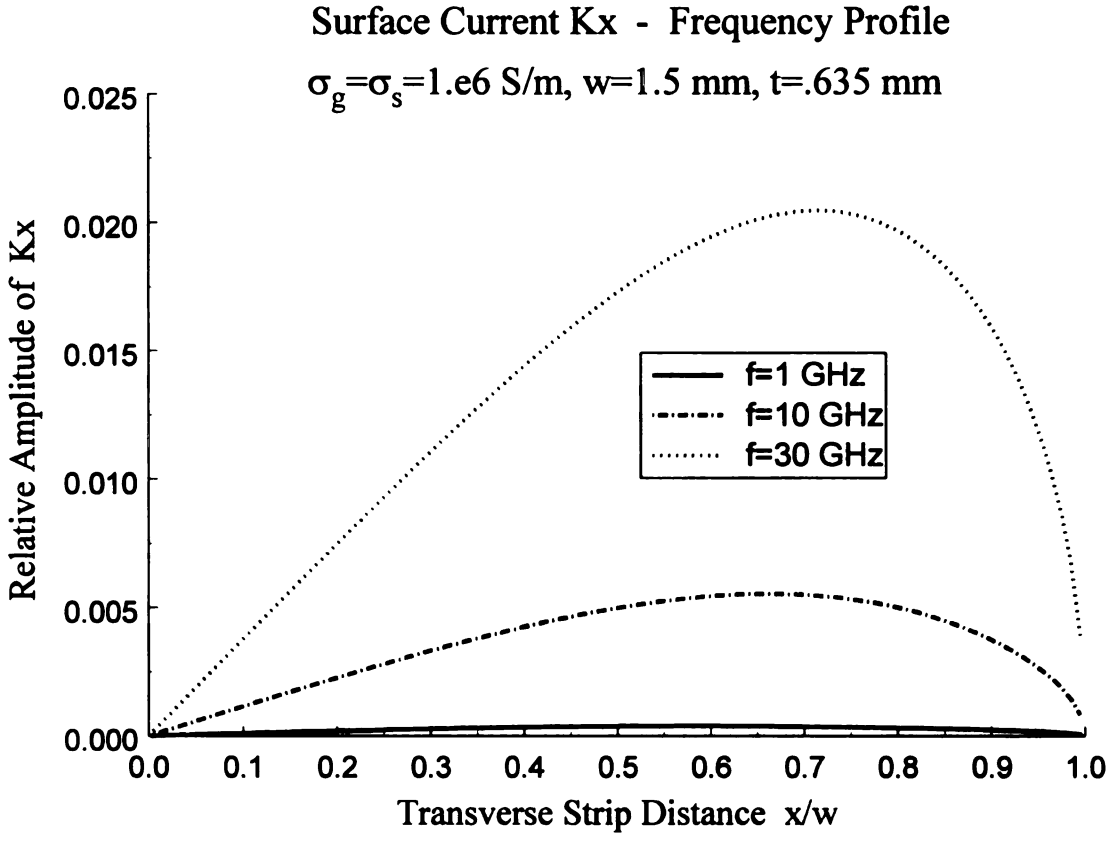

Figure 7.10 Effect of frequency on surface current k_x.

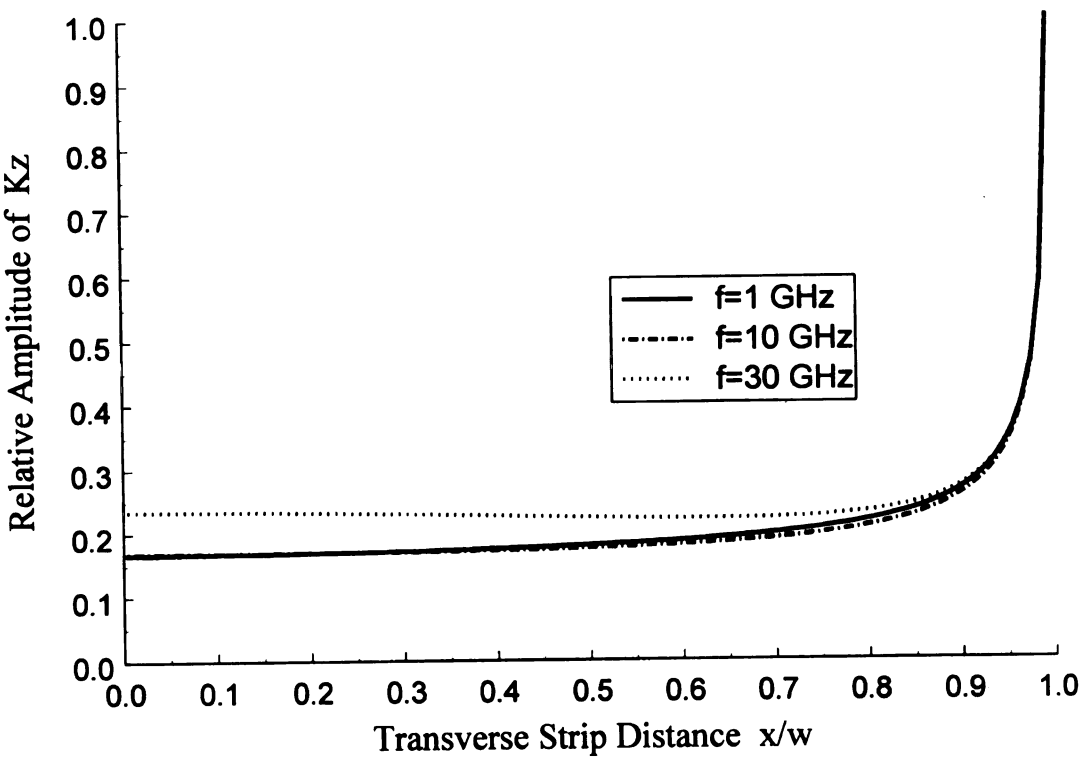
Relative Amplitude of Kz
1.0
0.9
0.8
0.7
0.6
0.5
0.4
0.3
0.2
0.1
0.0
0.0
0.1
0.2
0.3
0.4
0.5
0.6
0.7
0.8
0.9
1.0
Transverse Strip Distance x/w
f=1 GHz
f=10 GHz
f=30 GHz

Chapter 8

CONCLUSION

This dissertation has provided several methods and schemes, beyond the NRW technique, for accommodating errors in electromagnetic material characterization measurements. Chapter 2 discussed two methods, the direct and deembed techniques, for measuring and characterizing samples located within multi-layered materials. Experimental rectangular waveguide measurements were provided to verify the theoretical analysis. Although both methods are based on the wave-matrix approach, it was shown that the direct method must be used if sample homogeneity is to be accurately monitored.

Chapter 3 provided a theoretical technique for accommodating sample-to-wall gaps in rectangular waveguide measurements. The gaps were handled by regarding the waveguide as inhomogeneously filled in the cross-sectional plane with *LSM* and *LSE* propagation modes supported in the sample/gap region. Characteristic equations for the corresponding propagation constants were derived and solved numerically to determine shifts from the ideal TE_{10} propagation constant of a uniformly-filled guide. A modal analysis was utilized to obtain, under small gap conditions, approximate expressions for the wave impedance and interfacial reflection and transmission coefficients. This was done by considering a single TE_{10} mode incident upon, and reflected from, the sample and only a single *LSM* or *LSE* mode inside the sample region. Approximate expressions for the scattering parameters were also obtained using wave matrices. Gap

analysis measurements for a non-magnetic Alumina (Al_2O_3) sample were performed to substantiate the theoretical analysis. It was shown, as expected, that top/bottom gaps had a much more significant impact on constitutive parameter errors (5%) than left/right gaps (<1%) due to the electric field configuration for the TE_{10} rectangular waveguide mode.

In Chapter 4, a coupled-mode perturbation theory based on an impedance boundary condition was used to account for wall loss due to imperfectly-conducting boundaries in rectangular waveguide field applicators. The coupled-mode perturbation theory was specialized to single-mode operation and a complex correction to the ideal TE_{10} mode propagation constant was subsequently identified. This complex correction was compared with the standard power-loss method, which provides attenuation correction only. Rectangular waveguide measurements showed that obtaining the additional phase correction using the coupled-mode perturbation theory was crucial to accurately accommodating for the imperfectly-conducting walls. In addition, a high-dielectric resistive-card sample was measured to reveal the sensitivity that constitutive parameter computations have when changes in conductivity occur.

The main objective of Chapter 5 was to develop the dyadic Green's function for the electric field maintained by a general 3D current source immersed in a lossy stripline background environment. This goal was achieved by employing an intermediary electric-type Hertz potential in the Fourier transform domain and satisfying appropriate boundary conditions. The electric-field dyadic Green's function was formulated using two methodologies. The first method involved the analysis of a symmetric slab waveguide in which Hertz potential boundary conditions were invoked at the dielectric interfaces, the outer regions were allowed to become good conductors and the electric field was

carefully calculated using relations in Appendix A. The source-point singularity was discussed and appropriately handled using Leibnitz's rule. Although this singularity had no bearing on the results of Chapter 6, a clear understanding is vital for thick-strip analysis and applications. The second method utilized Hertzian-potential impedance boundary conditions to ultimately compute the electric-field dyadic Green's function. It was shown that both methods produced identical results, but the second method required considerably less effort. The magnetic-field dyadic Green's function, which was not required in this dissertation, was also computed for completeness.

Chapter 6 involved the analysis and numerical solution of a lossy stripline structure. These objectives were accomplished through the following sequence of steps. First, the general 3D current source of chapter 5 was specialized to an infinitely-long strip surface current symmetrically located between imperfectly-conducting plates. Next, an EFIE was developed by satisfying an impedance boundary condition on the strip conductor in the axial Fourier transform domain. As a final step, the EFIE was solved using a MoM technique and the principal-mode propagation constant and corresponding surface current distribution were subsequently identified. In regards to the MoM solution for the lossy stripline, a non-Galerkin's MoM technique using Chebyshev polynomials of the first and second kind had to be devised since the well-known Galerkin's method produced divergent integrals. The resulting integrals from the non-Galerkin's technique were identified and computed in closed form with the aid of Appendix E.

The results of the full-wave lossy stripline analysis and corresponding MoM solution revealed several expected phenomena. First, it was shown that the full-wave analysis lead to a complex correction to the propagation constant, which is vital in the

material characterization process. Next, it was observed that the MoM solution converged rapidly since the chosen Chebyshev polynomials closely modeled the real physical behavior of the surface currents. Indeed, it was shown that even one expansion term lead to highly accurate results for the surface currents and propagation constant. It was also demonstrated that the Galerkin and non-Galerkin MoM solutions produced identical results under lossless conditions. The full-wave theory compared closely with the standard power-loss perturbation method. Effects of ground and strip conductivity and frequency on the propagation constant and surface currents were examined and discussed. Finally, the influences of strip width and refractive index were reported.

A lossy microstrip transmission line was investigated in Chapter 7 using a procedure similar to Chapters 5 and 6. First, the dyadic Green's function was developed for the electric field maintained by a general 3D current source immersed in a lossy microstrip background environment. The general 3D current was then specialized to an infinitely-long strip surface current and boundary conditions were invoked on the imperfect strip conductor, leading to an EFIE. In the final step, the same non-Galerkin MoM technique of Chapter 6 was employed for solution of the lossy microstrip EFIE. The full-wave theory for the microstrip, as was the case for the stripline, compared closely with the power-loss perturbation method. Effects of ground-plane conductivity, strip conductivity and frequency on the principal-mode propagation constant and surface current were also examined.

This dissertation has also provided a basis for future investigations. For example, strip and microstrip transmission lines having thick, imperfect center conductors can now be investigated using the general electric-field dyadic Green's functions developed in

Chapters 5 and 7, respectively. The edge-singularity behavior will be different than the infinitesimally-thin conductors of Chapters 6 and 7, thus different expansion and testing functions will be required. A detailed study of the edge singularity reveals that Gegenbauer polynomials are the appropriate choice. Future investigations should also include coupled lossy strip and microstrip field applicators. Finally, higher-order modes of lossy strip and microstrip devices should be explored.

APPENDIX A

EM FIELDS AND HERTZIAN POTENTIALS

A.1 Introduction

Appendix A provides a brief overview of Maxwell's equations, EM fields and Hertzian potentials. Included in the analysis is the development of the wave equations for both the EM fields and the Hertzian potentials.

A.2 Maxwell's Equations and the Wave Equations for $\vec{E}$ and $\vec{H}$

Maxwell's equations for a simple medium (linear, homogeneous and isotropic) and the continuity equation in spectral-domain point form are

$$\nabla \times \vec{E}(\vec{r}) = -j\omega\mu\vec{H}(\vec{r}) \tag{A.1}$$

$$\nabla \times \vec{H}(\vec{r}) = \vec{J}(\vec{r}) + \sigma\vec{E}(\vec{r}) + j\omega\tilde{\varepsilon}\vec{E}(\vec{r}) = \vec{J}(\vec{r}) + j\omega\varepsilon\vec{E}(\vec{r}) \tag{A.2}$$

$$\nabla \bullet \vec{E}(\vec{r}) = \rho(\vec{r})/\varepsilon \tag{A.3}$$

$$\nabla \bullet \vec{H}(\vec{r}) = 0 \tag{A.4}$$

$$\nabla \bullet \vec{J}(\vec{r}) = -j\omega\rho(\vec{r}) \tag{A.5}$$

where $\vec{J}(\vec{r})$ is an electric source (i.e., impressed) current and $\varepsilon = \tilde{\varepsilon}(1 - j\sigma/\omega\tilde{\varepsilon})$ is the effective complex permittivity. In general, all the above quantities are also functions of ω (which has been dropped for notational convenience). If the excitation is time harmonic (i.e., sinusoidal steady state), then ω is interpreted as a frequency-domain variable and the peak field quantities in the time domain are recovered by multiplying by

$e^{j\omega t}$ and taking the real part. For example, $\vec{E}(\vec{r},t)$ in the time domain will be

$$\vec{E}(\vec{r},t) = \mathrm{Re}\{\vec{E}(\vec{r},\omega)e^{j\omega t}\} \tag{A.6}$$

If the excitation is non-sinusoidal, then ω must be interpreted as a Fourier-transform variable and the field quantities in the time domain are computed by taking the inverse transform. For example, $\vec{E}(\vec{r},t)$ in the time domain will be

$$\vec{E}(\vec{r},t) = \frac{1}{2\pi}\int_{-\infty}^{\infty} \vec{E}(\vec{r},\omega)e^{j\omega t}d\omega \tag{A.7}$$

The wave equation for $\vec{E}$ is determined by taking the curl of (A.1), substituting (A.2) into the resulting relation, applying the vector identity $\nabla\times\nabla\times\vec{E} = \nabla(\nabla\bullet\vec{E}) - \nabla^2\vec{E}$ and using equations (A.3) and (A.5). The result is

$$\nabla^2\vec{E} + k^2\vec{E} = j\omega\mu\vec{J} - \frac{1}{j\omega\varepsilon}\nabla(\nabla\bullet\vec{J}) \tag{A.8}$$

where $k^2 = \omega^2\varepsilon\mu$. The wave equation for $\vec{H}$ is found by taking the curl of (A.2), substituting (A.1) into the resulting equation and using $\nabla\times\nabla\times\vec{H} = \nabla(\nabla\bullet\vec{H}) - \nabla^2\vec{H}$ and (A.4). The result is

$$\nabla^2\vec{H} + k^2\vec{H} = -\nabla\times\vec{J} \tag{A.9}$$

A.3 Electric Hertzian Potential

Hertzian potentials are primarily used as an intermediate and simplifying step to determining electric and magnetic fields. An electric Hertzian potential can be identified by observing that (A.4) implies that $\vec{H}$ can be written as

$$\vec{H} = j\omega\varepsilon\nabla\times\vec{\pi} \tag{A.10}$$

since $\nabla \bullet \nabla \times \vec{\pi} = 0$ by vector identity. The electric field can be determined by substituting (A.10) into (A.1) and using the vector identity $\nabla \times \nabla \Phi = 0$. This leads to

$$\vec{E} = k^2 \vec{\pi} + \nabla \Phi \tag{A.11}$$

The wave equation for $\vec{\pi}$ can be identified by substituting (A.10) and (A.11) into (A.2), applying the identity $\nabla \times \nabla \times \vec{\pi} = \nabla(\nabla \bullet \vec{\pi}) - \nabla^2 \vec{\pi}$ and using the gauge $\Phi = \nabla \bullet \vec{\pi}$. The resulting Helmoltz wave equation is

$$\nabla^2 \vec{\pi} + k^2 \vec{\pi} = -\frac{\vec{J}}{j\omega\varepsilon} \tag{A.12}$$

Equation (A.12) can be decomposed into three scalar equations in Cartesian coordinates (hence reducing mathematical complexity) as follows

$$\nabla^2 \pi_\alpha + k^2 \pi_\alpha = -\frac{J_\alpha}{j\omega\varepsilon} \tag{A.13}$$

where $\alpha = x, y, z$. Substituting $\Phi = \nabla \bullet \vec{\pi}$ into (A.11) leads to

$$\vec{E} = k^2 \vec{\pi} + \nabla(\nabla \bullet \vec{\pi}) \tag{A.14}$$

Since (A.12) reveals that $\vec{\pi}$ is maintained by an electric current, it is called an electric Hertzian potential (magnetic Hertzian potentials are also used, but will not be discussed here). A comparison of (A.13) with (A.8) or (A.9) demonstrates why Hertzian potentials are introduced into the mathematical analysis of electromagnetic problems. In equation (A.13), each component of $\vec{\pi}$ is simply and directly related to each component of $\vec{J}$. The relationship between $\vec{E}, \vec{J}$ in (A.8) or $\vec{H}, \vec{J}$ in (A.9) is more complicated and therefore the solution is, in general, more difficult to determine and more strongly singular. It's easier to solve for $\vec{\pi}$ first then obtain $\vec{E}$ and $\vec{H}$ using (A.14) and (A.10).

APPENDIX B

EVALUATION OF THE FOURIER TRANSFORM INVERSION INTEGRAL FOR THE SPECTRAL-DOMAIN PRINCIPAL-WAVE GREEN'S FUNCTION

B.1 Introduction

It was stated in Chapter 5 that the solution to the Fourier transform inversion integral for the spectral-domain principal-wave Green's function was

$$\tilde{G}_2^p(\vec{\lambda}; y|y') = \tilde{G}_2^p(\vec{\lambda}; y-y') = \frac{1}{2\pi}\int_{-\infty}^{\infty} \frac{e^{j\eta(y-y')}}{(\eta+jp)(\eta-jp)}d\eta = \frac{e^{-p|y-y'|}}{2p} \tag{B.1}$$

where y is the field point, y' is the source point, p is the spectral-domain wavenumber and $\eta = \eta_{re}$ (a real axis integration). The purpose of this appendix is to prove the above result using Cauchy's integral theorem and formula. Cauchy's integral theorem states, if a function $f(z)$ is analytic (differentiable at a point and a neighborhood about that point) everywhere within and on a closed contour C, then

$$\oint_C f(z)dz = 0 \tag{B.2}$$

Actually, it is sufficient to require $f(z)$ to be differentiable strictly inside the contour and continuous in the closed region bounded by it, including points on the boundary [67], [68]. Cauchy's integral formula states, if $f(z)$ is analytic within and on a closed contour C, then if z_0 is interior to C

$$\oint_C \frac{f(z)}{z-z_0}dz = \pm j2\pi f(z_0) \tag{B.3}$$

depending on whether C is oriented in the counterclockwise/clockwise direction.

The parameter $p = p(\xi,\zeta)$ is not a function of η, thus equation (B.1) reveals that $\eta = \pm jp$ are simple poles in the complex η-plane (they are not branch points). Also, $\mathrm{Re}\{p\} > 0$ has been chosen (as mentioned in Chapter 5), thus $\eta = +jp$ must be located in the upper-half of the complex η-plane since $\mathrm{Re}\{p\} > 0 \Rightarrow \mathrm{Im}\{jp\} > 0$. Similarly, $\eta = -jp$ must be located in the lower-half of the complex η-plane since $\mathrm{Re}\{p\} > 0 \Rightarrow \mathrm{Im}\{-jp\} < 0$.

The integrand, for the original real-axis integration, is a complex function of a real variable and is therefore not an analytic function since it doesn't satisfy the Cauchy-Riemann equations [69]. In order to compute the integral in (B.1) using Cauchy's integral theorem, the integrand must be analytically continued off of the η_{re}-axis (avoiding the poles $\pm jp$ in the process) to establish a region of analyticity [70]. The above analytic continuation, in this case, is easily accomplished by allowing η in (B.1) to become complex [71], that is, $\eta = \eta_{re} + j\eta_{im}$. The integrand is now analytic in the entire complex η-plane, except at the simple pole singularities $\eta = \pm jp$, thus the original integration contour can be deformed off of the real axis and Cauchy's integral theorem invoked.

The specific closed-contour C chosen for application of Cauchy's integral theorem is motivated by an examination of the integrand, more specifically, the term $e^{j\eta(y-y')}$. If $y - y' > 0$, then $e^{j\eta(y-y')} = e^{-\eta_{im}(y-y')} e^{j\eta_{re}(y-y')}$, thus $\eta_{im} > 0$ provides exponential decay (important for mathematical convergence). This prompts closure of the real-axis contour in the upper-half plane (making sure to circumvent the pole

singularity $\eta = jp$ since Cauchy's integral theorem states that no singularities can be contained within or on the closed contour), as shown in Figure B.1. Similarly, Figure B.2 shows the proper closure and contour when $y - y' < 0$ since $\eta_{im} < 0$ provides the necessary exponential decay for convergence. The evaluation of the integral in equation (B.1) using Cauchy's integral theorem and formula will be carried out in detail in the following sections.

B.2 Evaluation of $\tilde{G}_2^p$ for $y - y' > 0$

Figure B.1 shows the closed contour $C = C_R + C_p^+ + C_\infty^+$ used in Cauchy's integral theorem for the evaluation of $\tilde{G}_2^p$ when $y - y' > 0$. The segment C_R is the real-axis contour, C_p^+ is the portion of C that circumvents the pole singularity at $\eta = jp$ and C_∞^+ is the semi-circular segment that closes the contour in the upper-half plane. Since $f(\eta) = e^{j\eta(y-y')}/(\eta + jp)(\eta - jp)$ is analytic everywhere within and on C, Cauchy's integral theorem can be applied, leading to

$$\oint_C f(\eta)d\eta = \int_{C_R} f(\eta)d\eta + \oint_{C_p^+} f(\eta)d\eta + \int_{C_\infty^+} f(\eta)d\eta = 0 \tag{B.4}$$

where

$$\int_{C_R} f(\eta)d\eta = \int_{-\infty}^{\infty} \frac{e^{j\eta(y-y')}}{(\eta + jp)(\eta - jp)}d\eta = \lim_{R\to\infty} \int_{-R}^{R} \frac{e^{j\eta(y-y')}}{(\eta + jp)(\eta - jp)}d\eta \tag{B.5}$$

Therefore, using (B.4) and (B.5), the following desired result is obtained

$$\int_{-\infty}^{\infty} \frac{e^{j\eta(y-y')}}{(\eta + jp)(\eta - jp)}d\eta = -\oint_{C_p^+} \frac{e^{j\eta(y-y')}}{(\eta + jp)(\eta - jp)}d\eta - \int_{C_\infty^+} \frac{e^{j\eta(y-y')}}{(\eta + jp)(\eta - jp)}d\eta \tag{B.6}$$

The contour integral along C_∞^+ can be determined by using the parameterization $\eta = Re^{j\theta}$, $d\eta = jRe^{j\theta}d\theta$ and Jordan's lemma [72]. The result is

$$\int_{C_\infty^+} \frac{e^{j\eta(y-y')}}{(\eta+jp)(\eta-jp)}d\eta = \lim_{R\to\infty}\int_0^\pi \frac{e^{jRe^{j\theta}(y-y')}}{(Re^{j\theta}+jp)(Re^{j\theta}-jp)}jRe^{j\theta}d\theta \to 0 \qquad \text{(B.7)}$$

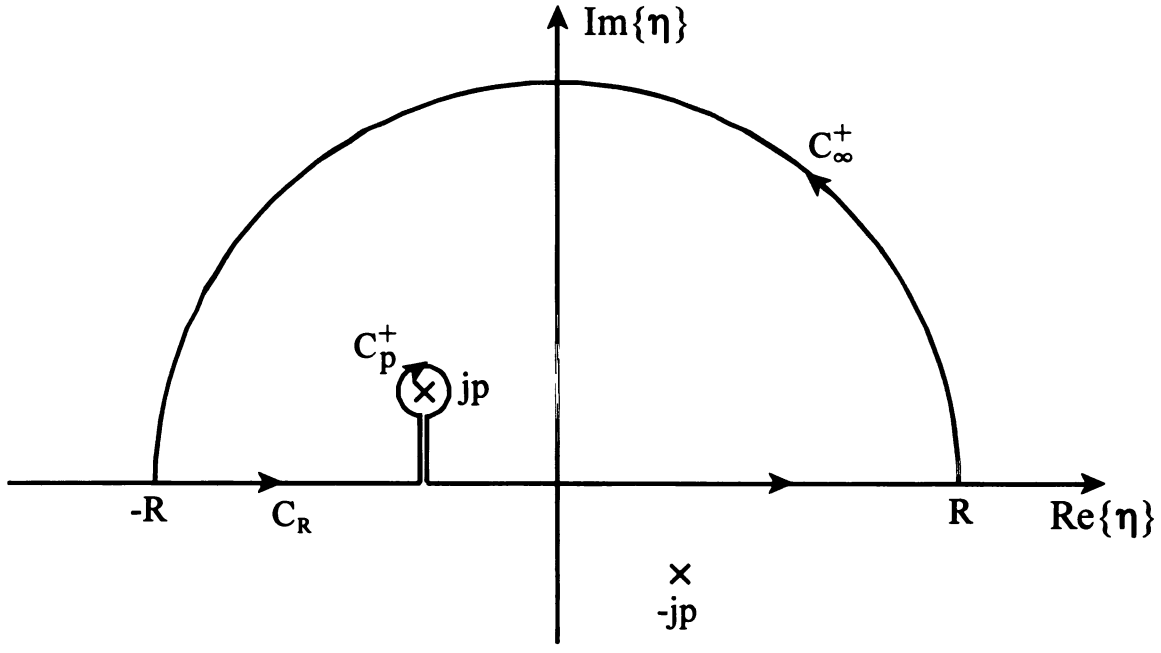

Figure B.1 Evaluation contour for $\tilde{G}_2^p$ when $y - y' > 0$.

The term $e^{j\eta(y-y')}$, as mentioned in the previous section, has an exponentially decaying behavior that provides the necessary convergence in (B.7). Note, the above result is also valid for $y - y' = 0$ (which is not always the case). The integral along the contour C_p^+ can be evaluated using Cauchy's integral formula. The pole $\eta = jp$ is interior to C_p^+ while $\eta = -jp$ is exterior to it, thus $e^{j\eta(y-y')}/(\eta + jp)$ is analytic everywhere within and on C_p^+. Therefore, application of Cauchy's integral formula leads to

$$\oint_{C_p^+} \frac{e^{j\eta(y-y')}}{(\eta+jp)(\eta-jp)}d\eta = -j2\pi \frac{e^{j\eta(y-y')}}{(\eta+jp)}\bigg|_{\eta=jp} = -\pi\frac{e^{-p(y-y')}}{p} \tag{B.8}$$

Combining the results of (B.6), (B.7) and (B.8) leads to the following desired result

$$\tilde{G}_2^p(\vec{\lambda};y|y') = \frac{1}{2\pi}\int_{-\infty}^{\infty} \frac{e^{j\eta(y-y')}}{(\eta+jp)(\eta-jp)}d\eta = \frac{e^{-p(y-y')}}{2p} \quad ...y-y' \geq 0 \tag{B.9}$$

B.3 Evaluation of $\tilde{G}_2^p$ for $y-y'<0$

The closed contour used for evaluating $\tilde{G}_2^p$ when $y-y'<0$ is shown in Figure B.2. In this case, $e^{j\eta(y-y')}$ provides the necessary convergence (i.e., exponential decay) along the C_∞^- contour due to the lower-half plane closure. An application of Cauchy's integral theorem leads to

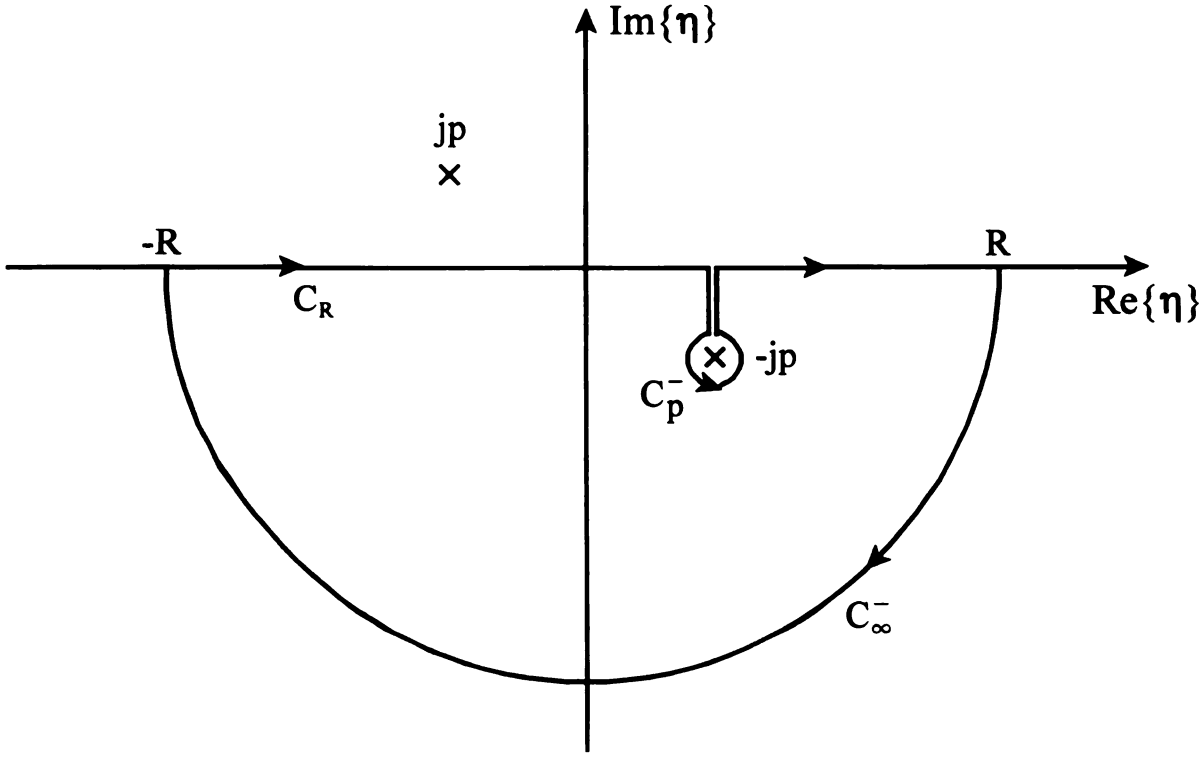

Figure B.2 Evaluation contour for $\tilde{G}_2^p$ when $y-y'<0$.

$$\int_{-\infty}^{\infty} \frac{e^{j\eta(y-y')}}{(\eta+jp)(\eta-jp)}d\eta = -\oint_{C_p^-} \frac{e^{j\eta(y-y')}}{(\eta+jp)(\eta-jp)}d\eta - \int_{C_\infty^-} \frac{e^{j\eta(y-y')}}{(\eta+jp)(\eta-jp)}d\eta \quad \text{(B.10)}$$

The contribution from C_∞^-, similar to C_∞^+, vanishes for $y-y' \le 0$ due to proper closure conditions and Jordan's lemma, that is

$$\int_{C_\infty^+} \frac{e^{j\eta(y-y')}}{(\eta+jp)(\eta-jp)}d\eta = \lim_{\mathrm{R}\to\infty} \int_0^{-\pi} \frac{e^{j\mathrm{R}e^{j\theta}(y-y')}}{(\mathrm{R}e^{j\theta}+jp)(\mathrm{R}e^{j\theta}-jp)} j\mathrm{R}e^{j\theta}d\theta \to 0 \quad \text{(B.11)}$$

An application of Cauchy's integral formula produces the result

$$\oint_{C_p^-} \frac{e^{j\eta(y-y')}}{(\eta+jp)(\eta-jp)}d\eta = j2\pi \frac{e^{j\eta(y-y')}}{(\eta-jp)}\bigg|_{\eta=-jp} = -\pi\frac{e^{p(y-y')}}{p} \quad \text{(B.12)}$$

Therefore, combining (B.10), (B.11) and (B.12) produces the result

$$\tilde{G}_2^p(\vec{\lambda}; y|y') = \frac{1}{2\pi}\int_{-\infty}^{\infty} \frac{e^{j\eta(y-y')}}{(\eta+jp)(\eta-jp)}d\eta = \frac{e^{p(y-y')}}{2p} \quad \ldots y-y' \le 0 \quad \text{(B.13)}$$

B.4 General Representation of $\tilde{G}_2^p$

The expressions for $\tilde{G}_2^p$ in (B.9) and (B.13) can be combined into a single result that is valid for all values of $y-y'$ by recognizing that

$$|y-y'| = \begin{cases} y-y' & \ldots y-y' > 0 \\ -(y-y') & \ldots y-y' < 0 \end{cases} \quad \text{(B.14)}$$

This leads to the final desired expression that was to be proved in (B.1), namely

$$\tilde{G}_2^p(\vec{\lambda}; y|y') = \tilde{G}_2^p(\vec{\lambda}; y-y') = \frac{1}{2\pi}\int_{-\infty}^{\infty} \frac{e^{j\eta(y-y')}}{(\eta+jp)(\eta-jp)}d\eta = \frac{e^{-p|y-y'|}}{2p} \quad \text{(B.15)}$$

APPENDIX C

ELECTRIC-TYPE HERTZIAN-POTENTIAL BOUNDARY CONDITIONS AT A MATERIAL INTERFACE

C.1 Introduction

Electric-type Hertzian-potential boundary conditions at a material interface are developed in Appendix C. These boundary conditions, which are based on the continuity of tangential electric and magnetic field components, are valid at the interface between two media having constitutive parameters (ε_1, μ_1) and (ε_2, μ_2). The analysis contained in this appendix directly follows the development of Nyquist [26], which is based upon the work of Sommerfeld [25] and Banos [27].

C.2 Geometry

Figure C.1 shows the material interface used in the development of the Hertzian-potential boundary conditions. The medium in region 1 $(y > 0)$ has an effective complex permittivity and permeability of (ε_1, μ_1) and the medium in region 2 $(y < 0)$ has an effective complex permittivity and permeability of (ε_2, μ_2).

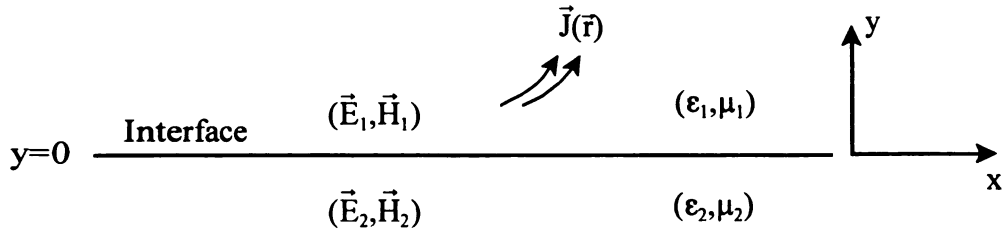

Figure C.1 Material interface for Hertzian potential boundary conditions.

C.3 Hertzian-Potential Boundary Conditions

The electric-type Hertzian-potential boundary conditions at a material interface can be identified by invoking continuity on the tangential electric and magnetic field components, that is (for all values of x and z along the $y = 0$ interface)

$$\hat{\alpha} \cdot \vec{E}_1(x, y = 0^+, z) = \hat{\alpha} \cdot \vec{E}_2(x, y = 0^-, z) \ \ldots \alpha = x, z \tag{C.1}$$

$$\hat{\alpha} \cdot \vec{H}_1(x, y = 0^+, z) = \hat{\alpha} \cdot \vec{H}_2(x, y = 0^-, z) \ \ldots \alpha = x, z \tag{C.2}$$

where (see Appendix A for details)

$$\vec{E} = k^2 \vec{\pi} + \nabla(\nabla \bullet \vec{\pi}) \tag{C.3}$$

$$\vec{H} = j\omega\varepsilon \nabla \times \vec{\pi} \tag{C.4}$$

$$\nabla^2 \vec{\pi} + k^2 \vec{\pi} = -\frac{\vec{J}}{j\omega\varepsilon} \tag{C.5}$$

and $k^2 = \omega^2 \varepsilon \mu$. Note that, in equation (C.2), it has been assumed that no surface current exists at the material interface.

Substitution of (C.3) into (C.1) and (C.4) into (C.2) (and dropping the functional dependence of the x and z variables for notational convenience) results in the following set of relations (for $\alpha = x, z$)

$$E_{1x}(y = 0^+) = E_{2x}(y = 0^-) \ \Rightarrow \ k_1^2 \pi_{1x} + \frac{\partial}{\partial x} \nabla \cdot \vec{\pi}_1 = k_2^2 \pi_{2x} + \frac{\partial}{\partial x} \nabla \cdot \vec{\pi}_2 \tag{C.6}$$

$$E_{1z}(y = 0^+) = E_{2z}(y = 0^-) \ \Rightarrow \ k_1^2 \pi_{1z} + \frac{\partial}{\partial z} \nabla \cdot \vec{\pi}_1 = k_2^2 \pi_{2z} + \frac{\partial}{\partial z} \nabla \cdot \vec{\pi}_2 \tag{C.7}$$

$$H_{1x}(y = 0^+) = H_{2x}(y = 0^-) \ \Rightarrow \ j\omega\varepsilon_1 \left(\frac{\partial \pi_{1z}}{\partial y} - \frac{\partial \pi_{1y}}{\partial z} \right) = j\omega\varepsilon_2 \left(\frac{\partial \pi_{2z}}{\partial y} - \frac{\partial \pi_{2y}}{\partial z} \right) \tag{C.8}$$

$$H_{1z}(y=0^+)=H_{2z}(y=0^-) \;\Rightarrow\; j\omega\varepsilon_1\left(\frac{\partial\pi_{1y}}{\partial x}-\frac{\partial\pi_{1x}}{\partial y}\right)=j\omega\varepsilon_2\left(\frac{\partial\pi_{2y}}{\partial x}-\frac{\partial\pi_{2x}}{\partial y}\right) \quad \text{(C.9)}$$

The above boundary conditions appear difficult to implement since all components of $\vec{\pi}$ and its derivatives are implicated. However, because of the uniqueness theorem, it is found that not all components of $\vec{\pi}$ are required to represent the EM field. Individual components of excitatory current (i.e., J_x, J_y, J_z) are studied to deduce (using the principle of superposition) which components of $\vec{\pi}$ are required to satisfy the above boundary conditions on tangential $\vec{E}, \vec{H}$ for a general electric current source $\vec{J}$.

C.3.1 Horizontal Source $\vec{J}=\hat{x}J_x$

An examination of (C.5) reveals that J_x maintains π_x only if the current source was immersed in unbounded space, that is, π_x alone maintains all fields (also see Appendix B for verification of this fact). The presence of the boundary in Figure C.1 may cause J_x to couple into other components of $\vec{\pi}$. However, as a starting point, the naïve conjecture that all fields can be represented by $\vec{\pi}=\hat{x}\pi_x$ only will be made. Substituting $\vec{\pi}=\hat{x}\pi_x$ into (C.7) leads to

$$E_{1z}(y=0^+)=E_{2z}(y=0^-) \;\Rightarrow\; \frac{\partial}{\partial z}\left(\frac{\partial\pi_{1x}}{\partial x}\right)=\frac{\partial}{\partial z}\left(\frac{\partial\pi_{2x}}{\partial x}\right) \quad \text{(C.10)}$$

Since this relation has to hold for all points x, z along the $y=0$ interface, it is concluded from (C.10) that

$$\pi_{1x}=\pi_{2x} \quad \text{(C.11)}$$

Similarly, substitution of $\vec{\pi}=\hat{x}\pi_x$ into (C.6) leads to

$$E_{1x}(y=0^+)=E_{2x}(y=0^-) \;\Rightarrow\; k_1^2\pi_{1x}+\frac{\partial}{\partial x}\left(\frac{\partial \pi_{1x}}{\partial x}\right)=k_2^2\pi_{2x}+\frac{\partial}{\partial x}\left(\frac{\partial \pi_{2x}}{\partial x}\right) \quad \text{(C.12)}$$

Inserting (C.11) into the partial derivative terms of (C.12) produces the following result

$$k_1^2\pi_{1x}=k_2^2\pi_{2x} \quad \text{(C.13)}$$

Equation (C.13) is in contradiction with (C.11), hence it is concluded that the conjecture of $\vec{\pi}=\hat{x}\pi_x$ maintaining all fields was incorrect. Thus, $\vec{\pi}=\hat{x}\pi_x$ alone is not sufficient to satisfy boundary conditions for the excitation $\vec{J}=\hat{x}J_x$.

The above analysis prompts the more educated conjecture that all fields are maintained by

$$\vec{\pi}=\hat{x}\pi_x+\hat{y}\pi_y \quad \text{(C.14)}$$

That is, the horizontal source $\vec{J}=\hat{x}J_x$ couples into both horizontal and vertical components of Hertzian potential π_x and π_y due to the presence of the boundary. Substitution of (C.14) into (C.7) results in

$$E_{1z}(y=0^+)=E_{2z}(y=0^-) \;\Rightarrow\; \frac{\partial}{\partial z}\nabla\cdot\vec{\pi}_1=\frac{\partial}{\partial z}\nabla\cdot\vec{\pi}_2 \;\Rightarrow\; \nabla\cdot\vec{\pi}_1=\nabla\cdot\vec{\pi}_2 \quad \text{(C.15)}$$

$$\frac{\partial \pi_{1x}}{\partial x}+\frac{\partial \pi_{1y}}{\partial y}=\frac{\partial \pi_{2x}}{\partial x}+\frac{\partial \pi_{2y}}{\partial y} \;\Rightarrow\; \frac{\partial \pi_{1y}}{\partial y}-\frac{\partial \pi_{2y}}{\partial y}=\frac{\partial \pi_{2x}}{\partial x}-\frac{\partial \pi_{1x}}{\partial x} \quad \text{(C.16)}$$

Inserting (C.14) into (C.6) and using the result from (C.15) leads to

$$E_{1x}(y=0^+)=E_{2x}(y=0^-) \;\Rightarrow\; k_1^2\pi_{1x}=k_2^2\pi_{2x} \quad \text{(C.17)}$$

$$\varepsilon_1\mu_1\pi_{1x}=\varepsilon_2\mu_2\pi_{2x} \quad \text{(C.18)}$$

Substitution of (C.14) into (C.8) gives

$$H_{1x}(y=0^+)=H_{2x}(y=0^-) \;\Rightarrow\; \varepsilon_1\frac{\partial \pi_{1y}}{\partial z}=\varepsilon_2\frac{\partial \pi_{2y}}{\partial z} \quad \text{(C.19)}$$

$$\varepsilon_1 \pi_{1y} = \varepsilon_2 \pi_{2y} \tag{C.20}$$

Substitution of (C.14) into (C.9) and using the result from (C.20) produces

$$H_{1z}(y=0^+) = H_{2z}(y=0^-) \;\Rightarrow\; \varepsilon_1\left(\frac{\partial \pi_{1y}}{\partial x} - \frac{\partial \pi_{1x}}{\partial y}\right) = \varepsilon_2\left(\frac{\partial \pi_{2y}}{\partial x} - \frac{\partial \pi_{2x}}{\partial y}\right) \tag{C.21}$$

$$\Rightarrow\; \varepsilon_1 \frac{\partial \pi_{1x}}{\partial y} - \varepsilon_2 \frac{\partial \pi_{2x}}{\partial y} = \varepsilon_1 \frac{\partial \pi_{1y}}{\partial x} - \varepsilon_2 \frac{\partial \pi_{2y}}{\partial x} = 0 \tag{C.22}$$

$$\varepsilon_1 \frac{\partial \pi_{1x}}{\partial y} = \varepsilon_2 \frac{\partial \pi_{2x}}{\partial y} \tag{C.23}$$

Finally, inserting (C.18) into (C.16) establishes the result

$$\frac{\partial \pi_{1y}}{\partial y} - \frac{\partial \pi_{2y}}{\partial y} = \left(1 - \frac{\varepsilon_2 \mu_2}{\varepsilon_1 \mu_1}\right)\frac{\partial \pi_{2x}}{\partial x} \tag{C.24}$$

No contradictions were encountered in the previous analysis, thus the above educated conjecture was correct.

C.3.2 Vertical Source $\vec{J} = \hat{y} J_y$

It will be assumed that $\vec{J} = \hat{y} J_y$ maintains only a vertical component of Hertzian potential. Thus, it will be conjectured that all fields can be represented by

$$\vec{\pi} = \hat{y} \pi_y \tag{C.25}$$

Substitution of (C.25) into (C.6) and (C.7) gives the following result

$$E_{1x}(y=0^+) = E_{2x}(y=0^-) \;\Rightarrow\; \frac{\partial}{\partial x}\left(\frac{\partial \pi_{1y}}{\partial y}\right) = \frac{\partial}{\partial x}\left(\frac{\partial \pi_{2y}}{\partial y}\right) \tag{C.26}$$

$$E_{1z}(y=0^+) = E_{2z}(y=0^-) \;\Rightarrow\; \frac{\partial}{\partial z}\left(\frac{\partial \pi_{1y}}{\partial y}\right) = \frac{\partial}{\partial z}\left(\frac{\partial \pi_{2y}}{\partial y}\right) \tag{C.27}$$

$$\frac{\partial \pi_{1y}}{\partial y} = \frac{\partial \pi_{2y}}{\partial y} \tag{C.28}$$

Note, the derivatives with respect to x and z in (C.26) and (C.27) can be removed (via integration) since these relations must hold for all values x, z. However, the derivative with respect to y cannot be removed since it holds only at a single point, namely, $y = 0$ (note, integration is an operation that can be performed only if an interval or some neighborhood about a point exists). Similarly, substitution of (C.25) into (C.8) and (C.9) gives

$$H_{1x}(y = 0^+) = H_{2x}(y = 0^-) \;\Rightarrow\; \varepsilon_1 \frac{\partial \pi_{1y}}{\partial z} = \varepsilon_2 \frac{\partial \pi_{2y}}{\partial z} \tag{C.29}$$

$$H_{1z}(y = 0^+) = H_{2z}(y = 0^-) \;\Rightarrow\; \varepsilon_1 \frac{\partial \pi_{1y}}{\partial x} = \varepsilon_2 \frac{\partial \pi_{2y}}{\partial x} \tag{C.30}$$

$$\varepsilon_1 \pi_{1y} = \varepsilon_2 \pi_{2y} \tag{C.31}$$

Note, no contradictions were encountered above, thus the conjecture was correct.

C.3.3 Horizontal Source $\vec{J} = \hat{z} J_z$

If the conjecture that all fields can be represented by

$$\vec{\pi} = \hat{y} \pi_y + \hat{z} \pi_z \tag{C.32}$$

for the current excitation $\vec{J} = \hat{z} J_z$ is correct, then an analogous set of steps as in section C.3.1 can be utilized, leading to the following relations

$$k_1^2 \pi_{1z} = k_2^2 \pi_{2z} \;\Rightarrow\; \varepsilon_1 \mu_1 \pi_{1z} = \varepsilon_2 \mu_2 \pi_{2z} \tag{C.33}$$

$$\varepsilon_1 \pi_{1y} = \varepsilon_2 \pi_{2y} \tag{C.34}$$

$$\varepsilon_1 \frac{\partial \pi_{1z}}{\partial y} = \varepsilon_2 \frac{\partial \pi_{2z}}{\partial y} \tag{C.35}$$

$$\frac{\partial \pi_{1y}}{\partial y} - \frac{\partial \pi_{2y}}{\partial y} = \left(1 - \frac{\varepsilon_2 \mu_2}{\varepsilon_1 \mu_1}\right) \frac{\partial \pi_{2z}}{\partial z} \tag{C.36}$$

C.3.4 General Source $\vec{J} = \hat{x}J_x + \hat{y}J_y + \hat{z}J_z$

Based upon the above special cases in sections C.3.1-C.3.3, the boundary conditions for Hertzian potential can be deduced (by linear superposition) when all components of $\vec{J}$ are active. A comparison of (C.17) with (C.33) leads to

$$k_1^2 \pi_{1\alpha} = k_2^2 \pi_{2\alpha} \quad \Rightarrow \quad \varepsilon_1 \mu_1 \pi_{1\alpha} = \varepsilon_2 \mu_2 \pi_{2\alpha} \quad ...\alpha = x, z \tag{C.37}$$

An examination of (C.20), (C.31) and (C.34) reveals, by superposition, that

$$\varepsilon_1 \pi_{1y} = \varepsilon_2 \pi_{2y} \tag{C.38}$$

Substitution of (C.37) into (C.6) and (C.7) gives

$$E_{1x}(y = 0^+) = E_{2x}(y = 0^-) \quad \Rightarrow \quad \frac{\partial}{\partial x} \nabla \cdot \vec{\pi}_1 = \frac{\partial}{\partial x} \nabla \cdot \vec{\pi}_2 \tag{C.39}$$

$$E_{1z}(y = 0^+) = E_{2z}(y = 0^-) \quad \Rightarrow \quad \frac{\partial}{\partial z} \nabla \cdot \vec{\pi}_1 = \frac{\partial}{\partial z} \nabla \cdot \vec{\pi}_2 \tag{C.40}$$

$$\Rightarrow \quad \nabla \cdot \vec{\pi}_1 = \nabla \cdot \vec{\pi}_2 \tag{C.41}$$

$$\Rightarrow \quad \frac{\partial \pi_{1y}}{\partial y} - \frac{\partial \pi_{2y}}{\partial y} = \frac{\partial \pi_{2x}}{\partial x} - \frac{\partial \pi_{1x}}{\partial x} + \frac{\partial \pi_{2z}}{\partial z} - \frac{\partial \pi_{1z}}{\partial z} \tag{C.42}$$

$$\frac{\partial \pi_{1y}}{\partial y} - \frac{\partial \pi_{2y}}{\partial y} = \left(1 - \frac{\varepsilon_2 \mu_2}{\varepsilon_1 \mu_1}\right)\left(\frac{\partial \pi_{2x}}{\partial x} + \frac{\partial \pi_{2z}}{\partial z}\right) \tag{C.43}$$

since $\pi_{1\alpha} = (\varepsilon_2 \mu_2 / \varepsilon_1 \mu_1)\pi_{2\alpha}$ from (C.37). Finally, substitution of (C.38) into (C.8) and (C.9) produces the result

$$H_{1x}(y=0^+) = H_{2x}(y=0^-) \;\Rightarrow\; \varepsilon_1 \frac{\partial \pi_{1z}}{\partial y} = \varepsilon_2 \frac{\partial \pi_{2z}}{\partial y} \tag{C.44}$$

$$H_{1z}(y=0^+) = H_{2z}(y=0^-) \;\Rightarrow\; \varepsilon_1 \frac{\partial \pi_{1x}}{\partial y} = \varepsilon_2 \frac{\partial \pi_{2x}}{\partial y} \tag{C.45}$$

Note, the boundary condition in (C.43) results in coupling of π_y to π_x and π_z. Also, if the interface is along x or z, the above components may be cyclically permutated to obtain the proper relationships.

C.4 Summary

The boundary conditions for components of electric-type Hertzian potential for a y-interface material boundary are

$$\begin{aligned} &\varepsilon_1 \mu_1 \pi_{1\alpha} = \varepsilon_2 \mu_2 \pi_{2\alpha} \quad , \quad \varepsilon_1 \frac{\partial \pi_{1\alpha}}{\partial y} = \varepsilon_2 \frac{\partial \pi_{2\alpha}}{\partial y} \quad ...\alpha = x, z \\ &\varepsilon_1 \pi_{1y} = \varepsilon_2 \pi_{2y} \quad , \quad \frac{\partial \pi_{1y}}{\partial y} - \frac{\partial \pi_{2y}}{\partial y} = \left(1 - \frac{\varepsilon_2 \mu_2}{\varepsilon_1 \mu_1}\right)\left(\frac{\partial \pi_{2x}}{\partial x} + \frac{\partial \pi_{2z}}{\partial z}\right) \end{aligned} \tag{C.46}$$

If $\mu_1 = \mu_2$, then the above boundary conditions simplify as follows

$$\begin{aligned} \varepsilon_1 \pi_{1\alpha} &= \varepsilon_2 \pi_{2\alpha} \quad ...\alpha = x, y, z \\ \varepsilon_1 \frac{\partial \pi_{1\alpha}}{\partial y} &= \varepsilon_2 \frac{\partial \pi_{2\alpha}}{\partial y} \quad ...\alpha = x, z \\ \frac{\partial \pi_{1y}}{\partial y} - \frac{\partial \pi_{2y}}{\partial y} &= \left(1 - \frac{\varepsilon_2}{\varepsilon_1}\right)\left(\frac{\partial \pi_{2x}}{\partial x} + \frac{\partial \pi_{2z}}{\partial z}\right) \end{aligned} \tag{C.47}$$

As mentioned earlier, the functional variables were dropped for notational convenience. It is therefore noted that $\pi_{1\alpha} = \pi_{1\alpha}(x, y=0^+, z)$ and that $\pi_{2\alpha} = \pi_{2\alpha}(x, y=0^-, z)$.

If the boundary conditions hold for all values of x and z $(-\infty < x, z < \infty)$, then the above relations can be Fourier transformed. Consider the generic Fourier transform

pair

$$\tilde{\pi}(\xi, y, \zeta) = \int_{-\infty}^{\infty} \int_{-\infty}^{\infty} \pi(x, y, z) e^{-j\vec{\lambda}\cdot\vec{r}} dx dz \tag{C.48}$$

$$\pi(x, y, z) = \frac{1}{(2\pi)^2} \int_{-\infty}^{\infty} \int_{-\infty}^{\infty} \tilde{\pi}(\xi, y, \zeta) e^{j\vec{\lambda}\cdot\vec{r}} d\xi d\zeta \tag{C.49}$$

where $\vec{\lambda} = \hat{x}\xi + \hat{z}\zeta$ and $\vec{r} = \hat{x}x + \hat{y}y + \hat{z}z$. If the above boundary conditions are multiplied by $e^{-j\vec{\lambda}\cdot\vec{r}}$ and integrated over x and z from $-\infty$ to ∞, then (C.46) and (C.47) become

$$\begin{gathered} \varepsilon_1 \mu_1 \tilde{\pi}_{1\alpha} = \varepsilon_2 \mu_2 \tilde{\pi}_{2\alpha} \quad , \quad \varepsilon_1 \frac{\partial \tilde{\pi}_{1\alpha}}{\partial y} = \varepsilon_2 \frac{\partial \tilde{\pi}_{2\alpha}}{\partial y} \quad \ldots \alpha = x, z \\ \varepsilon_1 \tilde{\pi}_{1y} = \varepsilon_2 \tilde{\pi}_{2y} \quad , \quad \frac{\partial \tilde{\pi}_{1y}}{\partial y} - \frac{\partial \tilde{\pi}_{2y}}{\partial y} = \left(1 - \frac{\varepsilon_2 \mu_2}{\varepsilon_1 \mu_1}\right)\left(j\xi \tilde{\pi}_{2x} + j\zeta \tilde{\pi}_{2z}\right) \end{gathered} \tag{C.50}$$

$$\begin{gathered} \varepsilon_1 \tilde{\pi}_{1\alpha} = \varepsilon_2 \tilde{\pi}_{2\alpha} \quad \ldots \alpha = x, y, z \\ \varepsilon_1 \frac{\partial \tilde{\pi}_{1\alpha}}{\partial y} = \varepsilon_2 \frac{\partial \tilde{\pi}_{2\alpha}}{\partial y} \quad \ldots \alpha = x, z \\ \frac{\partial \tilde{\pi}_{1y}}{\partial y} - \frac{\partial \tilde{\pi}_{2y}}{\partial y} = \left(1 - \frac{\varepsilon_2}{\varepsilon_1}\right)\left(j\xi \tilde{\pi}_{2x} + j\zeta \tilde{\pi}_{2z}\right) \end{gathered} \tag{C.51}$$

where $\tilde{\pi}_{1\alpha} = \tilde{\pi}_{1\alpha}(\xi, y = 0^+, \zeta)$ and $\tilde{\pi}_{2\alpha} = \tilde{\pi}_{2\alpha}(\xi, y = 0^-, \zeta)$.

APPENDIX D

HERTZIAN-POTENTIAL IMPEDANCE BOUNDARY CONDITIONS

D.1 Introduction

Electric-type Hertzian-potential impedance boundary conditions are developed in Appendix D. These boundary conditions, which are based on the electric and magnetic field impedance boundary conditions, are valid at the interface between a material and a good conductor. The Hertzian-potential boundary conditions at the surface of a perfect conductor will also be found as a limiting case of the impedance boundary conditions.

D.2 Geometry

Figure D.1 shows the material/conductor interface used in the development of the Hertzian-potential impedance boundary conditions. The upper material region ($y>0$) has an effective complex permittivity and permeability (ε,μ). Note that $\varepsilon=\tilde{\varepsilon}-j\sigma/\omega$, where $\tilde{\varepsilon}$ and σ are the permittivity and conductivity. The lower region ($y<0$) has a conductivity and permittivity ($\sigma_c,\tilde{\varepsilon}_c$), where $\sigma_c \gg \omega\tilde{\varepsilon}_c$ for a good conductor, and permeability μ_c. The effective complex permittivity is $\varepsilon_c=\tilde{\varepsilon}_c-j\sigma_c/\omega\approx -j\sigma_c/\omega$. The unit normal vector $\hat{n}=\hat{y}$ points out of the conductor and the fields are maintained by source excitation $\vec{J}$.

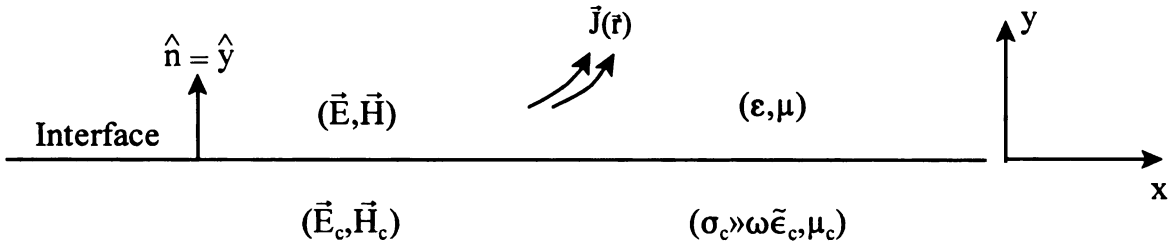

Figure D.1 Interface between material and good conductor.

D.3 Hertzian-Potential Impedance Boundary Conditions

The Hertzian-potential impedance boundary conditions are developed from the approximate electric and magnetic field impedance boundary condition [73]-[76]

$$\vec{E}_{tan} = Z_c \hat{n} \times \vec{H}_{tan} = Z_c \vec{K} \tag{D.1}$$

where

$$Z_c = (1+j)\sqrt{\frac{\omega\mu_c}{2\sigma_c}} \tag{D.2}$$

The vectors $\vec{E}_{tan}$ and $\vec{H}_{tan}$ represent the tangential electric and magnetic field components in the material region at $y = 0^+$, Z_c is the intrinsic impedance in the imperfectly-conducting region $y < 0$, $\vec{K}$ is the surface current and $\hat{n}$ is the unit normal vector that points out from the conductor and into the material, as shown in Figure D.1.

The justification of the above boundary condition is carried out in detail by Collin [3], but a brief overview is given here for the benefit of the reader. It is assumed that a plane EM wave in the material region is incident upon the conductor. Due to the high contrast between the material and conducting region, the wave penetrates normally into the conducting region, independent of the incidence angle (as verified by Snell's law).

The components of the electric and magnetic field inside the conductor are thus purely tangential to the surface and can be described by the well-known plane wave relationship $\vec{H}_c = \hat{u} \times \vec{E}_c / Z_c \Rightarrow \vec{H}_{tan,c} = \hat{u} \times \vec{E}_{tan,c} / Z_c$ or $\vec{E}_{tan,c} = -Z_c \hat{u} \times \vec{H}_{tan,c}$. The unit vector $\hat{u}$ is the direction of propagation and $Z_c = \sqrt{\mu_c / \varepsilon_c}$ is the intrinsic impedance of the conductor. Recall that $\varepsilon_c \approx -j\sigma_c / \omega$ for a good conductor, which implies that the intrinsic impedance becomes $Z_c \approx \sqrt{j\omega\mu_c / \sigma_c} = (1+j)\sqrt{\omega\mu_c / 2\sigma_c}$ (since the factor $\sqrt{j} = (1+j)/\sqrt{2}$). Note that this is in agreement with (D.2). The wave penetrates normally into the conductor ($\Rightarrow \hat{u} = -\hat{n}$), thus the above relation can be written $\vec{E}_{tan,c} = Z_c \hat{n} \times \vec{H}_{tan,c}$. Since the tangential components of the electric and magnetic fields must be continuous across the interface, the tangential fields just inside the conductor ($\vec{E}_{tan,c}, \vec{H}_{tan,c}$) can be replaced by the tangential fields just inside the material region ($\vec{E}_{tan}, \vec{H}_{tan}$), that is,

$$\vec{E}_{tan,c}(y = 0^-) = Z_c \hat{n} \times \vec{H}_{tan,c}(y = 0^-) \Rightarrow \vec{E}_{tan}(y = 0^+) = Z_c \hat{n} \times \vec{H}_{tan}(y = 0^+) \quad \text{(D.3)}$$

The current induced in the conductor is confined closely to the surface due to the high conductivity, therefore $\hat{n} \times \vec{H}_{tan} \approx \vec{K}$ (a well-known boundary condition), where $\vec{K}$ is the surface current. Thus, the above relation is written $\vec{E}_{tan} = Z_c \hat{n} \times \vec{H}_{tan} = Z_c \vec{K}$ and is the desired result (D.1), where it is understood that ($\vec{E}_{tan}, \vec{H}_{tan}$) are the tangential field components at $y = 0^+$. Note that an arbitrary field can always be decomposed into a sum of plane waves at various angles, thus the above results remain valid for any general EM field configuration. Besides, no matter what type of field exists in the material region,

the wave penetrates normally into the conducting region and will have field components that are planar to the interface and can therefore be described by a plane wave.

An examination of Figure D.1 shows that $\hat{n} = \hat{y}$, thus equation (D.1) becomes

$$\hat{x}E_x + \hat{z}E_z = Z_c\hat{y}\times(\hat{x}H_x + \hat{z}H_z) = Z_c(\hat{x}K_x + \hat{z}K_z) \quad \Rightarrow \tag{D.4}$$

$$E_x = Z_c H_z = Z_c K_x \tag{D.5}$$

$$E_z = -Z_c H_x = Z_c K_z \tag{D.6}$$

The first parts of (D.5) and (D.6) can be arranged as follows

$$\frac{E_x}{H_z} = Z = Z_c \quad , \quad \frac{E_z}{H_x} = -Z = -Z_c \tag{D.7}$$

where Z is the wave impedance in the material region. Essentially, (D.7) states that continuity of the tangential components of $\vec{E}$ and $\vec{H}$ is guaranteed by matching the impedances at the boundary/interface.

Now that the origin of (D.1) has been discussed, the electric-type Hertzian potential impedance boundary conditions are now developed. As mentioned previously, when $\hat{n} = \hat{y}$, the first part of (D.1) in scalar form becomes

$$E_x(y = 0^+) = Z_c H_z(y = 0^+) \tag{D.8}$$

$$E_z(y = 0^+) = -Z_c H_x(y = 0^+) \tag{D.9}$$

For electric-type Hertz potentials, the following relations prevail (see Appendix A)

$$\vec{E} = k^2\vec{\pi} + \nabla(\nabla\cdot\vec{\pi}) \tag{D.10}$$

$$\vec{H} = j\omega\varepsilon\nabla\times\vec{\pi} \tag{D.11}$$

$$\nabla^2\vec{\pi} + k^2\vec{\pi} = -\frac{\vec{J}}{j\omega\varepsilon} \tag{D.12}$$

where $k^2 = \omega^2 \varepsilon \mu$. Substitution of (D.10) and (D.11) into (D.8) and (D.9) leads to

$$E_x(y=0^+) = Z_c H_z(y=0^+) \;\Rightarrow\; k^2 \pi_x + \frac{\partial}{\partial x} \nabla \cdot \vec{\pi} = j\omega\varepsilon Z_c \left(\frac{\partial \pi_y}{\partial x} - \frac{\partial \pi_x}{\partial y} \right) \quad \text{(D.13)}$$

$$E_z(y=0^+) = -Z_c H_x(y=0^+) \;\Rightarrow\; k^2 \pi_z + \frac{\partial}{\partial z} \nabla \cdot \vec{\pi} = -j\omega\varepsilon Z_c \left(\frac{\partial \pi_z}{\partial y} - \frac{\partial \pi_y}{\partial z} \right) \quad \text{(D.14)}$$

The above boundary conditions appear difficult to implement since all components of $\vec{\pi}$ and its derivatives are implicated. However, because of the uniqueness theorem, it is found that not all components of $\vec{\pi}$ are required to represent the EM field. Individual components of excitatory current (i.e., J_x, J_y, J_z) are studied to deduce (using the principle of superposition) which components of $\vec{\pi}$ are required to satisfy the above boundary conditions on tangential $\vec{E}, \vec{H}$ for a general electric current source $\vec{J}$. An examination of Appendix C may help the reader better understand the following analysis.

D.3.1 Horizontal Source $\vec{J} = \hat{x} J_x$

It will be conjectured, for the horizontal source $\vec{J} = \hat{x} J_x$, that all fields can be represented by

$$\vec{\pi} = \hat{x} \pi_x + \hat{y} \pi_y \quad \text{(D.15)}$$

That is, $\vec{J} = \hat{x} J_x$ couples into both π_x and π_y (due to the presence of the interface) and only these components are required to satisfy boundary conditions. Substitution of (D.15) into (D.14) results in

$$E_z(y=0^+) = -Z_c H_x(y=0^+) \;\Rightarrow\; \frac{\partial}{\partial z} \nabla \cdot \vec{\pi} = j\omega\varepsilon Z_c \frac{\partial \pi_y}{\partial z} \quad \text{(D.16)}$$

$$\nabla \cdot \vec{\pi} = j\omega\varepsilon Z_c \pi_y \tag{D.17}$$

since the relation in (D.16) must hold for all values of x, z. Inserting (D.17) into (D.13) leads to

$$E_x(y=0^+) = Z_c H_z(y=0^+) \;\Rightarrow\; k^2\pi_x + j\omega\varepsilon Z_c \frac{\partial \pi_y}{\partial x} = j\omega\varepsilon Z_c \left(\frac{\partial \pi_y}{\partial x} - \frac{\partial \pi_x}{\partial y} \right) \tag{D.18}$$

$$\pi_x = -\frac{j\omega\varepsilon Z_c}{k^2} \frac{\partial \pi_x}{\partial y} = \frac{Z_c}{j\omega\mu} \frac{\partial \pi_x}{\partial y} \tag{D.19}$$

D.3.2 Vertical Source $\vec{J} = \hat{y} J_y$

It will be assumed that $\vec{J} = \hat{y} J_y$ maintains only a vertical component of Hertzian potential. Thus, it is conjectured that all fields can be represented by

$$\vec{\pi} = \hat{y} \pi_y \tag{D.20}$$

Substitution of (D.20) into (D.13) and (D.14) gives the following result

$$E_x(y=0^+) = Z_c H_z(y=0^+) \;\Rightarrow\; \frac{\partial}{\partial x} \nabla \cdot \vec{\pi} = j\omega\varepsilon Z_c \frac{\partial \pi_y}{\partial x} \tag{D.21}$$

$$E_z(y=0^+) = -Z_c H_x(y=0^+) \;\Rightarrow\; \frac{\partial}{\partial z} \nabla \cdot \vec{\pi} = j\omega\varepsilon Z_c \frac{\partial \pi_y}{\partial z} \tag{D.22}$$

$$\nabla \cdot \vec{\pi} = j\omega\varepsilon Z_c \pi_y \tag{D.23}$$

D.3.3 Horizontal Source $\vec{J} = \hat{z} J_z$

It will be conjectured, for the horizontal source $\vec{J} = \hat{z} J_z$, that all fields can be represented by

$$\vec{\pi} = \hat{y} \pi_y + \hat{z} \pi_z \tag{D.24}$$

Substitution of (D.24) into (D.13) results in

$$E_x(y=0^+) = Z_c H_z(y=0^+) \;\Rightarrow\; \frac{\partial}{\partial x}\nabla\cdot\vec{\pi} = j\omega\varepsilon Z_c \frac{\partial \pi_y}{\partial x} \tag{D.25}$$

$$\nabla\cdot\vec{\pi} = j\omega\varepsilon Z_c \pi_y \tag{D.26}$$

Inserting (D.26) into (D.14) leads to

$$E_z(y=0^+) = -Z_c H_x(y=0^+) \;\Rightarrow\; k^2\pi_z + j\omega\varepsilon Z_c \frac{\partial \pi_y}{\partial z} = -j\omega\varepsilon Z_c\left(\frac{\partial \pi_z}{\partial y} - \frac{\partial \pi_y}{\partial z}\right) \tag{D.27}$$

$$\pi_z = -\frac{j\omega\varepsilon Z_c}{k^2}\frac{\partial \pi_z}{\partial y} = \frac{Z_c}{j\omega\mu}\frac{\partial \pi_z}{\partial y} \tag{D.28}$$

D.3.4 General Source $\vec{J} = \hat{x}J_x + \hat{y}J_y + \hat{z}J_z$

Based upon the above special cases in sections D.3.1-D.3.3, the Hertzian-potential impedance boundary conditions can be deduced (by linear superposition) when all components of $\vec{J}$ are active. A comparison of (D.17), (D.23) and (D.26) leads to

$$\nabla\cdot\vec{\pi} = j\omega\varepsilon Z_c \pi_y \;\Rightarrow\; \frac{\partial \pi_x}{\partial x} + \frac{\partial \pi_y}{\partial y} + \frac{\partial \pi_z}{\partial z} = j\omega\varepsilon Z_c \pi_y \tag{D.29}$$

$$\frac{\partial \pi_y}{\partial y} = j\omega\varepsilon Z_c \pi_y - \frac{\partial \pi_x}{\partial x} - \frac{\partial \pi_z}{\partial z} \tag{D.30}$$

Note, the boundary condition in (D.30) results in coupling of π_y to π_x and π_z. Substitution of (D.29) into (D.13) and (D.14) produces the following results

$$E_x(y=0^+) = Z_c H_z(y=0^+) \;\Rightarrow\; k^2\pi_x + j\omega\varepsilon Z_c \frac{\partial \pi_y}{\partial x} = j\omega\varepsilon Z_c\left(\frac{\partial \pi_y}{\partial x} - \frac{\partial \pi_x}{\partial y}\right) \tag{D.31}$$

$$\pi_x = -\frac{j\omega\varepsilon Z_c}{k^2}\frac{\partial \pi_x}{\partial y} = \frac{Z_c}{j\omega\mu}\frac{\partial \pi_x}{\partial y} \tag{D.32}$$

$$E_z(y=0^+) = -Z_c H_x(y=0^+) \;\Rightarrow\; k^2\pi_z + j\omega\varepsilon Z_c \frac{\partial \pi_y}{\partial z} = -j\omega\varepsilon Z_c\left(\frac{\partial \pi_z}{\partial y} - \frac{\partial \pi_y}{\partial z}\right) \quad \text{(D.33)}$$

$$\pi_z = -\frac{j\omega\varepsilon Z_c}{k^2}\frac{\partial \pi_z}{\partial y} = \frac{Z_c}{j\omega\mu}\frac{\partial \pi_z}{\partial y} \quad \text{(D.34)}$$

If the permeabilities of both regions are equal (i.e., $\mu = \mu_c$), then

$$\frac{Z_c}{j\omega\mu} = \frac{Z_c Z_c^*}{j\omega\mu Z_c^*} = \frac{\omega\mu/\sigma_c}{\omega\mu j Z_c^*} = \frac{1}{\sigma_c Z_c} \quad \text{(D.35)}$$

therefore, the impedance boundary conditions can be written as

$$\frac{\partial \pi_y}{\partial y} = j\omega\varepsilon Z_c \pi_y - \frac{\partial \pi_x}{\partial x} - \frac{\partial \pi_z}{\partial z} \quad \text{(D.36)}$$

$$\pi_x = \frac{1}{\sigma_c Z_c}\frac{\partial \pi_x}{\partial y} \quad \text{(D.37)}$$

$$\pi_z = \frac{1}{\sigma_c Z_c}\frac{\partial \pi_z}{\partial y} \quad \text{(D.38)}$$

If $\hat{n} = -\hat{y}$, then a similar analysis leads to the following impedance boundary conditions when $\mu \neq \mu_c$

$$\pi_x = -\frac{Z_c}{j\omega\mu}\frac{\partial \pi_x}{\partial y}\;,\; \pi_z = -\frac{Z_c}{j\omega\mu}\frac{\partial \pi_z}{\partial y}\;,\; \frac{\partial \pi_y}{\partial y} = -j\omega\varepsilon Z_c \pi_y - \frac{\partial \pi_x}{\partial x} - \frac{\partial \pi_z}{\partial z} \quad \text{(D.39)}$$

and

$$\pi_x = -\frac{1}{\sigma_c Z_c}\frac{\partial \pi_x}{\partial y}\;,\; \pi_x = -\frac{1}{\sigma_c Z_c}\frac{\partial \pi_x}{\partial y}\;,\; \frac{\partial \pi_y}{\partial y} = -j\omega\varepsilon Z_c \pi_y - \frac{\partial \pi_x}{\partial x} - \frac{\partial \pi_z}{\partial z} \quad \text{(D.40)}$$

when $\mu = \mu_c$.

D.4 Hertzian-Potential Boundary Conditions at a Perfect Conductor

The Hertzian-potential boundary conditions at the surface of a perfect conductor can be found by considering the limiting case as $\sigma_c \to \infty$. Note that

$$\lim_{\sigma_c \to \infty} Z_c = \lim_{\sigma_c \to \infty} (1+j)\sqrt{\frac{\omega\mu_c}{2\sigma_c}} \to 0 \tag{D.41}$$

therefore (D.32), (D.34) and (D.30) reduce to

$$\pi_x, \pi_z, \frac{\partial \pi_y}{\partial y} = 0 \tag{D.42}$$

D.5 Summary

The electric-type Hertzian-potential impedance boundary conditions at a material/conductor interface are

$$\begin{aligned} \pi_\alpha &= \pm \frac{Z_c}{j\omega\mu} \frac{\partial \pi_\alpha}{\partial y} \quad \ldots \alpha = x, z \\ \frac{\partial \pi_y}{\partial y} &= \pm j\omega\varepsilon Z_c \pi_y - \frac{\partial \pi_x}{\partial x} - \frac{\partial \pi_z}{\partial z} \end{aligned} \quad \ldots \mu \neq \mu_c, \hat{n} = \pm\hat{y} \tag{D.43}$$

$$\begin{aligned} \pi_\alpha &= \pm \frac{1}{\sigma_c Z_c} \frac{\partial \pi_\alpha}{\partial y} \quad \ldots \alpha = x, z \\ \frac{\partial \pi_y}{\partial y} &= \pm j\omega\varepsilon Z_c \pi_y - \frac{\partial \pi_x}{\partial x} - \frac{\partial \pi_z}{\partial z} \end{aligned} \quad \ldots \mu = \mu_c, \hat{n} = \pm\hat{y} \tag{D.44}$$

where it is understood that $\pi_\alpha = \pi_\alpha(x, y = 0^+, z)$ for $\alpha = x, y, z$. The boundary conditions at the surface of a perfect conductor are

$$\pi_x, \pi_z, \frac{\partial \pi_y}{\partial y} = 0 \quad \ldots \sigma_c \to \infty \tag{D.45}$$

If the boundary conditions hold for all values of x and z $(-\infty < x,z < \infty)$, then the above relations can be Fourier transformed. Consider the generic Fourier transform pair

$$\tilde{\pi}(\xi,y,\zeta) = \int_{-\infty}^{\infty}\int_{-\infty}^{\infty} \pi(x,y,z)e^{-j\vec{\lambda}\cdot\vec{r}}\,dxdz \tag{D.46}$$

$$\pi(x,y,z) = \frac{1}{(2\pi)^2}\int_{-\infty}^{\infty}\int_{-\infty}^{\infty} \tilde{\pi}(\xi,y,\zeta)e^{j\vec{\lambda}\cdot\vec{r}}\,d^2\lambda \tag{D.47}$$

where $\vec{\lambda} = \hat{x}\xi + \hat{z}\zeta$, $d^2\lambda = d\xi d\zeta$ and $\vec{r} = \hat{x}x + \hat{y}y + \hat{z}z$. If the above boundary conditions are multiplied by $e^{-j\vec{\lambda}\cdot\vec{r}}$ and integrated over x and z from $-\infty$ to ∞, then (D.43), (D.44) and (D.45) become

$$\begin{aligned} \tilde{\pi}_\alpha &= \pm\frac{Z_c}{j\omega\mu}\frac{\partial\tilde{\pi}_\alpha}{\partial y} \quad ...\alpha = x,z \\ \frac{\partial\tilde{\pi}_y}{\partial y} &= \pm j\omega\varepsilon Z_c\tilde{\pi}_y - j\xi\tilde{\pi}_x - j\zeta\tilde{\pi}_z \end{aligned} \qquad ...\mu \neq \mu_c, \hat{n} = \pm\hat{y} \tag{D.48}$$

$$\begin{aligned} \tilde{\pi}_\alpha &= \pm\frac{1}{\sigma_c Z_c}\frac{\partial\tilde{\pi}_\alpha}{\partial y} \quad ...\alpha = x,z \\ \frac{\partial\tilde{\pi}_y}{\partial y} &= \pm j\omega\varepsilon Z_c\tilde{\pi}_y - j\xi\tilde{\pi}_x - j\zeta\tilde{\pi}_z \end{aligned} \qquad ...\mu = \mu_c, \hat{n} = \pm\hat{y} \tag{D.49}$$

$$\tilde{\pi}_x, \tilde{\pi}_z, \frac{\partial\tilde{\pi}_y}{\partial y} = 0 \quad ...\sigma_c \to \infty \tag{D.50}$$

where $\tilde{\pi}_\alpha = \tilde{\pi}_\alpha(\xi, y = 0^+, \zeta)$. If the interface is along x or z, the above components may be cyclically permutated to obtain the proper relationships.

APPENDIX E

OVERVIEW OF CHEBYSHEV POLYNOMIALS

E.1 Introduction

Appendix E provides a brief overview of Chebyshev polynomials. The overview will include fundamental expressions, relevant properties and several useful integrals that are commonly encountered in MoM solutions of integral equations. The primary references are [39], [50], [77]-[80].

E.2 Chebyshev Polynomial Properties

E.2.1 Fundamental Expressions

The Chebyshev polynomials of the first and second kind of order n are designated as $T_n(x)$ and $U_n(x)$, respectively. The Chebyshev polynomials, defined on the interval $-1 \le x \le 1$, can be expressed in the following power series representation

$$T_n(x) = U_n(x) = 1 \qquad \ldots n = 0 \tag{E.1}$$

$$T_n(x) = \frac{n}{2} \sum_{m=0}^{[n/2]} a_{mn} x^{n-2m} \qquad \ldots n = 1,2,3,\ldots \tag{E.2}$$

$$U_n(x) = \sum_{m=0}^{[n/2]} b_{mn} x^{n-2m} \qquad \ldots n = 1,2,3,\ldots \tag{E.3}$$

$$a_{mn} = (-1)^m 2^{n-2m} \frac{(n-m-1)!}{m!(n-2m)!} \tag{E.4}$$

$$b_{mn} = (-1)^m 2^{n-2m} \frac{(n-m)!}{m!(n-2m)!} \tag{E.5}$$

where $[n/2]$ means the greatest integer $\leq n/2$ ($[-1/2]=-1$, $[3/2]=1$, $[2]=2$ etc.). If n is even, then $[n/2]=n/2$. If n is odd, then $[n/2]$ can be equivalently represented by $[n/2]=(n-1)/2$. Thus, equations (E.2) and (E.3) can be written

$$T_n(x)=\frac{n}{2}\sum_{m=0}^{(n-1)/2} a_{mn}x^{n-2m} \quad ...n=1,3,5,... \tag{E.6}$$

$$T_n(x)=\frac{n}{2}\sum_{m=0}^{n/2} a_{mn}x^{n-2m} \quad ...n=2,4,6,... \tag{E.7}$$

$$U_n(x)=\sum_{m=0}^{(n-1)/2} b_{mn}x^{n-2m} \quad ...n=1,3,5,... \tag{E.8}$$

$$U_n(x)=\sum_{m=0}^{n/2} b_{mn}x^{n-2m} \quad ...n=2,4,6,... \tag{E.9}$$

Equations (E.6)-(E.9) are in a form conducive to numerical computation via computer. The trigonometric representations of the Chebyshev polynomials (defined on the interval $0\leq\theta\leq\pi$), using the c.o.v. (change-of-variable) $x=\cos\theta$, are

$$T_n(\cos\theta)=\cos n\theta \tag{E.10}$$

$$U_n(\cos\theta)=\frac{\sin(n+1)\theta}{\sin\theta} \tag{E.11}$$

Both the power series and trigonometric representations are useful for proving the various integrals in section E.3.

E.2.2 Parity and Recurrence Relations

Chebyshev polynomials of even/odd order are even/odd about the origin, thus the following parity relations prevail

$$T_n(-x)=(-1)^n T_n(x) \tag{E.12}$$

$$U_n(-x) = (-1)^n U_n(x) \tag{E.13}$$

The Chebyshev polynomials can be generated (in computer programs, for example) using the following recursive formulae

$$T_n(x) = 2xT_{n-1}(x) - T_{n-2}(x) \tag{E.14}$$

$$U_n(x) = 2xU_{n-1}(x) - U_{n-2}(x) \tag{E.15}$$

A few of the Chebyshev polynomials are

$$\begin{aligned}
T_0(x) &= 1 & U_0(x) &= 1 \\
T_1(x) &= x & U_1(x) &= 2x \\
T_2(x) &= 2x^2 - 1 & U_2(x) &= 4x^2 - 1 \\
T_3(x) &= 4x^3 - 3x & U_3(x) &= 8x^3 - 4x \\
T_4(x) &= 8x^4 - 8x^2 + 1 & U_4(x) &= 16x^4 - 12x^2 + 1 \\
T_5(x) &= 16x^5 - 20x^3 + 5x & U_5(x) &= 32x^5 - 32x^3 + 6x
\end{aligned} \tag{E.16}$$

E.3 Integrals Involving Chebyshev Polynomials

E.3.1 Preliminary Formulae and Well-Known Relations

The following well-known (and perhaps some not so well-known) relations are given here for the benefit of the reader and will be used in the following sections for proving the various integrals involving the Chebyshev polynomials, namely

$$\cos z = \frac{e^{jz} + e^{-jz}}{2} \tag{E.17}$$

$$\sin z = \frac{e^{jz} - e^{-jz}}{j2} \tag{E.18}$$

$$\sin A \sin B = \frac{1}{2}\left[\cos(A-B) - \cos(A+B)\right] \tag{E.19}$$

$$\int_0^1 x^{n-2m}\sin(\tilde{a}x)dx=\begin{cases}S_1\sin\tilde{a}+S_2\cos\tilde{a} & ...\tilde{a}\neq 0\\ 0 & ...\tilde{a}=0\end{cases};\ n=1,3,5,... \tag{E.20}$$

$$\int_0^1 x^{n-2m}\cos(\tilde{a}x)dx=\begin{cases}S_3\sin\tilde{a}+S_4\cos\tilde{a} & ...\tilde{a}\neq 0\\ 1/(n-2m+1) & ...\tilde{a}=0\end{cases};\ n=2,4,6,... \tag{E.21}$$

$$\int_0^1 x^{n-2m}dx=\frac{1}{n-2m+1} \tag{E.22}$$

$$S_1=S_1(m,n,\tilde{a})=\sum_{r=0}^{(n-2m-1)/2}(-1)^r\frac{(n-2m)!}{(n-2m-2r-1)!}\frac{1}{\tilde{a}^{2r+2}} \tag{E.23}$$

$$S_2=S_2(m,n,\tilde{a})=\sum_{r=0}^{(n-2m-1)/2}(-1)^{r+1}\frac{(n-2m)!}{(n-2m-2r)!}\frac{1}{\tilde{a}^{2r+1}} \tag{E.24}$$

$$S_3=S_3(m,n,\tilde{a})=\sum_{r=0}^{(n-2m)/2}(-1)^r\frac{(n-2m)!}{(n-2m-2r)!}\frac{1}{\tilde{a}^{2r+1}} \tag{E.25}$$

$$S_4=S_4(m,n,\tilde{a})=\sum_{r=0}^{(n-2m-2)/2}(-1)^r\frac{(n-2m)!}{(n-2m-2r-1)!}\frac{1}{\tilde{a}^{2r+2}} \tag{E.26}$$

$$J_n(\tilde{a})=\frac{(-j)^n}{\pi}\int_0^{\pi}\cos(n\theta)e^{j\tilde{a}\cos\theta}d\theta \quad\Rightarrow\quad \int_0^{\pi}\cos(n\theta)e^{j\tilde{a}\cos\theta}d\theta=\frac{\pi}{(-j)^n}J_n(\tilde{a}) \tag{E.27}$$

$$J_n(0)=\frac{(-j)^n}{\pi}\int_0^{\pi}\cos(n\theta)d\theta=\begin{cases}1 & ...n=0\\ 0 & ...n\neq 0\end{cases} \tag{E.28}$$

$$\lim_{\tilde{a}\to\infty}J_n(\tilde{a})\sim\sqrt{\frac{2}{\pi\tilde{a}}}\cos\left[\tilde{a}-\frac{\pi}{2}\left(n+\frac{1}{2}\right)\right] \tag{E.29}$$

$$J_n(\tilde{a}e^{jm\pi})=e^{jnm\pi}J_n(\tilde{a})\ \ ...m=integer \tag{E.30}$$

$$J_{n-1}(\tilde{a})+J_{n+1}(\tilde{a})=\frac{2n}{\tilde{a}}J_n(\tilde{a}) \tag{E.31}$$

Note that (E.20) and (E.21) are odd and even functions of $\tilde{a}$, respectively.

E.3.2 Orthogonality Relations

The Chebyshev polynomials, with respect to their resultant weight functions, satisfy the following orthogonality integrals

$$\int_{-1}^{1} \frac{T_m(x)T_n(x)}{\sqrt{1-x^2}}dx = \begin{cases} 0 & ...m \neq n \\ \pi/2 & ...m = n \neq 0 \\ \pi & ...m = n = 0 \end{cases} \tag{E.32}$$

$$\int_{-1}^{1} U_m(x)U_n(x)\sqrt{1-x^2}dx = \begin{cases} 0 & ...m \neq n \\ \pi/2 & ...m = n \end{cases} \tag{E.33}$$

The above relations can be easily proved by using the c.o.v. $x = \cos\theta$, the trigonometric definitions in equations (E.10)-(E.11) and the well-known orthogonality conditions of the sine/cosine functions on the interval $0 \leq \theta \leq \pi$.

E.3.3 Integrals Involving $T_n(x)$

Some of the common integrals involving Chebyshev polynomials of the first kind are given below. Proofs of the following integrals are also provided. It is noted that these types of integrals are typically encountered in MoM solutions.

$$\int_{0}^{1} T_n(x)\sin(\tilde{a}x)dx = \begin{cases} \frac{n}{2}\sum_{m=0}^{(n-1)/2} a_{mn}(S_1\sin\tilde{a} + S_2\cos\tilde{a}) & ...\tilde{a} \neq 0 \\ 0 & ...\tilde{a} = 0 \end{cases} ; n = 1,3,5,... \tag{E.34}$$

$$\int_{0}^{1} \frac{T_n(x)}{\sqrt{1-x^2}}\sin(\tilde{a}x)dx = \begin{cases} (-1)^{(n-1)/2}\frac{\pi}{2}J_n(\tilde{a}) & ...\tilde{a} \neq 0 \\ 0 & ...\tilde{a} = 0 \end{cases} ; n = 1,3,5,... \tag{E.35}$$

$$\int_{0}^{1} T_n(x)\cos(\tilde{a}x)dx = \begin{cases} \sin\tilde{a}/\tilde{a} & ...\tilde{a} \neq 0 \\ 1 & ...\tilde{a} = 0 \end{cases} ; n = 0 \tag{E.36}$$

$$\int_0^1 T_n(x)\cos(\tilde{a}x)dx = \begin{cases} \dfrac{n}{2}\displaystyle\sum_{m=0}^{n/2} a_{mn}(S_3\sin\tilde{a} + S_4\cos\tilde{a}) \;\; ...\tilde{a}\neq 0 \\ \dfrac{n}{2}\displaystyle\sum_{m=0}^{n/2}\dfrac{a_{mn}}{n-2m+1} \;\; ...\tilde{a}=0 \end{cases} ; \; n=2,4,6,... \qquad \text{(E.37)}$$

$$\int_0^1 \frac{T_n(x)}{\sqrt{1-x^2}}\cos(\tilde{a}x)dx = \begin{cases} (-1)^{n/2}(\pi/2)J_n(\tilde{a}) \;\; ...\tilde{a}\neq 0,\; n=0,2,4,... \\ \pi/2 \;\; ...\tilde{a}=0,\; n=0 \\ 0 \;\; ...\tilde{a}=0,\; n=2,4,6,... \end{cases} \qquad \text{(E.38)}$$

Note again, upon trivial inspection of the above integrands, that (E.34)-(E.35) are odd functions of $\tilde{a}$ and (E.36)-(E.38) are even functions of $\tilde{a}$.

Proof: (E.34)

The proof of (E.34) follows immediately by substituting (E.6) into the integral expression of (E.34) and using relation (E.20).

Proof: (E.35)

The relation in (E.35) can be more easily proved by examining the following integral

$$\int_0^1 \frac{T_{2k+1}(x)}{\sqrt{1-x^2}}\sin(\tilde{a}x)dx \quad ...k=0,1,2,... \qquad \text{(E.39)}$$

Note that $2k+1$ is an odd integer, therefore the substitution of $n=2k+1$ will be made at the end of the derivation to recover the desired result. Using the c.o.v. $x=\cos\theta$ and substitution of (E.10) into (E.39) leads to (since the integrand is even due to the odd parity of T_{2k+1})

$$\int_0^1 \frac{T_{2k+1}(x)}{\sqrt{1-x^2}} \sin(\tilde{a}x)dx = \frac{1}{2}\int_{-1}^1 \frac{T_{2k+1}(x)}{\sqrt{1-x^2}} \sin(\tilde{a}x)dx = \frac{1}{2}\int_0^\pi \cos(2k+1)\theta \sin(\tilde{a}\cos\theta)d\theta \quad \text{(E.40)}$$

Equation (E.40) can be computed in closed-form by expanding $\sin(\tilde{a}\cos\theta)$ with the aid of (E.18) and then using relation (E.27), leading to

$$\int_0^1 \frac{T_{2k+1}(x)}{\sqrt{1-x^2}} \sin(\tilde{a}x)dx = \frac{\pi}{4j(-j)^{2k+1}}\left[J_{2k+1}(\tilde{a}) - J_{2k+1}(-\tilde{a})\right] \quad \text{(E.41)}$$

Since $[j(-j)^{2k+1}]^{-1} = (-1)^k$ and $J_{2k+1}(-\tilde{a}) = -J_{2k+1}(\tilde{a})$ from the analytic continuation relation (E.30) with $m = 1$, equation (E.41) reduces to

$$\int_0^1 \frac{T_{2k+1}(x)}{\sqrt{1-x^2}} \sin(\tilde{a}x)dx = (-1)^k \frac{\pi}{2} J_{2k+1}(\tilde{a}) \quad \text{(E.42)}$$

Letting $n = 2k+1$ produces the desired result

$$\int_0^1 \frac{T_n(x)}{\sqrt{1-x^2}} \sin(\tilde{a}x)dx = (-1)^{(n-1)/2} \frac{\pi}{2} J_n(\tilde{a}) \quad \ldots \tilde{a} \neq 0,\ n = 1,3,5,\ldots \quad \text{(E.43)}$$

Since n is a positive odd integer, relation (E.28) implies that

$$\int_0^1 \frac{T_n(x)}{\sqrt{1-x^2}} \sin(\tilde{a}x)dx = 0 \quad \ldots \tilde{a} = 0,\ n = 1,3,5,\ldots \quad \text{(E.44)}$$

Besides, if $\tilde{a} = 0$, then the integrand is identically zero. Hence, integral relation (E.35) has been proved.

Proof: (E.36)

The proof follows immediately since $T_0(x) = 1$ and $\cos(\tilde{a}x) = 1$ if $a = \tilde{0}$.

Proof: (E.37)

Substitution of (E.7) into the integral expression of (E.37) and using (E.21) leads to the desired result.

Proof: (E.38)

The relation in (E.38) is more easily proved by examining

$$\int_0^1 \frac{T_{2k}(x)}{\sqrt{1-x^2}} \cos(\tilde{a}x)dx \quad ...k = 0,1,2,... \tag{E.45}$$

The integrand is even due to parity relation (E.12), thus using the c.o.v. $x = \cos\theta$ and (E.10) gives

$$\int_0^1 \frac{T_{2k}(x)}{\sqrt{1-x^2}} \cos(\tilde{a}x)dx = \frac{1}{2}\int_{-1}^1 \frac{T_{2k}(x)}{\sqrt{1-x^2}} \cos(\tilde{a}x)dx = \frac{1}{2}\int_0^\pi \cos(2k\theta)\cos(\tilde{a}\cos\theta)d\theta \tag{E.46}$$

Expanding $\cos(\tilde{a}\cos\theta)$ with the aid of (E.17), using (E.27) and invoking the relation $J_{2k}(-\tilde{a}) = J_{2k}(\tilde{a})$ produces [since $(-j)^{-2k} = (-1)^k$]

$$\int_0^1 \frac{T_{2k}(x)}{\sqrt{1-x^2}} \cos(\tilde{a}x)dx = (-1)^k \frac{\pi}{2} J_{2k}(\tilde{a}) \tag{E.47}$$

Letting $n = 2k$ gives the anticipated result

$$\int_0^1 \frac{T_n(x)}{\sqrt{1-x^2}} \cos(\tilde{a}x)dx = (-1)^{n/2} \frac{\pi}{2} J_n(\tilde{a}) \quad ...\tilde{a} \neq 0,\ n = 0,2,4,... \tag{E.48}$$

The use of equation (E.28) leads to the remaining relation, that is

$$\int_0^1 \frac{T_n(x)}{\sqrt{1-x^2}} \cos(\tilde{a}x)dx = \begin{cases} \pi/2 & ...n = 0 \\ 0 & ...n = 2,4,6,... \end{cases} \quad ...\tilde{a} = 0 \tag{E.49}$$

E.3.4 Integrals Involving $U_n(x)$

Some of the common integrals involving Chebyshev polynomials of the second kind are given below. Proofs that are similar to the previous section will be omitted for the sake of brevity.

$$\int_0^1 U_n(x)\sin(\tilde{a}x)dx = \begin{cases} \sum_{m=0}^{(n-1)/2} b_{mn}(S_1\sin\tilde{a} + S_2\cos\tilde{a}) & ...\tilde{a}\neq 0 \\ 0 & ...\tilde{a}=0 \end{cases} \quad ; n=1,3,5,... \qquad \text{(E.50)}$$

$$\int_0^1 U_n(x)\sqrt{1-x^2}\sin(\tilde{a}x)dx = \begin{cases} (-1)^{(n-1)/2}\dfrac{(n+1)\pi}{2\tilde{a}}J_{n+1}(\tilde{a}) & ...\tilde{a}\neq 0 \\ 0 & ...\tilde{a}=0 \end{cases} \quad ; n=1,3,5,... \qquad \text{(E.51)}$$

$$\int_0^1 U_n(x)\cos(\tilde{a}x)dx = \begin{cases} \sin\tilde{a}/\tilde{a} & ...\tilde{a}\neq 0 \\ 1 & ...\tilde{a}=0 \end{cases} \quad ; n=0 \qquad \text{(E.52)}$$

$$\int_0^1 U_n(x)\cos(\tilde{a}x)dx = \begin{cases} \sum_{m=0}^{n/2} b_{mn}(S_3\sin\tilde{a} + S_4\cos\tilde{a}) & ...\tilde{a}\neq 0 \\ \sum_{m=0}^{n/2}\dfrac{b_{mn}}{n-2m+1} & ...\tilde{a}=0 \end{cases} \quad ; n=2,4,6,... \qquad \text{(E.53)}$$

$$\int_0^1 U_n(x)\sqrt{1-x^2}\cos(\tilde{a}x)dx = \begin{cases} (-1)^{n/2}(n+1)(\pi/2)J_{n+1}(\tilde{a})/\tilde{a} & ...\tilde{a}\neq 0,\ n=0,2,4,... \\ \pi/4 & ...\tilde{a}=0,\ n=0 \\ 0 & ...\tilde{a}=0,\ n=2,4,6,... \end{cases} \qquad \text{(E.54)}$$

Note, (E.50)-(E.51) are odd functions of $\tilde{a}$ and (E.52)-(E.54) are even functions of $\tilde{a}$.

Proof: (E.51)

The relation in (E.51) is proved by examining

$$\int_0^1 U_{2k+1}(x)\sqrt{1-x^2}\sin(\tilde{a}x)dx \quad ...k=0,1,2,... \qquad \text{(E.55)}$$

Since U_{2k+1} is odd, substitution of (E.11) into (E.55), upon using the c.o.v. $x=\cos\theta$, leads to the following

$$\int_0^1 U_{2k+1}(x)\sqrt{1-x^2}\,\sin(\tilde{a}x)dx=\frac{1}{2}\int_0^{\pi}\sin\{[(2k+1)+1]\theta\}\sin\theta\sin(\tilde{a}\cos\theta)d\theta \quad \text{(E.56)}$$

Expanding $\sin\{[(2k+1)+1]\theta\}\sin\theta$ using (E.19) gives

$$\begin{aligned}&\int_0^1 U_{2k+1}(x)\sqrt{1-x^2}\,\sin(\tilde{a}x)dx=\\ &\frac{1}{4}\int_0^{\pi}\cos[(2k+1)\theta]\sin(\tilde{a}\cos\theta)d\theta-\frac{1}{4}\int_0^{\pi}\cos\{[(2k+1)+2]\theta\}\sin(\tilde{a}\cos\theta)d\theta\end{aligned} \quad \text{(E.57)}$$

Expansion of $\sin(\tilde{a}\cos\theta)$ with the aid of (E.18) and using (E.27) and (E.30) leads to

$$\begin{aligned}&\int_0^{\pi}\cos[(2k+1)\theta]\sin(\tilde{a}\cos\theta)d\theta=(-1)^k\pi J_{2k+1}(\tilde{a})\\ &\int_0^{\pi}\cos\{[(2k+1)+2]\theta\}\sin(\tilde{a}\cos\theta)d\theta=-(-1)^k\pi J_{(2k+1)+2}(\tilde{a})\end{aligned} \quad \text{(E.58)}$$

Substitution of (E.58) into (E.57) produces

$$\int_0^1 U_{2k+1}(x)\sqrt{1-x^2}\,\sin(\tilde{a}x)dx=(-1)^k\frac{\pi}{4}[J_{2k+1}(\tilde{a})+J_{(2k+1)+2}(\tilde{a})] \quad \text{(E.59)}$$

Finally, use of relation (E.31) gives the desired result

$$\int_0^1 U_{2k+1}(x)\sqrt{1-x^2}\,\sin(\tilde{a}x)dx=(-1)^k\frac{\pi[(2k+1)+1]}{2\tilde{a}}J_{(2k+1)+1}(\tilde{a}) \quad \text{(E.60)}$$

Letting $n=2k+1$ leads to the anticipated result

$$\int_0^1 U_n(x)\sqrt{1-x^2}\,\sin(\tilde{a}x)dx=(-1)^{(n-1)/2}\frac{\pi(n+1)}{2\tilde{a}}J_{n+1}(\tilde{a}) \quad ...\tilde{a}\neq 0,\ n=1,3,5,... \quad \text{(E.61)}$$

If $\tilde{a}=0$, then (E.61) becomes indeterminate since $J_{n+1}(0)=0$. Instead, one must look at

the relation in (E.59) prior to using (E.31), which takes the following form when $n = 2k+1$

$$\int_0^1 U_n(x)\sqrt{1-x^2}\,\sin(\tilde{a}x)dx = (-1)^{(n-1)/2}\frac{\pi}{4}[J_n(\tilde{a}) + J_{n+2}(\tilde{a})] \quad ...n = 1,3,5,... \quad \text{(E.62)}$$

Substitution of (E.28) into (E.62) leads to (since $n > 0$ here)

$$\int_0^1 U_n(x)\sqrt{1-x^2}\,\sin(\tilde{a}x)dx = 0 \quad ...\tilde{a} = 0,\ n = 1,3,5,... \quad \text{(E.63)}$$

This is anticipated, of course, since the integrand is identically zero when $\tilde{a} = 0$.

Proof: (E.54)

A comparable procedure, which will be left for the reader, leads to

$$\int_0^1 U_n(x)\sqrt{1-x^2}\,\cos(\tilde{a}x)dx = (-1)^{n/2}\frac{(n+1)\pi}{2\tilde{a}}J_{n+1}(\tilde{a}) \quad ...\tilde{a} \neq 0,\ n = 0,2,4,... \quad \text{(E.64)}$$

The following equivalent form, upon using (E.31), is best for analyzing the behavior when $\tilde{a} = 0$ (since the above is indeterminate again), namely

$$\int_0^1 U_n(x)\sqrt{1-x^2}\,\cos(\tilde{a}x)dx = (-1)^{n/2}\frac{\pi}{4}[J_n(\tilde{a}) + J_{n+2}(\tilde{a})] \quad ...\tilde{a} \neq 0,\ n = 0,2,4,... \quad \text{(E.65)}$$

Use of (E.28) reveals that

$$\int_0^1 U_n(x)\sqrt{1-x^2}\,\cos(\tilde{a}x)dx = \begin{cases} \pi/4 & ...\tilde{a} = 0,\ n = 0 \\ 0 & ...\tilde{a} = 0,\ n = 2,4,6,... \end{cases} \quad \text{(E.66)}$$

Therefore, relation (E.54) has been proved (although several steps have been left for the enjoyment of the reader).

E3.5 Asymptotic Form of Integrals Involving $T_n(x)$ and $U_n(x)$

A careful examination of the previous results reveals, with the aid of (E.29), that the various above integrals have the following asymptotic behavior

$$\lim_{\tilde{a}\to\infty} \int_0^1 T_n(x)\sin(\tilde{a}x)dx \sim \frac{\cos\tilde{a}}{\tilde{a}} \quad ...n=1,3,5,... \tag{E.67}$$

$$\lim_{\tilde{a}\to\infty} \int_0^1 \frac{T_n(x)}{\sqrt{1-x^2}}\sin(\tilde{a}x)dx \sim \frac{\cos\left[\tilde{a}-\frac{\pi}{2}\left(n+\frac{1}{2}\right)\right]}{\tilde{a}^{1/2}} \quad ...n=1,3,5,... \tag{E.68}$$

$$\lim_{\tilde{a}\to\infty} \int_0^1 T_n(x)\cos(\tilde{a}x)dx \sim \frac{\sin\tilde{a}}{\tilde{a}} \quad ...n=0,2,4,... \tag{E.69}$$

$$\lim_{\tilde{a}\to\infty} \int_0^1 \frac{T_n(x)}{\sqrt{1-x^2}}\cos(\tilde{a}x)dx \sim \frac{\cos\left[\tilde{a}-\frac{\pi}{2}\left(n+\frac{1}{2}\right)\right]}{\tilde{a}^{1/2}} \quad ...n=0,2,4,... \tag{E.70}$$

$$\lim_{\tilde{a}\to\infty} \int_0^1 U_n(x)\sin(\tilde{a}x)dx \sim \frac{\cos\tilde{a}}{\tilde{a}} \quad ...n=1,3,5,... \tag{E.71}$$

$$\lim_{\tilde{a}\to\infty} \int_0^1 U_n(x)\sqrt{1-x^2}\sin(\tilde{a}x)dx \sim \frac{\cos\left[\tilde{a}-\frac{\pi}{2}\left(n+\frac{3}{2}\right)\right]}{\tilde{a}^{3/2}} \quad ...n=1,3,5,... \tag{E.72}$$

$$\lim_{\tilde{a}\to\infty} \int_0^1 U_n(x)\cos(\tilde{a}x)dx \sim \frac{\sin\tilde{a}}{\tilde{a}} \quad ...n=0,2,4,... \tag{E.73}$$

$$\lim_{\tilde{a}\to\infty} \int_0^1 U_n(x)\sqrt{1-x^2}\cos(\tilde{a}x)dx \sim \frac{\cos\left[\tilde{a}-\frac{\pi}{2}\left(n+\frac{3}{2}\right)\right]}{\tilde{a}^{3/2}} \quad ...n=0,2,4,... \tag{E.74}$$

where the following asymptotic behavior for S_1 - S_4 has been utilized

$$\lim_{\tilde{a}\to\infty} S_1, S_4 \sim \frac{1}{\tilde{a}^2} \quad ; \quad \lim_{\tilde{a}\to\infty} S_2, S_3 \sim \frac{1}{\tilde{a}} \tag{E.75}$$

BIBLIOGRAPHY

[1] A.M. Nicolson, and G.F. Ross, "Measurement of the Intrinsic Properties of Materials by Time-Domain Techniques," *IEEE Trans. Instrum. Meas.*, vol. IM-19, pp. 377-382, Nov. 1970.

[2] W.B. Weir, "Automatic Measurement of Complex Dielectric Constant and Permeability at Microwave Frequencies," *Proc. IEEE*, vol. 62, pp. 33-36, Jan. 1974.

[3] R.E. Collin, *Field Theory of Guided Waves*, Second Edition, IEEE Press, New Jersey, 1991.

[4] W.J. English, "Vector Variational Solutions of Inhomogeneously Loaded Cylindrical Waveguide Structures," *IEEE Trans. Microwave Theory Tech.*, vol. 19, 1 January 1971, pp. 9-18.

[5] T.K. Findakly, "On the Design of Dielectric Loaded Waveguides," *IEEE Trans. Microwave Theory Tech.*, vol. 24, 1 January 1976, pp. 39-43.

[6] J. Baker-Jarvis, M.D. Janezic, J.H. Grosvenor, and R.G. Geyer, "Transmission/ Reflection and Short-Circuit Line Methods for Measuring Permittivity and Permeability," *NIST Technical Note 1355-R*, U.S. Dept. of Commerce, Dec. 1993.

[7] V.M. Papadopoulos, "Propagation of Electromagnetic Waves in Cylindrical Waveguides with Imperfectly Conducting Walls," *Quart. J. Mech. And Appl. Math.*, vol. 7, September 1954, pp. 325-334.

[8] R.E. Collin, "A Variational Integral for Propagation Constant of Lossy Transmission Lines," *IRE Trans. Microwave Theory Tech.*, May 1960, pp. 339-342.

[9] J. Allison, and F.A. Benson, "Surface Roughness and Attenuation of Precision Drawn, Chemically Polished, Electropolished, Electroplated and Electroformed Waveguides," *Proc. IEE (London)*, vol. 102, part B, March 1955, pp. 251-259.

[10] K. Kurokawa, "Electromagnetic Waves in Waveguides with Wall Impedance," *IRE Trans. Microwave Theory Tech.*, September 1962, pp. 314-320.

[11] H.E.M. Barlow, and H.G. Effemey, "Propagation Characteristics of Low-Loss Tubular Waveguides," *Proc. IEE (London)*, vol. 104, part B, May 1957, pp. 254-260.

[12] R.B. Dybdal, L. Peters, and W.H. Peake, "Rectangular Waveguides with Impedance Walls," *IEEE Trans. Microwave Theory Tech.*, vol. 19, 1 January

1971, pp. 2-9.

[13] P.I. Somlo, and J.D. Hunter, "On the TE_{10}-Mode Cutoff Frequency in Lossy-Walled Rectangular Waveguides," *IEEE Trans. Instrum. Meas.*, vol. 45, 1 February 1996, pp. 301-304.

[14] R. Plonsey, and R.E. Collin, *Principles and Applications of Electromagnetic Fields*, New York, McGraw-Hill, 1961.

[15] R.S. Elliott, *An Introduction to Guided Waves and Microwave Circuits*, New Jersey, Prentice Hall, 1993.

[16] K. Kurokawa, *An Introduction to the Theory of Microwave Circuits*, New York, Academic Press, 1969.

[17] R.E. Collin, *Foundations of Microwave Engineering*, New York, McGraw-Hill, 1966.

[18] D.M. Pozar, *Microwave Engineering*, Second Edition, New York, John Wiley & Sons, 1998.

[19] S. Ramo, J.R. Whinnery, and T. Van Duzer, *Fields and Waves in Communication Electronics*, Third Edition, New York, John Wiley & Sons, 1994.

[20] P.C. Clemmow, *The Plane Wave Representation of Electromagnetic Fields*, New York, Pergamon Press, 1966.

[21] L.B. Felsen, and N. Marcuvitz, *Radiation and Scattering of Electromagnetic Waves*, New Jersey, Prentice Hall, 1973.

[22] J.A. Kong, *Electromagnetic Wave Theory*, New York, John Wiley & Sons, 1986.

[23] W.C. Chew, *Waves and Fields in Inhomogeneous Media*, New York, Van Nostrand Reinhold, 1990.

[24] R.H. Jansen, "The Spectral Domain Approach for Microwave Integrated Circuits," *IEEE Trans. Microwave Theory Tech.*, vol. 33, 1985, pp. 1043-1056.

[25] A. Sommerfeld, *Partial Differential Equations in Physics*, New York, Academic Press, 1949.

[26] D.P. Nyquist, *EE929A Advanced Topics in Electromagnetics; Planar Waveguides and Circuits*, Course Notes, Michigan State University, 1989.

[27] A. Banos, *Dipole Radiation in the Presence of a Conducting Half-Space*, Oxford, Pergamon Press, 1966.

[28] J.S. Bagby, D.P. Nyquist, and B.C. Drachman, "Integral Formulation for Analysis of Integrated Dielectric Waveguides," *IEEE Trans. Microwave Theory Tech.*, vol. 33, 10 October 1985, pp. 906-915.

[29] R.F. Harrington, *Field Computations by Method of Moments*, New York, Macmillan, 1968.

[30] C.T. Tai, *Dyadic Green's Function in Electromagnetic Theory*, New York, Intext Publishers, 1971.

[31] R.N. Bracewell, *The Fourier Transform and its Applications*, New York, McGraw-Hill, 1965.

[32] N.S. Kapany, and J.J. Burke, Optical Waveguides, New York, Academic Press, 1972.

[33] D. Marcuse, *Light Transmission Optics*, Second Edition, New York, Van Nostrand Reinhold, 1982.

[34] D.J. Infante, *Full-Wave Integral-Operator Description of Propagation Modes Excited on Stripline Structures*, Doctoral Dissertation, Michigan State University, 1999.

[35] W.C. Chew, "Some Observations on the Spatial and Eigenfunction Representations of Dyadic Green's Function," *IEEE Trans. on Antennas and Propagation*, vol. 37, 1989, pp. 1322-1327.

[36] J. VanBladel, "Some Remarks on Green's Dyadic for Infinite Space," *IEEE Trans. on Antennas and Propagation*, vol. 9, 1961, pp. 563-566.

[37] M.S. Viola, and D.P. Nyquist, "An Observation on the Sommerfeld-Integral Representation of the Electric Dyadic Green's Function for Layered Media," *IEEE Trans. Microwave Theory Tech.*, vol. 36, 1988, pp. 1289-1292.

[38] J.S. Bagby, and D.P. Nyquist, "Dyadic Green's Functions for Integrated Electronic and Optical Circuits," *IEEE Trans. Microwave Theory Tech.*, vol. 35, 1987, pp. 206-210.

[39] W.H. Beyer, *CRC Standard Mathematical Tables*, 27th Edition, Florida, CRC Press, 1984.

[40] A. Papoulis, *The Fourier Integral and its Applications*, New York, McGraw-Hill, 1962.

[41] H. Howe, *Stripline Circuit Design*, Massachusetts, Artech House, 1974.

[42] J. Frey, *Microwave Integrated Circuits*, Massachusetts, Artech House, 1975.

[43] C.M. Krowne, "Relationships for Green's Function Spectral Dyadics Involving Anisotropic Imperfect Conductors Imbedded in Layered Anisotropic Media," *IEEE Trans. on Antennas and Propagation*, vol. 37, 1989, pp. 1207-1211.

[44] D.P. Nyquist, and D.J. Infante, "Discrete Higher-Order Leaky-Wave Modes and the Continuous Spectrum of Stripline," *IEICE Trans. Electronics*, vol. E78-C, no. 10, October 1995, pp. 1331-1338.

[45] D. Nyquist, J. Grimm, D. Infante, and H. Braunisch, "Classification of the Proper Propagation-Mode Spectrum and Leaky-Wave Modes on Open Planar Waveguides," *Electromagnetics*, Vol. 17, March/April 1997, pp. 105-130.

[46] J. Van Bladel, *Electromagnetic Fields*, New York, McGraw-Hill, 1964.

[47] T. Rozzi, and M. Mongiardo, *Open Electromagnetic Waveguides*, London, Institution of Electrical Engineers, 1997.

[48] A. Frenkel, "On Entire-Domain Basis Functions with Square-Root Edge Singularity," *IEEE Trans. on Antennas and Propagation*, vol. 37, 1989, pp. 1211-1214.

[49] J. S. Bagby, C. Lee, Y. Yuan, and D.P. Nyquist, "Entire-Domain Basis MoM Analysis of Coupled Microstrip Transmission Lines," *IEEE Trans. Microwave Theory Tech.*, vol. 40, 1992, pp. 49-57.

[50] M. Abramowitz, and I. Stegun, *Handbook of Mathematical Functions with Formulas, Graphs, and Mathematical Tables*, New York, Dover Publications, 1964.

[51] P.F. Combes, J. Graffeuil, and J.F. Sautereau, *Microwave Components, Devices and Active Circuits*, New York, John Wiley & Sons, 1987.

[52] K.C. Gupta, R. Garg, I. Bahl, and P. Bhartia, *Microstrip Lines and Slotlines*, Second Edition, London, Artech House, 1996.

[53] F. Gardiol, *Microstrip Circuits*, New York, John Wiley & Sons, 1994.

[54] E.H. Fooks, and R.A. Zakarevicius, *Microwave Engineering Using Microstrip Circuits*, New York, Prentice Hall, 1990.

[55] C.M. Krowne, "Microstrip Conductor Losses Calculated by Full-Wave and Perturbational Approaches," *Electronics Letters*, vol. 24, no. 9, 28th April 1988, pp. 552-553.

[56] T. Deventer, P. Katehi, and A. Cangellaris, "An Integral Equation Method for the Evaluation of Conductor and Dielectric Losses in High-Frequency Interconnects," *IEEE Trans. Microwave Theory Tech.*, vol. 37, 1989, pp. 1964-1972.

[57] J.S. Bagby, C. Lee, and D.P. Nyquist, "Identification of Propagation Regimes on Integrated Microstrip Transmission Lines," *IEEE Trans. Microwave Theory Tech.*, vol. 41, 1993, pp. 1887-1894.

[58] E.J. Denlinger, "Losses of Microstrip Lines," *IEEE Trans. Microwave Theory Tech.*, vol. 28, 1980, pp. 513-522.

[59] R.A. Pucel, D.J. Masse, and C.P. Hartwig, "Losses in Microstrip," *IEEE Trans. Microwave Theory Tech.*, vol. 16, 1968, pp. 342-350.

[60] B.E. Spielman, "Dissipation Loss Effects in Isolated and Coupled Transmission Lines," *IEEE Trans. Microwave Theory Tech.*, vol. 25, 1977, pp. 648-656.

[61] H.A. Wheeler, "Transmission-Line Properties of a Strip on a Dielectric Sheet on a Plane," *IEEE Trans. Microwave Theory Tech.*, vol. 25, 1977, pp. 631-647.

[62] E.F. Kuester, and D.C. Chang, "An Appraisal of Methods for Computation of the Dispersion Characteristics of Open Microstrip," *IEEE Trans. Microwave Theory Tech.*, vol. 27, 1979, pp. 691-694.

[63] N. Fache, and D. De Zutter, "Rigorous Full-Wave Space-Domain Solution for Dispersive Microstrip Lines," *IEEE Trans. Microwave Theory Tech.*, vol. 36, 1988, pp. 731-737.

[64] K.A. Michalski, and D. Zheng, "Rigorous Analysis of Open Microstrip Lines of Arbitrary Cross Section in Bound and Leaky Regimes," *IEEE Trans. Microwave Theory Tech.*, vol. 37, 1989, pp. 2005-2010.

[65] M. Hashimoto, "A Rigorous Solution for Dispersive Microstrip," *IEEE Trans. Microwave Theory Tech.*, vol. 33, 1985, pp. 1131-1137.

[66] D.M. Syahkal, and J.B. Davies, "Accurate Solution of Microstrip and Coplanar Structures for Dispersion and for Dielectric and Conductor Losses," *IEEE Trans. Microwave Theory Tech.*, vol. 27, 1979, pp. 694-699.

[67] A.D. Myskis, *Advanced Mathematics for Engineers*, Moscow, Mir Publishers, 1979.

[68] J.W. Dettman, *Applied Complex Variables*, New York, Dover Publications, 1965.

[69] L.V. Ahlfors, *Complex Analysis, An Introduction to the Theory of Analytic Functions of One Complex Variable*, Second Edition, New York, McGraw-Hill,

1966.

[70] W.R. LePage, *Complex Variables and the Laplace Transform for Engineers*, New York, Dover Publications, 1961.

[71] K. Knopp, *Theory of Functions, Parts I and II*, New York, Dover Publications, 1996.

[72] G.F. Carrier, M. Krook, and C. Pearson, *Functions of a Complex Variable*, New York, McGraw-Hill, 1966.

[73] J.A. Stratton, *Electromagnetic Theory*, New York, McGraw-Hill, 1941.

[74] T.B.A Senior, and J.L. Volakis, *Approximate Boundary Conditions in Electromagnetics*, Institution of Electrical Engineers, 1995.

[75] C.A. Balanis, *Advanced Engineering Electromagnetics*, New York, John Wiley & Sons, 1989.

[76] M.A. Leontovich, *Investigations on Radiowave Propagation, Part II*, Moscow, Printing House of the Academy of Sciences, 1948.

[77] I.S. Gradshteyn, and I.M. Ryzhik, *Table of Integrals, Series, and Products*, Sixth Edition", New York, Academic Press, 2000.

[78] T.J. Rivlin, *The Chebyshev Polynomials*, New York, John Wiley & Sons, 1974.

[79] G. Szego, *Orthogonal Polynomials*, New York, American Mathematical Society, 1939.

[80] J. Spanier, and K. Oldham, *An Atlas of Functions*, Washington, Hemisphere Publishing, 1987.